

HYSTERETIC RESPONSE OF STEEL-CLAD, WOOD-FRAMED SHEAR WALLS
UNDER REVERSE-CYCLIC LOADING

By

KHOI DUC MAI

A dissertation submitted in partial fulfillment of
the requirements for the degree of

DOCTOR OF PHILOSOPHY

WASHINGTON STATE UNIVERSITY
Department of Civil and Environmental Engineering

MAY 2016

To the Faculty of Washington State University:

The members of the Committee appointed to examine the dissertation of
KHOI DUC MAI find it satisfactory and recommend that it be accepted.

Donald A. Bender, Ph.D., Chair

James D. Dolan, Ph.D.

William Franklin Cofer, Ph.D.

Vikram Yadama, Ph.D.

ACKNOWLEDGMENTS

With the most gratefulness, I would like to thank the following for all that they did for me while I worked on this research:

- Buddhism: for my beliefs, and spirituality.
- Parents: Ba Thi Nguyen and Khai Van Mai for inspiring me to “Never give up” and for always being there at the drop of a hat to provide me advices, and most importantly to pray for me every day.
- Brothers and Sisters: Mai Thi Hong Thao, Mai Thi Thanh Thao, and Mai Thi Huong Thao for their laughter, consistent interest and continual supports.
- Committee members: Dr. Donald Bender, Dr. William Cofer, Dr. J Daniel Dolan and Dr. Vikram Yadama for keeping me on the right path and providing their invaluable knowledge to aid in my research.
- CMEC: Bob Duncan and Scott Lewis for their persistent help in my testing process. I would still be in the lab trying to figure out how to control the hydraulic actuator and to build the shear walls if it was not for their assistance.
- Extra hands: Dustin Gatchalian and everyone else who threw their backs out helping me build the post-frame shear walls.
- SFS Inc. and Maze Nail: for nails, and screws donations.
- National Frame Building Association: for funding this research.

HYSTERETIC RESPONSE OF STEEL-CLAD, WOOD-FRAMED SHEAR WALLS UNDER REVERSE-CYCLIC LOADING

Abstract

by Khoi Duc Mai, Ph.D.
Washington State University
May 2016

Chair: Donald A. Bender

Steel-Clad, Wood-Framed (SCWF) shear walls are used as the main lateral load resisting system in post-frame buildings under wind and earthquake lateral loadings. However, seismic design coefficients have not been developed for the design of SCWF shear walls as a main lateral force resisting system for seismic forces. Research is needed to help designers of post-frame construction with accurately determining the behavior of SCWF shear walls subjected to lateral loads. To address these needs, finite element analysis (FEA) models of SCWF shear walls under monotonic and cyclic loading as well as the reversed cyclic SCWF shear wall tests were developed. With validated FEA predictions, and experimental data on behavior of SCWF shear walls, design information can be developed for post-frame buildings in seismic and high wind regions.

FEA models were developed and validated to predict shear strength and effective shear modulus of SCWF shear walls under monotonic loading. Moreover, the

hysteretic behavior of SCWF shear walls was predicted using hysteretic behavior of sheathing-to-framing connector elements. Analyses were performed to assess the shear strength, stiffness, ductility, equivalent energy elastic plastic (EEEP), and hysteretic parameters of tested SCWF shear wall specimens. Experimental tests also provided the seismic design coefficients of SCWF shear walls, which are currently lacking in the building codes.

The dynamic implicit FEA models predicted well the shear strength and effective shear stiffness of SCWF shear walls under monotonic loading. The dynamic implicit FEA also overcame the deficiencies of the static implicit approach with regard to buckling, nonlinear geometry behavior of steel cladding. In addition, experimental test results showed that SCWF shear walls had high ductility, especially for unstitched shear wall configurations. Based on the research herein, shear walls with high ductility can be considered equivalent to light-framed wood shear walls with regard to behavior under seismic loading. Moreover, the hysteretic behavior of SCWF shear walls under cyclic loading was predicted well, especially for unstitched shear wall configurations. Good agreement was also obtained with regard to shear strength backbone curve, except for heavily stitched shear walls. Therefore, the FEA models can be used to determine the equivalency between SCWF shear walls and light-framed wood shear walls.

TABLE OF CONTENTS

	Page
ACKNOWLEDGMENTS.....	iii
ABSTRACT.....	iv
TABLE OF CONTENTS.....	vi
LIST OF TABLES.....	xi
LIST OF FIGURES.....	xiv
CHAPTER 1.....	1
INTRODUCTION.....	1
CHAPTER 2.....	3
ABSTRACT.....	3
INTRODUCTION.....	4
OBJECTIVES.....	6
LITERATURE REVIEW.....	6
TESTING OF SCWF SHEAR WALLS UNDER MONOTONIC LOADING.....	10
Materials and wall construction.....	10
Test methods.....	11
COMPARISON OF FEA APPROACHES.....	12
Static implicit FEA.....	12

Dynamic implicit FEA.....	13
MODEL DEVELOPMENT.....	14
Selection of elements.....	14
Material properties.....	15
Boundary conditions.....	18
RESULTS AND DISCUSSION.....	19
SUMMARY AND CONCLUSIONS.....	20
FUTURE RESEARCH.....	20
REFERENCES.....	22
FIGURES.....	26
TABLES.....	30
CHAPTER 3.....	34
ABSTRACT.....	34
INTRODUCTION.....	34
OBJECTIVES.....	38
LITERATURE REVIEW.....	39
METHOD AND MATERIALS.....	41
Material and wall constructions.....	41
Methods.....	41

Wood specific gravity	42
Steel coupon tension and bending yield strength for nail.....	42
EXPERIMENTALLY DETERMINED PARAMETERS	42
RESULTS AND DISCUSSION	44
Wall failure modes	44
Cyclic horizontal shear strength.....	45
Hysteresis parameters	46
Equivalency with light-framed shear wall using AC 322 criteria	47
DESIGN RECOMMENDATIONS.....	49
SUMMARY AND CONCLUSIONS	50
ACKNOWLEDGEMENTS.....	51
NOTATION	52
REFERENCES.....	53
FIGURES	57
TABLES.....	60
CHAPTER 4	64
ABSTRACT	64
INTRODUCTION	65
DEVELOPMENT OF HYSTERESIS MODEL FOR SCREW CONNECTOR	67

Overview of Heine’s hysteresis model	67
BWBN model development.....	70
Model solution.....	70
System identification	72
Screw connector tests and validation of BWBN model	73
FINITE ELEMENT MODEL DEVELOPMENT.....	75
Selection of elements.....	75
Material properties	76
TESTING OF STEEL-CLAD, WOOD-FRAMED SHEAR WALLS UNDER CYCLIC LOADING	78
Materials and wall construction	78
Test methods	79
RESULTS AND DISCUSSION	80
SUMMARY AND CONCLUSIONS	82
ACKNOWLEDGEMENTS.....	83
REFERENCES	84
FIGURES	89
TABLES.....	98
CHAPTER 5	104

SUMMARY AND CONCLUSIONS	104
APPENDIX A BEHAVIOR OF STEEL-CLAD, WOOD-FRAMED (SCWF) SHEAR WALLS UNDER MONOTONIC LOADING	108
APPENDIX B SEISMIC DESIGN COEFFICIENTS FOR STEEL-CLAD, WOOD- FRAMED SHEAR WALLS.....	127
APPENDIX C PREDICTING BEHAVIOR OF STEEL-CLAD, WOOD-FRAMED SHEAR WALLS UNDER CYCLIC LOADING	156

LIST OF TABLES

Table 2.1: Construction properties for each shear wall (Bender, 2012).....	30
Table 2.2: Load-slip modulus of nail connection	31
Table 2.3: Load-displacement parameters of screw connection	31
Table 2.4: Ultimate shear strength of SCWF shear walls from tests and FEA model....	32
Table 2.5: Effective shear modulus of SCWF shear wall from tests and FEA model	33
Table 3.1: Seismic design values and ductility ratio	60
Table 3.2: Wood Member Specific Gravity at Oven-Dry Volume.....	61
Table 3.3: Tension strength and bending yield strength of nails and steel sheathing ...	61
Table 3.4: Seismic design values and monotonic design values (Bender, 2012)	62
Table 3.5: Average hysteresis parameters of wall type 2	62
Table 3.6: AC 322 criteria for seismic equivalency with wood shear wall.....	63
Table 4.1: BWBN parameters for connection between SPF and steel cladding (no. 10x25.1 mm)	98
Table 4.2: BWBN parameters for connection between steel cladding and steel cladding (no. 12x19.1 mm)	99
Table 4.3: BWBN parameters for connection between steel cladding and steel cladding (no. 12x38.1 mm)	100
Table 4.4: Corrugated panel properties.....	101
Table 4.5: Load-slip modulus of nail connection	101
Table 4.6: Construction properties for each shear wall (Bender, 2015).....	102
Table 4.7: Energy dissipation between FEA models and tests.....	103
Table 4.8: AC 322 criteria check for tests and FEA models	103

Table B.1 Average calculated hysteresis parameters. Wall type 1.....	130
Table B.2: Average calculated hysteresis parameters. Wall type 2.....	133
Table B.3: Average calculated hysteresis parameters. Wall type 4.....	136
Table B.4: Average calculated hysteresis parameters. Wall type 5.....	139
Table B.5: Average calculated hysteresis parameters. Wall type 6.....	142
Table B.6: Average calculated hysteresis parameters. Wall type 7.....	145
Table B.7: Average calculated hysteresis parameters. Wall type 10.....	148
Table B.8: Average calculated hysteresis parameters. Wall type 11.....	151
Table B.9: Average calculated hysteresis parameters. Wall type 13.....	153
Table B.10: Average calculated hysteresis parameters. Wall type 14.....	155
Table C.1: Parameters estimation of screw connection test 1 (SPF to Grandrib 3)	158
Table C.2: Parameters estimation of screw connection test 2 (SPF to Grandrib 3)	160
Table C.3: Parameters estimation of screw connection test 3 (SPF to Grandrib 3)	162
Table C.4: Parameters estimation of screw connection test 4 (SPF to Grandrib 3)	164
Table C.5: Parameters estimation of screw connection test 5 (SPF to Grandrib 3)	166
Table C.6: Parameters estimation of screw connection test 6 (SPF to Grandrib 3)	168
Table C.7: Parameters estimation of No.12x19.1 mm screw connection test 1 (Grandrib 3 to Grandrib 3)	170
Table C.8: Parameters estimation of No.12x19.1 mm screw connection test 2 (Grandrib 3 to Grandrib 3)	172
Table C.9: Parameters estimation of No.12x19.1 mm screw connection test 3 (Grandrib 3 to Grandrib 3)	174

Table C.10: Parameters estimation of No.12x19.1 mm screw connection test 4 (Grandrib 3 to Grandrib 3)	176
Table C.11: Parameters estimation of No.12x19.1 mm screw connection test 5 (Grandrib 3 to Grandrib 3)	178
Table C.12: Parameters estimation of No.12x19.1 mm screw connection test 6 (Grandrib 3 to Grandrib 3)	180
Table C.13: Parameters estimation of No.12x19.1 mm screw connection test 7 (Grandrib 3 to Grandrib 3)	182
Table C.14: Parameters estimation of No.12x19.1 mm screw connection test 8 (Grandrib 3 to Grandrib 3)	184
Table C.15: Parameters estimation of No.12x38.1 mm screw connection test 1 (Grandrib 3 to Grandrib 3)	186
Table C.16: Parameters estimation of No.12x38.1 mm screw connection test 2 (Grandrib 3 to Grandrib 3)	188
Table C.17: Parameters estimation of No.12x38.1 mm screw connection test 3 (Grandrib 3 to Grandrib 3)	190
Table C.18: Parameters estimation of No.12x38.1 mm screw connection test 4 (Grandrib 3 to Grandrib 3)	192
Table C.19: Parameters estimation of No.12x38.1 mm screw connection test 5 (Grandrib 3 to Grandrib 3)	194
Table C.20: Parameters estimation of No.12x38.1 mm screw connection test 6 (Grandrib 3 to Grandrib 3)	196
Table C.21: AC 322 criteria check for tests and FEA models.....	206

LIST OF FIGURES

Figure 2.1: Simplified diagram of a post-frame building (National Frame Builders Association Design Manual, 1999)	26
Figure 2.2 : General shear wall configuration (Bender, 2012)	27
Figure 2.3: Shear wall screw patterns (Bender, 2012)	28
Figure 2.4: Connector load-displacement curve (Dolan, 1992)	28
Figure 2.5: Shear load-displacement of wall type 4.....	29
Figure 2.6: Shear load-displacement of wall type 5.....	29
Figure 3.1 : Hysteresis, Envelope and EEEP curves of wall 2-1	57
Figure 3.2: Hysteresis, Envelope and EEEP curves of wall 7-2	58
Figure 3.3: Performance Parameters of Specimen (ASTM E2126).....	59
Figure 4.1: Hysteretic behavior of a bolted joint in single shear stress beyond the elastic limit (Heine, 2001)	89
Figure 4.2: Typical load-slip of no.10x25.4 mm connection between SPF and steel panel. Test 1.	90
Figure 4.3: Typical hysteretic energy of no.10x25.4 mm connection between SPF and steel panel. Test 1.....	90
Figure 4.4: Energy of FEA model. Wall type 1.	91
Figure 4.5: Force vs. displacement. Wall type 1.....	92
Figure 4.6: Force vs. displacement of wall type 2	93
Figure 4.7: Force vs. displacement of wall type 4	94
Figure 4.8: Backbone curve for tests and FEA models	95
Figure 4.9: General shear wall configuration (Bender, 2015)	96

Figure 4.10: Shear wall screw patterns (Bender, 2015)	97
Figure A.1: Load versus displacement for SCWF shear wall type 1	109
Figure A.2: Load versus displacement for SCWF shear wall type 2.....	109
Figure A.3: Load versus displacement for SCWF shear wall type 3.....	110
Figure A.4: Load versus displacement for SCWF shear wall type 4.....	110
Figure A.5: Load versus displacement for SCWF shear wall type 5.....	111
Figure A.6: Load versus displacement for SCWF shear wall type 6.....	111
Figure A.7: Load versus displacement for SCWF shear wall type 7.....	112
Figure A.8: Load versus displacement for SCWF shear wall type 8.....	112
Figure A.9: Load versus displacement for SCWF shear wall type 9.....	113
Figure A.10: Load versus displacement for No.10x25.4mm screw connection test 1 (SPF to Grandrib 3)	114
Figure A.11: Load versus displacement for No.10x25.4mm screw connection test 2 (SPF to Grandrib 3)	114
Figure A.12: Load versus displacement for No.10x25.4mm screw connection test 3 (SPF to Grandrib 3)	115
Figure A.13: Load versus displacement for No.10x25.4mm screw connection test 4 (SPF to Grandrib 3)	115
Figure A.14: Load versus displacement for No.10x25.4mm screw connection test 6 (SPF to Grandrib 3)	116
Figure A.15: Load versus displacement for No.10x25.4mm screw connection test 7 (SPF to Grandrib 3)	116

Figure A.16: Load versus displacement for No.10x25.4mm screw connection test 8 (SPF to Grandrib 3)	117
Figure A.17: Load versus displacement for No.10x25.4mm screw connection test 9 (SPF to Grandrib 3)	117
Figure A.18: Load versus displacement for No.10x25.4mm screw connection test 10 (SPF to Grandrib 3)	118
Figure A.19: Average load versus displacement for No.10x25.4 mm screw (SPF to Grandrib 3)	118
Figure A.20: Average load versus displacement for No.10x25.4 mm screw (SPF to Grandrib 3) used in FEA model.....	119
Figure A.21: Load versus displacement for No.10x25.4mm screw connection test 1 (SPF to Wick)	119
Figure A.22: Load versus displacement for No.10x25.4mm screw connection test 2 (SPF to Wick)	120
Figure A.23: Load versus displacement for No.10x25.4mm screw connection test 3 (SPF to Wick)	120
Figure A.24: Load versus displacement for No.10x25.4mm screw connection test 4 (SPF to Wick)	121
Figure A.25: Load versus displacement for No.10x25.4mm screw connection test 6 (SPF to Wick)	121
Figure A.26: Load versus displacement for No.10x25.4mm screw connection test 7 (SPF to Wick)	122

Figure A.27: Load versus displacement for No.10x25.4mm screw connection test 8 (SPF to Wick)	122
Figure A.28: Load versus displacement for No.10x25.4mm screw connection test 9 (SPF to Wick)	123
Figure A.29: Load versus displacement for No.10x25.4mm screw connection test 10 (SPF to Wick)	123
Figure A.30: Average load versus displacement for No.10x25.4 mm screw (SPF to Wick)	124
Figure A.31: Average load versus displacement for No.10x25.4 mm screw (SPF to Wick) used in FEA model	124
Figure A.32: Average load versus displacement for No.12x19.1 mm screw (between Grandrib 3) used in FEA model	125
Figure A.33: Average load versus displacement for No.12x38.1 mm screw (between Grandrib 3) used in FEA model	125
Figure A.34: Average load versus displacement for No.12x19.1 mm screw (between Wick) used in FEA model	126
Figure B.1: Cyclic loading protocol, $\Delta = 91.44$ mm (ASTM E2126-11)	128
Figure B.2: Performance parameters of specimens (ASTM E2126-11)	128
Figure B.3: Hysteresis, Envelop, and EEEP curves of wall 1-1	129
Figure B.4: Average envelop, and EEEP curve of wall 1-1	129
Figure B.5: Hysteresis, Envelop, and EEEP curves of wall 2-1	131
Figure B.6: Average envelop, and EEEP curve of wall 2-1	131
Figure B.7: Hysteresis, Envelop, and EEEP curves of wall 2-2	132

Figure B.8: Average envelop, and EEEP curve of wall 2-2	132
Figure B.9: Hysteresis, Envelop, and EEEP curves of wall 4-1	134
Figure B.10: Average envelop, and EEEP curve of wall 4-1	134
Figure B.11: Hysteresis, Envelop, and EEEP curves of wall 4-2.....	135
Figure B.12: Average envelop, and EEEP curve of wall 4-2	135
Figure B.13: Hysteresis, Envelop, and EEEP curves of wall 5-1	137
Figure B.14: Average envelop, and EEEP curve of wall 5-1	137
Figure B.15: Hysteresis, Envelop, and EEEP curves of wall 5-2.....	138
Figure B.16: Average envelop, and EEEP curve of wall 5-2	138
Figure B.17: Hysteresis, Envelop, and EEEP curves of wall 6-1	140
Figure B.18: Average envelop, and EEEP curve of wall 6-1	140
Figure B.19: Hysteresis, Envelop, and EEEP curves of wall 6-2.....	141
Figure B.20: Average envelop, and EEEP curve of wall 6-2	141
Figure B.21: Hysteresis, Envelop, and EEEP curves of wall 7-2.....	143
Figure B.22: Average envelop, and EEEP curve of wall 7-2	143
Figure B.23: Hysteresis, Envelop, and EEEP curves of wall 7-3.....	144
Figure B.24: Average envelop, and EEEP curve of wall 7-3	144
Figure B.25: Hysteresis, Envelop, and EEEP curves of wall 10-1.....	146
Figure B.26: Average envelop, and EEEP curve of wall 10-1	146
Figure B.27: Hysteresis, Envelop, and EEEP curves of wall 10-2.....	147
Figure B.28: Average envelop, and EEEP curve of wall 10-2	147
Figure B.29: Hysteresis, Envelop, and EEEP curves of wall 11-2.....	149
Figure B.30: Average envelop, and EEEP curve of wall 11-2	149

Figure B.31: Hysteresis, Envelop, and EEEP curves of wall 11-3.....	150
Figure B.32: Average envelop, and EEEP curve of wall 11-3	150
Figure B.33: Hysteresis, Envelop, and EEEP curves of wall 13-1	152
Figure B.34: Average envelop, and EEEP curve of wall 13-1	152
Figure B.35: Hysteresis, Envelop, and EEEP curves of wall 14-1	154
Figure B.36: Average envelop, and EEEP curve of wall 14-1	154
Figure C.1: Load versus displacement of No.10x25.4mm screw connection test 1 (SPF to Grandrib 3)	157
Figure C.2: Cumulative Energy dissipated of No.10x25.4 mm screw connection test 1 (SPF to Grandrib 3)	157
Figure C.3: Load versus displacement of No.10x25.4mm screw connection test 2 (SPF to Grandrib 3)	159
Figure C.4: Cumulative Energy dissipated of No.10x25.4 mm screw connection test 2 (SPF to Grandrib 3)	159
Figure C.5: Load versus displacement of No.10x25.4mm screw connection test 3 (SPF to Grandrib 3)	161
Figure C.6: Cumulative Energy dissipated of No.10x25.4 mm screw connection test 3 (SPF to Grandrib 3)	161
Figure C.7: Load versus displacement of No.10x25.4mm screw connection test 4 (SPF to Grandrib 3)	163
Figure C.8: Cumulative Energy dissipated of No.10x25.4 mm screw connection test 4 (SPF to Grandrib 3)	163

Figure C.9: Load versus displacement of No.10x25.4mm screw connection	
test 5 (SPF to Grandrib 3)	165
Figure C.10: Cumulative Energy dissipated of No.10x25.4 mm screw connection	
test 5 (SPF to Grandrib 3)	165
Figure C.11: Load versus displacement of No.10x25.4mm screw connection	
test 6 (SPF to Grandrib 3)	167
Figure C.12: Cumulative Energy dissipated of No.10x25.4 mm screw connection	
test 6 (SPF to Grandrib 3)	167
Figure C.13: Load versus displacement of No.12x19.1 mm screw connection	
test 1 (Grandrib 3 to Grandrib 3)	169
Figure C.14: Cumulative Energy dissipated of No.12x19.1 mm screw connection	
test 1 (Grandrib 3 to Grandrib 3)	169
Figure C.15: Load versus displacement of No.12x19.1 mm screw connection	
test 2 (Grandrib 3 to Grandrib 3)	171
Figure C.16: Cumulative Energy dissipated of No.12x19.1 mm screw connection test 2 (Grandrib 3 to Grandrib 3)	171
Figure C.17: Load versus displacement of No.12x19.1 mm screw connection test 3 (Grandrib 3 to Grandrib 3)	173
Figure C.18: Cumulative Energy dissipated of No.12x19.1 mm screw connection test 3 (Grandrib 3 to Grandrib 3)	173
Figure C.19: Load versus displacement of No.12x19.1 mm screw connection	
test 4 (Grandrib 3 to Grandrib 3)	175

Figure C.20: Cumulative Energy dissipated of No.12x19.1 mm screw connection test 4 (Grandrib 3 to Grandrib 3)	175
Figure C.21: Load versus displacement of No.12x19.1 mm screw connection test 5 (Grandrib 3 to Grandrib 3)	177
Figure C.22: Cumulative Energy dissipated of No.12x19.1 mm screw connection test 5 (Grandrib 3 to Grandrib 3)	177
Figure C.23: Load versus displacement of No.12x19.1 mm screw connection test 6 (Grandrib 3 to Grandrib 3)	179
Figure C.24: Cumulative Energy dissipated of No.12x19.1 mm screw connection test 6 (Grandrib 3 to Grandrib 3)	179
Figure C.25: Load versus displacement of No.12x19.1 mm screw connection test 7 (Grandrib 3 to Grandrib 3)	181
Figure C.26: Cumulative Energy dissipated of No.12x19.1 mm screw connection test 7 (Grandrib 3 to Grandrib 3)	181
Figure C.27: Load versus displacement of No.12x19.1 mm screw connection test 8 (Grandrib 3 to Grandrib 3)	183
Figure C.28: Cumulative Energy dissipated of No.12x19.1 mm screw connection test 8 (Grandrib 3 to Grandrib 3)	183
Figure C.29: Load versus displacement of No.12x38.1 mm screw connection test 1 (Grandrib 3 to Grandrib 3)	185
Figure C.30: Cumulative Energy dissipated of No.12x38.1 mm screw connection test 1 (Grandrib 3 to Grandrib 3)	185

Figure C.31: Load versus displacement of No.12x38.1 mm screw connection test 2 (Grandrib 3 to Grandrib 3)	187
Figure C.32: Cumulative Energy dissipated of No.12x38.1 mm screw connection test 2 (Grandrib 3 to Grandrib 3)	187
Figure C.33: Load versus displacement of No.12x38.1 mm screw connection test 3 (Grandrib 3 to Grandrib 3)	189
Figure C.34: Cumulative Energy dissipated of No.12x38.1 mm screw connection test 3 (Grandrib 3 to Grandrib 3)	189
Figure C.35: Load versus displacement of No.12x38.1 mm screw connection test 4 (Grandrib 3 to Grandrib 3)	191
Figure C.36: Cumulative Energy dissipated of No.12x38.1 mm screw connection test 4 (Grandrib 3 to Grandrib 3)	191
Figure C.37: Load versus displacement of No.12x38.1 mm screw connection test 5 (Grandrib 3 to Grandrib 3)	193
Figure C.38: Cumulative Energy dissipated of No.12x38.1 mm screw connection test 5 (Grandrib 3 to Grandrib 3)	193
Figure C.39: Load versus displacement of No.12x38.1 mm screw connection test 6 (Grandrib 3 to Grandrib 3)	195
Figure C.40: Cumulative Energy dissipated of No.12x38.1 mm screw connection test 6 (Grandrib 3 to Grandrib 3)	195
Figure C.41: Load versus deflection of wall type 1 under cyclic loading.....	197
Figure C.42: Energy of wall type 1 under cyclic loading (FEA model)	197
Figure C.43: Load versus deflection of wall type 2 under cyclic loading.....	198

Figure C.44: Energy of wall type 2 under cyclic loading (FEA model)	198
Figure C.45: Load versus deflection of wall type 4 under cyclic loading.....	199
Figure C.46: Energy of wall type 4 under cyclic loading (FEA model)	199
Figure C.47: Load versus deflection of wall type 5 under cyclic loading.....	200
Figure C.48: Energy of wall type 5 under cyclic loading (FEA model)	200
Figure C.49: Load versus deflection of wall type 6 under cyclic loading.....	201
Figure C.50: Energy of wall type 6 under cyclic loading (FEA model)	201
Figure C.51: Load versus deflection of wall type 7 under cyclic loading.....	202
Figure C.52: Energy of wall type 7 under cyclic loading (FEA model)	202
Figure C.53: Backbone curve of FEA model and test. Wall type 1.....	203
Figure C.54: Backbone curve of FEA model and test. Wall type 2.....	203
Figure C.55: Backbone curve of FEA model and test. Wall type 4.....	204
Figure C.56: Backbone curve of FEA model and test. Wall type 5.....	204
Figure C.57: Backbone curve of FEA model and test. Wall type 6.....	205
Figure C.58: Backbone curve of FEA model and test. Wall type 7.....	205

CHAPTER 1

INTRODUCTION

Post-frame construction is becoming increasingly popular for the many low-rise building applications due to its advantages in cost, structural efficiencies, and open clear span spaces that are preferred for commercial and gathering spaces. Steel-clad, wood-framed (SCWF) shear walls are used as the main lateral force resisting systems in post-frame construction. Research was performed at Washington State University Composite Material and Engineering Center (CMEC) to gain a better understanding of the behavior of SCWF shear walls subjected to wind and seismic loading. The current design approach involves testing common SCWF shear wall configuration and publishing the design shear and stiffness. Design values derived from small-scale tests are limited and not a practical option for post-frame building design due to expense and considerable time consuming to conduct tests. Moreover, a majority of research data consisted of monotonic testing of diaphragms, and monotonic testing of connection used in SCWF diaphragms; and no research was found on the behavior of SCWF shear walls under cyclic loading. To address the need, three main goals of the research were performed and summarized as follows:

1. The first objective of this study was to develop and validate a finite element analysis (FEA) model to predict shear strength, and effective shear modulus of SCWF shear walls under monotonic loading.
2. The second objective was to gain insights on the behavior of SCWF and Oriented Strandboard, Wood-Framed (OSBWF) shear walls under cyclic

loading. Post-frame walls with steel and OSB sheathing were tested under cyclic loading to characterize the shear stiffness, shear strength, ductility ratio of post-frame shear walls, and to provide experimental basis for seismic design coefficients equivalent with traditional light-framed wood shear walls.

3. The third objective of this study was to develop a FEA model to predict the hysteretic behavior of SCWF shear walls under cyclic loading. The results from this model can be incorporated into the methodology for reliably quantifying building system performance and response parameters for use in seismic design. Moreover, this FEA model can provide the constitutive relationship for shear walls or diaphragms under cyclic loading and this constitutive relationship can be used as macro-element to model the entire post-frame building under dynamic loading.

CHAPTER 2

DYNAMIC IMPLICIT FINITE ELEMENT ANALYSIS OF STEEL-CLAD, WOOD-FRAMED SHEAR WALLS

ABSTRACT

Various finite element codes and solution techniques have been developed for Steel-Clad, Wood-Framed (SCWF) shear walls over the past few decades. Most previous finite element models for SCWF shear walls under monotonic loading were based on a static implicit solution technique. Previous researchers showed that the static implicit technique showed promise for modeling SCWF diaphragms; however, the solution technique failed to converge to equilibrium as local instabilities, snap-through bucking of steel cladding occurred or geometric nonlinearities were included in the model reported herein. In this paper, a nonlinear dynamic implicit finite element analysis (FEA) of SCWF shear walls subjected to monotonic loading was developed to overcome the deficiencies of the static implicit approach. Three types of elements were used, including beam elements to model wood framing, shell elements to model steel cladding, and nonlinear spring elements to model connectors. Screw connector tests were conducted to obtain the load-displacement constitutive relationships needed for finite element models. Nine types of SCWF shear walls with and without lap seam stitching were tested to validate the finite element model. The ratios of predicted-to-test values for ultimate shear strength averaged 0.97 with coefficient of variation of 8.1%; and the ratios for effective shear modulus averaged 1.13 with coefficient of variation of 30%. The dynamic implicit FEA was a significant improvement over previous static

implicit techniques, and should be a useful tool to predict the ultimate shear strength and effective shear modulus of SCWF shear walls under monotonic loading.

INTRODUCTION

Post-frame construction is becoming increasingly popular for the many low-rise building applications due to its advantages in cost, structural efficiencies, and open clear span spaces that are preferred for commercial and gathering spaces. Post-frame construction is typically a wood frame building system composed of main members such as posts and trusses and secondary members such as roof purlins and wall girts. Timber posts are usually embedded in the ground with concrete footings or surface mounted to concrete foundation or slab on grade. Girts are attached across the posts to form the wall frame. Trusses are typically mounted directly to posts and purlins are laid across the trusses to form the roof frame. The most common cladding material used in post-frame construction is corrugated steel attached to framing members with structural fasteners. Figure 2.1 illustrates the structural components of a common type of post-frame construction. While timber frames with embedded posts can provide some resistance to lateral loads, the diaphragm and shear wall actions resist most of the lateral loads from wind and earthquake.

The code referenced standard ANSI/ASAE EP484.2 gives provisions for diaphragm and shear wall design of post-frame buildings. The force distribution method (Anderson et al, 1989) or computer program DAFI (Bohnhoff, 1992) can be used to determine the load distribution between frames, diaphragms and shear walls in post-frame buildings. However, the stiffness for each building component need to be known

prior to analysis. While frame stiffness can be easily computed from static analysis, shear wall and diaphragm stiffness analysis is complex. Strength and stiffness of shear walls and diaphragms are typically derived from small-scale panel tests in accordance with ANSI/ASAE EP558. Several variables affect the strength and stiffness of shear walls and diaphragms. Whenever changes are made to the shear wall dimensions, cladding material, steel corrugated profile, framing geometry, fastener or framing pattern, new tests are required to obtain design values for specific configurations. The modified MCA model has also been used to derive shear wall design values (Luttrell and Mattingly, 2004; Leflar, 2008), but this model can only predict point estimates of the design shear strength and stiffness and not the entire load-displacement response needed for seismic analyses. Therefore, an analytical approach such as FEA is a desirable option for predicting strength and stiffness of shear wall panels and can reduce the number of tests required to determine shear wall performance.

Various FEA programs have been developed to model the performance of SCWF shear walls and diaphragms under monotonic loading with the understanding that the individual behavior of steel-to-framing fasteners has great influence on the overall lateral behavior (Wright and Manbeck, 1993; Keener and Manbeck, 1996b; and Williams and Bohnhoff, 1998). Therefore, the load-slip characteristics of various configurations of steel-to-framing connectors were tested for SCWF shear wall and diaphragm models (Troxell et al, 1989; Anderson and Kelley, 1998; Williams and Bohnhoff, 2000). Most of previous developed FEA models used static implicit methods to model SCWF diaphragms behavior. Although promising results have been obtained

based on these methods, general application has been shown to be limited due to failing to reach convergence with highly stitched SCWF shear walls (Wright and Manbeck, 1993), less accuracy in the load-deflection results in the nonlinear region (Keener and Manbeck, 1996b), and the need for complex testing and models for equivalent material properties of plane stress elements for steel sheathing (Williams and Bohnhoff, 1998). In this paper, the FEA based on a dynamic implicit method is developed to predict strength and effective shear modulus for various SCWF shear wall configurations under monotonic loading. The configurations considered include combinations of wood framing spacing, fastener patterns, steel cladding profiles, and types of stitch screws at lap joints.

OBJECTIVES

The primary objectives of this research were:

1. To develop a dynamic implicit finite element model to predict ultimate shear strength and effective shear modulus of SCWF shear walls under monotonic loading.
2. To validate the dynamic implicit finite element model by comparing with experimental tests.

LITERATURE REVIEW

Davies and Bryan (1982) developed a finite element model to predict effective shear moduli of corrugated steel panels. A four-node shell element was used to model the corrugated steel panels and the results showed that load-deflection behavior of corrugated steel panels was predicted well using the finite element model. Davies and

Bryan (1982) also derived an equation to estimate the shear modulus of a panel that consisted of the inverse of the summation of shear strain and profile distortion flexibility. This equation was used to predict the corrugation shear modulus used in the SCWF diaphragm model by many post-frame building researchers (Anderson, 1987; Boone, 1987; Boone and Manbeck, 1989, Keener and Manbeck, 1996a, Keener and Manbeck, 1996b, Williams and Bohnhoff, 1998).

Keener and Manbeck (1996a) conducted experiments and studied effective shear moduli for cold-formed steel panels which were used in many wood-frame diaphragms. The effective shear modulus was then adopted in their simplified model for predicting the behavior of steel-clad, wood-framed diaphragms (Keener and Manbeck, 1996b). Single major ribs and paired minor ribs were loaded separately in shear in order to accommodate the fastener pattern used in the model diaphragm. The length of the corrugations tested, which was the distance between cladding-purlin fasteners along the corrugation, varied from 304 mm to 1524 mm (1 foot to 5 feet). The shear modulus results were compared with the equation to calculate effective shear modulus developed by Davies and Bryan (1982). The shear modulus increased as the corrugation length increased to 609 mm (2 feet). Effective shear modulus decreased for lengths greater than 609 mm (2 feet). Keener and Manbeck also found that Davies and Bryan (1982) predicted well shear modulus for major rib lengths less than or equal to 609 mm (2 feet).

Relatively little literature exists for finite element modeling of SCWF diaphragms (Wright and Manbeck, 1993; Keener and Manbeck, 1996b; and Williams and Bohnhoff,

1998). In the Wright and Manbeck (1993) study, nonlinear finite element analysis of a steel-clad, wood-framed diaphragm was conducted with ABAQUS software. A four node shell element was used to model the cladding and a beam element was used to model framing members. Nonlinear springs were used to model the connections between framing members, panel and framing members, and panels. Connector tests were conducted to provide the required element properties for connection between framing members. Functional relationships for load-slip of steel panel connections and panel to framed member connections were adopted from Troxell (1989). Three panel tests were conducted in accordance with the ANSI/ASAE EP 558 standard to validate the finite element model. There was good agreement between model and laboratory results; however, a large number of degrees of freedom were required to model a relatively small section of corrugated diaphragm panels, and this result showed good agreement for only one specific SCWF diaphragm configuration.

Keener and Manbeck (1996b) used a simplified finite element model based on the research of Davies and Bryan (1982). Beam elements were used for framing members, nonlinear springs for connections, and equivalent truss elements for sheathing panels. Poor results were obtained since the connection and framing members were lumped. Only the initial portion of the load-displacement curve showed good agreement with experimental data, less accurate load-deflection results were obtained in the nonlinear region.

Williams and Bohnhoff (1998) proposed a more accurate finite element model to predict the static behavior of SCWF diaphragms. Beam elements were used for framing

members. The major differences between the Wright and Manbeck (1993) and Williams and Bohnhoff (1998) modeling approaches were the connection and sheathing elements. Williams and Bohnhoff used plane stress elements for sheathing with equivalent material properties for plane stress elements derived from corrugated steel panel and individual panel coupon testing. In-plane corrugated steel panel tests included shear, elongation parallel to corrugations, and elongation perpendicular to corrugations. Williams and Bohnhoff developed nonlinear spring element to model connection between steel cladding and wood frame elements. This element overcame overestimated connection strength and stiffness problem of non-oriented spring pair model assumed in the Wright and Manbeck (1993) model. Williams and Bohnhoff conducted a total of eighteen diaphragm tests under monotonic load following the ANSI/ASAE EP558 procedure to validate the finite element model. Load-displacement curves from experiment were observed and compared with those of the finite element model. The Williams and Bohnhoff model showed good agreement on monotonic behavior of steel-clad, wood-framed diaphragms; however, the method to obtain equivalent material properties for plane stress elements is complex and limited to one specific steel cladding geometry.

Recent efforts to develop a design shear strength and effective shear modulus table for SCWF shear walls and diaphragms was performed by Aguilera and Bender (2014). A mathematical model, typically referred as the Modified MCA procedure (Luttrell and Mattingly, 2004; Leflar, 2008) was used and the analysis results were compared with experimental tests (Bender, 2012). Good agreement was obtained with

regard to peak shear strength and effective shear modulus and while this model has good face validity with the low-rise metal building industry it only provides point estimates of ultimate shear strength and stiffness. It does not predict the entire load-displacement behavior that is needed for more sophisticated engineering analyses. However, the FEA model (Wright and Manbeck, 1993; Williams and Bohnhoff, 1998), and the FEA model herein predict the entire load displacement curve.

The technical literature on the behavior of SCWF shear walls and their connections under monotonic loading is lacking. A majority of data consists of monotonic performance of connections and diaphragms. Experimental data on monotonic performance of SCWF diaphragms can be found from Anderson (1987), Anderson and Bundy (1990) and more recently Bender (2012). There is a need to develop a finite element model to predict strength and effective shear modulus of SCWF shear walls.

TESTING OF SCWF SHEAR WALLS UNDER MONOTONIC LOADING

Materials and wall construction

Shear wall tests conducted by Bender (2012) were used to validate the model reported herein. SCWF shear walls were constructed using 0.343 mm thickness (29-gage), 0.55 GPa (80 ksi) yield strength steel cladding with profiled ribs. Fabral Grandrib 3 or Wick steel panels were attached to wood framing using structural screws [no. 10 x 25.4 mm (1 inch) on the field, no. 12 x 38.1 mm (1.5 inch) or no. 12 x 19.1 mm (3/4 inch) through steel lap joints]. All SCWF shear walls were 4877 mm (16 feet) wide by 3658 mm (12 feet) high with 2 bays spacing at 2438mm (8 feet). The 38 x 140 mm

(nominal 2 x 6 inch) pressure preservative treated (PPT) Hem-Fir No.2 and Douglas Fir-Larch Select Structural lumber were used to construct the base and top of the 3-ply nail-laminated posts. The 38 x 190 mm (nominal 2 x 8 inch) PPT Hem-Fir No.2, and 38 x 140 mm (nominal 2 x 6 inch) Douglas Fir-Larch Select Structural lumber were used for skirt board, and simulated truss chord at top of the wall respectively. Girts and blockings were 38 x 89 mm (nominal 2 x 4 inch) Spruce-Pine-Fir 1650Fb-1.5E lumber. The 88.9 x 4.1 mm (3-1/2x0.162 inch) ring shank nails were used to connect secondary members such as girts, skirt board, blocking, and simulated truss chord to posts. All secondary members were laid flat on the posts. General shear wall configuration and screw patterns are shown in Figure 2.2 and Figure 2.3, respectively. Table 2.1 shows details of girt spacing, cladding profile, field screw, and seam screw pattern for each shear wall. Details of materials and wall construction can be found in the technical report (Bender, 2012).

Test methods

SCWF shear wall tests were conducted in accordance with the ANSI/ASAE EP558 procedure using a cantilever configuration. The load-displacement on the top of wall was monitored during the tests. Deflection was measured at the four gage locations specified by ANSI/ASAE EP558 for the cantilever test. These deflection measurements were used to calculate the adjusted point load-deflection, which omits displacement resulting from rigid body rotation and translation. Additional testing details can be found in Bender (2012).

COMPARISON OF FEA APPROACHES

Static implicit FEA

Most SCWF diaphragms and shear walls have been tested under a quasi-static loading condition in which the inertia effect is insignificant. The load-deformation response of SCWF shear walls is highly nonlinear under monotonic loading (Bender, 2012), so the solution for a nonlinear system should be obtained incrementally. The equation of motion in the equilibrium state at the end of load increment at time $t + \Delta t$ can be represented as:

$$R_{t+\Delta t} - F_{t+\Delta t} = 0 \quad (2.1)$$

Where $R_{t+\Delta t}$ and $F_{t+\Delta t}$ are external and internal force vectors, respectively,

The response of SCWF shear walls is highly nonlinear, so the solution for (2.1) cannot be obtained like a linear static problem. Because $F_{t+\Delta t}$ depends on the history of nodal displacements, the finite element solution needs to be solved using an iterative process such as the Newton Raphson, modified Newton Raphson, or Newton methods. The algorithm for these methods is to search for equilibrium at each time step increment. Because of local instabilities, out-of-plane deformation of steel cladding or large deformation when the steel clad buckles, the solution fails to achieve to convergence within the tolerance required for accurate results, or a very small time increment is required. An attempt to analyze SCWF shear walls under monotonic loading required an increment time of less than 10^{-5} second (virtual time scale of static analysis is one second) and failed to obtain to convergence, especially with highly stitched SCWF shear walls. Note that stitch screws located at the steel panel overlaps

result in stiff shear walls with buckling being the primary failure mode. Because of the poor performance of the static implicit method, the dynamic implicit method was chosen for the analysis of SCWF shear walls under monotonic loading.

Dynamic implicit FEA

The dynamic implicit procedure can be used to solve a wide variety of nonlinear solid and structural mechanics problems. With proper control of energy dissipation and kinetic energy, this approach can be used for quasi-static problems to determine the final static response. Numerical energy dissipation can be introduced to improve convergence without degrading solution accuracy. Moreover, the main advantage of dynamic implicit FEA is the ability to continue when the cladding buckles, since equilibrium can be attained with internal and viscous forces. The equation of motion in the equilibrium state at the end of load increment at time $t + \Delta t$ can be expressed in the following form:

$$[M]\{\ddot{D}\}_{t+\Delta t} + [C]\{\dot{D}\}_{t+\Delta t} + [K]\{D\}_{t+\Delta t} = R_{t+\Delta t} \quad (2.2)$$

Where $[M]$ is mass matrix; $\{\ddot{D}\}$ is nodal acceleration vector; $\{C\}$ is viscous damping matrix; $\{\dot{D}\}$ is nodal velocity vector; $[K]$ is system stiffness matrix; and $\{D\}$ is nodal displacement vector; $R_{t+\Delta t}$ is external force vector

The solution of equation (2.2) can be solved using the backward Euler time integration operator. The details of the iterative nonlinear equation solver can be found in ABAQUS (2011). The algorithm for this method requires equilibrium to be solved at each time step increment. The dynamic implicit finite element method is based on a

dynamic formulation in which inertial forces resulting from acceleration and mass of a system play important roles. Therefore, applying dynamic implicit method to a quasi-static problem requires special consideration. The main goal is to simulate the analysis in the shortest period in which the kinetic energy, dissipation energy, and inertia forces remain insignificant. In most structural problems, a load duration corresponding to 10 times the largest natural period is recommended to obtain a quasi-static solution. Lower and upper boundaries of natural frequencies in seismic analysis of timber shear wall structures are 3 Hz and 30 Hz, which correspond to 0.33 second and 0.03 second periods (Cook 1989), so total time for the dynamic analysis of SCWF shear walls was chosen to be 45 seconds, which is greater than 10 times the largest mode period of timber shear walls.

MODEL DEVELOPMENT

The dynamic implicit method was chosen for the analysis of SCWF shear walls under monotonic loading. ABAQUS (2011) finite element software was used to develop the post-frame shear wall model since it contains a variety of element types suitable for modelling the steel clad sheathing, girt, posts, skirts, blockings and the screw connection.

Selection of elements

Steel cladding

A four-node shell element labeled "S4R" was selected to model the steel cladding. This element is a general-purpose 4-node double curve element with reduced integration which can significantly reduce running time compared to full integration "S4"

shell element, especially in three dimensional model herein. The element accounts for large membrane strains and arbitrarily finite rotations and it can be used to model both thick and thin shells. Each of the four nodes typically maintains six degrees of freedom which are three translations and three rotations, defined in the global coordinate system.

Posts, girts, skirts, trusses, and blockings

Two-node beam elements, called "B31" elements in ABAQUS, were used to model girts, truss, blockings, and posts. "B31" is a two-node linear interpolation beam element and each node has six degrees of freedom.

Screws and nails

ABAQUS contains an element named "CONN3D2" which can be used to model the fasteners. This element has six relative movements, namely, three relative displacements and three relative rotations in the element local coordinate system. Moreover, this element has the option to define the nonlinear springs, and dashpots in any or all of six degrees of freedom, making it a suitable element for fastener simulation.

Material properties

Steel cladding

The steel cladding was assumed to follow elastic behavior and was assigned the modulus and Poisson ratio of 200 GPa (2.9×10^7 psi) and 0.3 based on manufacturer's data (Fabral Grandrib 3 and Wick panel). The density of steel was assigned 7850 Kg/m^3 (0.284 lb/in^3).

Posts, girts, skirts, trusses, and blockings

Wood framing members were assumed to remain elastic throughout the analysis. The average elastic modulus and Poisson ratio for framing members are 10.34 GPa (1.5×10^6 psi) and 0.3, which were based on Tables 4A and 4D of the National Design Specification (NDS) supplement and the USDA Wood Handbook. The average density was specified as 450 Kg/m^3 (0.0163 lb/in^3).

Screws and nails

Nails were used to connect the wood framing members. Since functional relationships for load-slip characteristics of wood framing connectors were not available, load-slip characteristics were adopted from section 10.3.6 of NDS provision. The load-slip response of a single nail connection was assumed to be elastic behavior with load-slip modulus calculated from equation (2.3). Table 2.2 shows the load-slip moduli of connectors in wood framing members.

$$\gamma = \left(\frac{180,000}{5710}\right)\left(\frac{D}{25.4}\right)^{1.5} = 0.25 \times D^{1.5} \quad (2.3)$$

Where:

γ = load-slip modulus (kN/mm)

D = diameter of nail (mm)

Screws were used to connect steel cladding to wood framing members, and steel cladding to steel cladding (stitch screws). Screw connection data between steel panels was obtained from the Bender (2012) study and the steel-to-wood framing connections were tested at the Composite Materials & Engineering Center laboratory under

monotonic loading to determine force displacement properties for the finite element model. Dolan (1992) used five parameters to describe the load-displacement curve for a single nail connection under monotonic loading. He used an exponential curve with four parameters fit to data up to peak load, and linear regression to fit the data after peak load. Both curves were analyzed using the least square regression method. These parameters were then averaged for a set of nails to obtain the average load-displacement relationship for the finite element model. Although this method fit the data from the Dolan connection tests, it failed to predict the ultimate load for the screw connection tests used herein. Williams and Bohnhoff (2000) developed a linear piecewise regression program that included the specific gravity of wood in the equation to perform the load-displacement relationship in screw connection tests under monotonic loading. Good curve agreement was obtained up to peak load, but not the degradation portion after the peak load, so the linear piecewise regression program is not suitable to describe the load-displacement relationship of screws herein, especially after the peak load. The main failure modes of screw connections between wood and steel were crushing of wood, tearing of steel, or combination of wood crushing and steel tearing, which are different from the failure mode of nail connections in wood shear walls. A modified Dolan method that includes specific gravity in the equation (Eq. 2.4, and 2.5) was used to describe the behavior of screw connection between wood and steel. Detail of parameters used in Eq. 2.3, and 2.4 are shown in Figure 2.4. Specific gravity was not included in the equation to describe the behavior of steel panel connection. In order to capture the ultimate load in the connection test, one set of parameters was derived from all sets of the connection tests. Table 2.3 shows the

results for the monotonic connection tests for both Fabral Grandrib 3 and Wick panels. The load-slip curve of screws under monotonic tests can be found in more detail in appendix A.

$$F_{con} = SG(P_0 + K_2\Delta) \left\{ 1 - \exp\left(-\frac{K_0\Delta}{P_0}\right) \right\} \text{ for } \Delta \leq \Delta_{max} \quad (2.4)$$

$$F_{con} = SG \left[(P_0 + K_2\Delta_{max}) \left\{ 1 - \exp\left(-\frac{K_0\Delta_{max}}{P_0}\right) \right\} - K_3(\Delta - \Delta_{max}) \right] \text{ for } \Delta \geq \Delta_{max} \quad (2.5)$$

Where:

F_{con} = the connection force (kN)

SG = specific gravity

Δ = relative displacement (mm)

Δ_{max} = displacement corresponding to peak load (mm)

P_0 = intercept of asymptote with slope K_2 (kN/mm)

K_2 = stiffness at large displacement (kN/mm)

K_0 = initial stiffness (kN/mm)

K_3 = stiffness after post peak (kN/mm)

Boundary conditions

All of the nodes at the base of the posts were pinned and were only allowed to rotate on the axis perpendicular to plane of shear wall. The assumption of pinned boundary condition is reasonable because blocking was laid between posts to prevent

movement at the base of posts. Displacement control analysis rather than load control analysis was used because load control analysis will result in an unstable solution when the steel cladding buckles or applied load exceeds the load carrying capacity of shear wall. All of the top truss elements were subjected to the displacement at which the SCWF shear wall reached ultimate shear strength on the test.

RESULTS AND DISCUSSION

The predicted force-displacement results for two typical post-frame shear wall models are shown in Figures 2.5 and 2.6. The load-displacement of other SCWF shear walls can be found in appendix A. The load in the figure is the total shear load in the panel, and the displacement refers to the displacement at the top of the panel, where the load was applied. Ultimate shear strength, and the effective shear modulus from the finite element model and experiment were calculated using the ANSI/ASAE EP 558 procedure. Tables 2.4 and 2.5 show the results of ultimate shear strength and effective shear stiffness of post-frame shear walls. Based on the performance of the finite element model, the ultimate strength of the panels is predicted well. The predicted stiffness averaged 13% higher in the finite element model compared to experiment. The high variation in stiffness result is similar to the studies from Aguilera and Bender (2014) and Wright and Manbeck (1993). For the Wright and Manbeck (1993) study, the panel ultimate shear strength was predicted to within 3%; the panel shear stiffness was predicted to within 28%. For the Aguilera and Bender (2014) study, the ratio of predicted to tested design effective shear modulus averaged 0.81 with coefficient of variation of 39%. One reason for the higher shear stiffness could be that the decoupled orthogonal

spring element overestimates the strength and stiffness of the connection between wood-to-steel, and steel-to-steel.

SUMMARY AND CONCLUSIONS

The results show that predicted ultimate shear strength and effective shear modulus were in good agreement with test data. The ratios of predicted-to-test values for ultimate shear strength averaged 0.972, and the ratios for effective shear modulus averaged 1.134. The ratios of predicted-to-test values for effective shear modulus had larger differences relative to those of ultimate shear strength. However, the overall results are reasonable when one considers that the same average load-slip characteristics of screw connections were used in the entire model, the inherent variability in wood properties, and the lack of load-slip relationship for connectors used in wood frames. Moreover, it can be concluded that:

- Dynamic FEA is appropriate for predicting the structural behavior of SCWF shear walls, and improved accuracy may be obtained with improved load-slip characterizations of connectors used in the shear wall constructions.
- Failure modes due to tearing of the steel cladding at the fastener locations, buckling of the steel cladding, or combination of fastener tearing and steel buckling were accounted for nonlinear connection behavior, large-deflection analysis and geometric nonlinearity.

FUTURE RESEARCH

The dynamic implicit method is currently being used for further investigation into the behavior of SCWF shear walls and diaphragms under cyclic loading. Openings are

necessary in shear walls to provide doors and windows, but no modeling research and limited experimental tests have been conducted to examine the effect of openings shear wall and diaphragm behavior under monotonic and cyclic loading. The dynamic implicit method showed good agreement for both ultimate shear strength and effective shear modulus for shear walls with an aspect ratio of 4:3. The effect of aspect ratio is another area that needs to be examined further. Moreover, this method can provide the constitutive relationship for shear walls or diaphragms under monotonic or cyclic loading and this constitutive relationship can be used as a macro-element to model the entire post-frame building under dynamic loading.

REFERENCES

- ABAQUS. 2011. ABAQUS analysis user's manual. Version 6.11. Hibbitt, Karlsson, and Sorenson, Pawtucket, R.I.
- Aguilera, D. 2014. Development of strength and stiffness design values for steel-clad, wood-framed diaphragms. MS thesis. Department of Civil Engineering, Washington State University, Pullman, Wash.
- American Forest & Paper Association, Inc., National Design Specification (NDS) for Wood Construction, 2015 edition, Washington, DC.
- ASTM. 2007. ASTM D4442. Standard Test Methods for Direct Moisture Content Measurement of Wood and Wood-Base Materials. ASTM Standards, West Conshohocken, PA.
- ASTM. 2007. ASTM D2395. Standard Test Methods for Specific Gravity of Wood and Wood-Based Materials. ASTM Standards, West Conshohocken, PA.
- ASTM. 2008. ASTM F1575-03. Standard Test Method for Determining Bending Yield Moment of Nails. ASTM Standards, West Conshohocken, PA.
- ASAE. 2012. ANSI/ASAE Standard EP484.2. Diaphragm Design of Metal-Clad, Wood-Frame Rectangular Buildings. ASABE Standards, Engineering Practices, and Data. St. Joseph, MI.
- ASAE. 2004. ASAE EP 558. Load tests for metal clad, wood frame diaphragms. American Society of Agriculture Engineers, St Joseph, MI.

- Anderson, G.A., and Bundy, D.S. 1990. Stiffness of screw fastened, metal-clad, timber-framed roof diaphragms with opening in the sheeting. Transaction of the ASAE 33(1):266-273.
- Anderson, G. A., D. S. Bundy, and N. F. Meador. 1989. The force distribution method: Procedure and application to the analysis of buildings with diaphragm action. Transactions of the ASAE 32(5):1791-1796.
- Anderson, G.A., and Kelley, V.C. 1998. Lateral load strength of screw connections in 29ga metal. Fourteenth International Specialty Conference on Cold-Formed Steel Structures, St. Louis, Missouri U.S.A.
- Anderson, G.A., and Kelley, V.C. 1996a. Strength and stiffness of wood screws in metal to wood connections. International Wood Engineering Conference '96.
- Anderson, G.A., and Kelley, V.C. 1996b. Light-gage metal diaphragms on dimension lumber frames. International Wood Engineering Conference '96.
- Anderson, G.A. 1987. Evaluation of light-gage metal diaphragm behavior and diaphragms interaction with post-frames. Ph.D. dissertation, Iowa State University, Ames, Iowa.
- Bender, D.A. 2012. Development of design data for steel-clad, wood-framed shear walls. NFBA Shear Wall Project – CMEC technical report 12-004, Pullman, Washington.

- Bohnhoff, D. R. 1992. Expanding diaphragm analysis for post-frame buildings. *Applied Engineering in Agriculture* 35(4):509-517
- Boone, G.R. 1987. Predicting the elastic behavior of metal-clad timber-framed diaphragms with an analytical model. M.S. thesis, Pennsylvania State University, PA.
- Boone, G.R., and Manbeck H. B. 1989. Analytical modeling of metal-clad wood-framed diaphragms. *Transactions of the ASAE* 32(2):697-705.
- Cook, R. D., Malkus, D.S., Plesha, M.E., and Witt, R. J. 2002. *Concepts and applications of Finite Element Analysis*. John Wiley & Sons. Inc.
- Davies J., and Bryan E. 1982. *Manual of stressed skin diaphragm design*. John Wiley and Sons, Inc, New York.
- Dolan, J. D., and Madsen B. 1992. Monotonic and cyclic nail connection test. *Canadian Journal of Civil Engineering* 19(1): 97-104, 10.1139/l92-010
- Keener, J. D., and Manbeck, H. B. 1996a. Effective shear modulus trends for cold-formed steel panels *Transactions of the ASAE* VOL. 39(5): 1817-1824.
- Keener, J. D., and Manbeck, H. B. 1996b. A simplified model for predicting the behavior of metal-clad, wood-framed diaphragms *Transactions of the ASAE* VOL.39(3):1113-1122.

- Leflar, J.A. 2008. A mathematical model of steel-clad, wood-frame shear diaphragms. MS thesis. Fort Collins, Colorado: Colorado State University, Department of Civil and Environmental Engineering.
- Luttrell, L.D. and J.A. Mattingly. 2004. A Primer on Diaphragm Design. Metal Construction Association, Glenview, IL.
- NFBA. 1999. Post-frame building design manual. National Frame Builders Association Design Manual, Wisconsin, Madison.
- Troxell, D., Manbeck, H., and Blankenhorn, P. 1989. Shear response of fasteners in metal-clad timber-framed diaphragms. ASAE Paper No. 89-4506. St Joseph, MI.
- USDA Wood handbook - Wood as an engineering material. General Technical Report FPL-GTR-190. Madison, WI: U.S. Department of Agriculture, Forest Service, Forest Products Laboratory: 508 p. 2010
- Williams, G. D., and Bohnhoff, D. R. 1998. Modeling metal-clad, wood frame diaphragm behavior An ASAE Meeting Presentation, paper No. 974088.
- Williams, G. D. and Bohnhoff, D. R. 2000. Load-displacement characteristics of metal-clad wood framed diaphragm joints. An ASAE Meeting Presentation, Paper No. 004003, St. Joseph, MI.
- Wright, B. W., and Manbeck, H. B. 1993. Finite element analysis of wood-framed, metal-clad diaphragm panels. Transactions of the ASAE VOL. 36(3): 895-904- MAY-JUNE 1993.

FIGURES

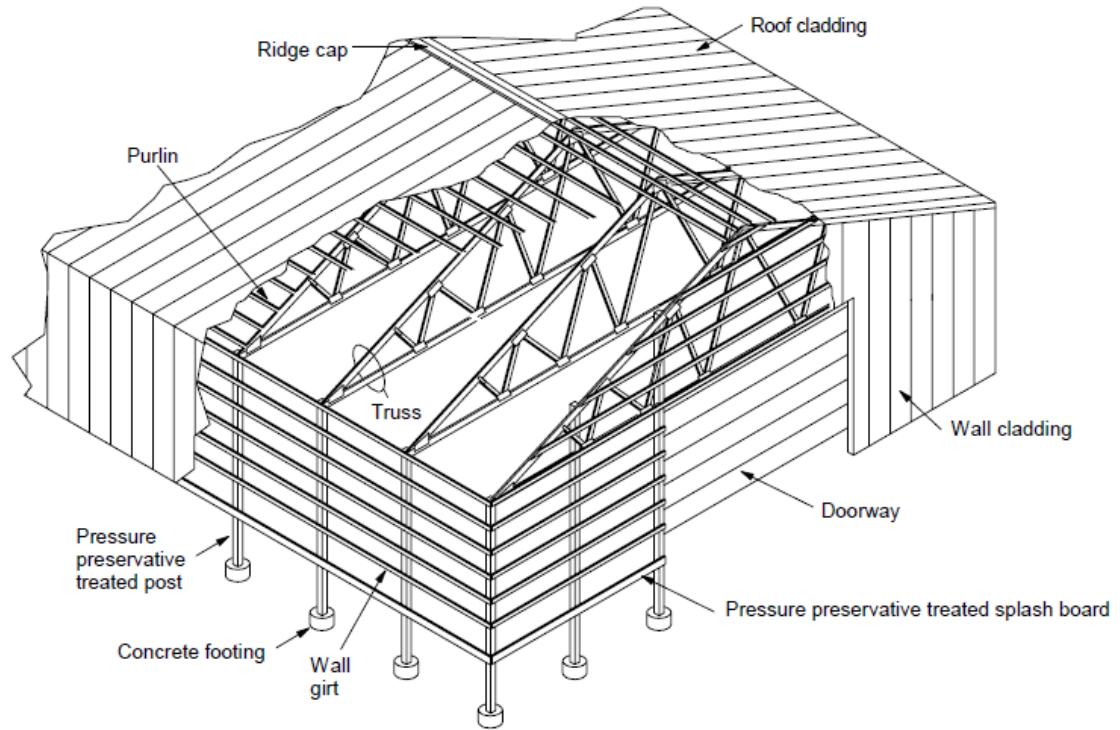


Figure 2.1: Simplified diagram of a post-frame building (National Frame Builders Association Design Manual, 1999)

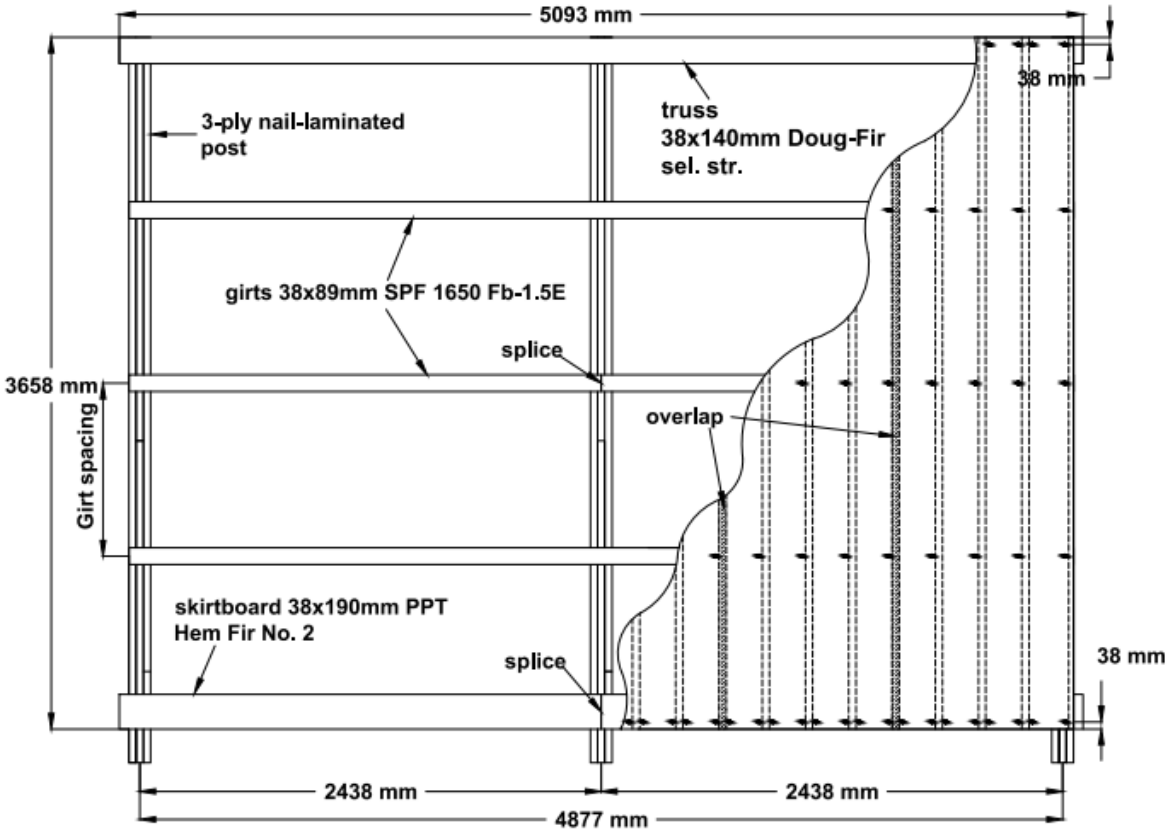


Figure 2.2 : General shear wall configuration (Bender, 2012)

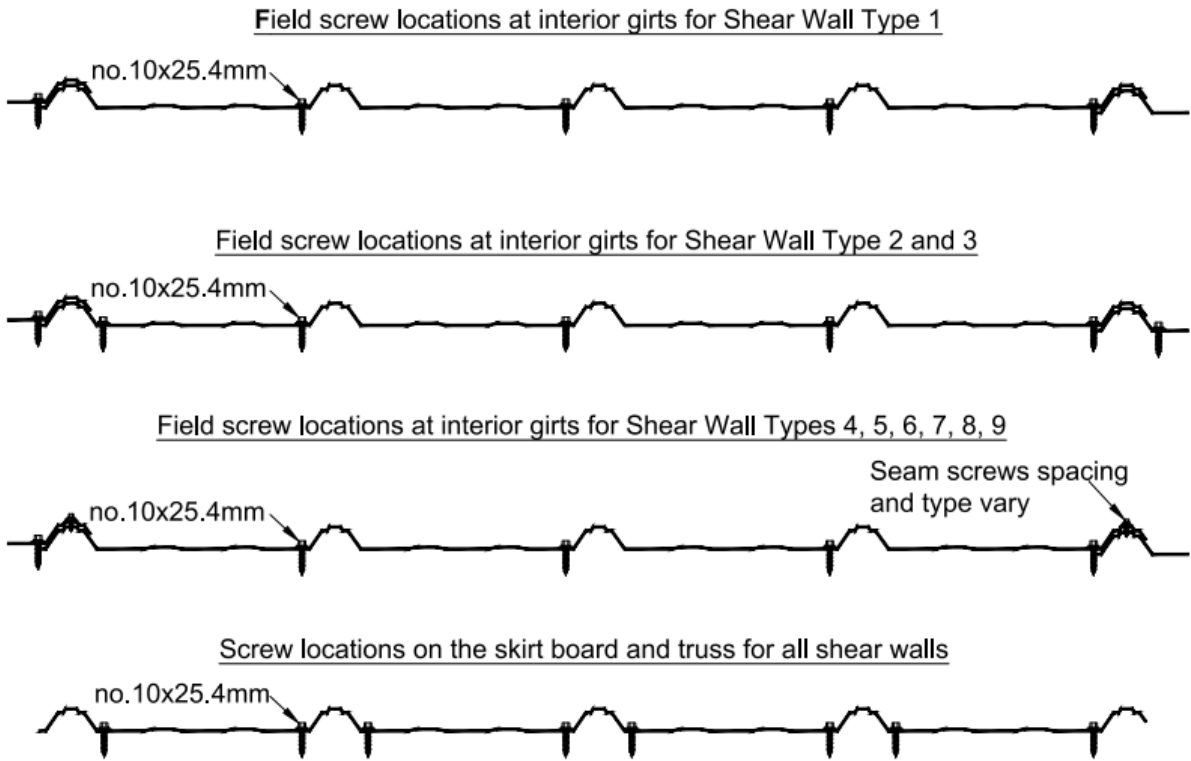


Figure 2.3: Shear wall screw patterns (Bender, 2012)

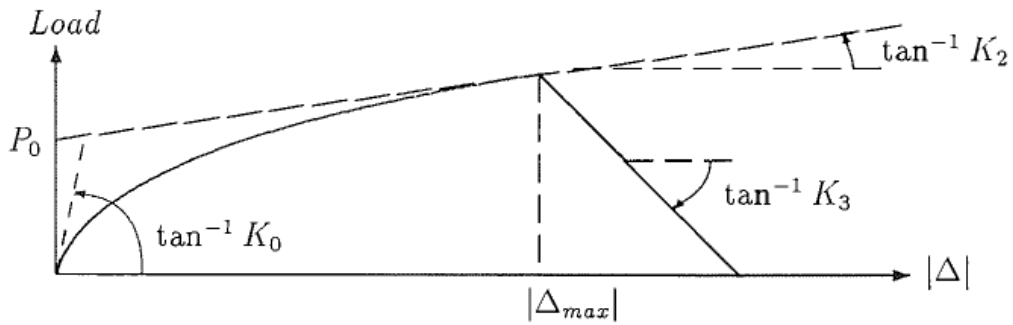


Figure 2.4: Connector load-displacement curve (Dolan, 1992)

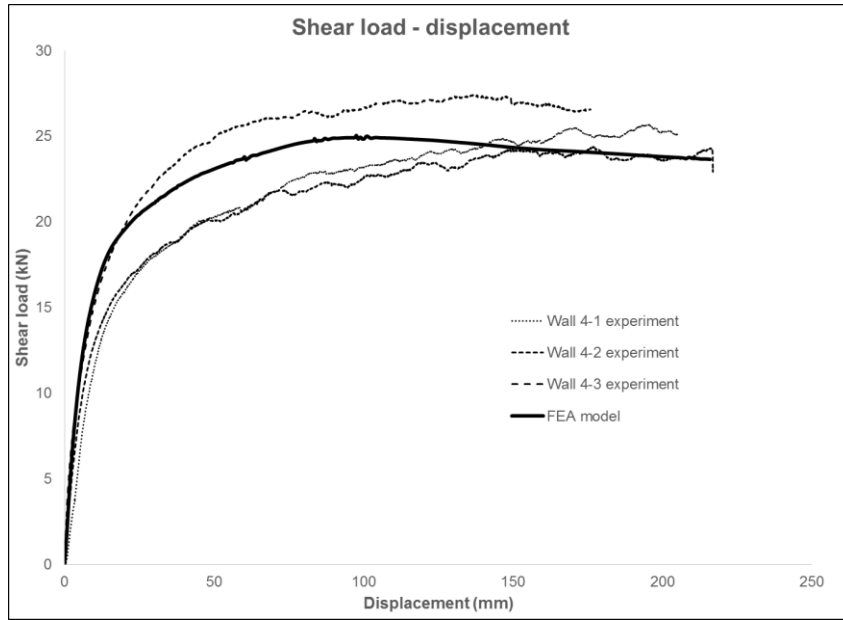


Figure 2.5: Shear load-displacement of wall type 4

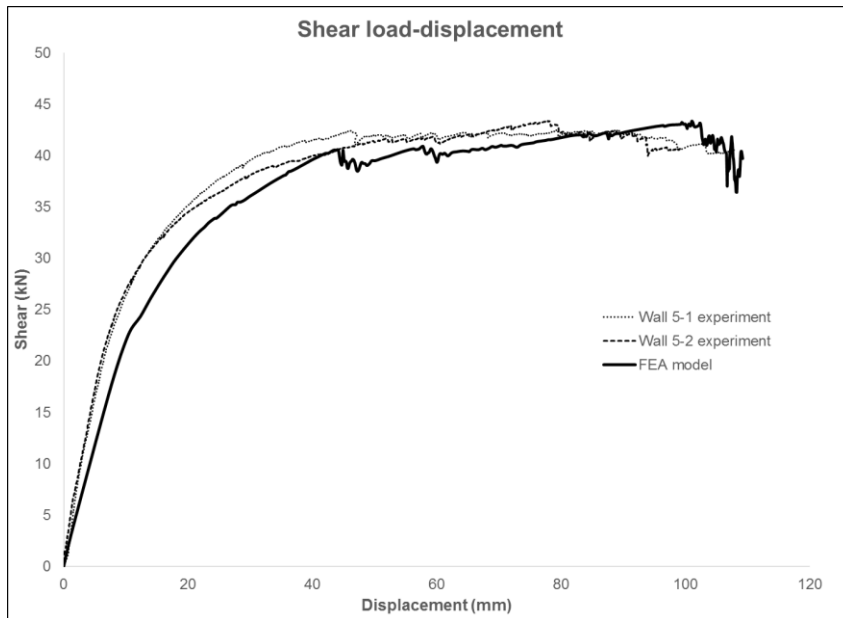


Figure 2.6: Shear load-displacement of wall type 5

TABLES

Table 2.1: Construction properties for each shear wall (Bender, 2012)

Shear Wall Type	Reps	Cladding Type	Girt Spacing (mm)	no.10x25.4 mm	no. 12x38.1	no.12x19.1
				structural fasteners adjacent to the overlap rib in flats	mm elevated sidelap structural fasteners	mm stitch fastener
1	1	Grandrib3	914	1 side	----	----
2	3	Grandrib3	914	Both sides	----	----
3	1	Grandrib3	610	Both sides	----	----
4	3	Grandrib3	610	1 side	609 mm off center	----
5	2	Grandrib3	610	1 side	----	203 mm off center
6	2	Grandrib3	610	1 side	----	609 mm off center
7	3	Grandrib3	914	1 side	----	457 mm off center
8	1	Wick	914	1 side	----	457 mm off center
9	1	Wick	610	1 side	----	203 mm off center

Table 2.2: Load-slip modulus of nail connection

Connector location	Load-slip modulus (KN/mm)
Truss to end post	12.33
Truss to center post	12.33
Skirt board to end post	12.33
Skirt board to center post	12.33
Girt to end post	6.17
Girt to center post	6.17
Girt to center post at splice	12.33
Blocking at end post	4.11

Table 2.3: Load-displacement parameters of screw connection

Connector type	Replication	SG	K_0	P_0	K_2	Δ_{max}	K_3
SPF to Grandrib 3	9	0.45	10.76	2.45	0.15	6.76	0.07
Grandrib 3 to Grandrib 3	10	-	4.66	1.03	0.13	6.12	0.05
SPF to Wick	9	0.45	11.06	2.2	0.20	7.16	0.05
Wick to Wick	8	-	4.84	2.18	-0.02	3.1	0.08

Table 2.4: Ultimate shear strength of SCWF shear walls from tests and FEA model

Ultimate shear strength			
Wall ID	Experimental (KN)	FEA model (KN)	Ratio: Predicted/Test
Wall 1-1	13.23	12.85	0.971
Wall 2-2	15.17	15.54	1.025
Wall 2-3	19.75	15.54	0.787
Wall 2-4	18.74	15.54	0.829
Wall 3-1	21.22	21.14	0.996
Wall 4-1	25.71	25.04	0.974
Wall 4-2	24.39	25.04	1.027
Wall 4-3	27.41	25.04	0.914
Wall 5-1	42.48	43.33	1.02
Wall 5-2	43.35	43.33	0.999
Wall 6-1	26.12	25.5	0.976
Wall 6-2	24.49	25.5	1.041
Wall 7-1	24.94	25.18	1.009
Wall 7-2	26.64	25.18	0.945
Wall 7-3	26.84	25.18	0.938
Wall 8-1	26.43	24.95	0.944
Wall 9-1	45.55	51.27	1.126
		Average =	0.972
		COV =	8.1%

Table 2.5: Effective shear modulus of SCWF shear wall from tests and FEA model

Effective shear modulus^a			
Wall ID	Experimental (KN/mm)	FEA model (KN/mm)	Ratio: Predicted/Test
Wall 1-1	0.53	0.79	1.5
Wall 2-2	0.77	1.03	1.341
Wall 2-3	1.16	1.03	0.894
Wall 2-4	0.98	1.03	1.054
Wall 3-1	0.79	1.38	1.756
Wall 4-1	0.96	1.7	1.764
Wall 4-2	1.24	1.7	1.366
Wall 4-3	1.54	1.7	1.102
Wall 5-1	2.43	1.73	0.712
Wall 5-2	2.57	1.73	0.673
Wall 6-1	1.31	1.65	1.253
Wall 6-2	1.33	1.65	1.237
Wall 7-1	2.33	1.66	0.714
Wall 7-2	1.86	1.66	0.896
Wall 7-3	1.54	1.66	1.08
Wall 8-1	2.54	2.01	0.793
Wall 9-1	2.05	2.33	1.137
		Average =	1.134
		COV =	30.0%

^a Effective shear stiffness is the secant modulus of load-displacement curve taken at the design level of ultimate divided by safety factor of 2.5 and multiple aspect ratio, as per ANSI/ASAE EP553

CHAPTER 3

DEVELOPMENT OF SEISMIC DESIGN COEFFICIENTS FOR STEEL-CLAD, WOOD-FRAMED SHEAR WALLS

ABSTRACT

This paper presents the lateral-loading test results of Steel-Clad, Wood-Framed (SCWF), and Oriented Strandboard, Wood-Framed (OSBWF) shear walls. A total of eighteen walls of ten different configurations were tested under reverse-cyclic loading to develop design shear strength, stiffness and seismic response coefficients of SCWF and OSBWF to resist lateral loads from seismic or wind events. Tested result shows that these walls exhibited high ductility and withstood large-in-plane displacements with minor load reduction, especially for the unstitched SCWF shear wall constructions. These walls also showed similar hysteresis behavior to light-frame wood shear wall construction. The seismic response coefficients for a number of SCWF shear walls with high ductility were judged to be equivalent to light-frame wood shear walls.

INTRODUCTION

Post-frame construction is becoming increasingly popular throughout the U.S. due to its advantages from the large clear span openings and the steel-clad, wood-framed structural envelope system. Key to the performance of post-frame construction is the diaphragm and shear wall actions to resist lateral loads from wind and earthquake. The code-recognized standard ANSI/ASCE 7-10 gives provisions for determining seismic loads and Table 12.2-1 lists seismic design coefficients and factors for a range of building types. Of particular interest for post-frame is Section B.23 for

Building Frame Seismic Force-Resisting Systems. This section of ASCE 7-10 is limited to cold-formed steel framing, sheathed with wood panels rated for shear resistance or steel panels - wood framing is not mentioned. Currently, seismic design coefficients are not provided in model building codes for the design of post-frame shear walls as a lateral force resisting system for seismic forces. Therefore, there is need to develop rational seismic design coefficients for steel-clad, wood-framed (SCWF) shear walls.

In 2004, the Federal Emergency Management Agency (FEMA) developed and documented a method for quantifying the building system seismic performance factors and response parameters used in seismic design (FEMA P-695). Seismic performance factors, including response modification factor (R), system overstrength factor (Ω_0), and deflection amplification factor (C_d), are used to estimate strength and deformation demands on seismic force-resisting systems that are designed using linear method of analysis but behave nonlinearly during an earthquake. The methodology for establishing seismic performance factors requires testing under pushover and cyclic loading of different configurations of a structural system and extensive computer analyses. The shape of the backbone curve on the hysteretic diagram and the strength at the maximum displacement for each configuration are factors in determining seismic performance factors for the system. The selection of configurations is important and will affect the outcomes. The configurations should represent all probable configurations of framing, construction details and material property variations. The nonlinear analysis techniques are performed after the development of configurations. Performance of structural systems is evaluated using Collapse Margin Ratio, which is the ratio between

the median collapse intensity and the intensity at maximum considered earthquake-level ground motions. The whole process is iteratively performed until the Collapse Margin Ratio is satisfied. The methodology in FEMA P-695 requires extensive physical testing and computer modeling, at a cost that can exceed \$500,000. Instead of using the costly and extensive FEMA P-695 approach, an alternate approach can be used to establish equivalency at the component level using FEMA P-795 procedure.

The Component Equivalency Methodology (FEMA P-795) evaluates the seismic performance equivalency of components such as connections, structural elements, or subassemblies experiencing inelastic response that controls the collapse performance of a seismic-force-resisting system. The FEMA P-795 is an adaption of the FEMA P-695, which is used to quantify collapse behavior and establish seismic performance factors for proposed components. A major difference between FEMA P-695 and FEMA P-795 is that the FEMA P-695 evaluates the level of collapse safety based on the response of the entire seismic-force resisting system. In contrast, Component Methodology evaluates the seismic performance equivalency of structural components that are substituted for reference components in seismic-force-resisting systems. Moreover, ICC Acceptance Criterion AC 322 was developed to establish seismic equivalency of proposed components with specific case of nailed wood shear walls in light-frame construction. The performance parameters in appendix A of AC 322 were developed from data set for nailed wood shear walls with aspect ratios ranging from 2:1 to 1:1, tested using the CUREE loading protocol. The possible replacement system can be used and share the same seismic design coefficients as light-frame (wood framed or

cold-form steel framed) wood bearing walls sheathed with wood structural panels or steel panels constructed in accordance with appendix A in the AC 322 document.

Simpson Strong-Tie demonstrated equivalency for Steel Strong Wall (SSW) component with light-frame wood shear wall (ICC-ES ESR-1679) using the Equivalency Method following the AC322 procedure. The SSW shear panel is prefabricated steel shear panel composed of wood studs, steel shear panels, steel top plate and steel base plate. The wood studs attached to SSW are normally 38 x 89 mm or 38 x 140 mm (2 x 4 or 2 x 6 nominal) sawn lumber with minimum specific gravity of 0.42. Steel shear panels are usually zinc-coated steel sheet with thickness of No.10 gage. Steel top plate and steel base plate are pre-attached to SSW to form a shear wall. The SSW is connected to a concrete foundation and installed in single- or multi-story buildings of light-framed wood construction. SSW is designed and constructed to resist gravity and to resist lateral loads from wind and earthquake. The design evaluations comply with 2009 International Building Code (2009 IBC), 2009 International Residential Code (2009 IRC) and based on the Acceptance Criteria for Prefabricated, Cold Formed, Steel Lateral Force Resisting Vertical Assemblies AC322. The performance of the SSW is associated with bearing wall that resist gravity loads and lateral loads from wind and earthquake. The steel shear panel is used in the wall instead of wood panel in wood shear walls that primary use in residential house construction. SSW panels are used as components within a seismic force-resisting system consisting of light frames with steel panels, provided seismic design coefficients and factors conform to recognized-code ASCE 7-10 Section 12.3.1. This was the method followed to develop the design values for Steel

Strong Wall (SSW) for a range of aspect ratios, wood framing, material properties, and wall heights.

Post-frame buildings are typically one-story, clear span buildings with shear walls providing resistance to lateral loading. As such, we contend that the component equivalency approach is sufficient. Therefore, this research evaluated the performance of SCWF and OSBWF shear walls tested under reverse-cyclic loading in accordance with ASTM E2126-11. The seismic design coefficients were also established to be equivalent to light-framed shear wall using FEMA P-795 methodology. The performance parameters of SCWF and OSBWF shear walls were compared with nailed wood shear walls using the criteria in appendix A of AC 322.

OBJECTIVES

This research was intended to provide insights on the behavior of Steel-Clad, Wood-Framed (SCWF) and Oriented Strandboard, Wood-Framed (OSBWF) shear walls under cyclic loading. The main goals of the research were:

- To characterize cyclic force-displacement relationships for commonly wood framed walls with steel and wood sheathed panels.
- To characterize the shear stiffness, shear strength, ductility ratio of post-frame shear walls subjected to reverse cyclic loading.
- To provide experimental analysis to support seismic design coefficients equivalent with all-wood shear walls, using the ICC AC322 approach.

LITERATURE REVIEW

Low-rise buildings in North America are typically built with shear walls and horizontal diaphragms to resist wind or seismic loads. ANSI/AWC SDPWS-2015 provides design shear strength and stiffness of wood shear walls to resist wind or seismic loads based on experimental data and modelling. Cyclic loading protocols have been developed (SEAOSC 1997, Krawinkler et al. 2000) for wood shear walls, and experimental research (He et al. 1998) has been performed to study the inelastic response and ductility of light-framed wood shear walls under these loading protocols. Effects of panel size (Lam et al. 1997), shear walls with openings (He et al. 1998), hold downs (Lebeda et al. 2005) have also been experimentally investigated. While extensive research has been done on the cyclic response of wood shear walls, there is no reported study on the cyclic performance of SCWF shear walls. More research is needed to improve our understanding of dynamic response of these walls, as well as provide seismic design codes.

Finite element models, along with experimental research, have been performed to predict behavior of wood shear walls. White and Dolan (1995) developed a finite element program to perform nonlinear analysis of timber shear walls subject to monotonic and dynamic loadings. Beam elements, plate elements, and nonlinear springs were used to model the framing, sheathing, and sheathing to framing connection, respectively. Judd and Fonseca (2005) developed an analytical model for sheathing to framing connection to model the hysteretic behavior of wood shear walls, in which oriented coupled spring pairs were used to model the nail connections.

Hysteretic and dynamic behavior of wood framed shear walls under lateral loads were further developed by Xu and Dolan (2009a, 2009b), Li et al. (2012) using the hysteretic behavior of nail connections. All research showed that nail connections governed ductility, energy dissipation, and fully contributed to global behavior of wood framed shear walls.

Limited research addressed the behavior of SCWF shear walls and diaphragms under monotonic loading. Only three publications were located that perform modeling of steel-clad, wood-framed diaphragms (Wright and Manbeck, 1993; Keener and Manbeck, 1996; and Williams and Bohnhoff, 1998). In these projects, a four node shell, plane stress or equivalent truss element was used to model the cladding and a beam element was used to model framing members. Nonlinear springs were used to model to connection between framing members, panel and framing members, and between panels. All research models showed good agreement on *monotonic* behavior of SCWF diaphragms; however, studies were limited to monotonic loading; no data for cyclic behavior was presented.

Technical literature on the behavior of SCWF diaphragms and their connections under reverse-cyclic loading is lacking. A majority of data consisted of monotonic performance of connections and diaphragms. Experimental data on monotonic performance of SCWF diaphragms can be found from Anderson (1987), Anderson and Bundy (1990) and Bender (2012). There is urgent need to study the seismic response of SCWF shear walls and diaphragms to understand load degradation, energy dissipation, and load-displacement hysteretic behavior.

METHOD AND MATERIALS

Material and wall constructions

Many of the shear wall constructions reported herein mirrored those from a previous study on monotonic loading of post-frame shear walls (Bender, 2012). Walls had materials and features that would allow for conservative substitution. For example, 3-ply 38 x 140 mm (2 x 6 nominal) columns with splice joints were used, so a denser species grouping such as Southern Pine, or a solid or glulam post could be conservatively substituted. Wall girts (S-P-F) and skirt boards (PPT incised Hem-fir) included splice joints at the center post. The strategy was to test as many different wall types as possible to learn the relative effects of construction details to dynamic behavior of shear walls under reversed cyclic loading. Details of wall construction can be found in more detail on Table 3.1 and Bender (2015) report.

Methods

Shear wall tests were conducted in accordance with ASTM E2126. Cyclic protocols require a reference displacement to characterize the displacement history. Since the monotonic tests of SCWF shear wall never reached $0.8P_{\text{peak}}$ (P_{peak} is ultimate load) from the Bender (2012) study, reference displacement was chosen of $2.5\%h_x = 91.44 \text{ mm}$ [(3.6 in), and (h_x is wall height)]. Each specimen was subjected to 52 cycles with displacement amplitudes that are based on percentage of reference displacement. Displacement rate was chosen of 15.24 mm/s (0.6 in/s) based on the provisions of ASTM E2126-11.

Wood specific gravity

Specific gravities were determined according to ASTM D2395-14, which involved cutting samples from each member after testing was complete, and implementing the oven-dry method to calculate specific gravity. Specific gravity was first computed using oven dry-dry mass and volume at equilibrium moisture content. Conversion formulas were then used to compute the specific gravity on a basis of oven-dry mass and oven-dry volume according to ASTM D2395.

Steel coupon tension and bending yield strength for nail

Steel samples from different panels were tested for yield strength and tensile strength. A total of fifteen specimens were tested from the Fabral Grandrib 3 panels. ASTM A370-12 was followed for the testing of sheet-type specimens.

Bending yield strength for Grip Rite smooth shank nails and Maze ring shank nails were determined in accordance with ASTM F1575-03. Five replicates were tested for each type of nail, and data for each replicate can be found in the electronic archive. All nails were loaded at a rate of 5.08 mm/min (0.2 in/min). The length between bearing points for Grip Rite nails and Maze nails was 38.1 mm (1.5 inches) and 43.2 mm (1.7 inches), respectively.

EXPERIMENTALLY DETERMINED PARAMETERS

Design values were computed in accordance with sections 9.1.1 through 9.1.5 of ASTM E2126. The ultimate load, P_{peak} , is the maximum load resisted by the wall in a given envelope curve. The ultimate shear strength is calculated by Equation 3.1.

$$v_{\text{peak}} = P_{\text{peak}}/L \quad (3.1)$$

The allowable design shear strength, v_a , is calculated by Equation 3.2.

$$v_a = 0.40 \cdot v_{\text{peak}} \quad (3.2)$$

Effective shear stiffness is calculated using Equation 3.3.

$$c = 0.40 \cdot P_{\text{peak}}/D_{T,d} \quad (3.3)$$

The effective shear modulus is computed by multiplying the effective shear stiffness by the aspect ratio as shown by Equation 3.4.

$$G' = c \cdot H/L \quad (3.4)$$

Ductility ratio is ratio of ultimate displacement and yield displacement as shown by Equation 3.5.

$$D = \Delta_u/\Delta_{\text{yield}} \quad (3.5)$$

Elastic shear stiffness is computed by dividing the $0.40 \cdot P_{\text{peak}}$ by the displacement at $0.40 \cdot P_{\text{peak}}$ as shown by Equation 3.6.

$$K_e = 0.40 \cdot P_{\text{peak}}/\Delta_e \quad (3.6)$$

Yield load is computed as shown by Equation 3.7.

$$P_{\text{yield}} = \left(\Delta_u - \sqrt{\Delta_u^2 - \frac{2 \cdot A}{K_e}} \right) \cdot K_e \quad (3.7)$$

Yield displacement is computed as shown by Equation 3.8.

$$\Delta_{yield} = P_{yield} / K_e \quad (3.8)$$

RESULTS AND DISCUSSION

Specific gravities for each type of framing member are summarized in Table 3.2. Table 3.3 shows tension strength and bending yield strength of nails and steel sheathing used in the experimental tests.

Wall failure modes

All walls tested typically exhibited the failure modes caused by crushing of wood, tearing of steel at connection between wood frame and steel sheathings. For the unstitched walls (wall type 1, and 2) and less stitched walls (wall type 4, 6, and 7), failure was dominated by tearing of the steel cladding at the fastener locations. Once the steel began tearing the individual panels began to rotate and slip with respect to each other. Rotation of the steel cladding caused some screws to partially pull-out and the screw head turned in the direction of panel displacement. When screws were rotated and pulled-out, steel panels were also pulled away from the wood frame. For these walls, there was minor or no buckling of the steel cladding.

For the walls that were heavily stitched (wall type 5), failure is due to buckling of the steel cladding coupled with the tearing of the steel cladding at the fastener locations. The individual panels rotated and slipped with respect to each other. Some screws were partially pulled out and turned in the direction of panel displacement.

For the walls with OSB panels (wall types 10 and 11), failure was due to fastener withdrawal and buckling of the OSB panel. Tearing of OSB, and steel cladding at the

connection location and nail pull-out were also observed. There was minor or no buckling of the steel cladding. The OSB was inset on the back side of the wall (interior side) and was recessed between the posts and nailed to the wall girts and blocking. As the tests progressed, the contact with the posts resisted OSB panel rotation, improving the performance as compared to just perimeter nailing as in all-wood shear walls.

Cyclic horizontal shear strength

Table 3.1 presents the values for seismic design shear strength and stiffness of SCWF shear walls. Allowable design unit shear was calculated by taking the ultimate test value divided by 4877 mm (16 ft.) wall length and a safety factor of 2.5. Shear modulus was calculated as the secant shear stiffness multiplied by the wall aspect ratio, as specified in Eq. 3.4. Table 3.4 shows the design shear strength, and effective shear modulus derived from cyclic tests herein and Bender (2012) monotonic test results. The cyclic unit design shear strength was lower than those of the monotonic tests (Bender 2012) for wall types 2, 4, 5, 6, and 7. The differences in unit design shear strength ranged from 4% (wall type 6, and 7) to 18% (wall type 2). The lower unit design shear strength in cyclic test is due to the damaging effects of the cyclic loading. The design shear stiffness in the cyclic test was higher than those of monotonic tests for wall type 2, 4, 5, 6, and 7. The percentage difference in effective shear stiffness ranged from 5% for wall type 2 to 72% for wall type 6. The difference in shear stiffness is due to the variation of lumber density, screws, and boundary conditions used in the experimental tests. However, the higher shear stiffness can provide the benefit to reduce the non-

structural components damage under large displacement caused by strong wind or earthquake loads.

The ANSI/AWC SDPWS-2015 provides the provision to determine design shear strength for shear walls with dissimilar materials on opposite sides. According to SDPWS-2015, the seismic design shear strength is the greater value of two times the smaller design shear strength or the larger design shear strength. Tested result shows that wall type 11 with rated OSB and steel panel (combination of wall type 10 on one side and wall type 4 on opposite side) has the highest design shear strength, which is 5% greater than the summation of design shear stiffness of wall type 10, and 4, so it is suitable for using to resist high wind. Wall type 14 provides the highest effective shear modulus and it can be used for low drift limit wall construction.

Hysteresis parameters

Figures 3.1 and 3.2 show the typical hysteresis, *equivalent energy elastic-plastic* (EEEP) behavior of post-framed shear walls under cyclic loading. The hysteresis, EEEP behavior of other shear wall types can be found in appendix B. All walls tested exhibited pinching behavior similar to that of light-framed wood shear walls, as shown in Figures 3.1 and 3.2. Pinching in SCWF shear walls results from crushing of wood, tearing of steel panel, and combination or crushing and tearing that cause the load capacity to decrease. Table 3.5 illustrates the typical changing hysteresis parameters on a cycle-by-cycle basis for SCWF shear walls. Hysteretic parameters of other shear walls can be found in more detail in appendix B. These parameters were calculated based on the primary cycle. Equivalent viscous damping is ratio of hysteresis energy to strain energy

per cycle per radian, and provides a measure of the dissipated energy of the cyclic loaded systems. Strain energy is representative of energy due to deformation of the system, while hysteresis energy is associated with the energy dissipated by the system for each cycle displacement. The hysteresis energy is due to the failure of material, and friction in the systems.

A high drop in cyclic stiffness was observed between the first and last primary cycle for all of the walls tested. The degradation in cyclic stiffness is similar to those found in light-framed wood shear walls. Although engineers tend to use the elastic stiffness for designing the drift limit in post-frame building, the cyclic stiffness degradation can provide useful information in performing the nonlinear analysis of SCWF systems following the provisions and methodology in the FEMA P-695 project.

Equivalent viscous damping ratio showed significant increase between the 1st and 11th primary cycle, and remained constant with fair variation until the end of most of the walls tested. SCWF shear walls exhibit high equivalent viscous damping, which is much close to those found in light-frame wood shear walls. High equivalent viscous damping ratio show good sign for SCWF shear walls, which can dissipate the energy under the earthquake.

Equivalency with light-framed shear wall using AC 322 criteria

The majority of the shear walls tested exhibited ductile behavior with high ductility ratios as shown in Table 3.1. These walls also withstood large in-plane displacement with minor load degradation, especially with the unstitched wall configurations (wall type 1 and 2). Moreover, the envelopes of the hysteresis loops are close to monotonic curve

(Bender, 2012) up until to the point that the shear walls reach their ultimate shear strengths. However, the strength degradation of the hysteresis loops is more severe than the monotonic curves due to the cumulative damage of cyclic loading such as screws being ejected as the holes in the steel enlarged. Design shear strength, and shear stiffness are shown in Table 3.1. These design values are close to those of shear walls tested under monotonic load (Bender, 2012) because there is not much difference between the envelope of hysteresis loops and monotonic curves up until to ultimate strength point.

The results of the AC 322 equivalency criteria are shown in Table 3.6. The majority of the shear walls tested demonstrated ductile behavior, resulting in easily passing the AC322 equivalency criteria. Shear wall type 6, 7, 10 and 14 failed the AC322 criteria regarding the displacement at 80% post-peak load as shown in Table 3.6. The primary reason was that the stitch screws that improved the initial stiffness and strength of the walls, were soon ejected after reaching peak load as the holes around the stitch screws enlarged and the panels buckled during cyclic loading. As soon as the stitch screws were ejected, the shear capacity quickly diminished as shown in Figure 3.2. With wall type 10, the OSB panels were inset between the posts (on the opposite side from the steel). The posts helped restrain panel rotation, causing the post-frame OSB shear walls to have approximately 12% higher capacity than conventional light-frame OSB shear walls. As the ultimate capacities were reached, the OSB panels buckled causing nail withdrawal and rapid reduction in the shear capacity. Hence, the displacement at 80% post-peak load did not meet the AC322 criterion. Finally, in wall

type 11, steel panels were used on one side of the wall with OSB on the other. The steel added sufficient ductility to the wall to pass the AC322 criteria, and the capacities of OSB sheathed walls and steel sheathed walls proved to be additive (actually the combined OSB/steel wall was 5% higher than the sum of wall type 10 and 6). The combined OSB/steel wall system appears to be an excellent choice when high seismic or wind forces must be resisted.

DESIGN RECOMMENDATIONS

This study provides a better understanding of how these walls respond to cyclic loading such as that cause by earthquakes. Based on our research, the recommendations for designing SCWF shear walls follow the guidelines below:

1. Proposed seismic design values for common post-framed shear walls in Table 3.1 could be used in designs to resist wind.
2. The unstitched constructions (wall type 1, and 2) had the greatest ductility values and easily passed all the three AC 322 criteria. These wall systems can be an excellent choice when light seismic or wind loads must be resisted.
3. The seismic design coefficients for those walls that passed all the AC 322 criteria can be considered equivalent to wood light-framed shear walls (response modification coefficient $R = 6.5$, overstrength factor $\Omega_0 = 3$, and deflection amplification factor $C_d = 4$).
4. The strength degradations of stitched wall configurations failed the AC 322 criteria (wall type 6, 7, and 14) are greater than those of unstitched wall

configurations (wall type 1, and 2) due to the ejection of stitched screws during the cyclic loading. Therefore, these wall configurations are not recommended to use in high seismic region.

5. The stitched wall constructions displayed behavior similar to those of unstitched constructions after the stitched screw ejected. Therefore, the seismic design coefficients (response modification coefficient $R = 6.5$, overstrength factor $\Omega_0 = 3$, and deflection amplification factor $C_d = 4$) can be used for those walls that fail the AC 322 criteria. However, these wall configurations are recommended to use only in low seismic region.
6. For the combine OSB/steel wall system in which steel panels were used on one side of the wall with OSB on the other, the steel added sufficient ductility to the wall, and the capacities of OSB sheathed walls and steel sheathed walls proved to be additive (actually the combined OSB/steel wall was 5% higher in design shear strength than the sum of wall type 10 and 6). Therefore this wall system appears to be an excellent choice when high seismic or wind forces must be resisted.

SUMMARY AND CONCLUSIONS

Tests on eighteen walls of ten different configurations were conducted under reverse-cyclic loading to develop design strength, stiffness and seismic design coefficients of SCWF and OSBWF shear walls. The test results show that SCWF and OSBWF shear walls have high ductility, as well as the ability to meet design requirements by current design timber code, especially for the unstitched SCWF shear

wall constructions. Moreover, similar load degradations caused by crushing of wood or tearing of wood panels in light-frame shear walls also occurs in SCWF shear walls, due to hysteresis pinching at the connections between wood frames and steel sheathing panels.

The comparative study with light-framed wood shear walls was performed using the ACC 322 criteria. The seismic design coefficients (response modification coefficient $R = 6.5$, overstrength factor $\Omega_0 = 3$, and deflection amplification factor $C_d = 4$) can be used for walls with high ductility (wall 1, 2, 4, 5, 11, and 13). Walls failed the ACC 322 criteria (6, 7, and 14) are recommended to use in low seismic region. However, the results in this research is limited to typical SCWF shear wall segments. The nonlinear analysis of SCWF systems following the provisions and methodology in the FEMA P-695 project [Applied Technology Council (ATC), 2007] should be investigated further to determine the seismic response factor.

Furthermore, openings are necessary in shear walls to provide doors and windows, but no research or limited experimental test has been conducted to examine the effect of openings to response of shear walls and diaphragm under monotonic and cyclic loading. The effect of aspect ratio is another area that needs to be examined further.

ACKNOWLEDGEMENTS

This research was supported by the National Frame Building Association. Donation of fasteners from SFS intec Inc. and Maze Nails are gratefully acknowledged.

NOTATION

v_{peak} = ultimate shear strength (N/mm)

v_a = allowable design shear strength (N/mm)

P_{peak} = ultimate load (KN) as shown in Figure 3.3

$D_{T,d}$ = adjusted point-load deflection, D_T , at $0.40 \cdot P_{peak}$ (mm)

c = effective shear stiffness (N/mm)

H = height of shear wall [3658 mm (12 feet) for all walls]

L = length of shear wall [4877 mm (16 feet) for all walls]

Δ_u = ultimate displacement corresponding to post peak load ($0.80 \cdot P_{peak}$)

Δ_{yield} = yield displacement as shown in Figure 3.3

Δ_e = displacement at $0.40 \cdot P_{peak}$

K_e = elastic shear stiffness (N/mm)

A = area under envelope curve from zero to ultimate displacement (Δ_u) of wall (lb.in)

ζ = equivalent viscous damping ratio

REFERENCES

- American Forest & Paper Association, Inc., Wind & Seismic, Special Design Provisions for Wind and Seismic, 2015 edition, Washington, DC.
- ASCE. 2010. Minimum design loads for buildings and other structures. ASCE/SEI 7-10, ASCE, Reston, Va.
- ASTM. 2012. Standard Test Methods and Definitions for Mechanical Testing of Steel Products. ASTM A370, ASTM International, West Conshohocken, PA.
- ASTM. 2007. Standard Test Methods for Specific Gravity of Wood and Wood-Based Materials. ASTM D2395-07a, ASTM International, West Conshohocken, PA.
- ASTM. 2008. Standard Test Method for Determining Bending Yield Moment of Nails. ASTM F1575, ASTM International, West Conshohocken, PA.
- ASTM. 2011. Standard test methods for cyclic reversed load test for shear resistance of walls for buildings. ASTM E2126-11, ASTM, West Conshohocken, Pa.
- Anderson, G.A. 1987. Evaluation of light-gage metal diaphragm behavior and diaphragms interaction with post-frames. Ph.D. dissertation, Iowa State University, Ames, Iowa.
- Anderson, G.A., and Bundy, D.S. 1990. Stiffness of screw fastened, metal-clad, timber-framed roof diaphragms with opening in the sheeting. Transaction of the ASAE 33(1):266-273.

Bender, D.A. 2012. Development of design data for steel-clad, wood-framed shear walls. NFBA Shear Wall Project – CMEC technical report 12-004, Pullman, Washington.

Bender, D.A. 2015. Development of seismic design data and seismic response factor for steel-clad, wood-framed shear walls. NFBA Shear Wall Project – CMEC technical report, Pullman, Washington.

Federal Emergency Management Agency. 2011. Quantification of Building Seismic Performance Factors: Component Equivalency Methodology. FEMA P-795, Washington D.C.

Federal Emergency Management Agency .2009. Quantification of Building Seismic Performance Factors. FEMA P-695, Washington D.C.

He, M., Lam, F., and Prion, H. G. L. 1998. Influence of cyclic test protocols on performance of wood-based shear walls. Can. J. Civ. Engrg., Ottawa, 25(3), 539–550.

ICC Evaluation Service, Inc. 2009. Acceptance criteria for prefabricated, cold-formed steel lateral-force-resisting vertical assemblies. AC322, Birmingham, Ala., <http://www.icc-es.org> (2009).

ICC-ES Evaluation Report (ICC). 2011. ESR -1679: Steel Strong Wall SSW Shear Panels and S/SSW shear panels. Simpson Strong Tie Company, Inc., Pleasanton, California.

- International Code Council. 2009. International building code. Whittier, CA.
- International Code Council. 2009. International residential code. Whittier, CA.
- Judd, J. and Fonseca, F. 2005. Analytical Model for Sheathing-to-Framing Connections in Wood Shear Walls and Diaphragms. *J. Struct. Eng.*, 131(2), 345–352.
- Keener, J. D., and Manbeck, H. B. 1996. A simplified model for predicting the behavior of metal-clad, wood-framed diaphragms. *Transactions of the ASAE VOL.39(3):1113-1122.*
- Krawinkler, H., Parisi, F., Ibarra, L., Ayoub, A., and Medina, R. 2000. Development of a testing protocol for wood frame structures. CUREe Publ. No. W-02, Consortium of Universities for Research in Earthquake Engineering, Richmond, Calif.
- Lam, F., Prion, H. G. L., and He, M. 1997. Lateral resistance of wood shear walls with large sheathing panels. *J. Struct. Eng., ASCE*, 123(12), 1666–1673.
- Lebeda, D., Gupta, R., Rosowsky, D., and Dolan, J. 2005. Effect of Hold-Down Misplacement on Strength and Stiffness of Wood Shear Walls. *Pract. Period. Struct. Des. Constr.*, 10(2), 79–87.
- Li, M., Foschi, R., and Lam, F. 2012. Modeling Hysteretic Behavior of Wood Shear Walls with a Protocol-Independent Nail Connection Algorithm. *J. Struct. Eng.*, 138(1), 99–108.
- Structural Engineers Association of California SEAOC. 1999. Recommended lateral force requirements and commentary, 7th Ed., Sacramento, Calif.

- White, M. and Dolan, J. 1995. Nonlinear Shear-Wall Analysis. *J. Struct. Eng.*, 121(11), 1629–1635.
- Williams, G. D., and Bohnhoff, D. R. 1998. Modeling metal-clad, wood frame diaphragm behavior. An ASAE Meeting Presentation, paper No. 974088.
- Wright, B. W., and Manbeck, H. B. 1993. Finite element analysis of wood-framed, metal-clad diaphragm panels. *Transactions of the ASAE VOL. 36(3): 895-904- MAY-JUNE 1993.*
- Xu, J. and Dolan, J. 2009a. Development of Nailed Wood Joint Element in ABAQUS. *J. Struct. Eng.*, 135(8), 968–976.
- Xu, J. and Dolan, J. 2009b. Development of a Wood-Frame Shear Wall Model in ABAQUS. *J. Struct. Eng.*, 135(8), 977–984.

FIGURES

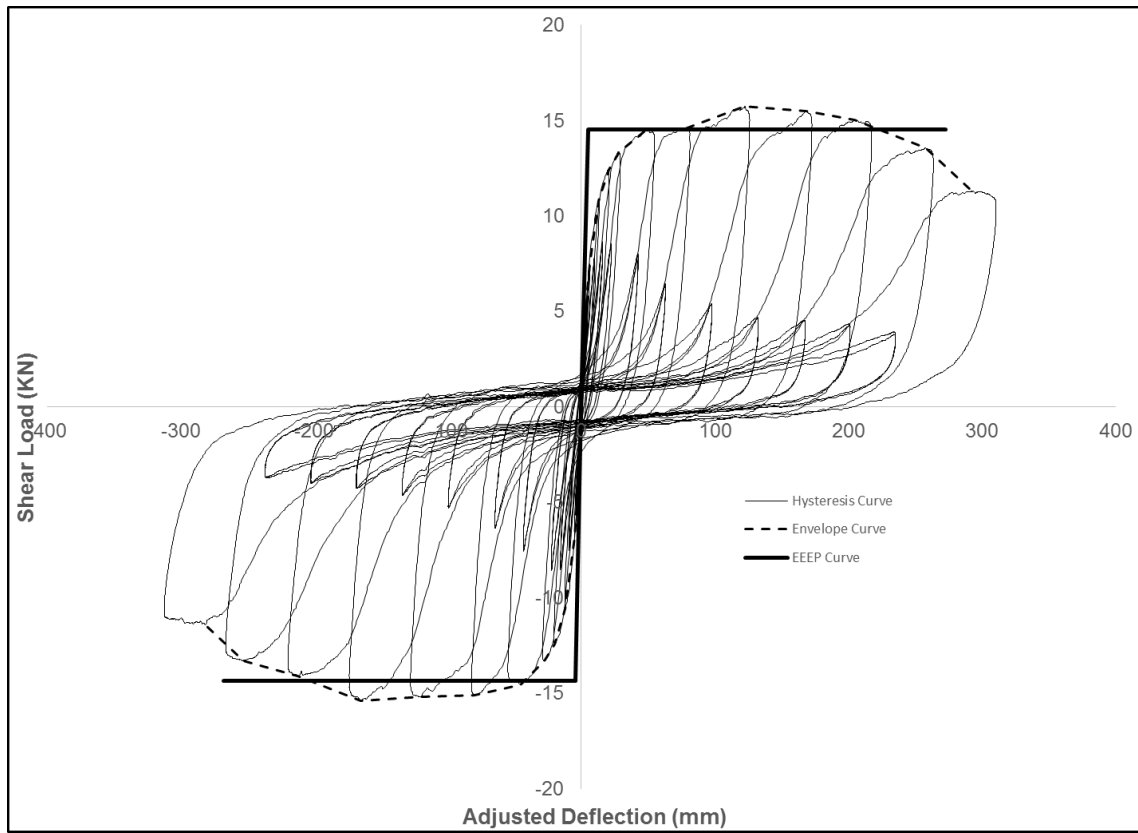


Figure 3.1 : Hysteresis, Envelope and EEEP curves of wall 2-1

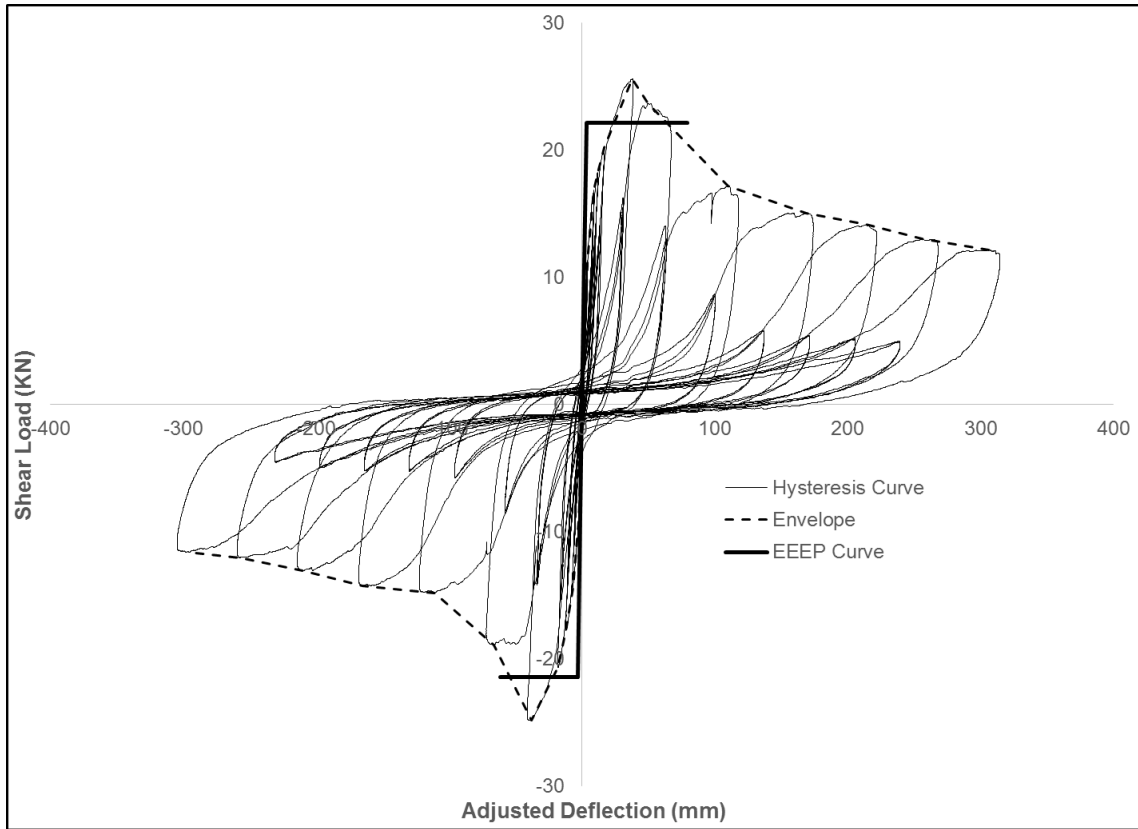


Figure 3.2: Hysteresis, Envelope and EEEP curves of wall 7-2

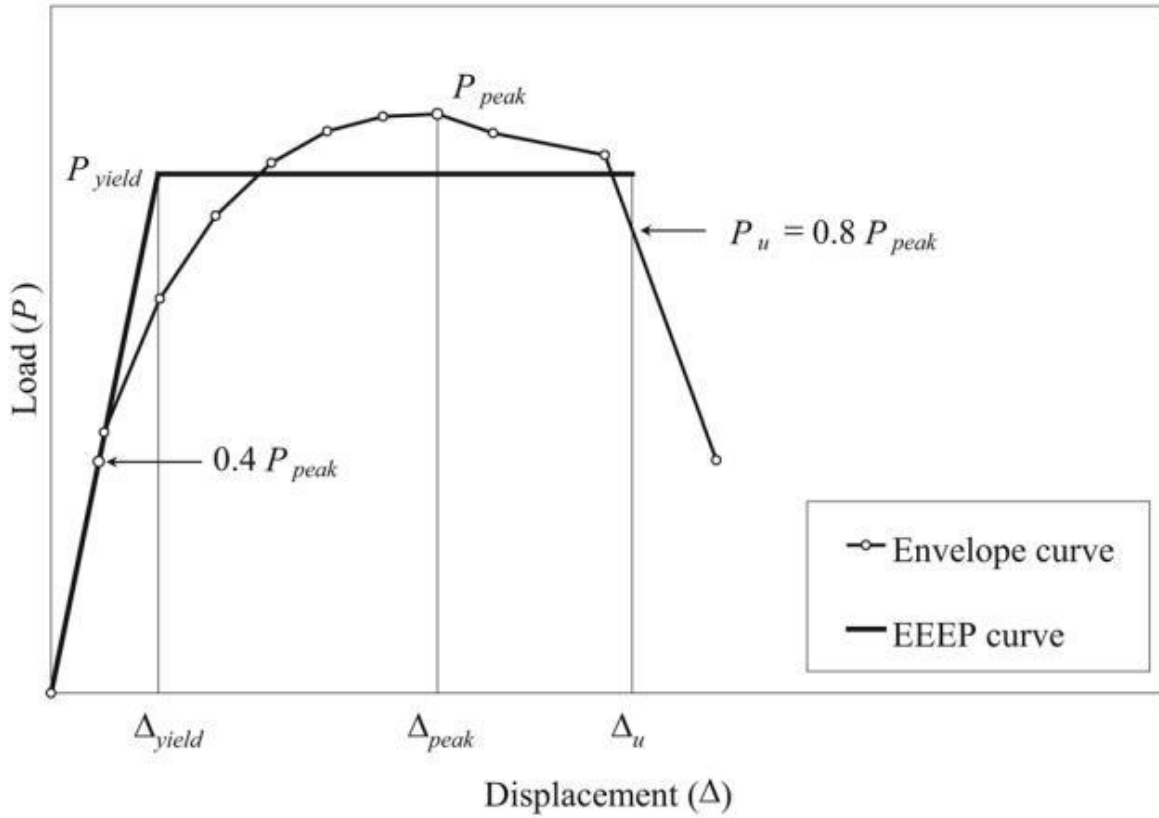


Figure 3.3: Performance Parameters of Specimen (ASTM E2126)

TABLES

Table 3.1: Seismic design values and ductility ratio

Shear Wall ID	Description	Average Statistics		
		allowable design unit shear, v (N/mm)**	shear modulus, G (N/mm)**	Ductility ratio (D)
1	914 mm girt, no.10x25.4 mm screws in field. no.10x25.4 mm structural screws on the left side at lap joints, 229 mm off center major rib panel	1.17	770.56	18.6
2	914 mm girt, no.10x25.4 mm screws throughout, screws on both sides of major rib, 229 mm off center major rib panel	1.24	1015.74	21.7
4	610 mm girt, no.10x25.4 mm screws in field, no.12x38.1 mm structural screw through overlap rib at girts, 229 mm off center major rib panel	1.97	2119.03	23.1
5	610 mm girt, no.10x25.4 mm screws in field, no.12x19.1 mm stitch at 203 mm off center and blocking with 203 mm off center no.10x25.4 mm, 229 mm off center major rib panel	3.5	2679.44	10
6	610 mm girt, no.10x25.4 mm screws in field, no.12x19.1 mm stitch through overlap rib at girts, 229 mm off center major rib panel	1.97	2294.16	14.4
7	914 mm girt, no.10x25.4 mm screws in field, no.12x19.1 mm stitch at 457 mm off center and blocking with 457 mm off center no.10x25.4 mm, 229 mm off center major rib panel	2.04	2189.09	9.7
10	11.1 mm (7/16) Rated OSB sheathing inset between posts on interior wall side. 44.5x3.1 mm coil nails spaced at 152 mm on panel edges and 305 mm field (panels will be fully blocked)	4.38	1961.42	5.4
11	11.1 mm (7/16) Rated OSB sheathing on interior side, and Wall Type 4 on exterior side	6.64	2994.67	7.3
13	Similar to wall type 7 but using 38.1 mm stitch screw at girt, and 19.1 mm stitch screw between girts	2.19	2399.24	26.8
14	Similar to wall type 5, except using 38.1 mm stitch at girts, and 19.1 mm between girts	3.65	3992.89	13.4

** Average value was calculated from average envelope curve. Allowable unit shear rounded to nearest 0.88N/mm (5 lb/ft), and shear modulus reported at 2 significant digits (similar rounding rules as in AWC SDPWS-2015)

Table 3.2: Wood Member Specific Gravity at Oven-Dry Volume

Member	Species	Size (mm)	Grade	Average	COV**
Skirt board	Hem Fir (PPT)	38x191	No. 2	0.52	0.13
Laminates at top of post	Douglas Fir-Larch	38x140	Select Structural	0.47	0.1
Girts	Spruce Pine Fir	38x89	1650 Fb-1.5E	0.44	0.09
Truss	Douglas Fir-Larch	38x140, 38x191	Select Structural	0.54	0.15
OSB				0.58	0.05
Blocking between posts under the truss	Douglas Fir-Larch	38x140	No. 2	-	-
Blocking between girts	Spruce Pine Fir	38x89	1650 Fb-1.5E	-	-

** Coefficient of Variation

Table 3.3: Tension strength and bending yield strength of nails and steel sheathing

Member	Diameter or thickness (mm)	Tensile strength (Gpa)	Bending yield strength (GPa)
Grip Rite Nail (bright coated)	3.264	-	0.85
Grip Rite Nail (exterior galvanized)	3.289	-	0.88
Maze Nails (Ring shank)	3.772	-	1.33
Maze Nails (Ring shank stormguard hot-dipped)	3.772	-	1.33
Collated Roofing Nails	2.982	-	0.7
Fabral Grandrib 3	0.356	0.77	-

Table 3.4: Seismic design values and monotonic design values (Bender, 2012)

Shear Wall ID	Average Statistics Cyclic tests		Average Statistics Monotonic tests (Bender, 2012)	
	allowable design	shear modulus, G (N/mm)**	allowable design	shear modulus, G (N/mm)**
	unit shear, v (N/mm)**		unit shear, v (N/mm)**	
1	1.17	771	1.09	525
2	1.24	1016	1.46	963
4	1.97	2119	2.12	1243
5	3.5	2679	3.5	2452
6	1.97	2294	2.04	1331
7	2.04	2189	2.12	1926

** Average value was calculated from average envelope curve. Allowable unit shear rounded to nearest 0.88N/mm (5 lb/ft), and shear modulus reported at 2 significant digits (similar rounding rules as in AWC SDPWS-2015)

Table 3.5: Average hysteresis parameters of wall type 2

Primary Cycle Number	Δ at F_{max} (mm)	F_{max} (kN)	Δ at F_{min} (mm)	F_{min} (kN)	Strain Energy (kN mm)	Hysteresis Energy (kN mm)	ζ	Cyclic stiffness (kN/mm)
1	2.74	4.245	-2.356	-4.001	10.6	2.517	0.038	1.644
3	4.131	5.915	-3.721	-5.418	22.361	7.593	0.054	1.454
5	5.604	7.214	-5.204	-6.476	37.141	16.038	0.069	1.271
7	12.119	10.431	-11.586	-9.667	119.679	90.142	0.12	0.848
9	19.218	12.107	-18.901	-11.546	226.076	192.24	0.136	0.621
11	26.838	13.031	-26.486	-12.578	342.207	291.612	0.136	0.481
13	49.115	14.807	-47.003	-14.318	700.11	906.349	0.207	0.304
15	77.029	15.226	-75.658	-14.821	1147.139	1207.082	0.168	0.198
17	119.955	16.08	-117.155	-14.489	1814.122	1926.301	0.169	0.129
19	158.255	15.165	-161.195	-13.902	2325.196	2125.307	0.146	0.092
21	205.582	13.428	-211.433	-12.084	2658.165	2108.642	0.127	0.062
23	255.039	11.9	-250.289	-11.127	2915.27	2129.998	0.117	0.046
25	299.317	10.047	-284.658	-10.315	2965.421	2149.904	0.116	0.035

Table 3.6: AC 322 criteria for seismic equivalency with wood shear wall

Shear Wall ID	reps	ICC AC322 Criteria			Equivalent to light-frame wood shear walls
		$2.5 \leq V_p/V_{asd} \leq 5.0$	$\Delta_{0.8V_p}/\Delta_{V_{asd}} \geq 11$	$\Delta_{0.8V_p} \geq 2.8\%h_x$	
1	1	PASS	PASS	PASS	YES
2	2	PASS	PASS	PASS	YES
4	2	PASS	PASS	PASS	YES
5	2	PASS	PASS	PASS	YES
6	2	PASS	PASS	FAIL (99.6<102.4)	NO
7	2	PASS	PASS	FAIL (70.1<102.4)	NO
10	2	PASS	PASS	FAIL (93.0<102.4)	NO
11	3*	PASS	PASS	PASS	YES
13	1	PASS	PASS	PASS	YES
14	1	PASS	PASS	FAIL (101.6<102.4)	NO

* Two reps were checked with AC 322 criteria since one wall failed prematurely at the load strut.

V_p : peak strength capacity

V_{asd} : allowable design capacity = $V_p/2.5$

$\Delta_{0.8V_p}$: displacement at 0.8 V_p

$\Delta_{V_{asd}}$: displacement at V_{asd}

h_x : height of wall = 3658 mm (144 in)

CHAPTER 4

PREDICTING BEHAVIOR OF STEEL-CLAD, WOOD-FRAMED SHEAR WALLS UNDER CYCLIC LATERAL LOADING

ABSTRACT

This paper presents the finite element (FEA) model results of Steel-Clad, Wood-Framed (SCWF) shear walls under cyclic lateral loading. The shear wall model consists of beam elements to model framing members, equivalent orthotropic plane stress elements to model corrugated steel cladding, linear spring elements to model nail connectors between framing members, and nonlinear hysteresis spring elements to model screw connectors. Screw connectors attaching steel panels to wood framing, and steel to steel panels at lap joints were tested under cyclic loading to provide the constitutive relationships for the model. A modified Bouc-Wen-Barber-Noori (BWBN) model was developed to capture the slack, pinching, and strength and stiffness degradation of screw connectors under cyclic loading. The material properties of equivalent orthotropic plane stress elements were determined from FEA models and properties of the material of the corrugated steel sheathing. The finite element models were validated by comparing them with experimental test results of six different SCWF shear wall configurations. The predicted shear strength was higher than that from experimental tests, especially for stitched shear walls. However, the FEA models can capture well the pinching, strength, and stiffness degradation of SCWF shear walls. These model results demonstrate the utility of the FEA model for SCWF shear walls.

INTRODUCTION

Low-rise buildings in North America are typically built with shear walls and horizontal diaphragms to resist wind or seismic loads. ANSI/AWC SDPWS-2015 (2015) provides design shear strength and stiffness properties of wood shear walls in resisting wind or seismic loads based on experimental data. The design values for shear and stiffness of wood shear walls were derived from monotonic tests in accordance with ASTM E 564 or from Dolan (1999). Since the design values were derived from monotonic tests, they do not represent the actual behavior of seismic or cyclic loading. Therefore, cyclic loading protocols have been developed (SEAOSC 1997, Krawinkler et al. 2000) to characterize the cyclic behavior of wood shear walls and provide conservative design values for strength and stiffness.

Experimental research (Gatto and Uang, 2003; He et al. 1998) was performed to study the effect of loading protocols on the inelastic response and ductility of light-framed wood shear walls. The effect of panel size (Lam et al. 1997), shear walls with openings (He et al. 1999), hold downs (Lebeda et al. 2005), and fluid dampers (Du, 2003; Symans et al. 2002) were also experimentally investigated. While extensive research has been performed to study the cyclic response of wood shear walls, nothing has been reported regarding the cyclic performance of SCWF shear walls. Research is needed to improve understanding of the dynamic response of these walls, as well as to provide seismic design values for SCWF shear walls.

Finite element models, along with experimental research, have been performed to predict the behavior of wood shear walls. White and Dolan (1995) developed a finite

element program to perform nonlinear analysis of timber shear walls subjected to monotonic and dynamic loads. Beam elements, plate elements, and nonlinear springs were used to model the framing, sheathing, and sheathing to framing connections, respectively. Judd and Fonseca (2005) developed an analytical model for sheathing to framing connections to model the hysteretic behavior of wood shear walls, in which oriented coupled spring pairs were used to model the nail connections. Hysteretic and dynamic behavior of wood framed shear walls under lateral loads were further developed by Xu and Dolan (2009a, 2009b), and Li et al. (2012) using the hysteretic behavior of nail connections. All research showed that nail connections governed ductility, energy dissipation, and fully contributed to the global behavior of wood framed shear walls.

Limited research has addressed the behavior of SCWF shear walls and diaphragms under monotonic loading, and nothing on cyclic loading. Only a few studies have been published that focus on modeling of steel-clad, wood-framed diaphragms (Wright and Manbeck, 1993; Keener and Manbeck, 1996; and Williams and Bohnhoff, 1998). In these investigations, four node shell, plane stress, or equivalent truss elements were used to model the cladding, and beam elements were used to model framing members. Nonlinear springs were used to model the connection between framing members, panel and framing members, and between panels. All research models showed good agreement with monotonic behavior of SCWF diaphragms. However, these studies were limited to monotonic loading; no data for cyclic behavior was presented.

Technical literature on the behavior of SCWF diaphragms and their connections under simulated seismic loading is lacking. A majority of the data has consisted of monotonic performance of connections and diaphragms. Experimental data on monotonic performance of SCWF diaphragms can be found from Anderson (1987), Anderson and Bundy (1990), and more recently Bender (2012). Therefore, this paper addresses the lack of data on the seismic response of SCWF shear walls and diaphragms, and provides insight on their load degradation, energy dissipation, and load-displacement hysteretic behavior.

DEVELOPMENT OF HYSTERESIS MODEL FOR SCREW CONNECTOR

Overview of Heine's hysteresis model

Heine (2001) developed a generic hysteresis model derived from the Bouc, Wen, Baber, and Noori (Baber and Noori 1986) model for a bolt connection under reverse-cyclic loading. The model is capable of representing the softening hysteresis as a function of dissipation energy, and pinching as a function of slack growth based on displacement rather than energy dissipation. The hysteresis model is a mass-normalized equation of motion [Eq. (4.1)] for a single-degree-of-freedom system consisting of a linear spring, a nonlinear hysteresis spring, and a viscous damper connected in parallel to a mass.

$$\ddot{u}(t) + 2 \times \xi_0 \times \omega \times \dot{u}(t) + \alpha \times \omega^2 \times u(t) \times \left(1.0 - e^{\left(\frac{-(z(t))^2}{(\psi_0 + \delta \psi \times |\Delta(t)|)^2} \right)} \right) + (1 - \alpha) \times \omega^2 \times z(t) = f(t) \quad (4.1)$$

where u = total displacement of the mass; ξ_0 = the viscous damping ratio of the linear system; ω = pseudo-natural frequency of the nonlinear system; α = the rigidity ratio; z = the hysteresis displacement; ψ_0 = a parameter controlling the initial slack; δ_ψ = the slack growth parameter; and Δ = the global maximum or minimum displacement. Hysteresis displacement, which was modified by Heine (2001), is expressed with the following differential equation form:

$$\dot{z}(t) = \left(1.0 - e^{\left(\frac{-(z(t))^2}{(\psi_0 + \delta_\psi \times |\Delta(t)|)^2} \right)} \right) \times \left(\frac{\dot{u}(t) - v \times (\beta \times |\dot{u}(t)| \times |z(t)|^{n-1} \times z(t) + \gamma \times \dot{u}(t) \times |z(t)|^n)}{\eta} \right) \quad (4.2)$$

where β , γ , and n determine the shape of hysteresis curve. The combination of β and γ determine whether the curve is hardening or softening. The hysteresis of a connection in wood structures is usually weak softening. Therefore, the following constraints are the most suitable:

$$\begin{aligned} \beta + \gamma &> 0 \\ \gamma - \beta &< 0 \end{aligned} \quad (4.3)$$

In the BWBN model, the degradation is represented in terms of dissipated energy. The dissipation energy is the continuous integral of hysteresis force, F_h , over the total displacement, u , as given in the following equation:

$$\begin{aligned} \varepsilon(t) = \int_{u(0)}^{u(T)} F_h du &= (1 - \alpha) \times \omega^2 \times \int_{u(0)}^{u(T)} z(u, t) \times du \times \frac{dt}{dt} = (1 - \alpha) \times \omega^2 \times \\ &\int_0^T z(u, t) \times \dot{u}(t) \times dt \end{aligned} \quad (4.4)$$

The strength and stiffness degradation are represented by the parameters ν and η , and they are linearly related to dissipation energy, as giving in the following equation:

$$\begin{aligned} \nu(\varepsilon) &= 1 + \delta_\nu \times \varepsilon(t) \\ \eta(\varepsilon) &= 1 + \delta_\eta \times \varepsilon(t) \end{aligned} \quad (4.5)$$

where δ_ν and δ_η are the strength and stiffness degradation rates, respectively.

Heine (2001) modified the pinching function and incorporated the two parameters that control the initial slack and slack growth into the system. Fig. 4.1 shows the hysteretic behavior of a bolted joint in single shear beyond the elastic limit. The hole gets larger as the displacement increases. Slack and pinching occur in the bolt connection as the hole in the connection gets larger (Heine, 2001). Heine used the following function to describe the pinching in the system:

$$h(z) = 1.0 - \zeta \times e^{\left(\frac{-(z(t))^2}{(\psi_0 + \delta_\psi \times |\Delta(t)|)^2} \right)} \quad (4.6)$$

where ζ = the parameter that controls the level of pinching.

The inclusion of slack in the Heine model allows it to modify both the nonlinear hysteresis element and the linear element since the connector element comes in contact with the wood member when the lateral displacement is larger than slack in the movement direction. Therefore, the linear element force, F_k in Heine's model, was modified to include the slack in the system.

$$F_k = \alpha \times \omega^2 \times u(t) \times \left(1.0 - e^{\left(\frac{-(z(t))^2}{(\psi_0 + \delta\psi \times |\Delta(t)|)^2} \right)} \right) \quad (4.7)$$

BWBN model development

Unlike a bolt connection, in which the slack is available in the system immediately due to oversized holes and slot formation, slack in a screw connection only occurs when the wood crushes or the steel tears. Therefore, the Heine model requires modification to model the strength and stiffness of a screw connection under small displacement when the screw is in contact with wood or steel. A parameter that determines the rate of pinching (p) was added to the pinching function to overcome this limitation. The rate of pinching parameter controls the level of pinching of a screw connection under cyclic loading. There is only minor pinching in a screw connection when the displacement is small. The level of pinching increases as the displacement gets larger. The pinching function was modified from equation (4.7) to the following:

$$h(z) = 1.0 - \zeta \times (1 - e^{-p \times |\Delta(t)|}) \times e^{\left(\frac{-(z(t))^2}{(\psi_0 + \delta\psi \times |\Delta(t)|)^2} \right)} \quad (4.8)$$

The linear restoring force was also modified to the following:

$$F_k = \alpha \times \omega^2 \times u(t) \times \left(1.0 - (1.0 - e^{-p \times |\Delta(t)|}) \times e^{\left(\frac{-(z(t))^2}{(\psi_0 + \delta\psi \times |\Delta(t)|)^2} \right)} \right) \quad (4.9)$$

Model solution

The equation of motion in the state of vector form is represented as follows:

$$y = \begin{cases} y_1(t) \\ y_2(t) \\ y_3(t) \end{cases} = \begin{cases} u(t) \\ z(t) \\ \varepsilon(t) \end{cases} \quad (4.10)$$

The model has a set of ordinary differential equations (ODE), as given in equation 4.11:

$$\dot{y}_1 = V \quad (4.11a)$$

$$\dot{y}_2 = \left(1.0 - \zeta \times (1 - e^{-p \times |\Delta(t)|}) \times e^{\left(\frac{-(z(t))^2}{(\psi_0 + \delta \psi \times |\Delta(t)|)^2} \right)} \right) \times$$

$$\left(\frac{\dot{u}(t) - v \times (\beta \times |\dot{u}(t)| \times |z(t)|^{n-1} \times z(t) + \gamma \times \dot{u}(t) \times |z(t)|^n)}{\eta} \right) \quad (4.11b)$$

$$\dot{y}_3 = (1 - \alpha) \times \omega^2 \times y_2 \times V \quad (4.11c)$$

where $V = \dot{u}(t)$ is the time derivative of the input displacement loading protocol.

Most screw connection tests are quasi-static and displacement controlled. These tests were performed at a slow rate, in which the force contribution from the mass ($m\ddot{u}(t)$) is not significant. Therefore, the restoring force on the system is reduced to the following:

$$F = \alpha \times \omega^2 \times u(t) \times \left(1.0 - e^{\left(\frac{-(z(t))^2}{(\psi_0 + \delta \psi \times |\Delta(t)|)^2} \right)} \right) + (1 - \alpha) \times \omega^2 \times z(t) + 2 \times \xi_0 \times \omega \times \dot{u}(t) \quad (4.12)$$

All of the derivatives in the BWBN model are first-order and variables vary with time at highly different rates. Hence, the BWBN model consists of a stiff set of linear ordinary differential equations (ODE). The solution is obtained using the Livermore Solver for Ordinary Differential Equations (LSODE) (Radhakrishnan and Hindmarsh 1993). In this model, the time and corresponding displacement are input at the discrete data points. Integrating the ODE solver over the time step yields the solution vector. The restoring force is obtained from Equation 4.12.

System identification

The modified BWBN model contains 12 parameters, which includes strength and stiffness degradation parameters δ_v and δ_η , hysteresis shape parameters β , γ , n , and α , pinching parameters ζ , ψ_0 , δ_ψ , and p , the pseudo-natural frequency ω , and the viscous damping ratio ξ_0 .

A problem in which the output response of a given input is known, but the values of the parameters are unknown, is referred to as a system identification problem. The goal of the method is to obtain the set of hysteresis parameters by minimizing the error between the computed force and the experimentally measured force. In this model, the objective function that needs to be minimized is the sum square error between the experimental values of force and those of the BWBN model for all given displacements. The objective function is:

$$E = \sum_{i=1}^M \{F_{EXP_i} - F_{BWBN_i}(\delta_v, \delta_\eta, \beta, \gamma, n, \alpha, \zeta, \psi_0, \delta_\psi, p, \omega, \xi_0)\}^2 \quad (4.13)$$

Where F_{EXP_i} = experimental force at the i_{th} measurement point; F_{BWBNI} = the computed force at the displacement corresponding to the i_{th} measurement point; and M = the total number of data points.

A genetic algorithm (GA) was selected for the optimization problem because it is capable of solving a wide range of problems in which the objective function is non-differentiable, stochastic, highly nonlinear, or discontinuous. GA is based on a natural selection process that mimics biological evolution. Heine (2001) developed a highly efficient and robust GA written in FORTRAN for a multi-bolt model. The model was modified and used for estimating the BWBN hysteresis parameters for screw connections. Details of the GA model can be found in Heine (2001).

Screw connector tests and validation of BWBN model

Screw connection tests were performed to provide the material constitutive relationships for the FEA model. Screw tests include connections of steel cladding to wood, steel cladding to steel cladding (i.e. a stitch connection at the ridge of the cladding profile), and metal cladding to metal cladding in which the screw penetrated the wood behind the steel panel. Fabral Grandrib 3 steel cladding at 29 gage and SPF lumber were used for all of the connection tests. No. 10x25.4 mm, no 12x38.1 mm, and no. 12x19.1 mm screws were used to connect wood framing members to steel panels, steel panels to steel panels at elevated sidelaps, and steel panels to steel panels, respectively. The connection tests were conducted in accordance with ASTM E2126-11 specifications.

All of the experimental results were smoothed using the locally weighted scatterplot smooth (LOWESS, MATLAB 2015) model to remove the data noise. An initial guess of the parameter set was made and the GA program was run for each experimental test result.

Validation of the BWBN model is shown in Fig. 4.2, and 4.3. The figure also illustrates that the BWBN model agrees well with the experimental tests for all types of screw connections that are used in SCWF shear walls. Tables 4.1, 4.2, and 4.3 show the parameter estimation results for SPF wood to steel cladding, steel panel to steel panel, and steel panel to steel panel at elevated sidelaps. Observation from the experiments showed that the shear strength and stiffness for the connection test decrease to zero when the displacement reaches beyond the limit, d_{fail} , which is the point at which the connector fails due to tearing of the steel sheathing, crushing of the wood, or a combination of crushing and tearing. The parameters from the BWBN model are highly dependent, so averaging the parameters for a series of specimens is not suitable. Therefore, screw connections were randomized throughout the simulated walls. A total of six typical no. 10x 25.1 mm screws, eight typical no. 12x19.1 mm screws, and six typical no. 12x38.1 mm screws were used and uniformly randomized throughout the simulated walls. A C++ program (Visual Studio 2012 Integrated Development Environment) was used to randomize the screws for each wall configuration.

FINITE ELEMENT MODEL DEVELOPMENT

The dynamic implicit method was chosen for the analysis of SCWF shear walls under cyclic loading. ABAQUS (2011) finite element software was used to develop the post-frame shear wall model since it contains a number of element types suitable for modelling the steel cladding, girt, posts, skirts, blockings, and screw connections.

Selection of elements

Steel Cladding

A four-node membrane element labeled "M3D4R" was selected as an orthotropic plane stress element to represent the steel cladding. It is a general-purpose, 4-node, double curve element with reduced integration. This type of element is used to represent thin surfaces in space that have in-plane stiffness, but no bending stiffness.

Posts, girts, skirt, truss and blockings

A two-node beam element, called "B31" in ABAQUS, was used to model girts, truss, blockings, and posts. It is a two-node, linear interpolation beam element and each node has six degrees of freedom.

Nails

ABAQUS contains an element named "CONN3D2" which can be used to model the fasteners. This element has six relative movements, namely three relative displacements and three relative rotations in the element local coordinate system. Moreover, this element has the option to define nonlinear springs and dashpots in any or all of the six degrees of freedom, making it a suitable element for fastener simulation.

Screws

ABAQUS allows the user to develop elements which are not included in ABAQUS element library. A user defined element, which is call UEL, was implemented to simulate the screw connections (program in Visual Studio 2012 Integrated Development Environment), and it works similarly to existing elements in ABAQUS. The oriented spring pair model, developed by Judd (2005) and used for wood shear wall simulation by Xu and Dolan (2009), was used in this UEL element. This spring element is oriented using the initial deformation trajectory of the connection. K_u is the tangent stiffness of the nonlinear spring in the trajectory direction and K_v is the tangent stiffness in the orthogonal direction, which is perpendicular to the trajectory direction. Tearing through the steel edge is the dominant failure mode of SCWF shear walls under reversed-cyclic loading (Bender, 2015). This tearing restricts the movement of the screw in the narrow direction. Therefore, this model represents the actual behavior of a screw connection and it relieves the problem experienced with uncoupled springs (Dolan 1989, Judd 2005).

Material properties

Steel Cladding

There are three main material constants that represent the behavior of corrugated panels under in-plane loading. These are the effective shear modulus (G), the modulus of elasticity perpendicular to panel corrugations (E_{11}), and the modulus of elasticity parallel to panel corrugations (E_{22}). The modulus of elasticity parallel to panel corrugations was determined from the properties of the material. The modulus of

elasticity perpendicular to panel corrugations and the effective shear modulus were determined from finite element models. The method to determine the material properties for equivalent plane stress elements can be found in Williams (1997). Table 4.4 shows the material properties of equivalent plane stress elements that were used in the FEA model. The density of steel was assigned as 7.85×10^{-8} kN/mm³.

Posts, girts, skirt, truss and blockings

Wood framing members were assumed to remain elastic throughout the analysis. The average elastic modulus and Poisson ratio for framing members were taken as 10.34 kN/mm² and 0.3, respectively, which were based on Tables 4A and 4D of the National Design Specification (NDS) supplement and the USDA Wood Handbook. The average density was specified as 6×10^{-9} kN/mm³.

Nails

Nails were used to connect the wood framing members. Since functional relationships for load-slip characteristics of wood framing connectors were not available, load-slip properties were adopted from section 10.3.6 of the NDS provision. The load-slip response of a single nail connection was assumed to be elastic behavior with the load-slip modulus calculated from equation (4.14). Table 4.5 shows the load-slip modulus of connectors in wood framing members.

$$\gamma = \left(\frac{180,000}{5710}\right)\left(\frac{D}{25.4}\right)^{1.5} = 0.25 \times D^{1.5} \quad (4.14)$$

where: γ = load-slip modulus (kN/mm); D = diameter of nail (mm)

Screws

The BWBN hysteresis model was used for screw connections. Tables 4.1, 4.2, and 4.3 show the required parameters. The strength and stiffness of the screw connections were set to zero when a displacement goes beyond the failure displacement, (d_{fail}). The parameter representing hysteretic behavior of each screw connection can be found in appendix C.

Damping

Rayleigh damping was assigned for both wood and steel cladding with a damping factor of 0.015 for mass proportional damping, and 0.015 for stiffness proportional damping. The purpose of this damping is to damp the lower and higher frequency range behavior and to make the solution stable.

TESTING OF STEEL-CLAD, WOOD-FRAMED SHEAR WALLS UNDER CYCLIC LOADING

Materials and wall construction

Shear wall tests conducted by Bender (2015) were used to validate the model reported herein. SCWF shear walls were constructed using 0.343 mm thickness, 0.55 GPa yield strength steel cladding with profiled ribs. Fabral Grandrib3 steel panels were attached to wood framing using structural screws (no.10x25.4 mm on the field, no. 12x38.1 mm or no.12x19.1 mm through steel lap joints). All SCWF shear walls were 4877 mm wide by 3658 mm high with 2 bays spacing at 2438 mm. The 38 x 140 mm pressure preservative treated (PPT) Hem-Fir No.2 and Douglas Fir-Larch Select Structural lumber were used to construct the base and top of the 3-ply nail-laminated

posts. The 38 x 190 mm PPT Hem-Fir No.2, and 38 x 140 mm Douglas Fir-Larch Select Structural lumber were used for the skirt board and the simulated truss chord at the top of the wall, respectively. Girts and blockings were 38 x 89 mm Spruce-Pine-Fir 1650Fb-1.5E lumber. The 88.9 x 4.1 mm ring shank nails were used to connect secondary members such as girts, the skirt board, blocking, and the simulated truss chord to posts. All secondary members were laid flat on the posts. The general shear wall configuration and screw patterns are shown in Fig. 4.8 and 4.9, respectively. Table 4.6 shows a detail of the girt spacing, cladding profile, field screw, and seam screw pattern for each shear wall. Details of materials and wall construction can be found in the technical report by Bender (2015).

Test methods

Shear wall tests were conducted in accordance with *Standard Test Methods for Cyclic (Reversed) Load Test for Shear Resistance of Walls for Buildings* (ASTM E2126-11). The load and displacement on the top of wall was monitored during the tests. Deflection was measured at the four gage locations specified by ANSI/ASAE EP558 for the cantilever test. These deflection measurements were used to calculate the adjusted point load-deflection, which omits displacement resulting from rigid body rotation and translation. Cyclic protocols require a reference displacement to characterize the displacement history. Since the monotonic tests of SCWF shear wall tests never reached $0.8P_{peak}$ (P_{peak} is ultimate load), from the Bender (2012) study, the reference displacement was chosen to be $2.5\%h_x = 91.44$ mm (h_x is wall height). The

displacement rate was chosen to be 15.24 mm/s based on the provisions of ASTM E2126-11. Additional testing details can be found in the report by Bender (2015).

RESULTS AND DISCUSSION

Different types of energy, including external work, kinetic energy, and viscous damping energy, were obtained to evaluate the inertial effect in the dynamic analyses. Fig. 4.4 shows their variation with time. It was found that kinetic energy and viscous damping energy were negligible compared to the external energy during the dynamic analysis. Therefore, it can be concluded that the load model adequately simulated a quasi-static condition.

The hysteresis loops that were generated from the base shear vs. drift at the top of the wall from the FEA models and experimental tests are presented in Fig. 4.5 to 4.7. The hysteretic behavior of all shear walls modeled can be found in appendix C. The FEA model was found to slightly overestimate the ultimate shear strength, especially for the heavily stitched screw walls. The higher predicted strength could be due to the equivalent plane stress element that restrains the steel panel from buckling out of plane, which actually occurred for steel cladding under experimental tests. The pinching of the hysteresis curves and the strength degradation of the shear walls, which are the important features of SCWF behavior, are captured well by the FEA models.

Figure 4.8 shows the backbone curve comparison between tests and FEA model predictions for a typical unstitched wall configuration. Good agreements were obtained with regard to the shear strength envelope curve, except for heavily stitched walls, as shown in appendix C. According to AC 322, the backbone curve of shear strength is key

in determining the equivalency of proposed lateral load resisting system to light-framed wood shear walls. The possible replacement system can be used and share the same seismic design coefficients as light-framed wood shear wall in accordance with appendix A in the AC 322 document. Table 4.8 shows the AC 322 criteria check for tests and FEA models. Good agreements were obtained with regard to the AC 322 criteria for unstitched, and lightly stitched (wall used no.10x38.1 mm at seam lap) walls, except for heavily stitched, and lightly stitched (wall used no.10x19.1 mm at seam lap) walls. Therefore, the FEA models can be used to determine the seismic equivalency between unstitched, and lightly stitched (wall used no.10x38.1 mm at seam lap) walls with light-framed wood shear walls.

Energy dissipation is a key parameter for evaluating the performance of a system under earthquake excitation. The inelastic seismic performance of a system is quantified by the seismic response factor. The seismic response factor reduces the elastic demands based on the shear of a system when the system possesses a significant inelastic behavior during an earthquake. The enclosed area by a hysteresis loop generated by the load vs displacement history is used as the measure of energy dissipation. Table 4.7 shows the result of energy dissipation between the FEA model and experimental tests. The FEA model was found to underestimate the dissipation energy for all of the SCWF shear walls modeled. The lower energy dissipation could be due to the fact that friction and contact between framing members, steel to wood, and steel panel to steel panel were not included in the FEA model. However, the low

dissipation energy values in the FEA model make it more conservative when it is used as a macro-element for simulating a whole building under dynamic loading.

SUMMARY AND CONCLUSIONS

A finite element model based on a dynamic implicit formulation was developed for the analysis of SCWF shear walls under quasi-static cyclic loading. The solution for the analysis was obtained without any numerical difficulty because kinetic and viscous damping were used to make the model solution stable. The hysteresis constitutive relationships of screw connections obtained from experimental tests were included in the models. Constitutive relationships for several tested screw connections were randomized throughout the simulated shear walls, which enabled the FEA model results to capture some of the effects of screw variability. Equivalent orthotropic plane stress elements, instead of shell elements, were used in the model, which reduced simulation run time.

A general hysteresis model, BWBN, was also developed and used successfully for the screw connection simulation. The rate of pinching parameter was introduced to the pinching function, which is used to control the slack behavior of screw connections during reversed-cyclic loading. Slack was also incorporated into the pinching function. Pinching was modified to be a function of peak displacement history rather than hysteresis energy. The BWBN model is nonlinear and history dependent, and it included strength and stiffness degradation. The parameters of the BWBN models were obtained from experimental tests using the GA method. A failure displacement for each screw connection was also included in the FEA model.

A total of six SCWF shear wall configurations with 4:3 aspect ratio were modeled and compared with experimental tests. In general, good agreement was observed between the FEA models and the experimental tests. The FEA models predicted the shear strength backbone curve well for most of shear wall configurations, except for the heavily stitched shear wall configuration. The predicted shear strength was slightly higher for the FEA models than that for the tests, especially for stitched shear walls. Energy dissipation from the FEA models was lower than for the tests, which make the FEA model more conservative if it is used to define the properties of a macro-element that could be used in whole building simulation. The pinching effect and strength and stiffness degradation of shear walls subjected to cyclic loading were captured well in the FEA model, although FEA model results of shear strength show slightly greater than observed results in the physical tests. These model results demonstrate the validity of the development of FEA models for SCWF shear walls.

ACKNOWLEDGEMENTS

This research was supported by the National Frame Building Association. Donation of fasteners from SFS intec Inc. and Maze Nails are gratefully acknowledged.

REFERENCES

- ABAQUS. (2011). ABAQUS analysis user's manual (version 6.11), Hibbitt, Karlsson, and Sorenson, Pawtucket, R.I.
- American Forest & Paper Association, Inc., National Design Specification (NDS) for Wood Construction, 2015 edition, Washington, DC.
- ASTM. (2011). "Standard test methods for cyclic reversed load test for shear resistance of walls for buildings." ASTM E2126-11, ASTM, West Conshohocken, Pa.
- ASAE. (2004). "Load tests for metal clad, wood frame diaphragms." ASAE EP 558, American Society of Agriculture Engineers, St Joseph, MI.
- Anderson, G.A. (1987). "Evaluation of light-gage metal diaphragm behavior and diaphragms interaction with post-frames." Ph.D. dissertation, Iowa State University, Ames, Iowa.
- Anderson, G.A., and Bundy, D.S. (1990). "Stiffness of screw fastened, metal-clad, timber-framed roof diaphragms with opening in the sheeting." Transaction of the ASAE 33(1):266-273.
- Baber, T. T., and Noori, M. N. (1985). "Random vibration of degrading, pinching systems." J. Eng. Mech., 1118, 1010–1026.
- Bender, D.A. (2012). "Development of design data for steel-clad, wood-framed shear walls". NFBA Shear Wall Project – CMEC technical report 12-004, Pullman, Washington.

- Bender, D.A. (2015). "Development of seismic design data and seismic response factor for steel-clad, wood-framed shear walls". NFBA Shear Wall Project – CMEC technical report, Pullman, Washington.
- Bouc, R. (1967). "Force vibration of mechanical systems with hysteresis." Proc., 4th Conf. on Nonlinear Oscillation, Prague, Czechoslovakia.
- Dolan, J. D. (1999). "Code development for seismic design of woodframe structures: Testing needs." Proc., Invitational Workshop on Seismic Testing, Analysis and Design of Woodframe Construction, Pub. No. W-01, California Universities for Research in Earthquake Engineering, Richmond, Calif., 9–14.
- Du, Y. (2003). "The development and use of a novel finite element for the evaluation of embedded fluid dampers within light-frame timber structures with seismic loading." Ph.D. dissertation, Dept. of Civil and Environmental Engineering. Washington State Univ., Pullman, Wash.
- He, M., Magnusson, H., Lam, F., and Prion, H. G. L. (1999). "Cyclic performance of perforated wood shear walls with oversize OSB panels." J. Struct. Engrg., ASCE, 125(1), 10–18.
- He, M., Lam, F., and Prion, H. G. L. (1998). "Influence of cyclic test protocols on performance of wood-based shear walls." Can. J. Civ. Engrg., Ottawa, 25(3), 539–550.

- Heine, C. P. (2001). "Simulated response of degrading hysteretic joints with slack behavior." Ph.D. dissertation, Dept. of Wood Science and Forest Products, Virginia Polytechnic Institute and State Univ., Blacksburg, Va.
- ICC Evaluation Service, Inc. 2009. Acceptance criteria for prefabricated, cold-formed steel lateral-force-resisting vertical assemblies. AC322, Birmingham, Ala., <http://www.icc-es.org> (2009).
- Judd, J. and Fonseca, F. (2005). "Analytical Model for Sheathing-to-Framing Connections in Wood Shear Walls and Diaphragms." *J. Struct. Eng.*, 131(2), 345–352.
- Keener, J. D., and Manbeck, H. B. (1996). "A simplified model for predicting the behavior of metal-clad, wood-framed diaphragms" *Transactions of the ASAE VOL.39(3):1113-1122.*
- Krawinkler, H., Parisi, F., Ibarra, L., Ayoub, A., and Medina, R. (2000). "Development of a testing protocol for wood frame structures." CUREe Publ. No. W-02, Consortium of Universities for Research in Earthquake Engineering, Richmond, Calif.
- Lam, F., Prion, H. G. L., and He, M. (1997). "Lateral resistance of wood shear walls with large sheathing panels." *J. Struct. Eng., ASCE*, 123(12), 1666–1673.
- Lebeda, D., Gupta, R., Rosowsky, D., and Dolan, J. (2005). "Effect of Hold-Down Misplacement on Strength and Stiffness of Wood Shear Walls." *Pract. Period. Struct. Des. Constr.*, 10(2), 79–87.

Li, M., Foschi, R., and Lam, F. (2012). "Modeling Hysteretic Behavior of Wood Shear Walls with a Protocol-Independent Nail Connection Algorithm." J. Struct. Eng., 138(1), 99–108.

Radhakrishnan, K., and Hindmarsh, A. C. (1993). "Description and use of LSODE, the Livermore solver for ordinary differential equations." Rep. No. UCRL-ID-113855 (NASA Reference Publication No. 1327), Lawrence Livermore National Laboratory, Livermore, Calif.

Structural Engineers Association of California SEAOC. (1999). "Recommended lateral force requirements and commentary." 7th Ed., Sacramento, Calif.

Symans, M.D., Cofer, W.F., Du, Y., and Fridley, K.J. (2002b). "Evaluation of Fluid Dampers for Seismic Energy Dissipation of Woodframe Structures," CUREE Report No. W-20, Consortium of Universities for Research in Earthquake Engineering (CUREE), Richmond, CA.

USDA Wood handbook - Wood as an engineering material. General Technical Report FPL-GTR-190. Madison, WI: U.S. Department of Agriculture, Forest Service, Forest Products Laboratory: 508 p. 2010

Wen, Y.-K. 1976. "Method for random vibration of hysteretic systems." J. Eng. Mech. Div., 102EM2, 249–263.

White, M. and Dolan, J. (1995). "Nonlinear Shear-Wall Analysis." J. Struct. Eng., 121(11), 1629–1635.

Williams, G. D. (1997). "Modelling Metal-Clad Wood-Framed Diaphragm Assemblies."
Ph.D. dissertation, Dept. of Agricultural Engineering, University of Wisconsin-
Madison, Madison, Wisconsin.

Williams, G. D., and Bohnhoff, D. R. (1998). "Modeling metal-clad, wood frame
diaphragm behavior" An ASAE Meeting Presentation, paper No. 974088.

Wright, B. W., and Manbeck, H. B. (1993). "Finite element analysis of wood-framed,
metal-clad diaphragm panels" Transactions of the ASAE VOL. 36(3): 895-904-
MAY-JUNE 1993.

Xu, J. and Dolan, J. (2009a). "Development of Nailed Wood Joint Element in ABAQUS."
J. Struct. Eng., 135(8), 968–976.

Xu, J. and Dolan, J. (2009b). "Development of a Wood-Frame Shear Wall Model in
ABAQUS." J. Struct. Eng., 135(8), 977–984.

FIGURES

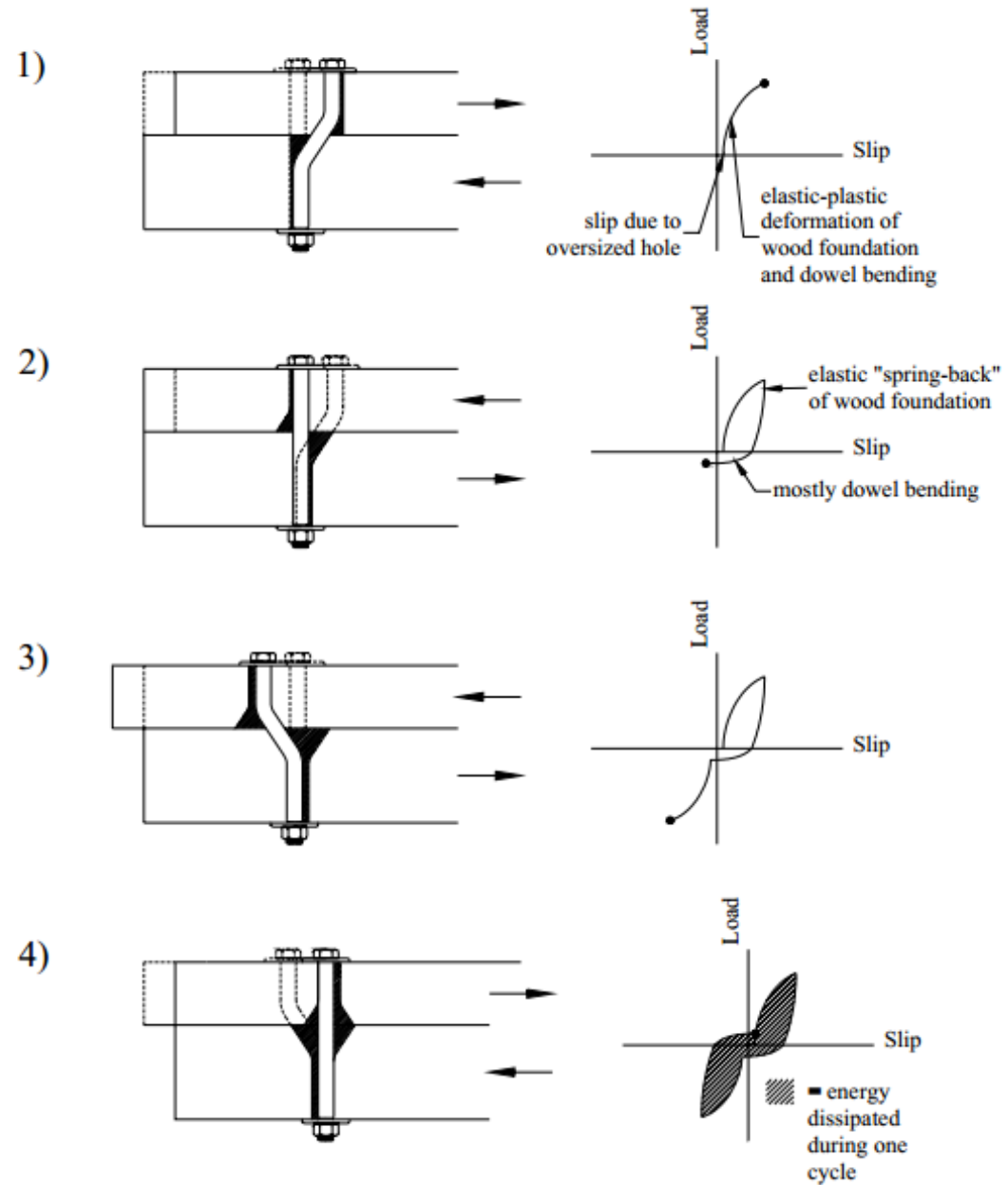


Figure 4.1: Hysteretic behavior of a bolted joint in single shear stress beyond the elastic limit (Heine, 2001)

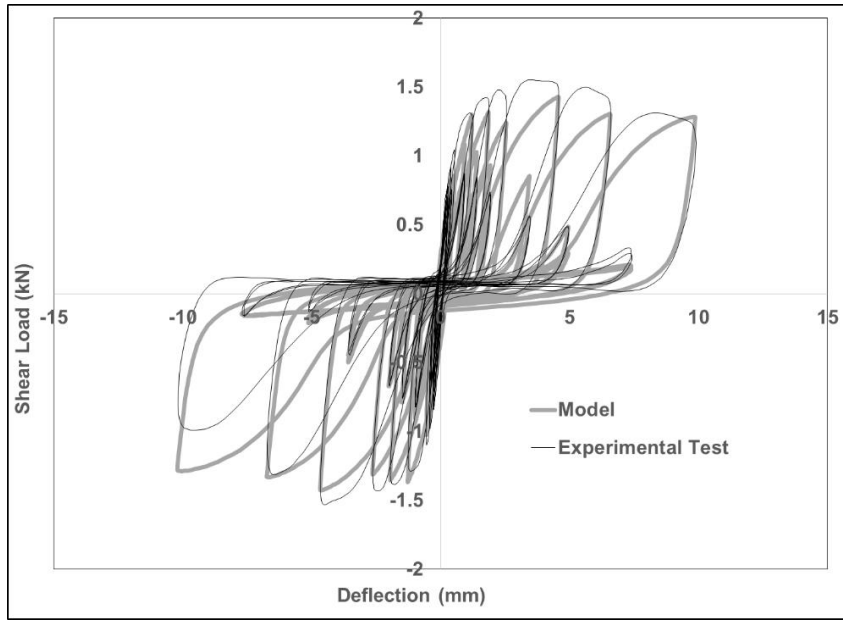


Figure 4.2: Typical load-slip of no.10x25.4 mm connection between SPF and steel panel. Test 1.

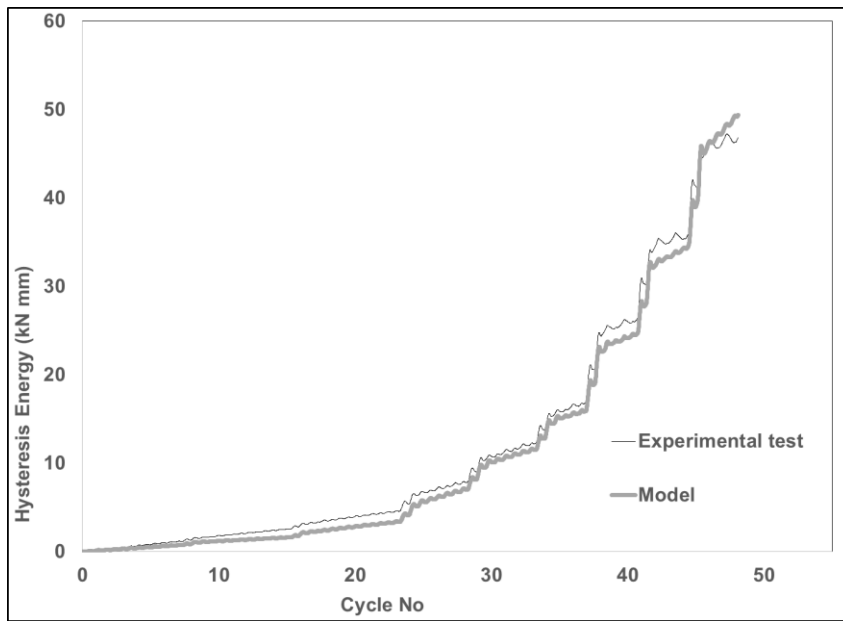


Figure 4.3: Typical hysteretic energy of no.10x25.4 mm connection between SPF and steel panel. Test 1.

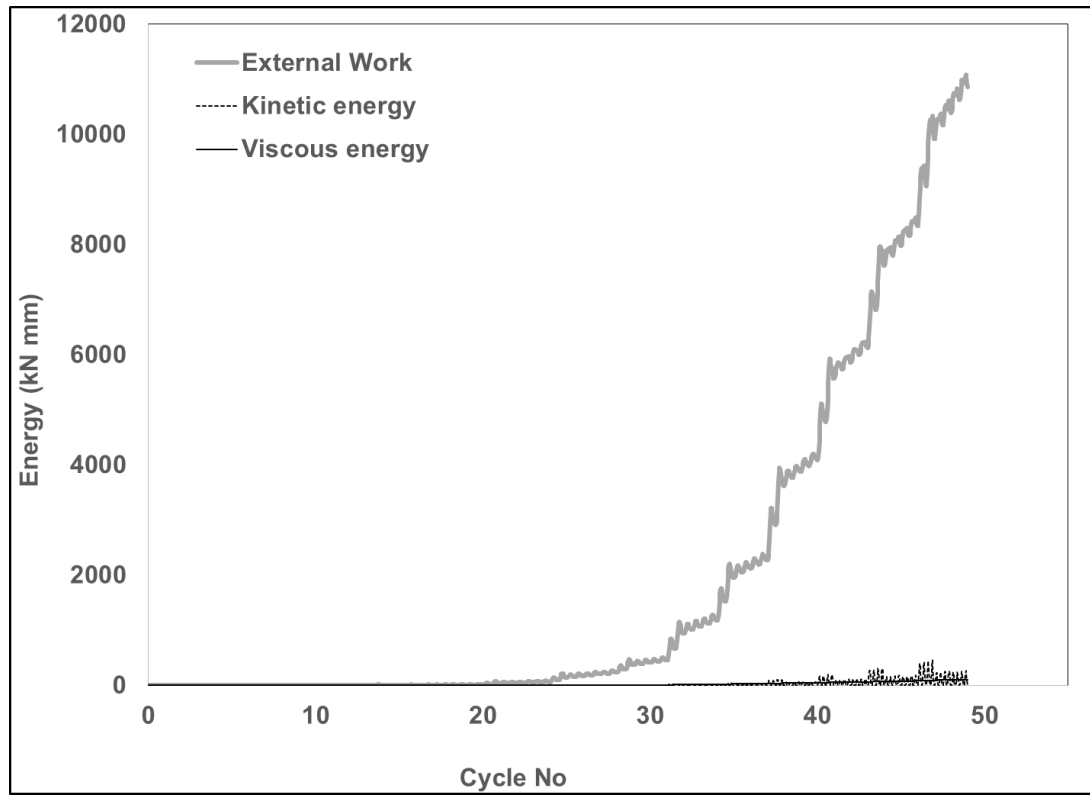


Figure 4.4: Energy of FEA model. Wall type 1.

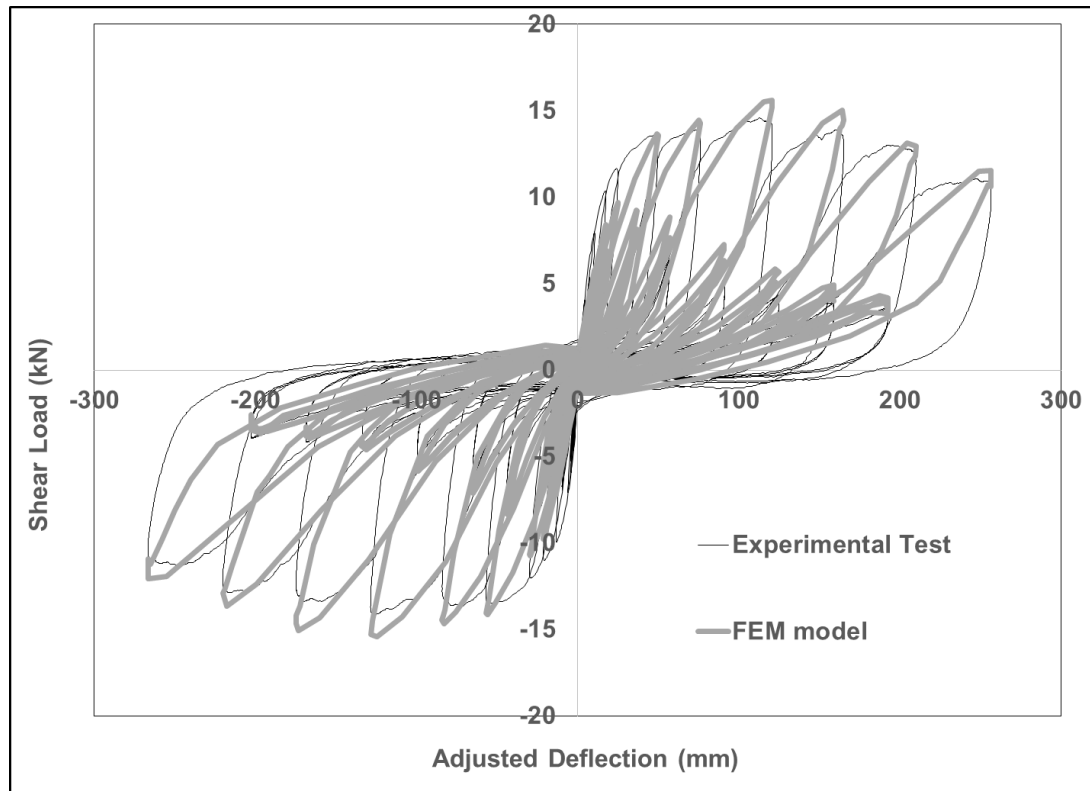


Figure 4.5: Force vs. displacement. Wall type 1.

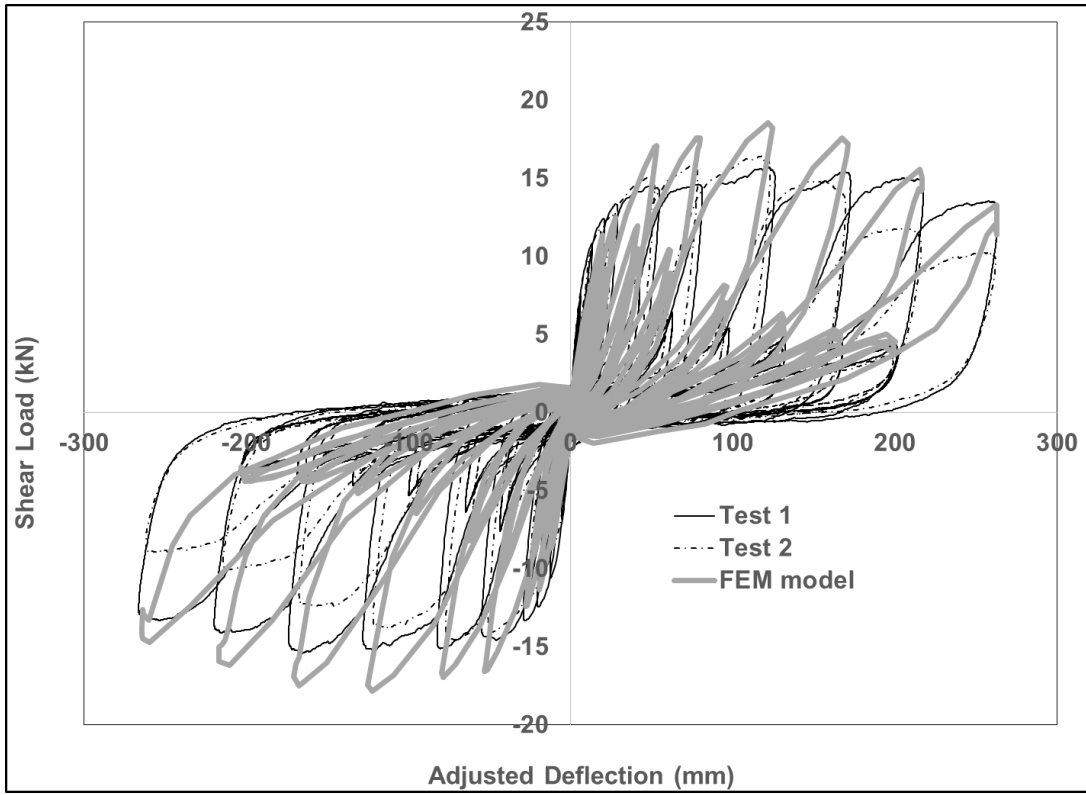


Figure 4.6: Force vs. displacement of wall type 2

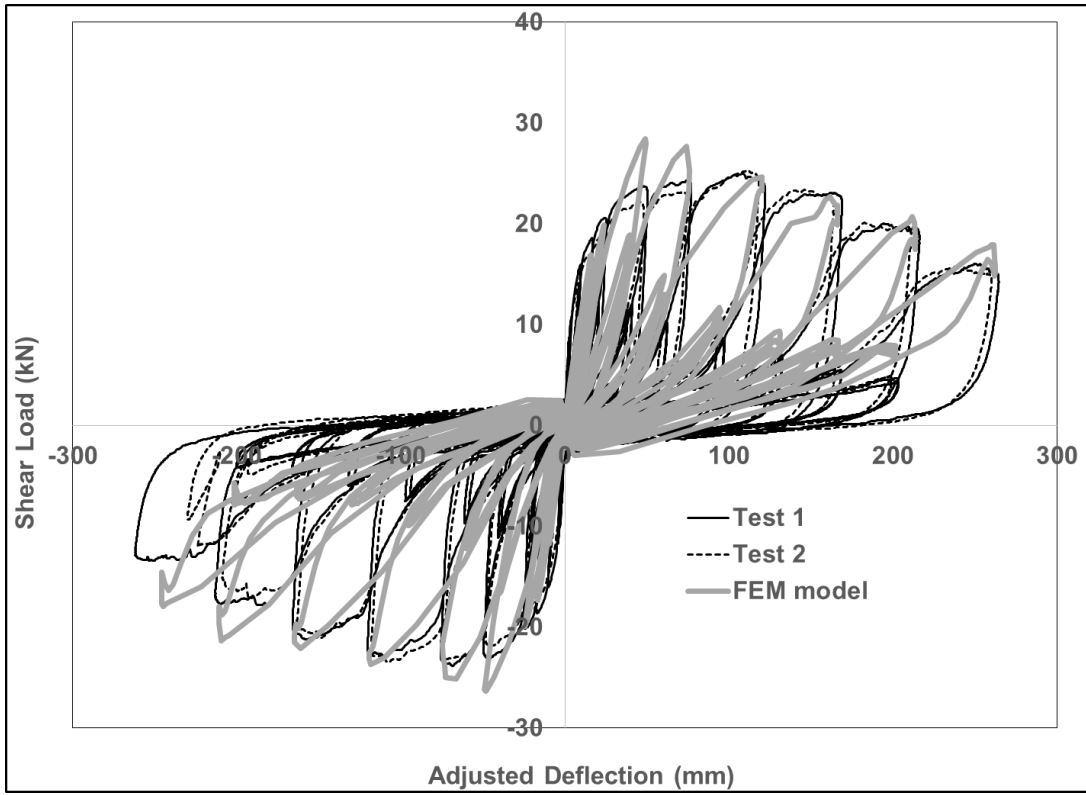


Figure 4.7: Force vs. displacement of wall type 4

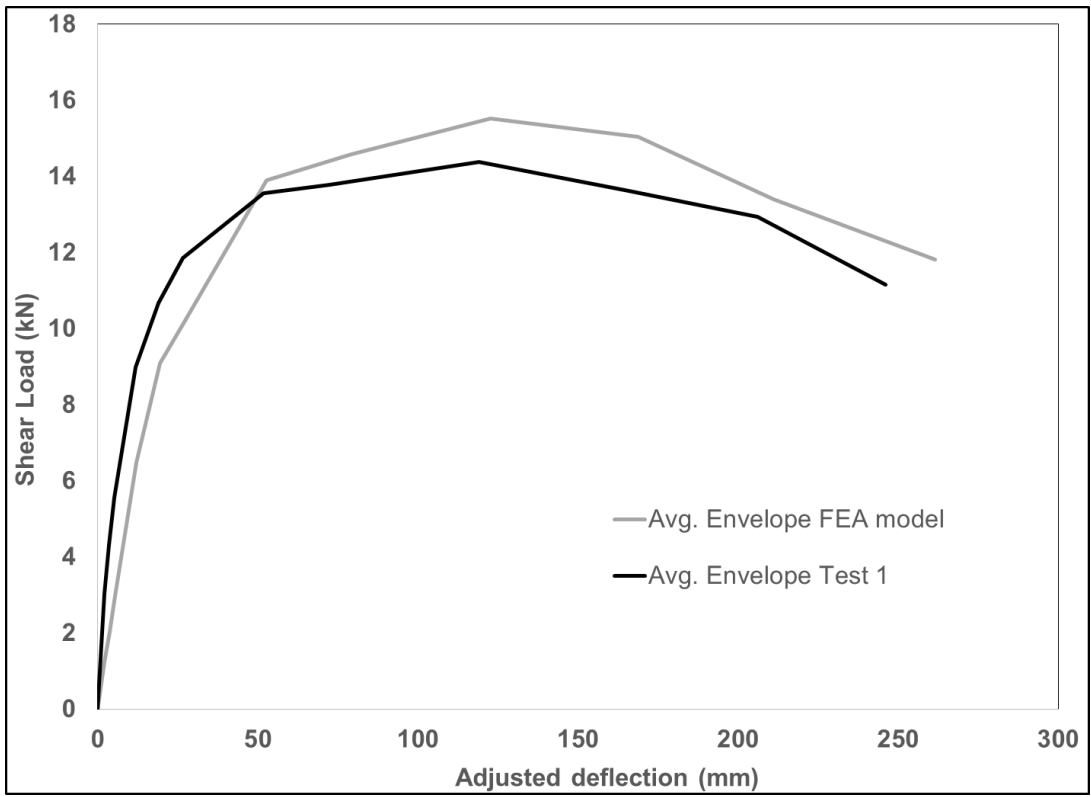


Figure 4.8: Backbone curve for tests and FEA models

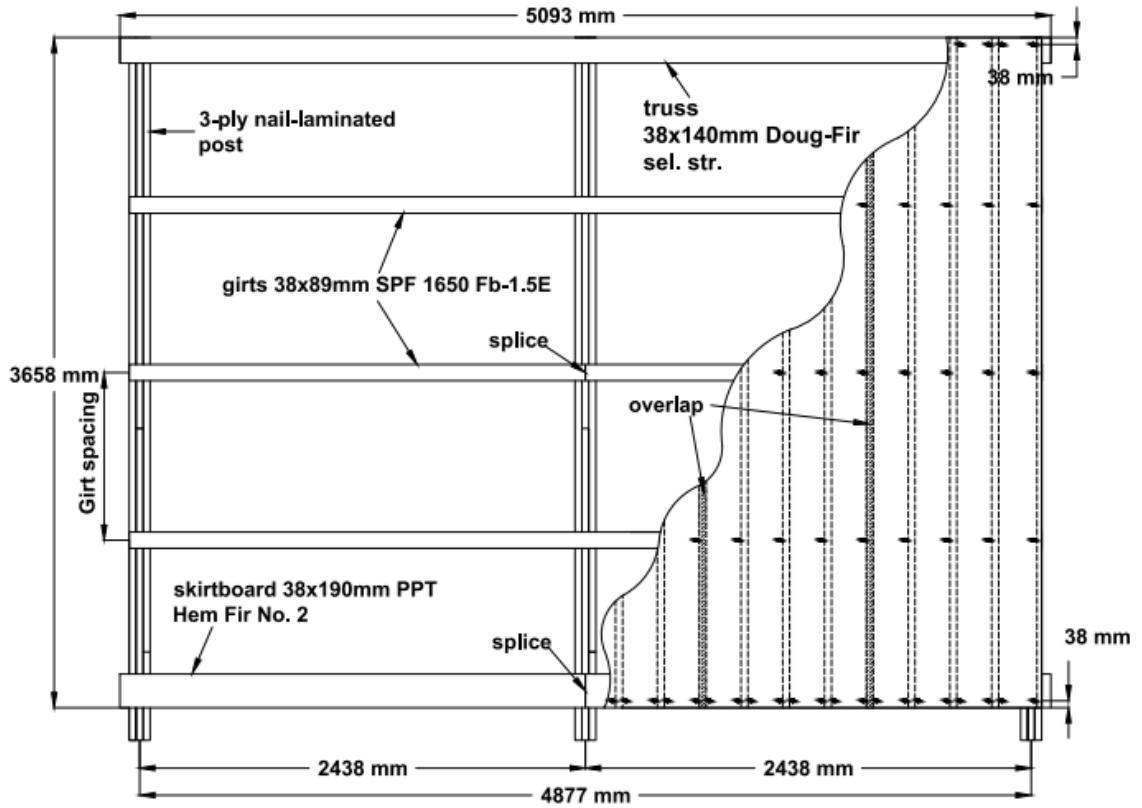


Figure 4.9: General shear wall configuration (Bender, 2015)

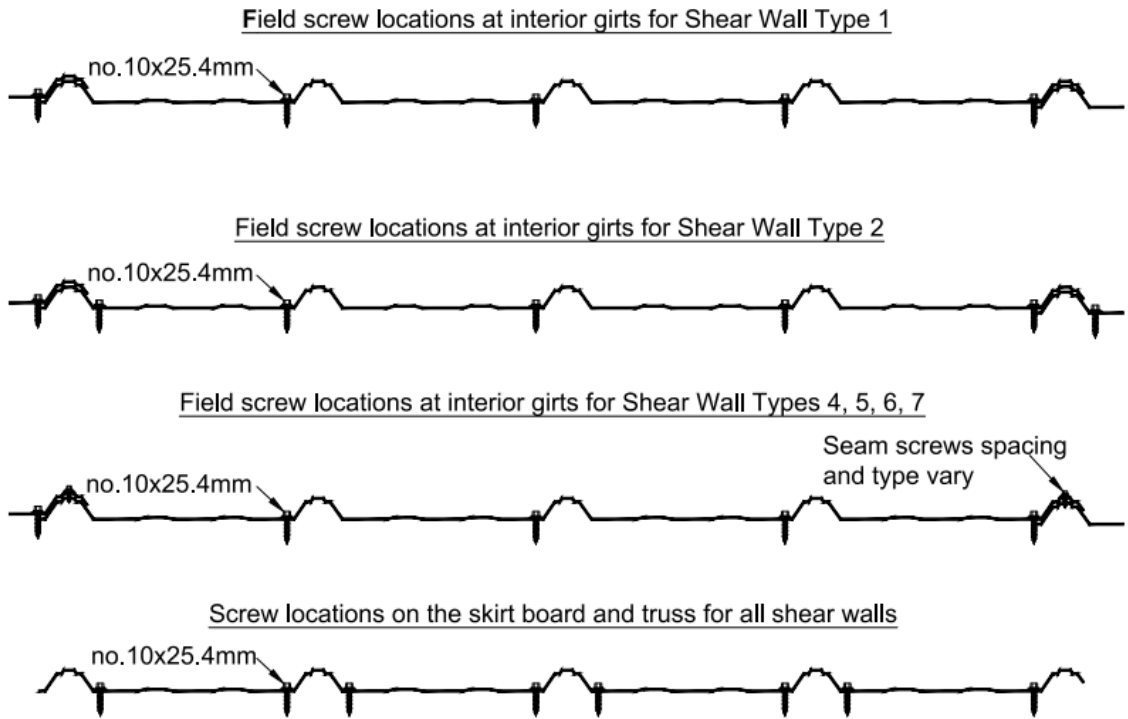


Figure 4.10: Shear wall screw patterns (Bender, 2015)

TABLES

Table 4.1: BWBN parameters for connection between SPF and steel cladding (no. 10x25.1 mm)

	Test 1	Test 2	Test 3	Test 4	Test 5	Test 6
α	0.001715	0.02313	0.012723	0.037093	0.020119	0.028502
β	2.49905	3.576251	2.282357	2.482788	3.268586	4.205177
ω	1.498048	1.618767	1.436525	1.344332	1.459071	1.522016
ζ	0.976314	0.986264	0.982136	0.983281	0.988848	0.981786
n	1.031465	1.107239	1.054614	1.183527	1.285907	1.614665
ψ_0	0.002562	0.003591	0.008641	0.008966	0.010931	0.043733
δ_ψ	0.020648	0.010735	0.007529	0.012802	0.005418	0.01094
δ_ν	0.014016	0.035177	0.032848	0.097589	0.166067	0.17757
ξ_0	0.002624	0.002869	0.002588	0.002266	0.002053	0.002343
γ	-1.419993	-2.549417	-1.817625	-1.553872	-2.848378	-2.687436
δ_η	0.106234	0.152997	0.143176	0.21506	0.293825	0.246575
p	3.723502	4.728824	2.764136	3.397975	3.97309	2.156789
d_{fail}	10.04	16.5	19.81	16.53	19.78	19.69

**Table 4.2: BWBN parameters for connection between steel cladding and steel cladding
(no. 12x19.1 mm)**

	Test 1	Test 2	Test 3	Test 4	Test 5	Test 6	Test 7	Test 8
α	0.001182	0.02672	0.00263	0.03072	0.00037	0.00817	0.0175	0.005
β	3.72756	3.09421	3.13569	3.5295	2.13538	2.92786	3.1195	2.8821
ω	1.899963	1.89638	1.89961	1.89383	2.19422	2.19715	2.1961	2.1994
ζ	0.975715	0.97976	0.97862	0.97765	0.98917	0.98274	0.971	0.9864
n	1.246145	1.14233	1.04898	1.02127	1.0062	1.01689	1.0001	1.4253
ψ_0	0.001228	0.00024	0.00019	0.00663	0.00039	0.00103	0.0002	0.0004
δ_ψ	0.026973	0.03706	0.0242	0.02356	0.01055	0.01899	0.0201	0.0346
δ_ν	0.102096	0.23127	0.20842	0.27596	0.27021	0.09093	0.1945	0.258
ξ_0	0.00436	0.00262	0.00085	0.00324	0.00195	0.00333	0.0035	0.0028
γ	-2.80719	-2.32083	-2.5797	-2.7607	-1.534	-1.7517	-2.174	-1.313
δ_η	0.204871	0.09441	0.13327	0.23341	0.23303	0.17926	0.2506	0.084
p	4.899828	4.8783	4.71118	4.95085	5.97144	5.98335	5.9363	5.8622
d_{fail}	7.81	7.68	10.21	7.7	10.4	10.3	7.76	10.28

**Table 4.3: BWBN parameters for connection between steel cladding and steel cladding
(no. 12x38.1 mm)**

	Test 1	Test 2	Test 3	Test 4	Test 5	Test 6
α	0.011081	0.013684	0.016321	0.011072	0.009709	0.012729
β	2.798202	2.669789	3.191365	3.310131	3.222305	3.47183
ω	1.699091	1.69258	1.899135	1.778656	1.899652	1.89929
ζ	0.98969	0.989887	0.987698	0.989794	0.986729	0.989343
n	1.001066	1.041919	1.000829	1.092169	1.000896	1.000134
ψ_0	0.033303	0.015633	0.011786	0.012143	0.015437	0.007355
δ_ψ	0.009167	0.006193	0.004732	0.004266	0.006043	0.003965
δ_ν	0.075755	0.080234	0.277255	0.188539	0.277035	0.16033
ξ_0	0.001438	0.001187	0.003229	0.002477	0.003423	0.002646
γ	-1.862902	-1.879151	-2.890809	-2.887135	-2.894989	-2.893847
δ_η	0.155305	0.207109	0.369118	0.315528	0.356066	0.364467
p	3.830046	3.815286	4.940647	4.95107	4.717811	3.260874
d_{fail}	15.4	18.08	18.11	18.21	15.61	18.22

Table 4.4: Corrugated panel properties

Value	Modulus of elasticity (kN/mm²)	Shear modulus (kN/mm²)
Shear	-	6.41
Parallel to corrugations	216.15	-
Perpendicular to corrugations	1.25	-

Table 4.5: Load-slip modulus of nail connection

Connector location	Load-slip modulus (kN/mm)
Truss to end post	12.33
Truss to center post	12.33
Skirt board to end post	12.33
Skirt board to center post	12.33
Girt to end post	6.17
Girt to center post	6.17
Girt to center post at splice	12.33
Blocking at end post	4.11

Table 4.6: Construction properties for each shear wall (Bender, 2015)

Shear Wall Type	Reps	Cladding Type	Girt Spacing (mm)	no.10x25.4 mm		
				structural fasteners adjacent to the overlap rib in flats	no. 12x38.1 mm elevated sidelap structural fasteners	no.12x19.1 mm stitch fastener
1	1	Grandrib3	914	1 side	----	----
2	3	Grandrib3	914	Both sides	----	----
4	3	Grandrib3	610	1 side	609 mm off center	----
5	2	Grandrib3	610	1 side	----	203 mm off center
6	2	Grandrib3	610	1 side	----	609 mm off center
7	3	Grandrib3	914	1 side	----	457 mm off center

Table 4.7: Energy dissipation between FEA models and tests

Wall ID	No. of cycles	Energy dissipation (kN.mm)		Predicted/Test
		Experimental	FEA model	
Wall 1-1	49	17107	8189	0.48
Wall 2-1	49	18662	9563	0.51
Wall 2-2	49	15895	9563	0.60
Wall 4-1	49	24794	13385	0.54
Wall 4-2	49	23570	13385	0.57
Wall 5-1	46	24086	15579	0.65
Wall 5-2	46	24562	15579	0.63
Wall 6-1	49	17156	10813	0.63
Wall 6-2	49	18067	10813	0.60
Wall 7-2	46	15907	9387	0.59
Wall 7-3	46	13965	9387	0.67
			Average	0.59
			COV	10.1%

Table 4.8: AC 322 criteria check for tests and FEA models

Shear Wall ID	reps	Equivalent to light-frame wood shear walls	
		Tests	FEA models
1	1	YES	YES
2	2	YES	YES
4	2	YES	YES
5	2	YES	NO
6	2	NO	YES
7	1	NO	YES

CHAPTER 5

SUMMARY AND CONCLUSIONS

Relative little literature addressed the finite element modeling of SCWF shear walls under monotonic loading, and no literature exists regarding the performance of SCWF shear walls under reverse-cyclic loading. Moreover, seismic design coefficients have not been developed in model building codes for the design of post-frame shear walls as a lateral force resisting system for seismic forces, yet there is a growing market for post-frame construction, especially in seismic regions. This research improves our understanding of the dynamic response of these walls, as well as providing data for seismic design codes. The conclusions and recommendations of this research are summarized as follows:

1. Behavior of SCWF shear walls under monotonic loading:

- Screw connections (between SPF and steel panel, and between steel panel and steel panel) have great influence on the overall performance of SCWF shear walls.
- The load-slip behavior of screw connections need to be obtained to provide the material constitutive relationship for finite element model.
- The dynamic implicit procedure should be used to solve the finite element model because the solution for the model is unstable due to buckling of the metal cladding, geometry nonlinearity, and nonlinear behavior of screw connection.

- The finite element model provides a good prediction for strength and stiffness of SCWF shear walls; however, hundreds of connector elements were used in the FEA model, making it computationally inefficient.

2. Seismic design coefficients for SCWF shear walls:

- The unstitched wall constructions had the greatest ductility values. The seismic design coefficients for those walls, which satisfied the AC 322 criteria for equivalency with light-frame wood shear walls, can be considered equivalent to wood light-framed shear walls (response modification coefficient $R = 6.5$, overstrength factor $\Omega_0 = 3$, and deflection amplification factor $C_d = 4$).
- Some of the lightly stitched shear wall configurations failed the AC 322 criteria due to the ejection of stitched screws during the cyclic loading, are not recommended for use in high seismic regions.
- For the combined OSB/steel wall system in which steel panels were used on one side of the wall with OSB on the other, the steel added sufficient ductility to the wall, and the capacities of OSB sheathed walls and steel sheathed walls proved to be additive. Therefore this wall system appears to be an excellent choice when high seismic or wind forces must be resisted.

3. Predicting behavior of SCWF shear walls under cyclic loading:

- A generic hysteresis model was developed to model the slack and hysteretic behavior of screw connections (SPF to steel panel, and steel panel to steel panel). The hysteretic model is capable of capturing the

stiffness and strength degradation, pinching, and slack on the screw connection. Moreover, the post failure stage of the screw connection (shear strength and stiffness for the screw connector decrease to zero when the displacement reaches beyond the maximum displacement) was also included in the finite element model.

- Equivalent orthotropic plane stress elements, instead of shell elements were used in the model, which reduces simulation run time. Therefore, three main material constant properties that represent the behavior of corrugated panels under in plane loading need to be determined for the finite element model.
- The accuracy of the FEA models were validated through six SCWF shear wall examples with different configurations. Although, good agreement was observed between FEA model and experimental tests, hundreds of connector elements were used in the model which made the model inefficient. Therefore, a more robust and simplified model should be developed for SCWF shear walls under cyclic loading.

Some future research is needed to expand this study:

1. More research is needed to examine the effect of openings, and aspect ratio to response of shear walls and diaphragm under monotonic and cyclic loading.

2. Macro-element based on cyclic response data from tests or FEA models should be developed to model the whole post-frame building under earthquake loading, to examine cases such as two-story, and irregular post-frame buildings.

**APPENDIX A BEHAVIOR OF STEEL-CLAD, WOOD-FRAMED (SCWF) SHEAR
WALLS UNDER MONOTONIC LOADING**

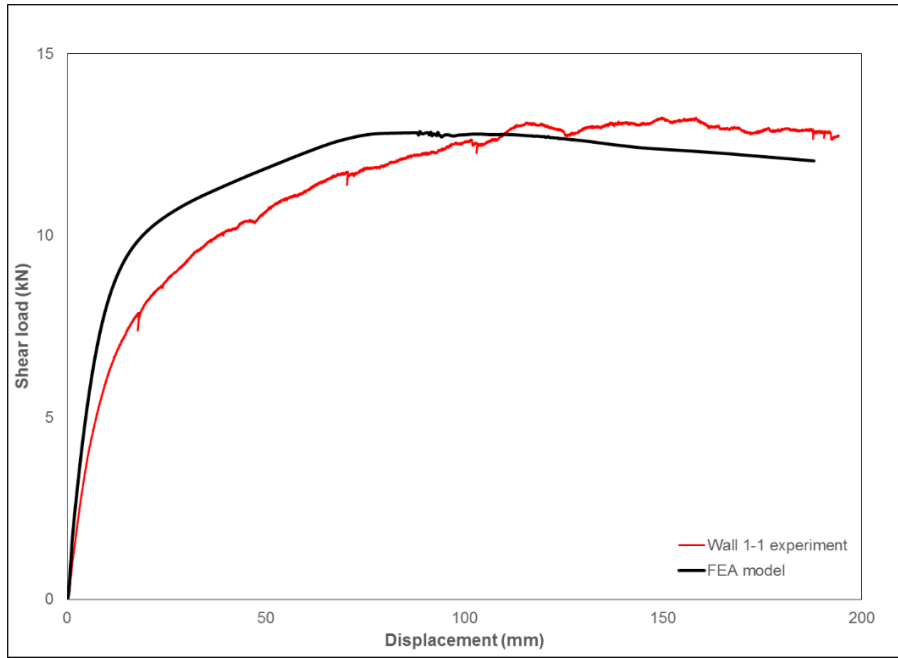


Figure A.1: Load versus displacement for SCWF shear wall type 1

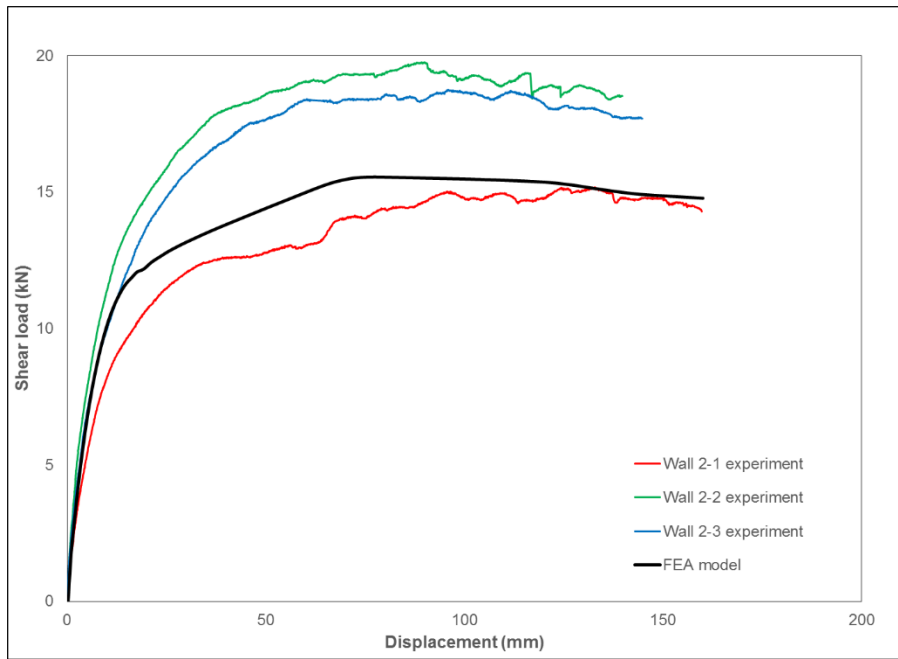


Figure A.2: Load versus displacement for SCWF shear wall type 2

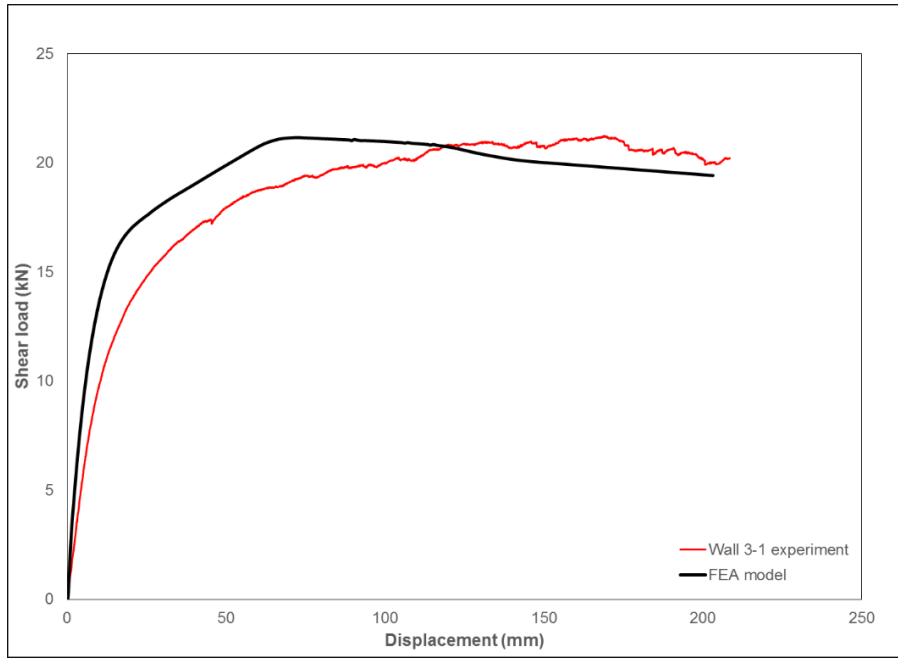


Figure A.3: Load versus displacement for SCWF shear wall type 3

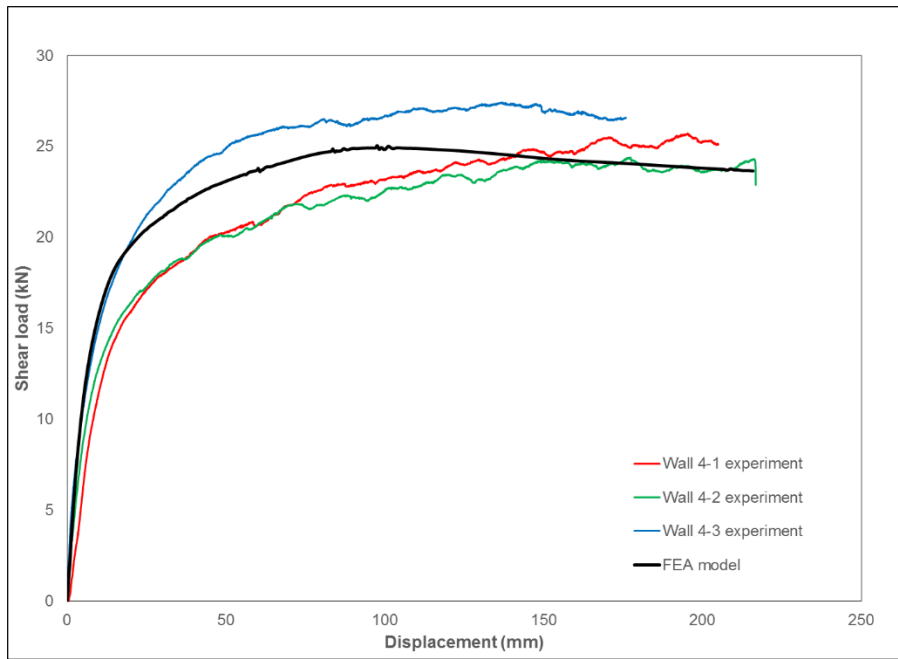


Figure A.4: Load versus displacement for SCWF shear wall type 4

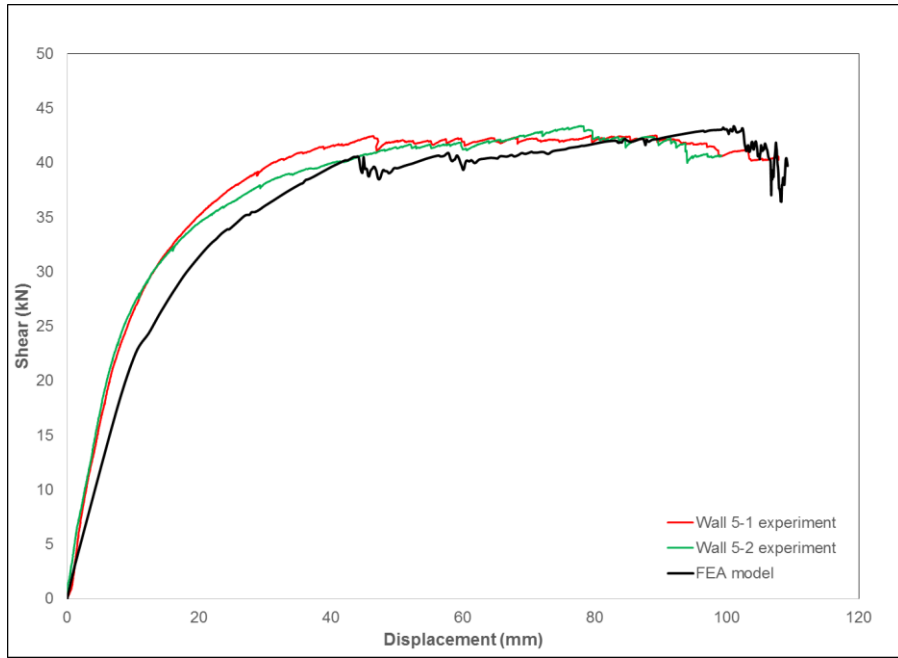


Figure A.5: Load versus displacement for SCWF shear wall type 5

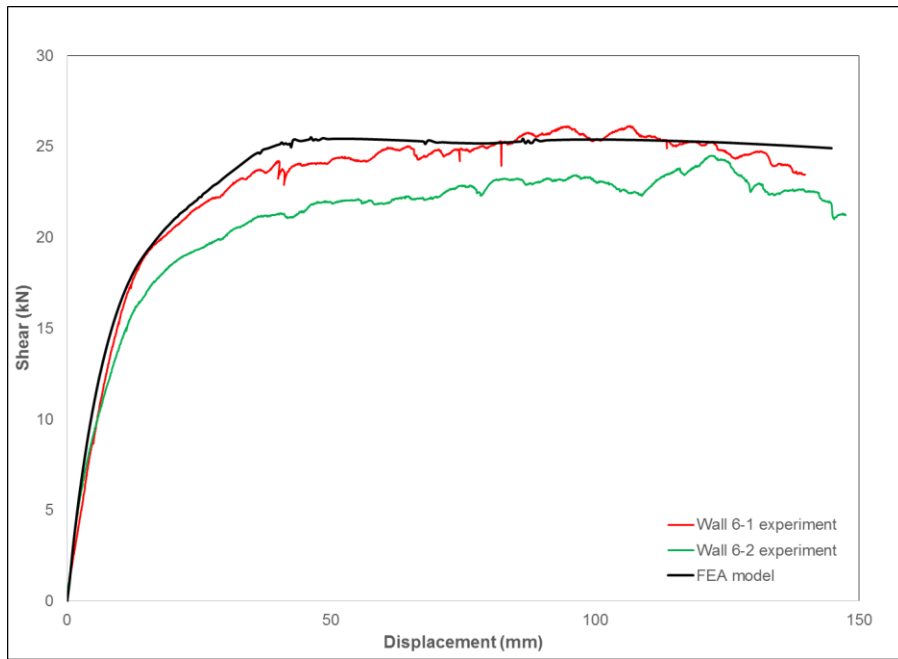


Figure A.6: Load versus displacement for SCWF shear wall type 6

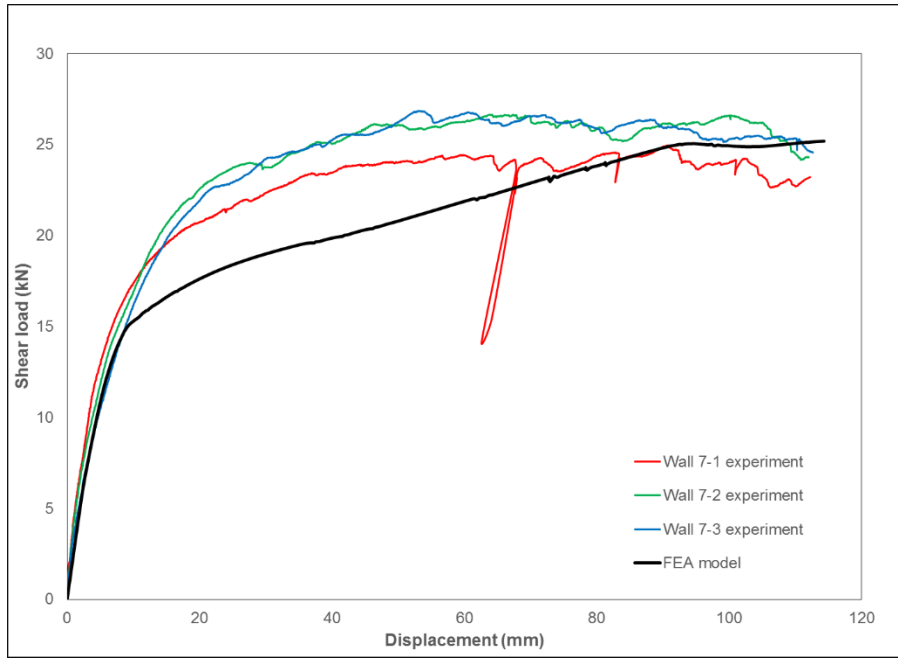


Figure A.7: Load versus displacement for SCWF shear wall type 7

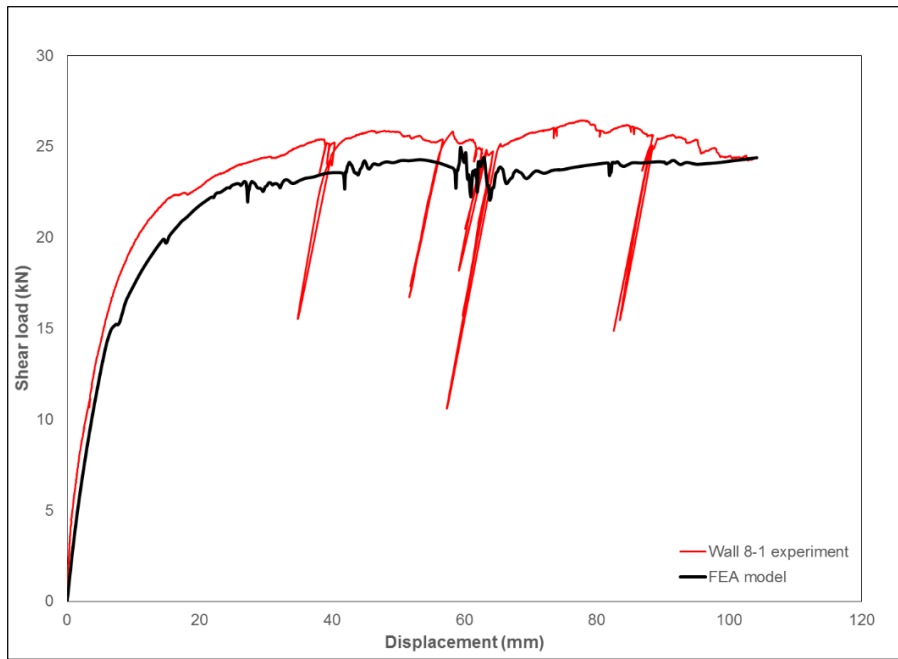


Figure A.8: Load versus displacement for SCWF shear wall type 8

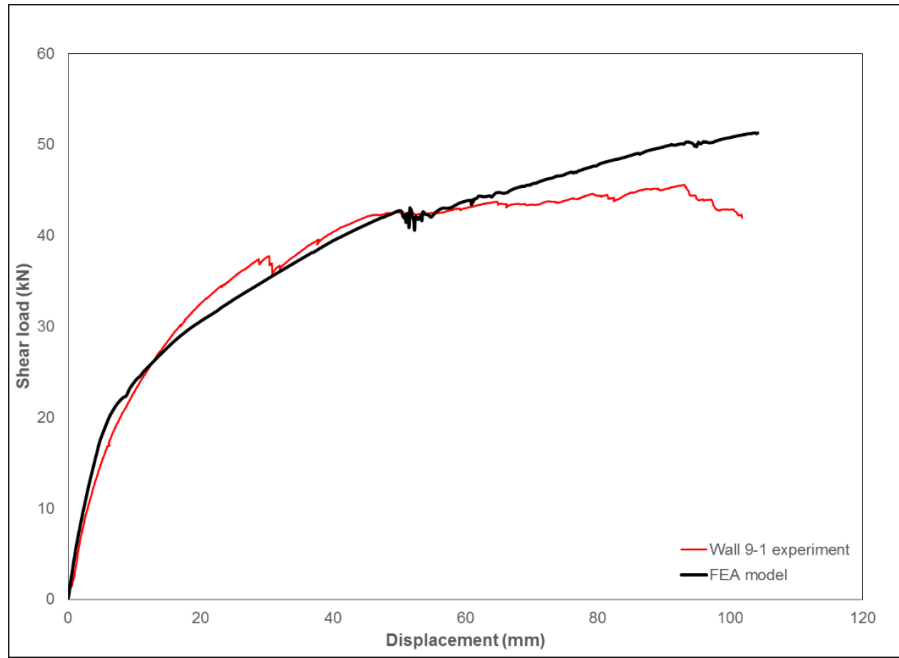
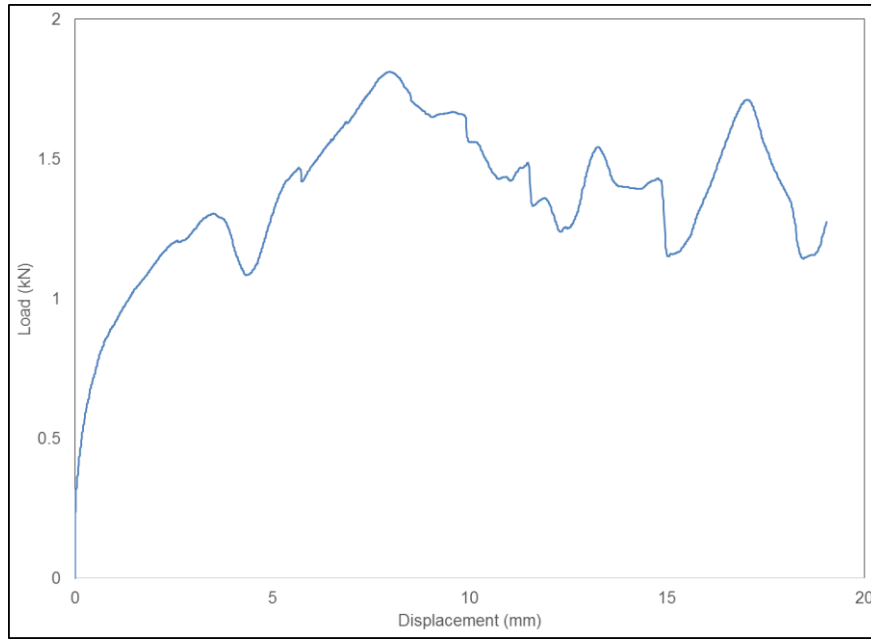
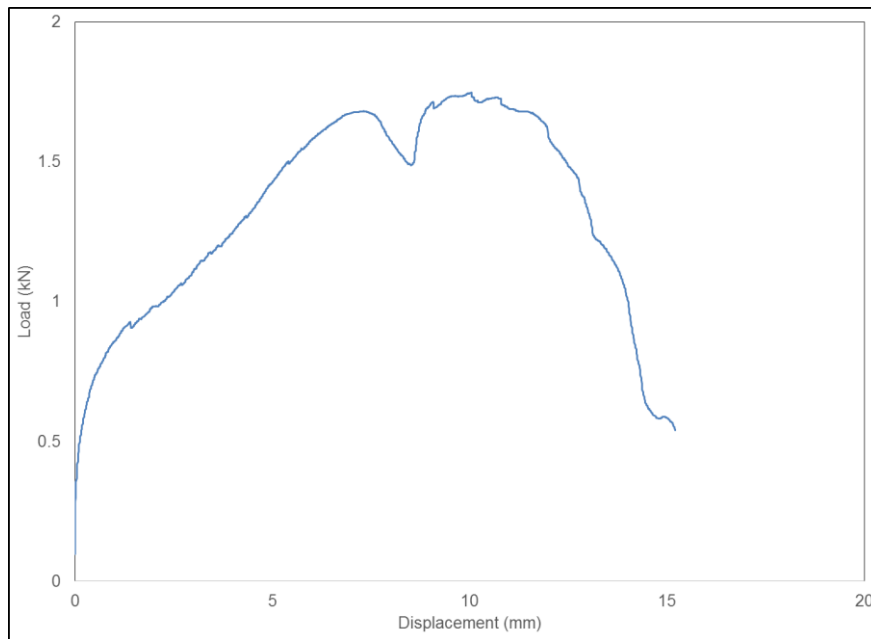


Figure A.9: Load versus displacement for SCWF shear wall type 9



**Figure A.10: Load versus displacement for No.10x25.4mm screw connection
test 1 (SPF to Grandrib 3)**



**Figure A.11: Load versus displacement for No.10x25.4mm screw connection
test 2 (SPF to Grandrib 3)**

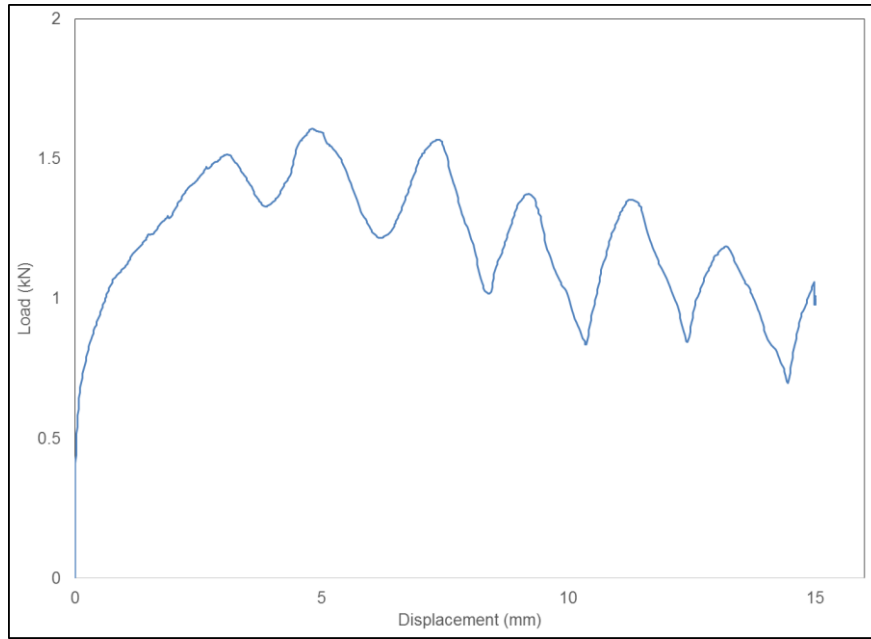


**Figure A.12: Load versus displacement for No.10x25.4mm screw connection
test 3 (SPF to Grandrib 3)**

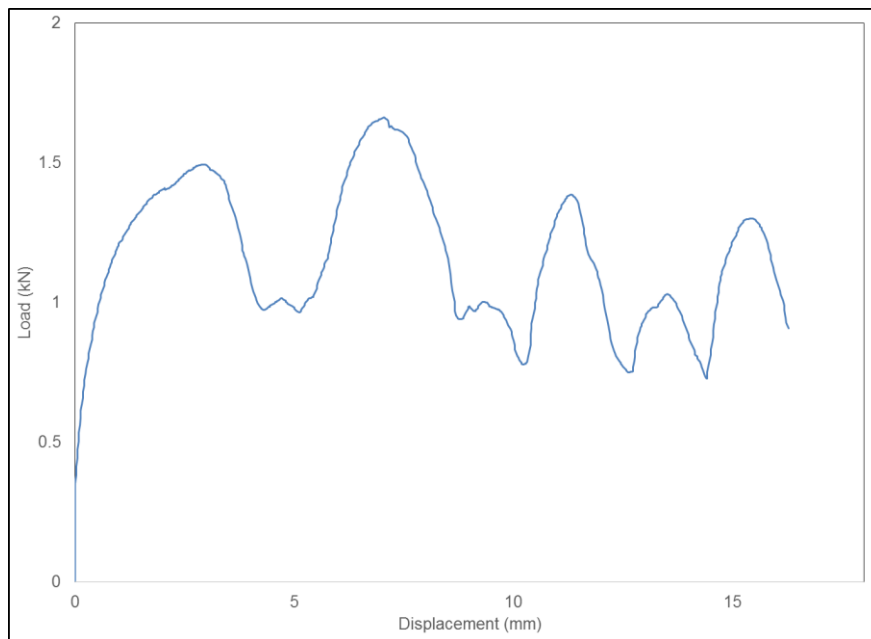


**Figure A.13: Load versus displacement for No.10x25.4mm screw connection
test 4 (SPF to Grandrib 3)**

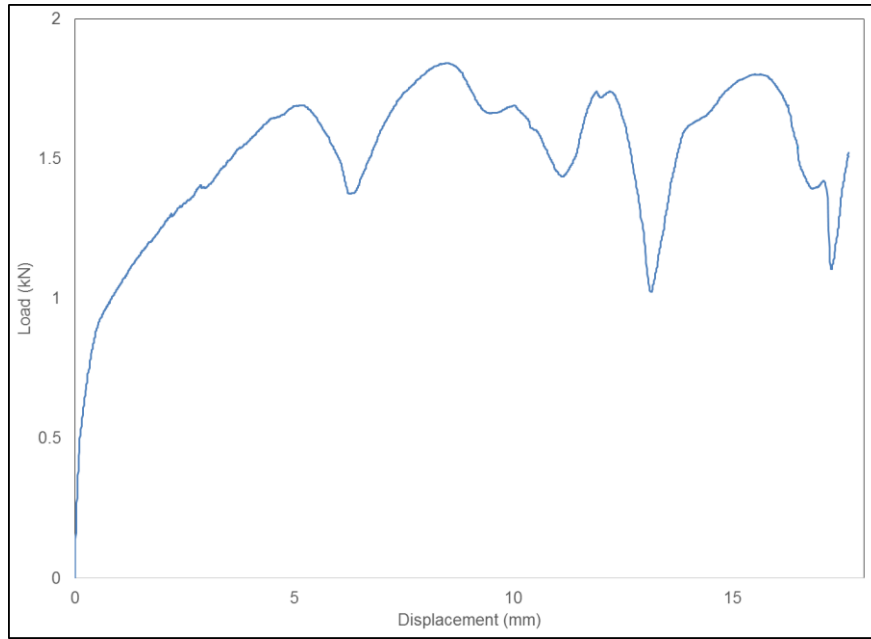


**Figure A.14: Load versus displacement for No.10x25.4mm screw connection
test 6 (SPF to Grandrib 3)**

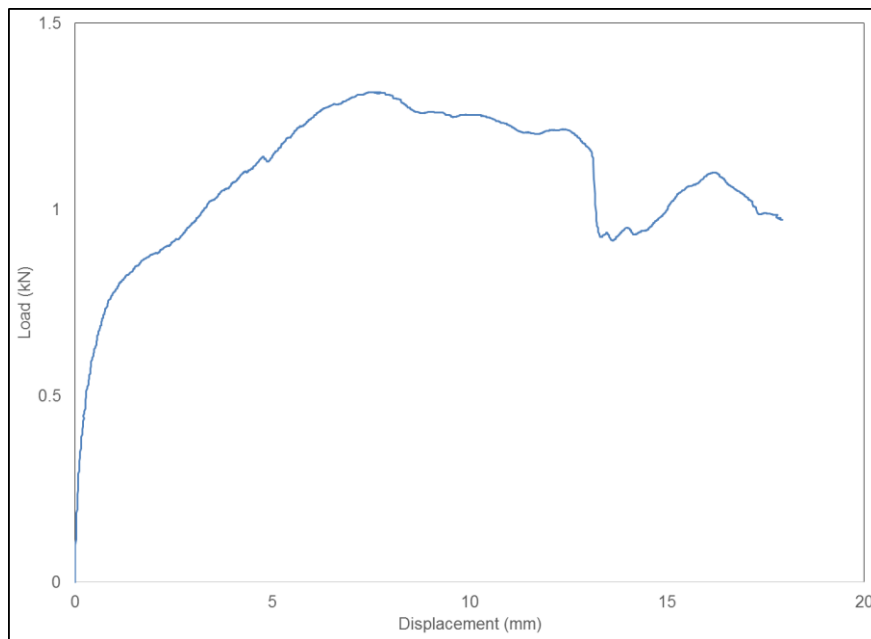


**Figure A.15: Load versus displacement for No.10x25.4mm screw connection
test 7 (SPF to Grandrib 3)**

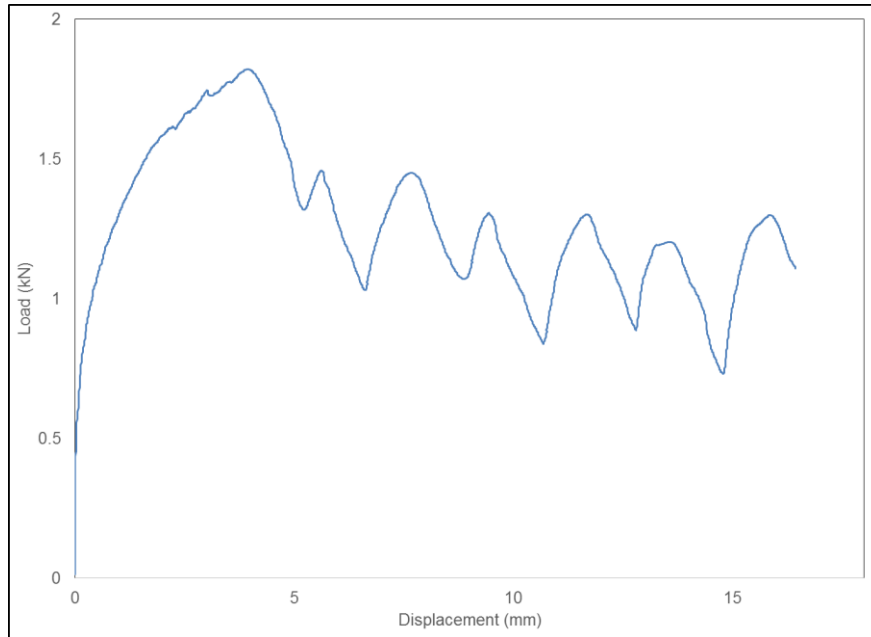


Figure A.16: Load versus displacement for No.10x25.4mm screw connection test 8 (SPF to Grandrib 3)

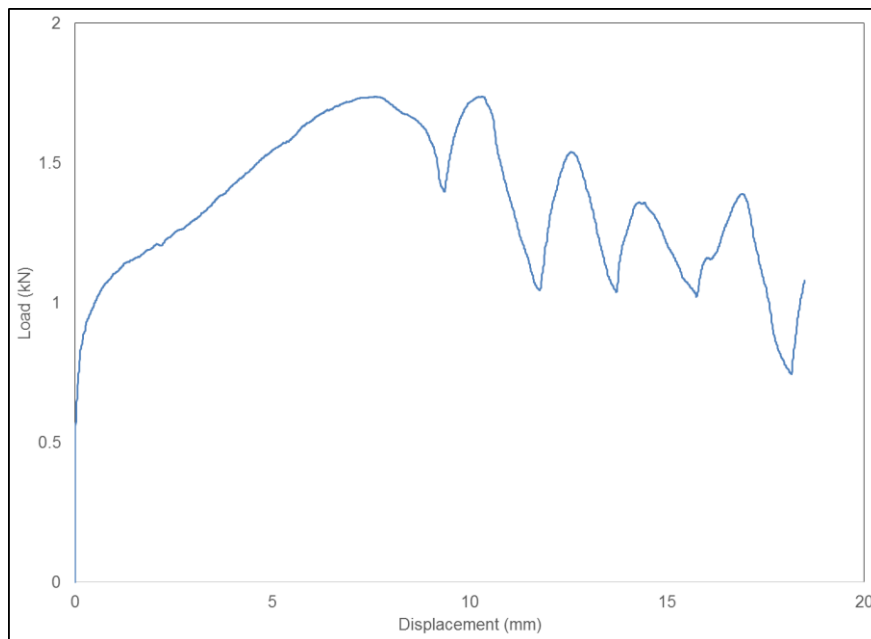


Figure A.17: Load versus displacement for No.10x25.4mm screw connection test 9 (SPF to Grandrib 3)

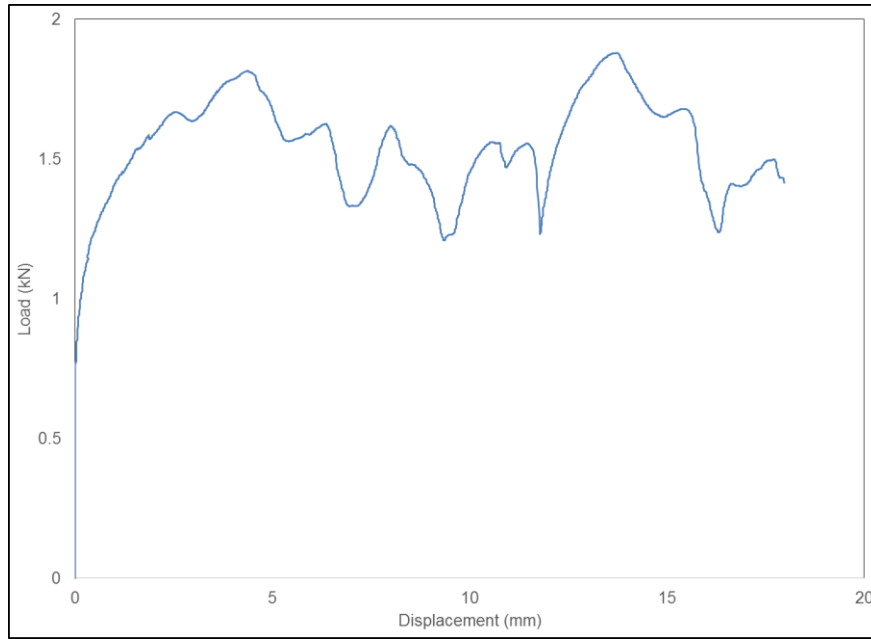


Figure A.18: Load versus displacement for No.10x25.4mm screw connection test 10 (SPF to Grandrib 3)

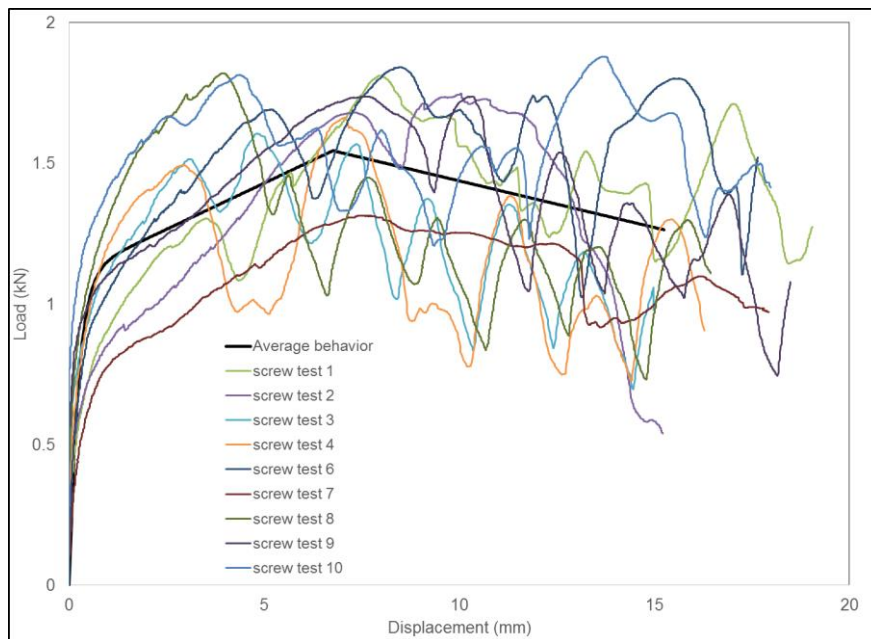


Figure A.19: Average load versus displacement for No.10x25.4 mm screw (SPF to Grandrib 3)

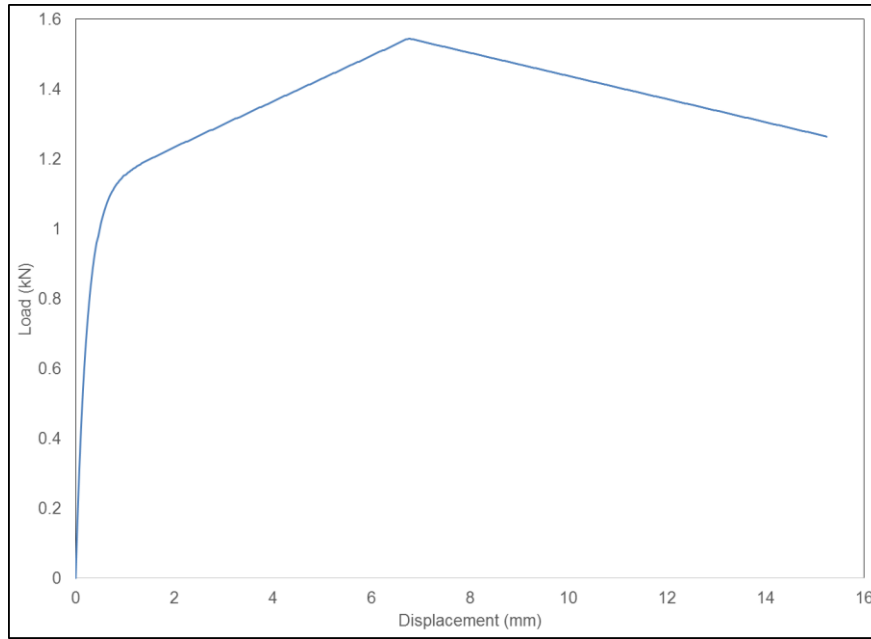


Figure A.20: Average load versus displacement for No.10x25.4 mm screw (SPF to Grandrib 3) used in FEA model

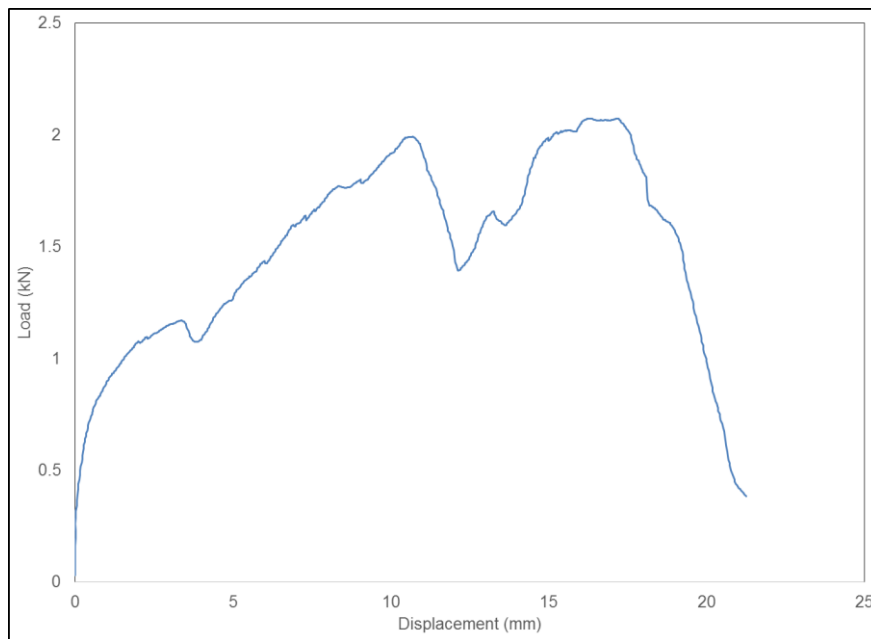


Figure A.21: Load versus displacement for No.10x25.4mm screw connection test 1 (SPF to Wick)

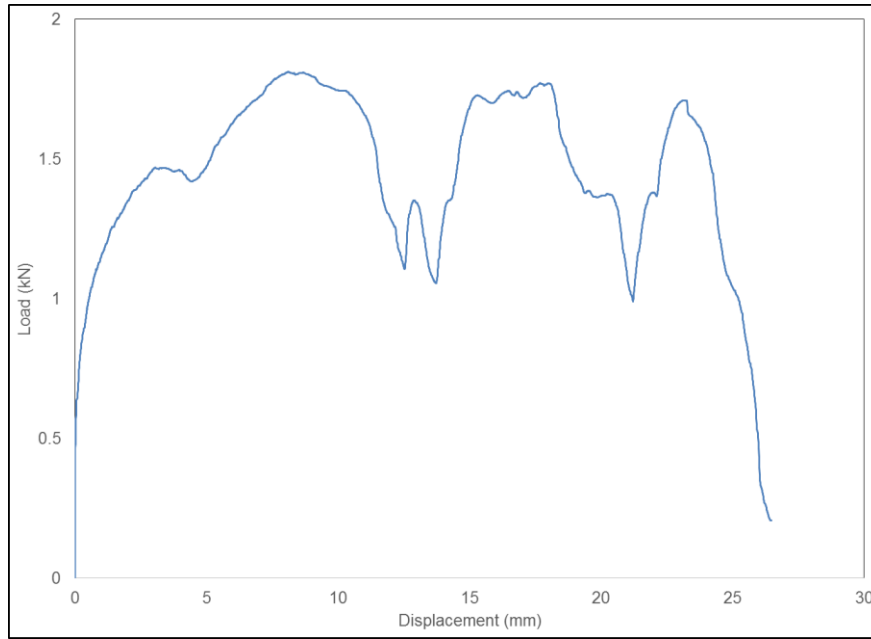


Figure A.22: Load versus displacement for No.10x25.4mm screw connection test 2 (SPF to Wick)

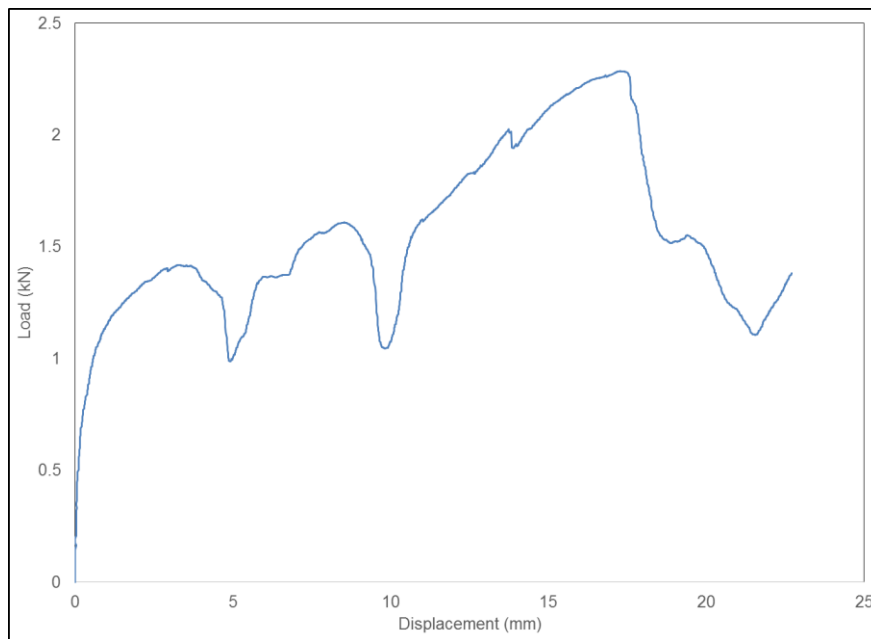
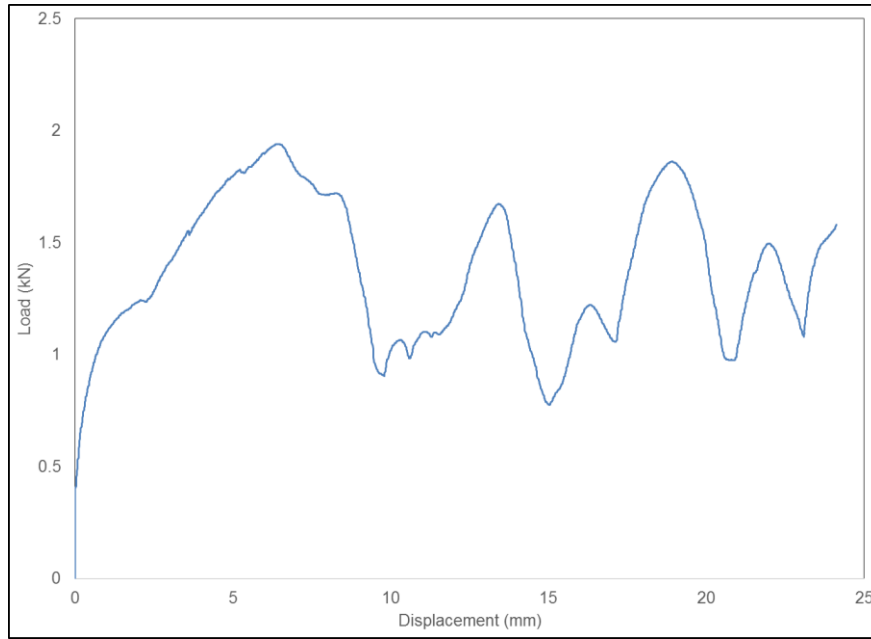
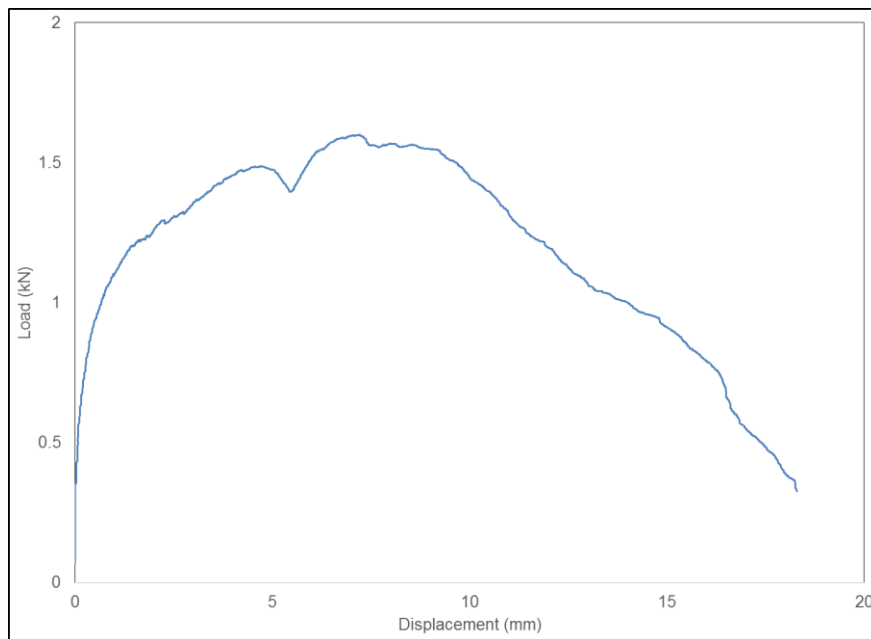


Figure A.23: Load versus displacement for No.10x25.4mm screw connection test 3 (SPF to Wick)



**Figure A.24: Load versus displacement for No.10x25.4mm screw connection
test 4 (SPF to Wick)**



**Figure A.25: Load versus displacement for No.10x25.4mm screw connection
test 6 (SPF to Wick)**

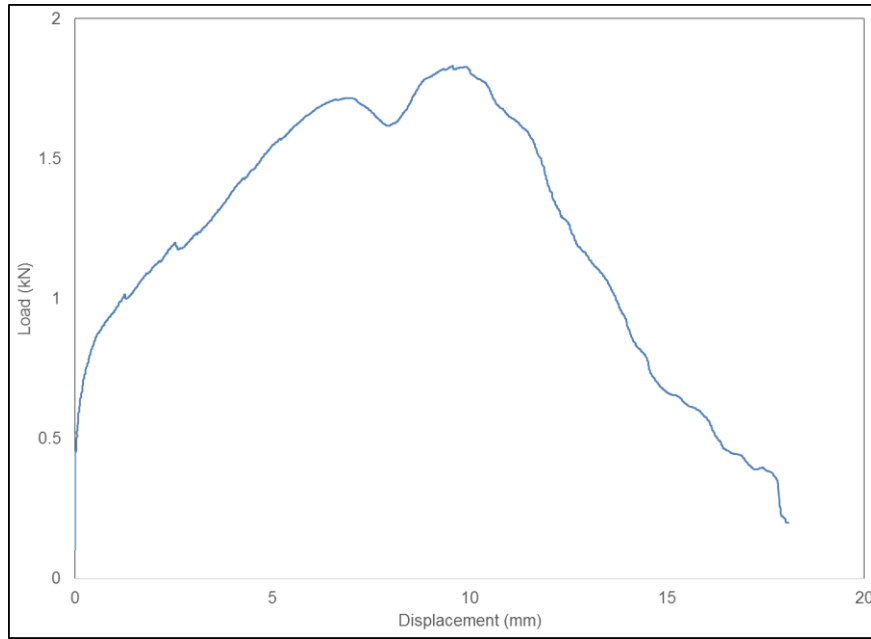


Figure A.26: Load versus displacement for No.10x25.4mm screw connection test 7 (SPF to Wick)

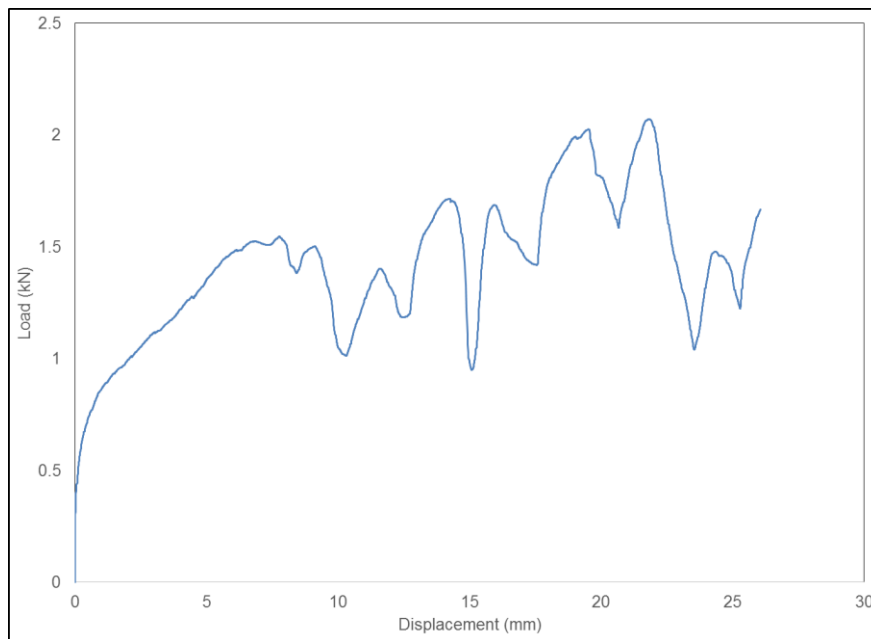


Figure A.27: Load versus displacement for No.10x25.4mm screw connection test 8 (SPF to Wick)

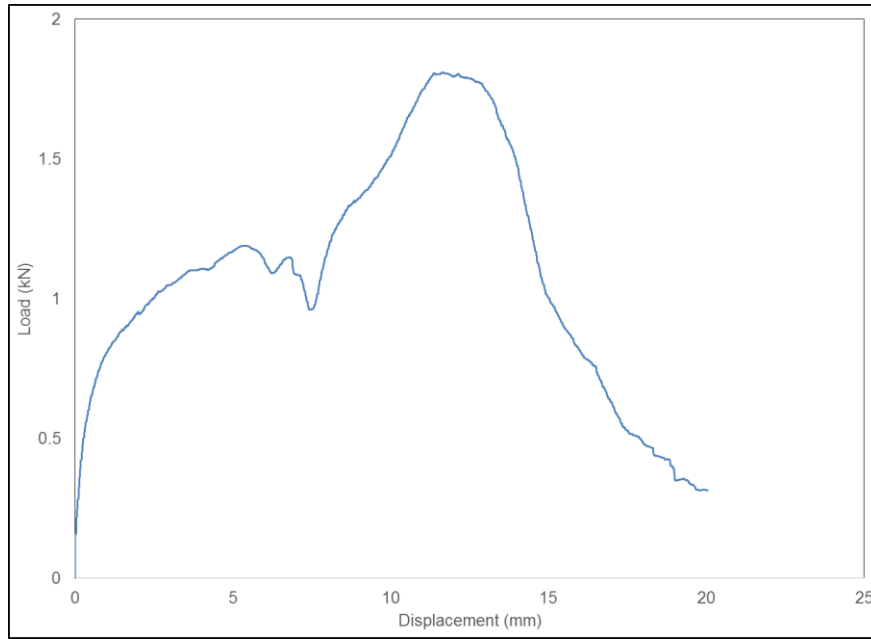


Figure A.28: Load versus displacement for No.10x25.4mm screw connection test 9 (SPF to Wick)

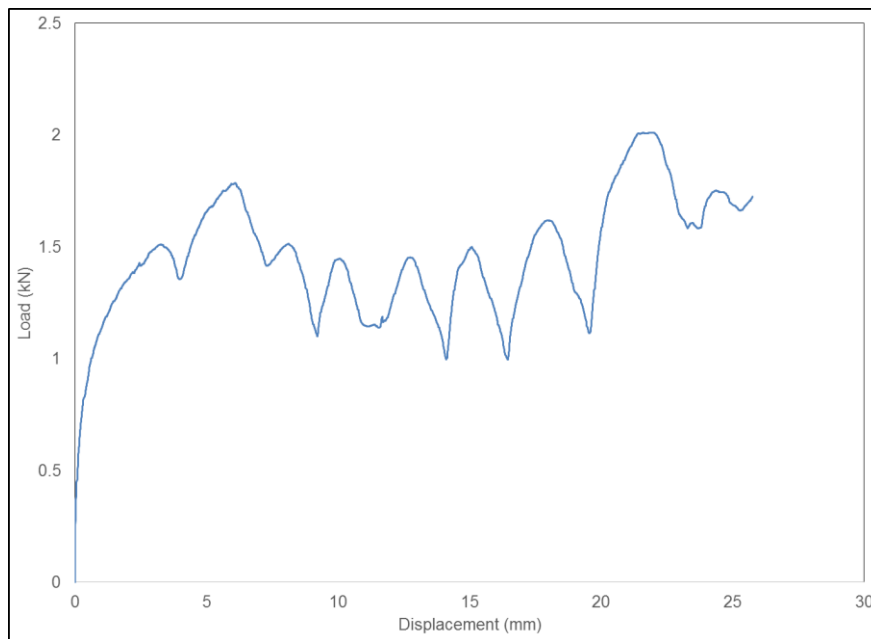


Figure A.29: Load versus displacement for No.10x25.4mm screw connection test 10 (SPF to Wick)

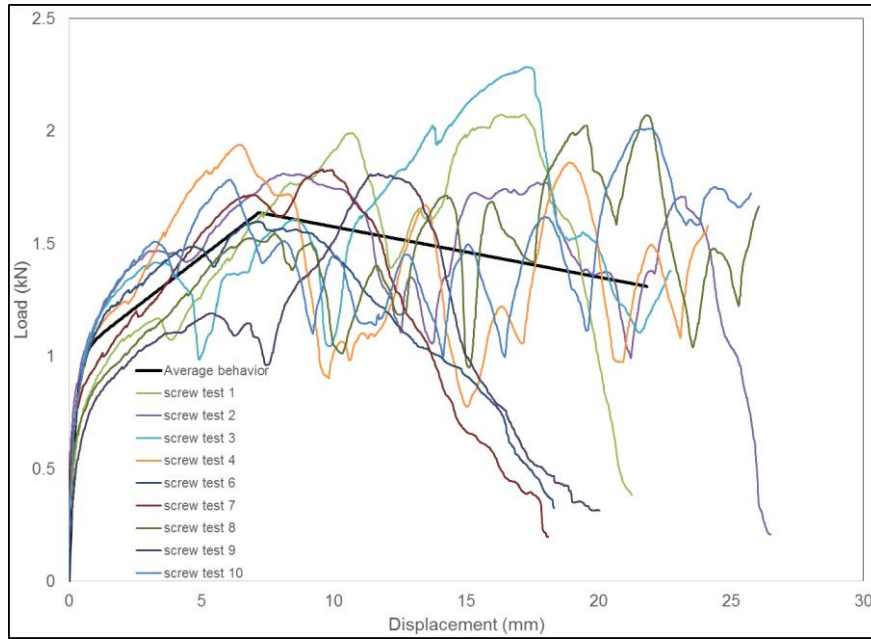


Figure A.30: Average load versus displacement for No.10x25.4 mm screw (SPF to Wick)

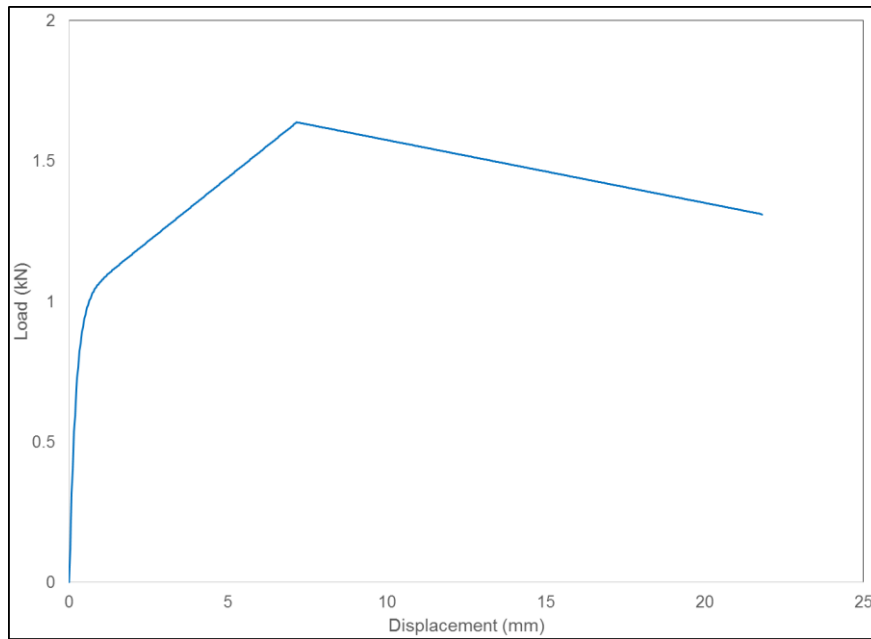
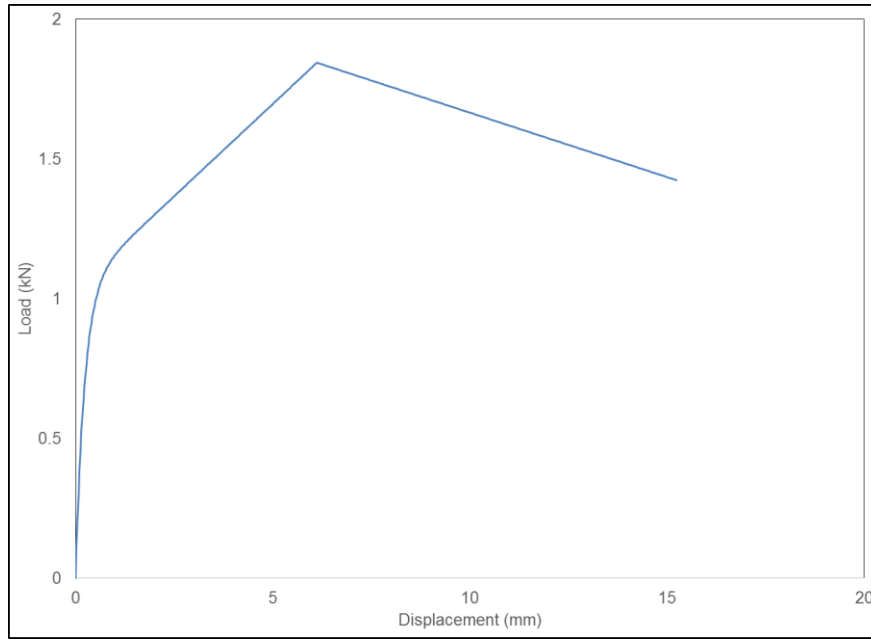
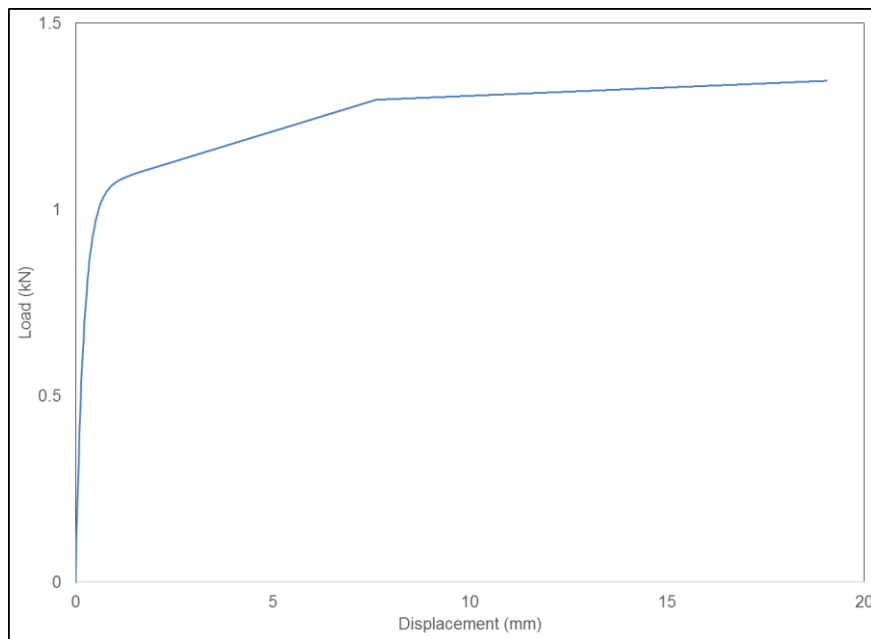


Figure A.31: Average load versus displacement for No.10x25.4 mm screw (SPF to Wick) used in FEA model



**Figure A.32: Average load versus displacement for No.12x19.1 mm screw
(between Grandrib 3) used in FEA model**



**Figure A.33: Average load versus displacement for No.12x38.1 mm screw
(between Grandrib 3) used in FEA model**

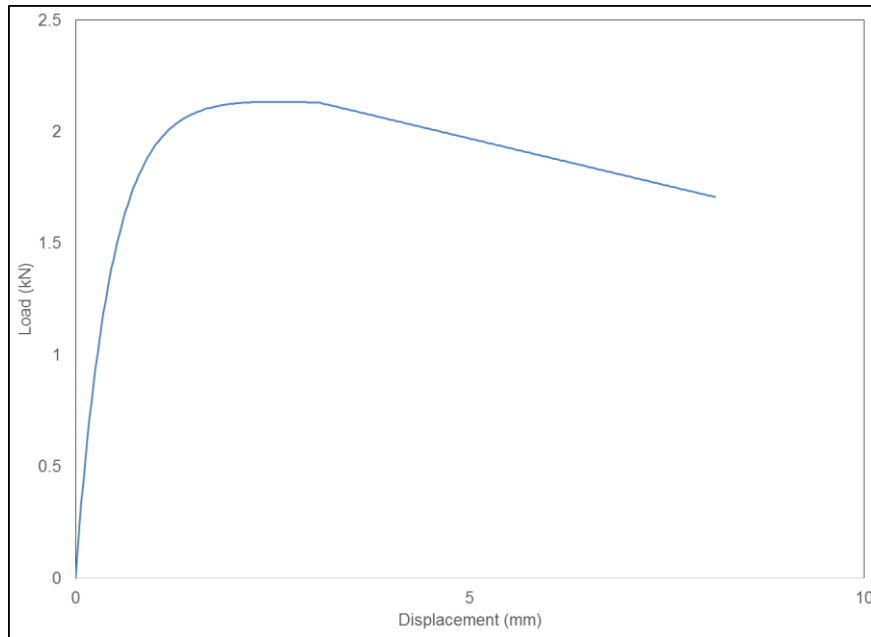


Figure A.34: Average load versus displacement for No.12x19.1 mm screw (between Wick) used in FEA model

**APPENDIX B SEISMIC DESIGN COEFFICIENTS FOR STEEL-CLAD, WOOD-
FRAMED SHEAR WALLS**

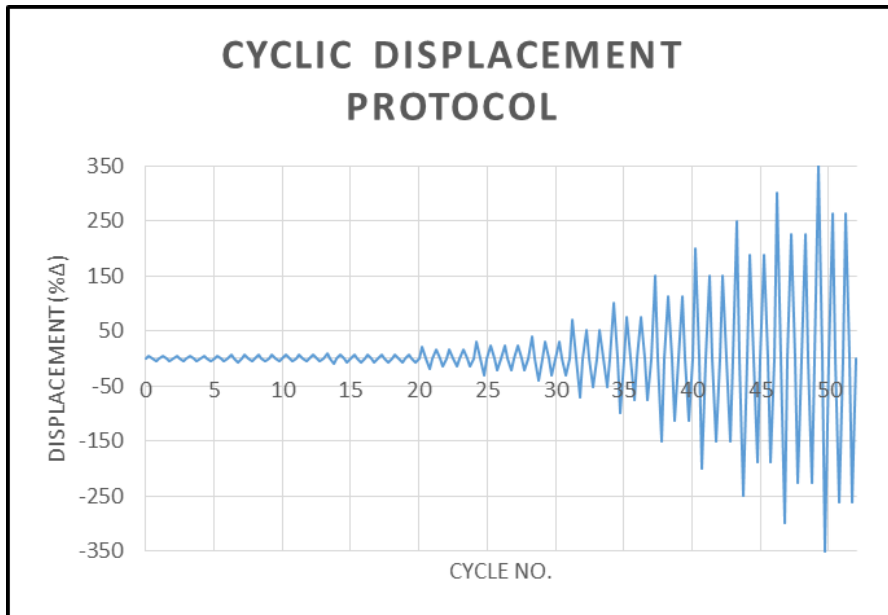


Figure B.1: Cyclic loading protocol, $\Delta = 91.44$ mm (ASTM E2126-11)

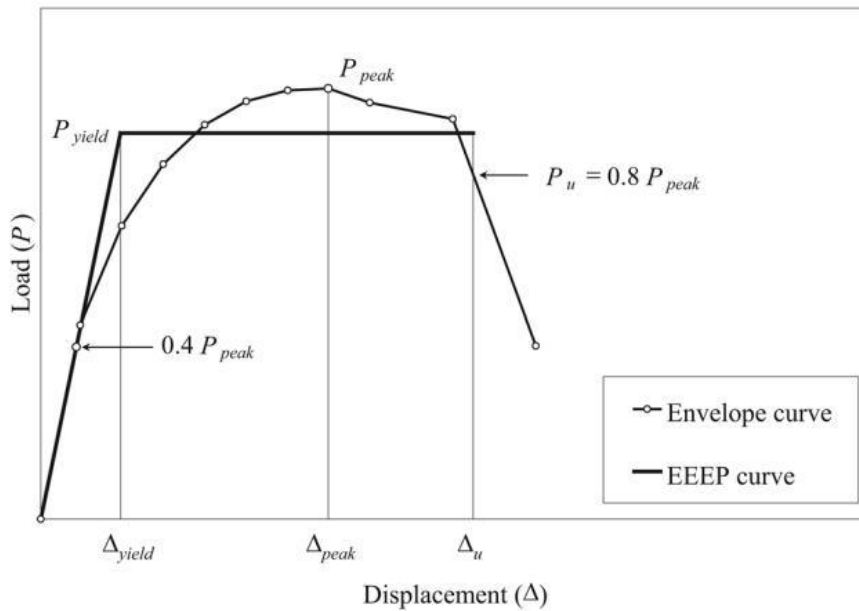


Figure B.2: Performance parameters of specimens (ASTM E2126-11)

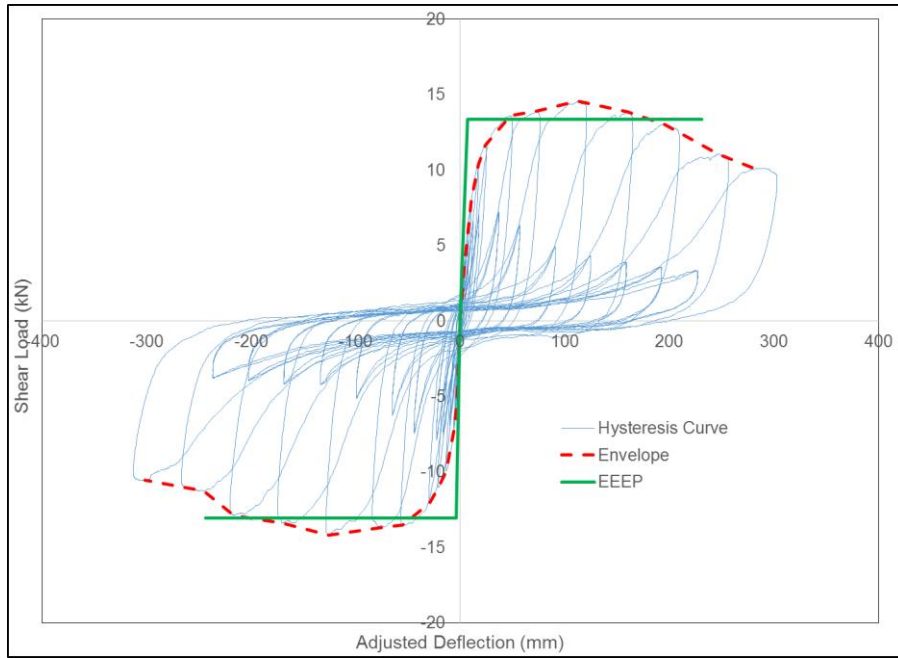


Figure B.3: Hysteresis, Envelop, and EEEP curves of wall 1-1

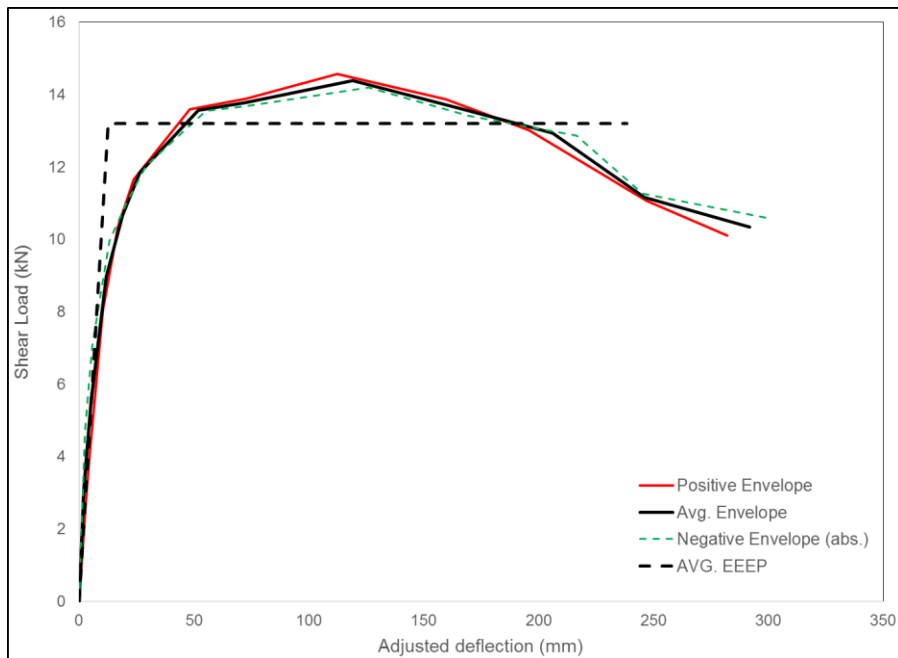


Figure B.4: Average envelop, and EEEP curve of wall 1-1

Table B.1 Average calculated hysteresis parameters. Wall type 1.

Primary Cycle #	$\Delta @$ F_{max} (mm)	F_{max} (kN)	$\Delta @$ F_{min} (mm)	F_{min} (kN)	Strain Energy (kN mm)	Hysteresis Energy (kN mm)	ζ	Cyclic Stiffness (kN/mm)
1	1.702	1.434	-2.483	-4.651	6.995	1.896	0.043	1.358
3	3.086	2.743	-4.089	-5.921	16.338	7.788	0.076	1.168
5	4.496	4.045	-5.944	-7.094	30.177	16.234	0.086	1.047
7	10.351	8.022	-13.227	-9.95	107.322	82.974	0.123	0.764
9	17.082	10.343	-20.739	-11.007	202.477	169.054	0.133	0.568
11	23.889	11.658	-29.153	-12.039	314.735	267.015	0.135	0.45
13	48.254	13.592	-55.359	-13.541	702.742	874.108	0.198	0.263
15	72.803	13.889	-71.704	-13.663	995.426	1191.028	0.19	0.191
17	112.376	14.572	-125.901	-14.185	1711.724	1896.091	0.176	0.121
19	159.633	13.869	-169.786	-13.405	2244.966	2079.739	0.147	0.083
21	195.675	13.012	-216.376	-12.877	2666.198	2092.334	0.125	0.063
23	246.99	11.065	-245.193	-11.265	2747.522	2156.404	0.125	0.045
25	282.061	10.111	-301.542	-10.569	3019.458	2172.348	0.115	0.035

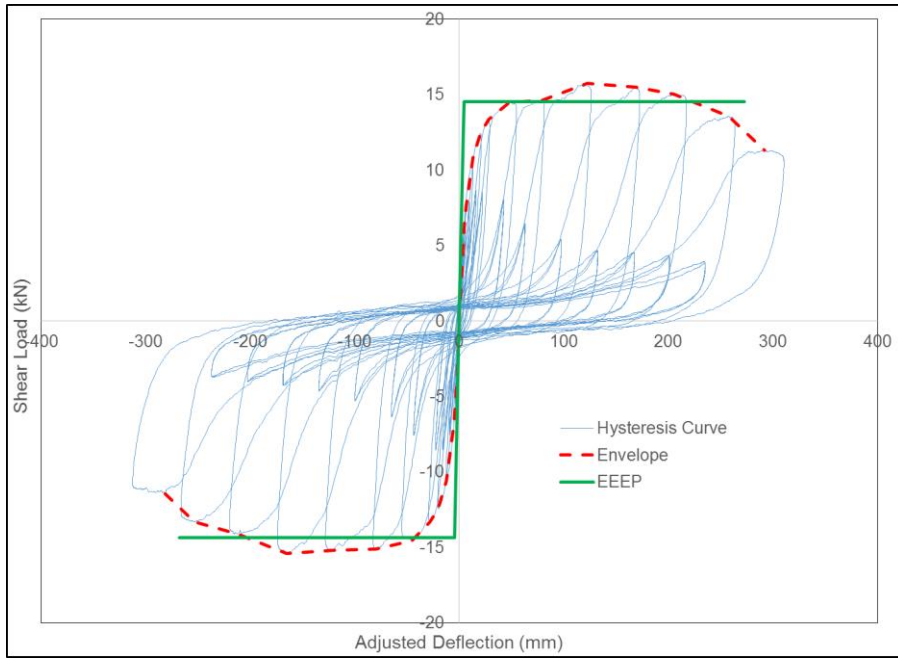


Figure B.5: Hysteresis, Envelop, and EEEP curves of wall 2-1

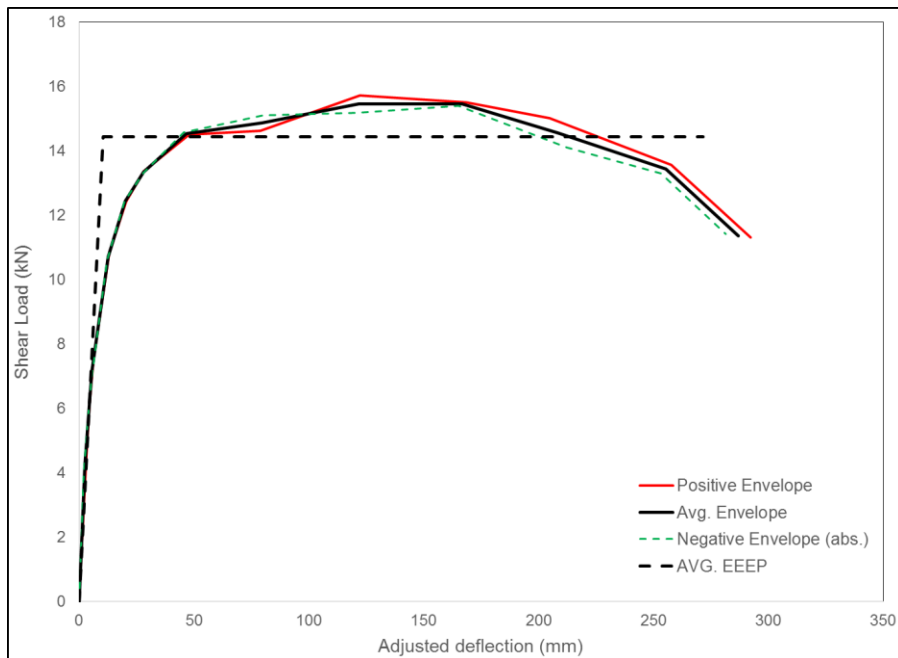


Figure B.6: Average envelop, and EEEP curve of wall 2-1

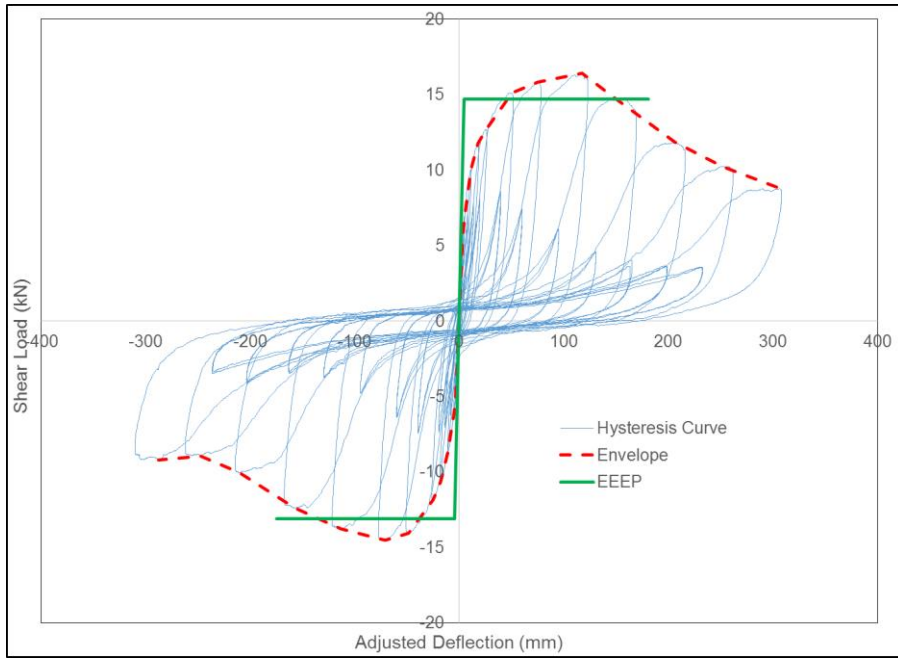


Figure B.7: Hysteresis, Envelop, and EEEP curves of wall 2-2

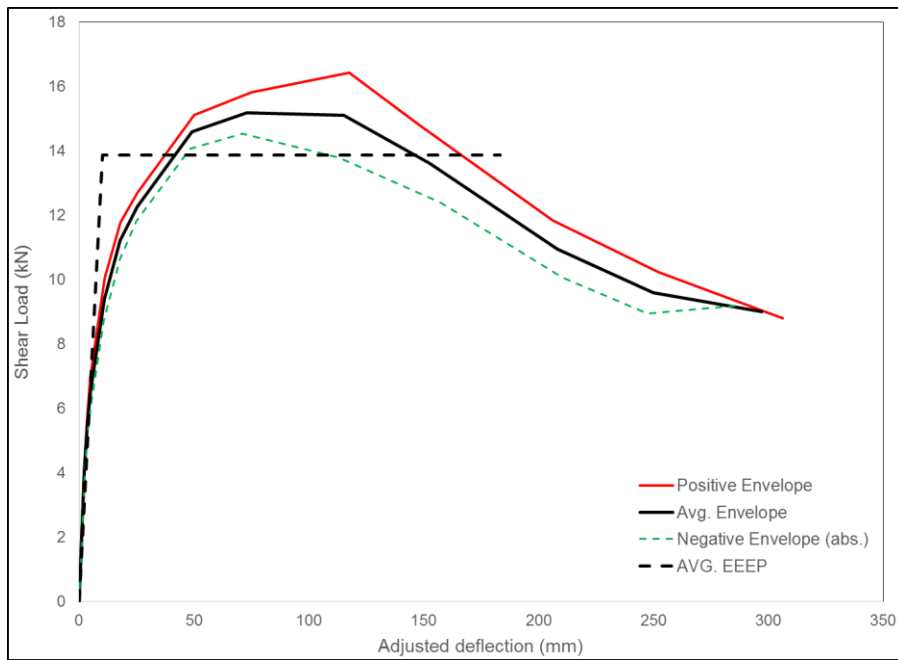


Figure B.8: Average envelop, and EEEP curve of wall 2-2

Table B.2: Average calculated hysteresis parameters. Wall type 2.

Primary Cycle #	$\Delta @$ F_{\max} (mm)	F_{\max} (kN)	$\Delta @$ F_{\min} (mm)	F_{\min} (kN)	Strain Energy (kN mm)	Hysteresis Energy (kN mm)	ζ	Cyclic Stiffness (kN/mm)
1	2.74	4.245	-2.356	-4.001	10.6	2.517	0.038	1.644
3	4.131	5.915	-3.721	-5.418	22.361	7.593	0.054	1.454
5	5.604	7.214	-5.204	-6.476	37.141	16.038	0.069	1.271
7	12.119	10.431	-11.586	-9.667	119.679	90.142	0.12	0.848
9	19.218	12.107	-18.901	-11.546	226.076	192.24	0.136	0.621
11	26.838	13.031	-26.486	-12.578	342.207	291.612	0.136	0.481
13	49.115	14.807	-47.003	-14.318	700.11	906.349	0.207	0.304
15	77.029	15.226	-75.658	-14.821	1147.139	1207.082	0.168	0.198
17	119.955	16.08	-117.155	-14.489	1814.122	1926.301	0.169	0.129
19	158.255	15.165	-161.195	-13.902	2325.196	2125.307	0.146	0.092
21	205.582	13.428	-211.433	-12.084	2658.165	2108.642	0.127	0.062
23	255.039	11.9	-250.289	-11.127	2915.27	2129.998	0.117	0.046
25	299.317	10.047	-284.658	-10.315	2965.421	2149.904	0.116	0.035

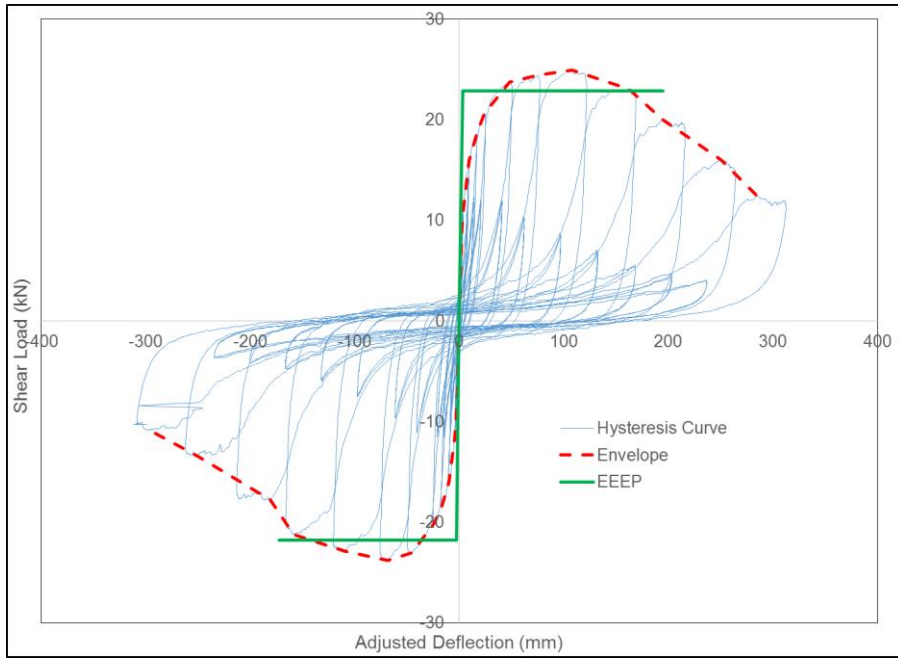


Figure B.9: Hysteresis, Envelop, and EEEP curves of wall 4-1

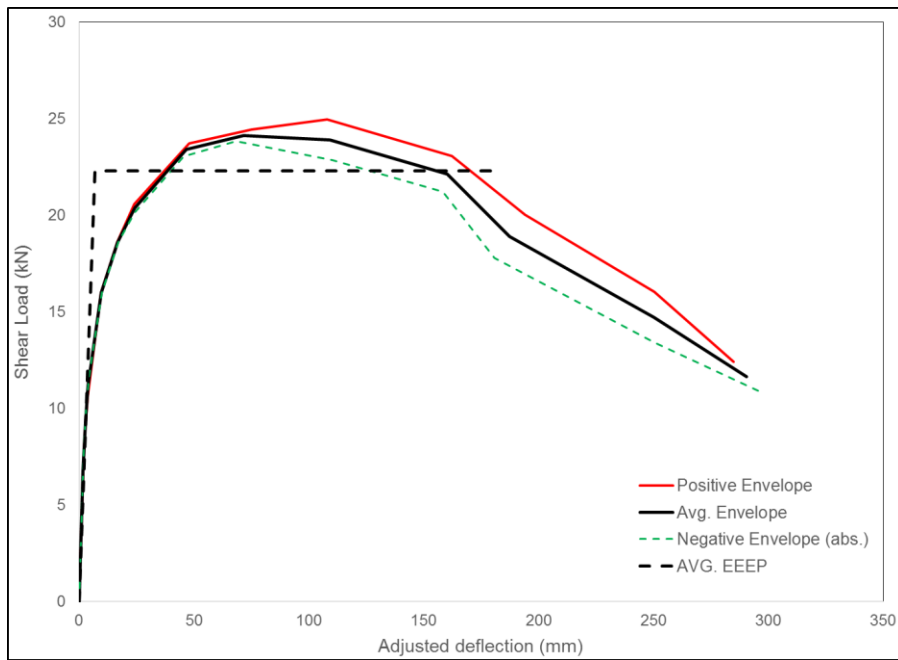


Figure B.10: Average envelop, and EEEP curve of wall 4-1

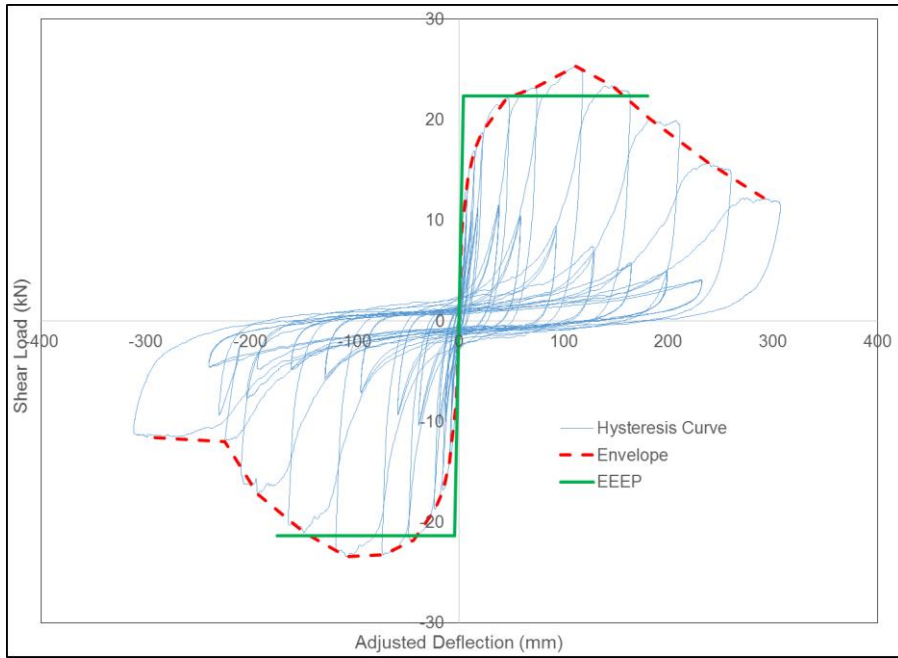


Figure B.11: Hysteresis, Envelop, and EEEP curves of wall 4-2

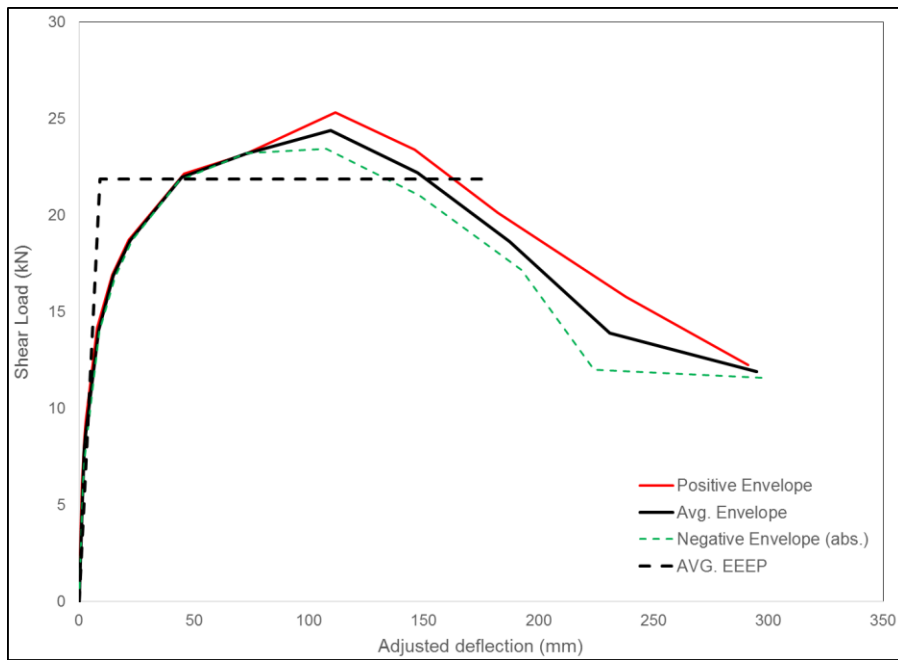


Figure B.12: Average envelop, and EEEP curve of wall 4-2

Table B.3: Average calculated hysteresis parameters. Wall type 4.

Primary Cycle #	$\Delta @$ F_{max} (mm)	F_{max} (kN)	$\Delta @$ F_{min} (mm)	F_{min} (kN)	Strain Energy (kN mm)	Hysteresis Energy (kN mm)	ζ	Cyclic Stiffness (kN/mm)
1	1.518	5.998	-1.88	-6.872	11.013	0.548	0.009	3.817
3	2.41	8.532	-2.744	-8.639	22.36	5.699	0.039	3.335
5	3.379	9.999	-3.883	-10.076	36.952	15.416	0.062	2.775
7	8.735	15.065	-9.509	-14.998	137.705	116.763	0.134	1.653
9	15.526	17.763	-16.332	-17.702	283.227	254.193	0.143	1.115
11	22.867	19.662	-23.775	-19.423	456.467	389.738	0.135	0.839
13	46.87	22.943	-44.628	-22.431	1038.88	1285.336	0.197	0.496
15	73.832	23.8	-70.555	-23.52	1708.383	1762.914	0.164	0.328
17	109.735	25.15	-108.982	-23.146	2641.128	2936.018	0.177	0.221
19	154.331	23.23	-153.353	-21.112	3410.901	3167.031	0.148	0.145
21	188.17	20.071	-186.786	-17.483	3520.132	3024.115	0.137	0.101
23	244.126	15.903	-237.297	-12.71	3454.173	2559.375	0.118	0.06
25	287.998	12.322	-297.469	-11.214	3442.3	2576.968	0.119	0.04

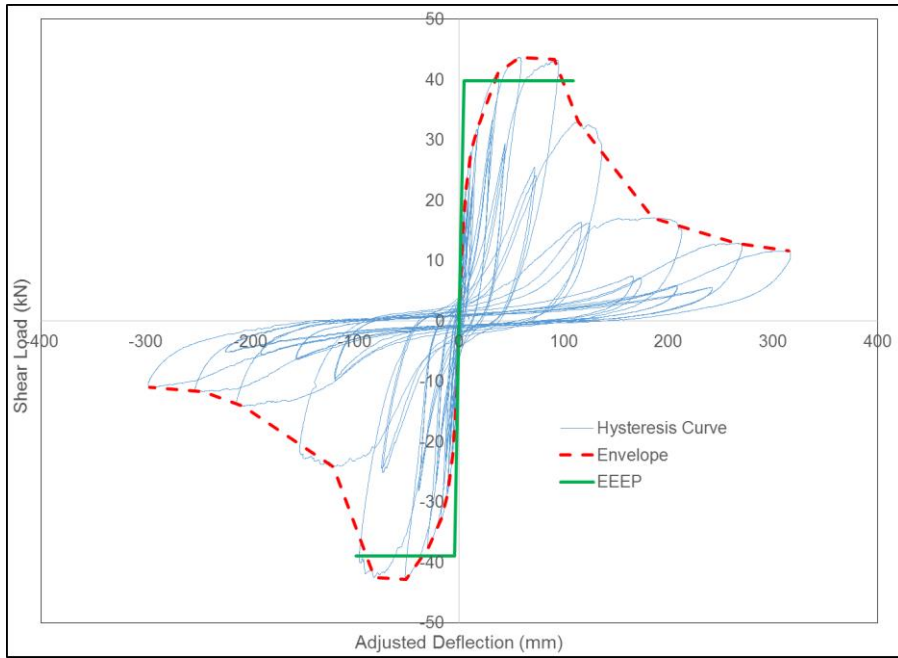


Figure B.13: Hysteresis, Envelop, and EEEP curves of wall 5-1

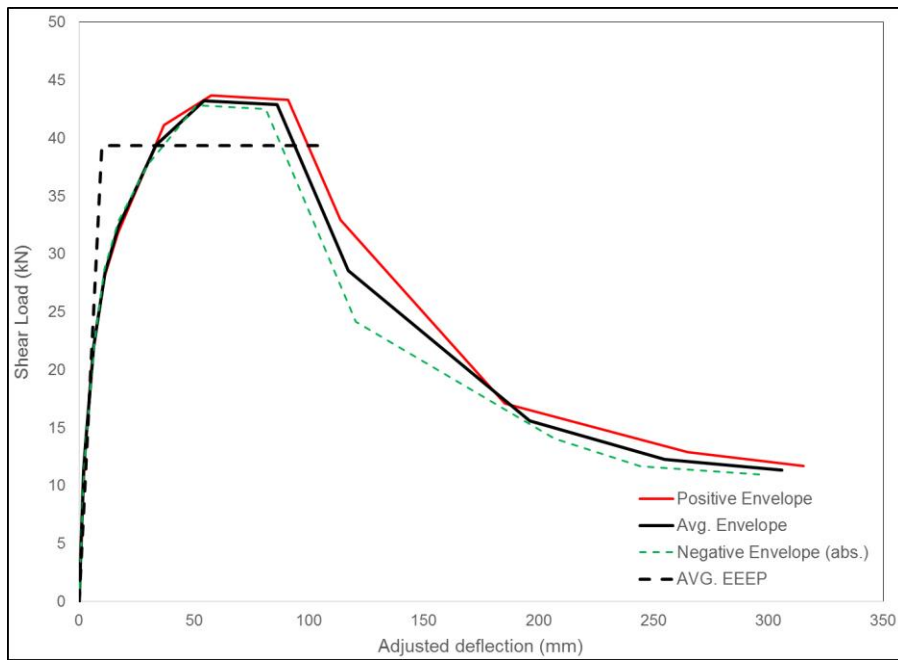


Figure B.14: Average envelop, and EEEP curve of wall 5-1

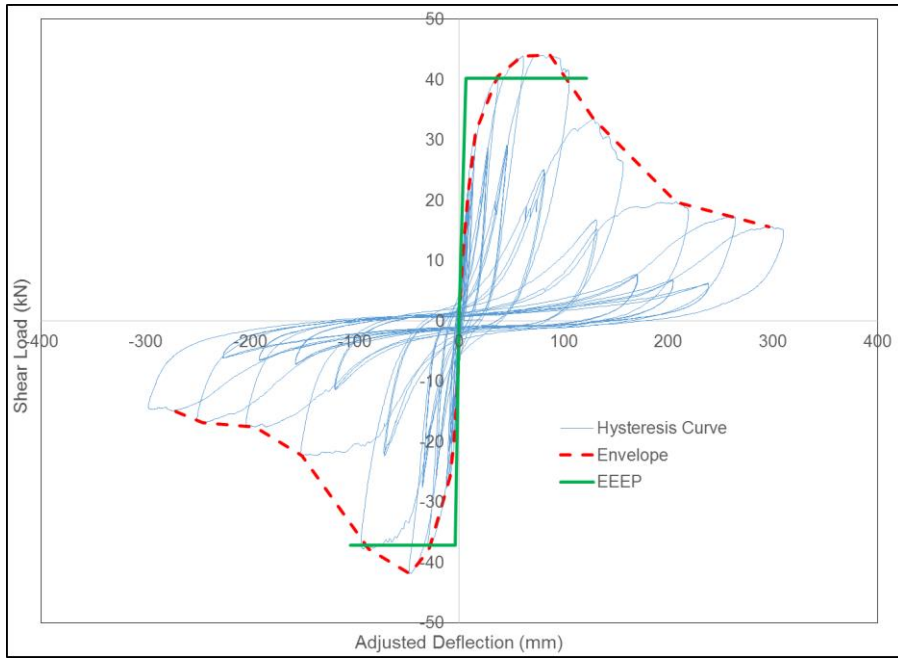


Figure B.15: Hysteresis, Envelop, and EEEP curves of wall 5-2

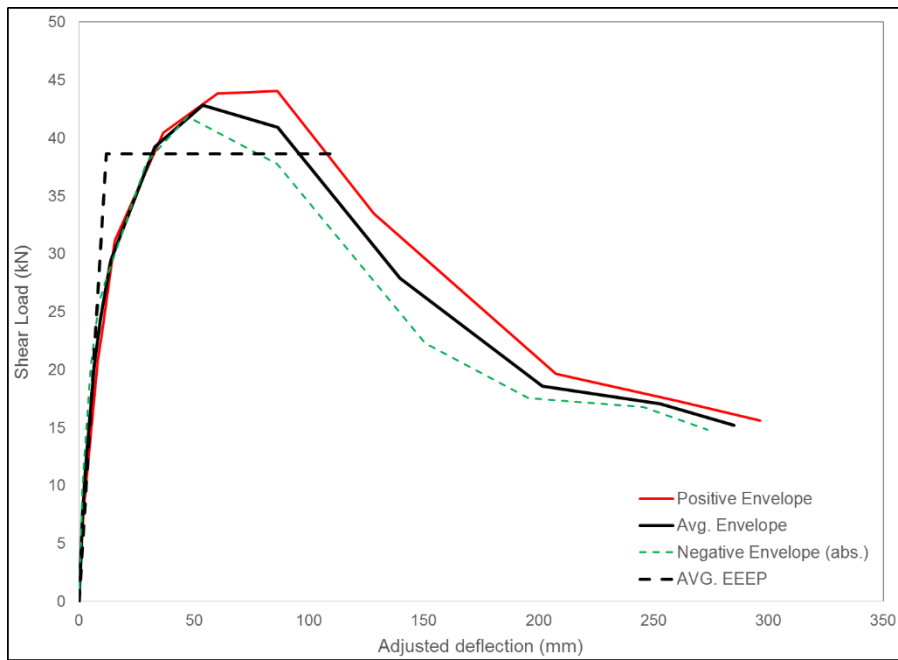


Figure B.16: Average envelop, and EEEP curve of wall 5-2

Table B.4: Average calculated hysteresis parameters. Wall type 5.

Primary Cycle #	$\Delta @$ F_{\max} (mm)	F_{\max} (kN)	$\Delta @$ F_{\min} (mm)	F_{\min} (kN)	Strain Energy (kN mm)	Hysteresis Energy (kN mm)	ζ	Cyclic Stiffness (kN/mm)
1	1.753	7.826	-1.257	-7.61	11.623	2.144	0.029	5.348
3	2.55	10.392	-1.861	-10.744	23.275	1.919	0.014	5.091
5	3.442	12.612	-2.6	-13.154	38.85	9.143	0.038	4.468
7	7.249	21.25	-5.826	-21.199	138.933	84.919	0.098	3.335
9	10.694	25.686	-9.887	-27.178	273.349	184.16	0.106	2.585
11	16.374	31.481	-14.336	-30.234	477.957	337.68	0.113	2.038
13	36.865	40.802	-29.636	-37.825	1312.569	1117.476	0.136	1.192
15	58.938	43.755	-49.178	-42.331	2330.778	1825.369	0.125	0.802
17	88.776	43.69	-83.811	-40.142	3618.086	3860.563	0.17	0.487
19	121.095	33.218	-135.604	-23.233	3580.536	4419.188	0.197	0.225
21	196.514	18.375	-201.228	-15.817	3399.035	3515.603	0.166	0.086
23	262.735	15.078	-245.028	-14.25	3724.626	2643.11	0.114	0.058
25	305.943	13.64	-284.877	-12.9	3903.685	2602.174	0.106	0.045

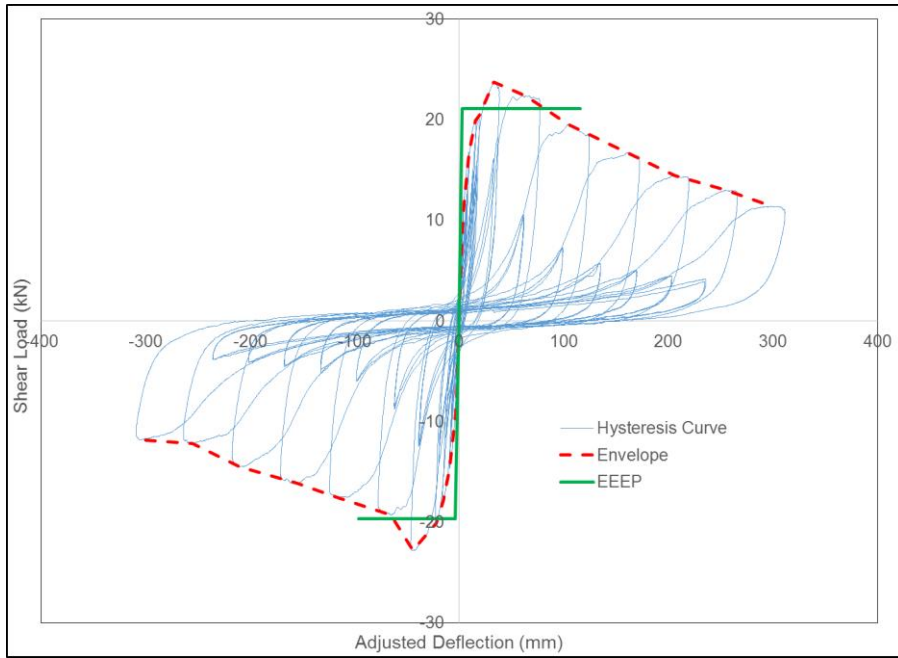


Figure B.17: Hysteresis, Envelop, and EEEP curves of wall 6-1

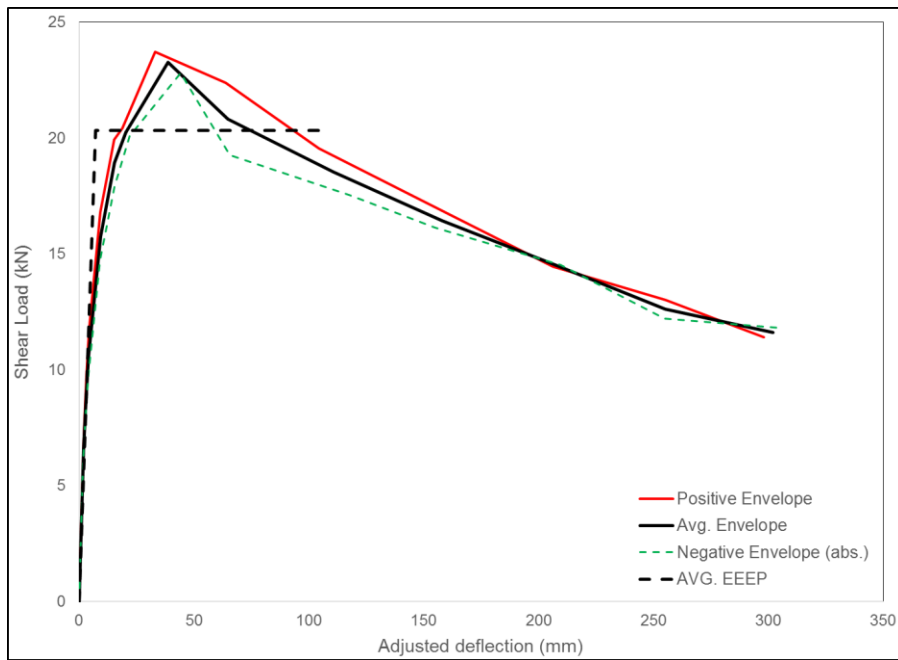


Figure B.18: Average envelop, and EEEP curve of wall 6-1

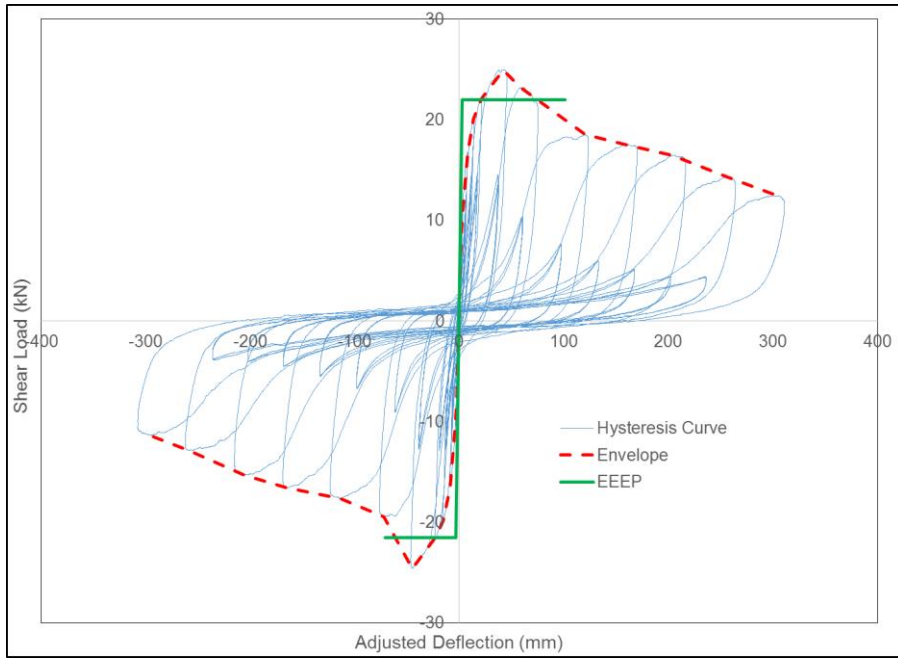


Figure B.19: Hysteresis, Envelop, and EEEP curves of wall 6-2

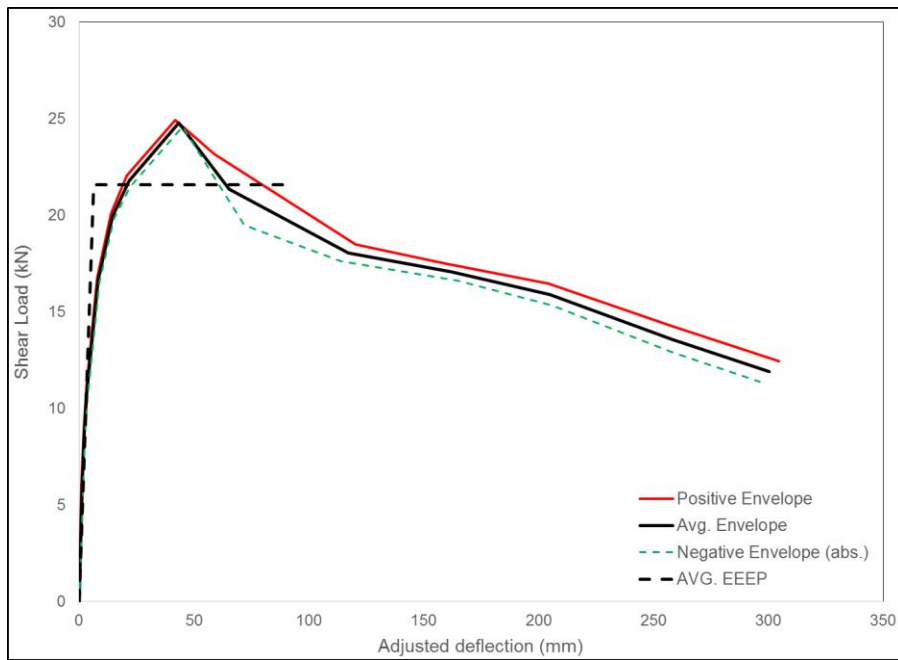


Figure B.20: Average envelop, and EEEP curve of wall 6-2

Table B.5: Average calculated hysteresis parameters. Wall type 6.

Primary Cycle #	$\Delta @$ F_{\max} (mm)	F_{\max} (kN)	$\Delta @$ F_{\min} (mm)	F_{\min} (kN)	Strain Energy (kN mm)	Hysteresis Energy (kN mm)	ζ	Cyclic Stiffness (kN/mm)
1	1.601	6.618	-1.893	-6.286	11.413	0.469	0.008	3.934
3	2.737	9.347	-2.712	-8.204	23.973	4.611	0.031	3.262
5	3.817	11.404	-3.775	-10.018	40.698	14.987	0.059	2.855
7	8.671	16.783	-9.055	-15.624	143.408	111.354	0.124	1.839
9	14.653	20.016	-15.342	-18.863	291.223	241.53	0.132	1.3
11	19.873	21.238	-22.206	-20.787	442.304	336.523	0.121	1.003
13	37.485	24.329	-44.673	-23.707	986.959	1194.884	0.193	0.594
15	61.459	22.775	-68.838	-19.378	1366.514	1860.655	0.217	0.327
17	112.402	19.02	-115.618	-17.583	2083.26	2471.705	0.189	0.161
19	160.074	17.115	-159.972	-16.368	2679.395	2493.299	0.148	0.105
21	205.162	15.465	-207.636	-14.924	3134.901	2559.182	0.13	0.074
23	256.512	13.65	-256.8	-12.545	3362.129	2447.95	0.116	0.051
25	301.378	11.926	-301.057	-11.588	3542.656	2439.315	0.11	0.039

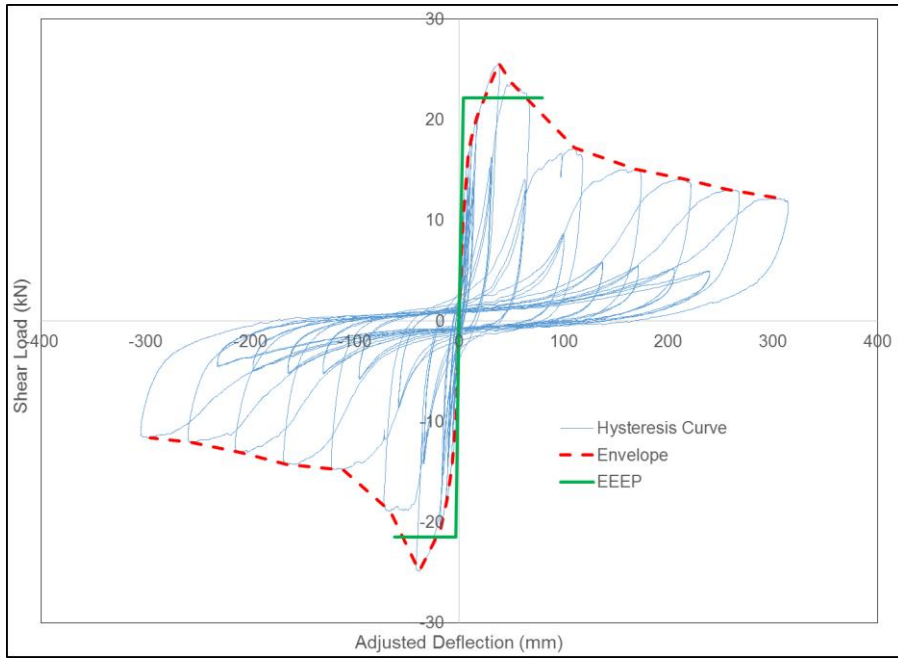


Figure B.21: Hysteresis, Envelop, and EEEP curves of wall 7-2

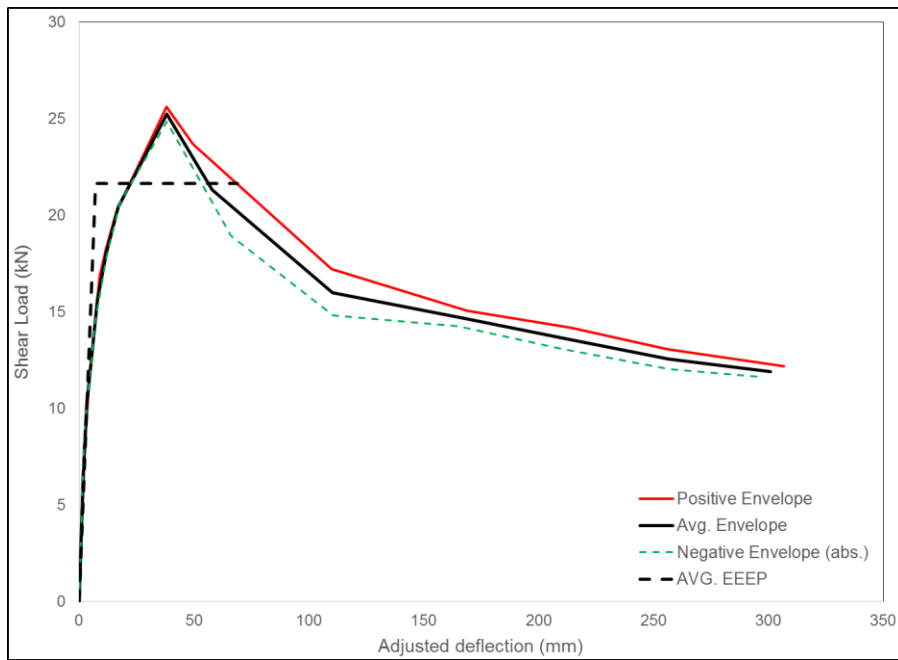


Figure B.22: Average envelop, and EEEP curve of wall 7-2

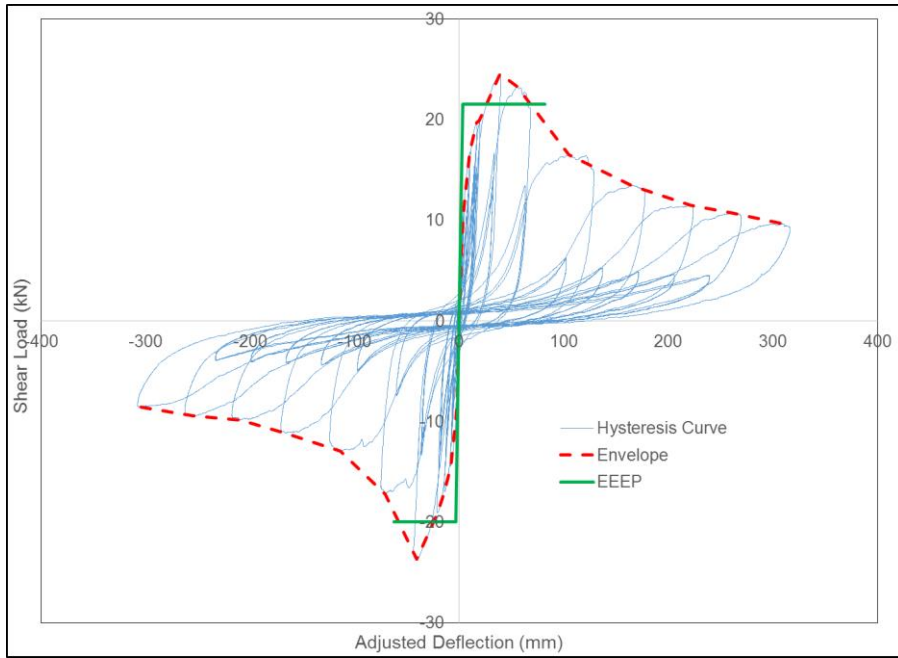


Figure B.23: Hysteresis, Envelop, and EEEP curves of wall 7-3

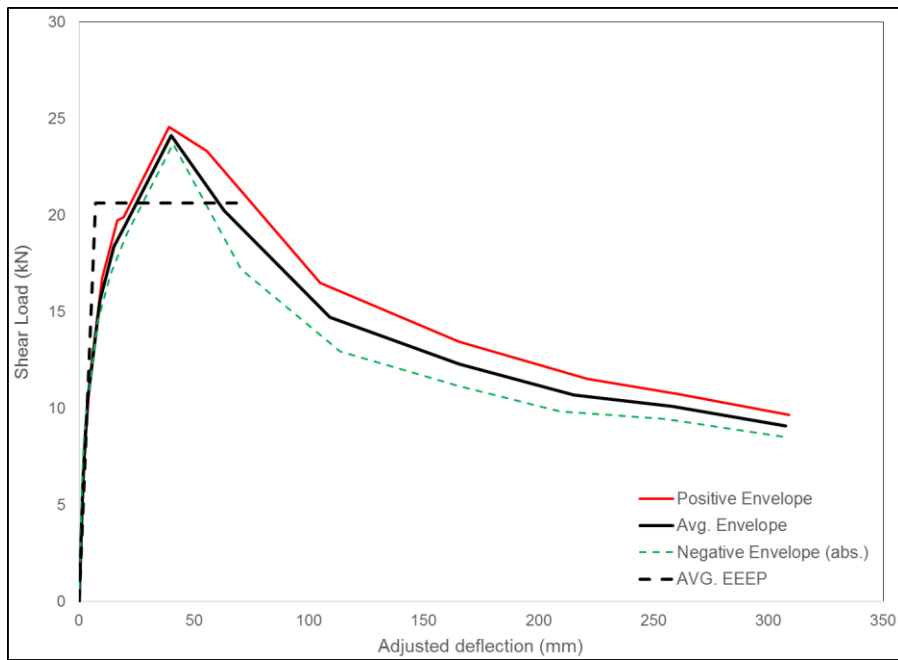


Figure B.24: Average envelop, and EEEP curve of wall 7-3

Table B.6: Average calculated hysteresis parameters. Wall type 7.

Primary Cycle #	Δ @ F_{max} (mm)	F_{max} (kN)	Δ @ F_{min} (mm)	F_{min} (kN)	Strain Energy (kN mm)	Hysteresis Energy (kN mm)	ζ	Cyclic Stiffness (kN/mm)
1	2.071	6.888	-1.359	-5.673	10.988	0.304	0.005	3.757
3	3.398	9.438	-2.039	-7.791	23.99	6.684	0.044	3.302
5	4.512	11.381	-2.956	-9.441	39.682	17.371	0.07	2.872
7	9.595	16.812	-7.579	-14.428	135.315	112.685	0.132	1.838
9	14.237	19.01	-12.884	-17.386	248.082	195.933	0.124	1.365
11	17.93	20.052	-19.377	-19.875	371.595	270.415	0.116	1.081
13	38.675	25.102	-39.548	-24.268	964.72	1057.047	0.175	0.633
15	52.604	23.507	-68.453	-18.057	1235.019	1679.332	0.217	0.357
17	107.506	16.848	-112.132	-13.867	1682.748	2074.583	0.197	0.14
19	167.196	14.266	-165.228	-12.709	2243.083	1986.153	0.141	0.081
21	217.675	12.844	-209.76	-11.452	2596.928	1931.965	0.119	0.057
23	258.579	11.9	-255.959	-10.737	2911.794	1982.851	0.109	0.044
25	307.946	10.92	-300.733	-10.082	3192.494	2075.52	0.103	0.035

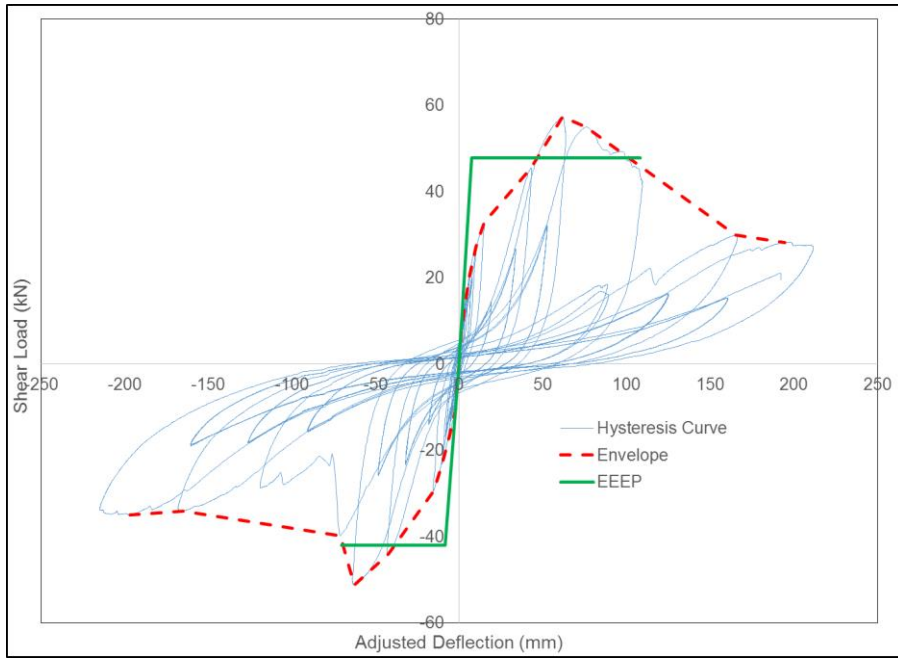


Figure B.25: Hysteresis, Envelop, and EEEP curves of wall 10-1

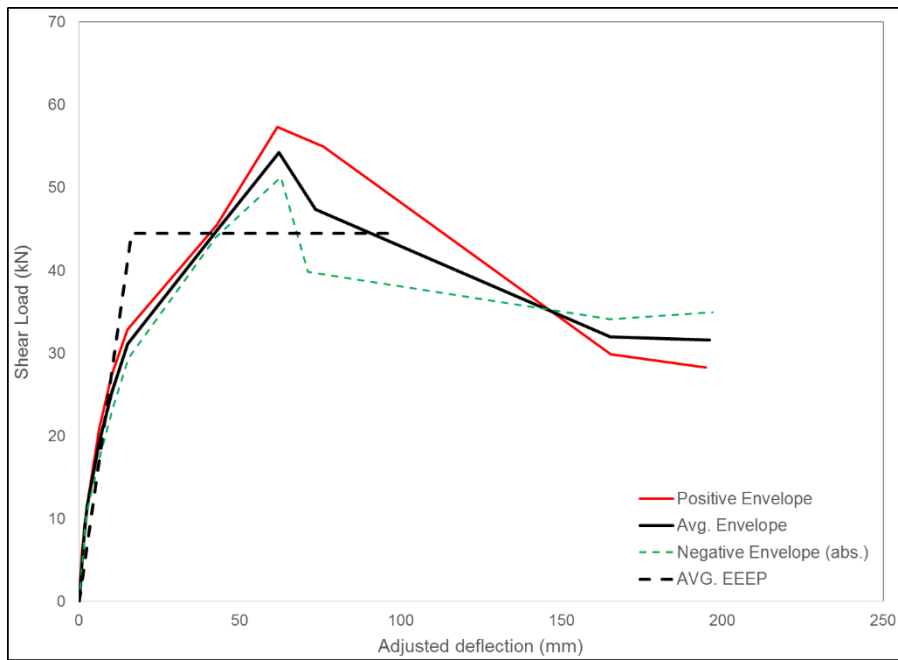


Figure B.26: Average envelop, and EEEP curve of wall 10-1

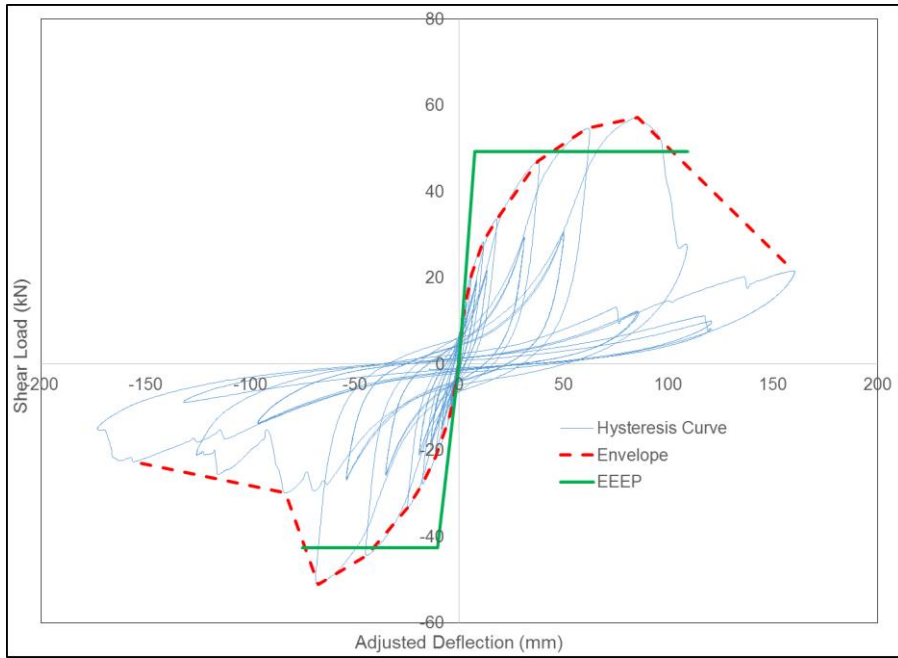


Figure B.27: Hysteresis, Envelop, and EEEP curves of wall 10-2

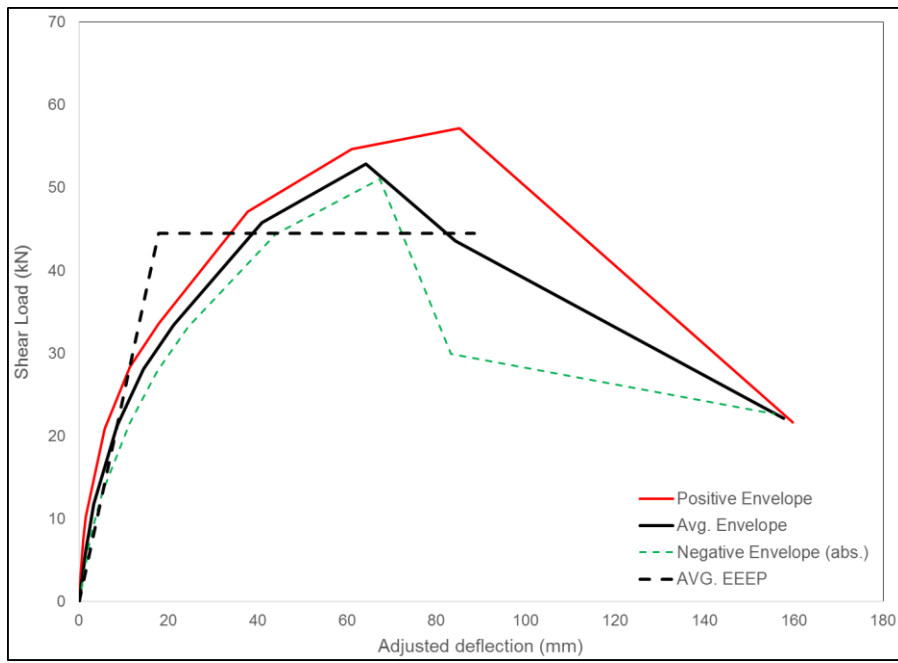


Figure B.28: Average envelop, and EEEP curve of wall 10-2

Table B.7: Average calculated hysteresis parameters. Wall type 10.

Primary Cycle #	$\Delta @$ F_{\max} (mm)	F_{\max} (kN)	$\Delta @$ F_{\min} (mm)	F_{\min} (kN)	Strain Energy (kN mm)	Hysteresis Energy (kN mm)	ζ	Cyclic Stiffness (kN/mm)
1	0.819	5.763	-2.004	-6.865	9.366	2.646	0.047	5.34
3	1.378	8.361	-2.839	-9.617	20.033	0.935	0.007	5.128
5	2.194	11.404	-3.861	-11.967	36.878	9.135	0.04	4.537
7	6.011	20.837	-8.963	-19.664	152.863	99.652	0.103	2.883
9	10.827	27.853	-13.957	-25.569	333.444	249.539	0.118	2.247
11	16.437	33.254	-19.904	-31.294	589.417	455.848	0.123	1.837
13	40.316	46.294	-43.352	-44.211	1890.517	1605.875	0.136	1.088
15	61.379	55.993	-65.094	-51.143	3383.008	3073.667	0.145	0.85
17	80.556	56.073	-77.216	-34.842	3591.303	5027.445	0.223	0.579
19	162.589	25.755	-160.455	-28.38	4389.787	2968.288	0.109	0.167
21	194.818	28.237	-196.99	-34.941	6192.052	4327.46	0.111	0.161

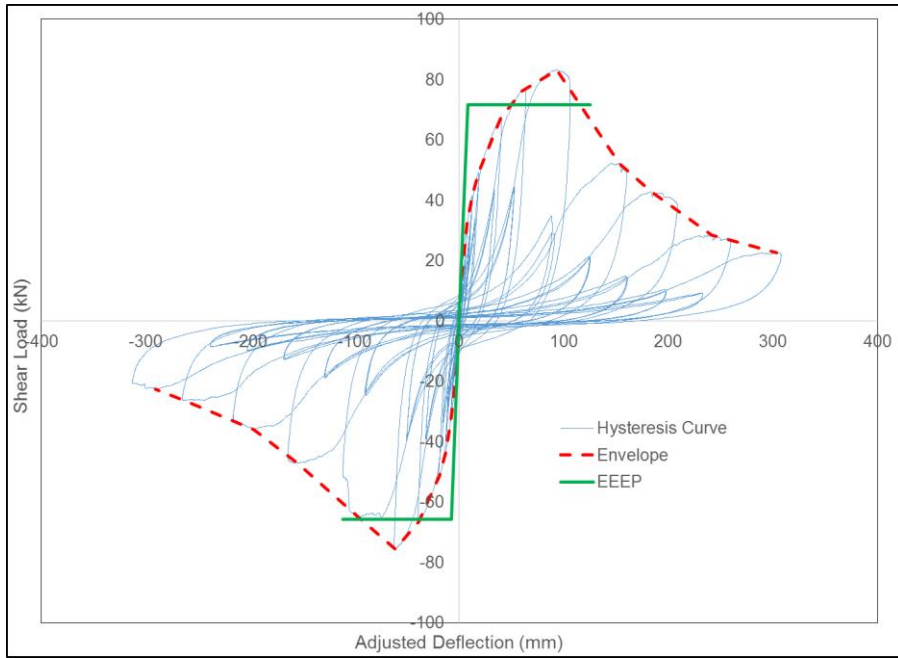


Figure B.29: Hysteresis, Envelop, and EEEP curves of wall 11-2

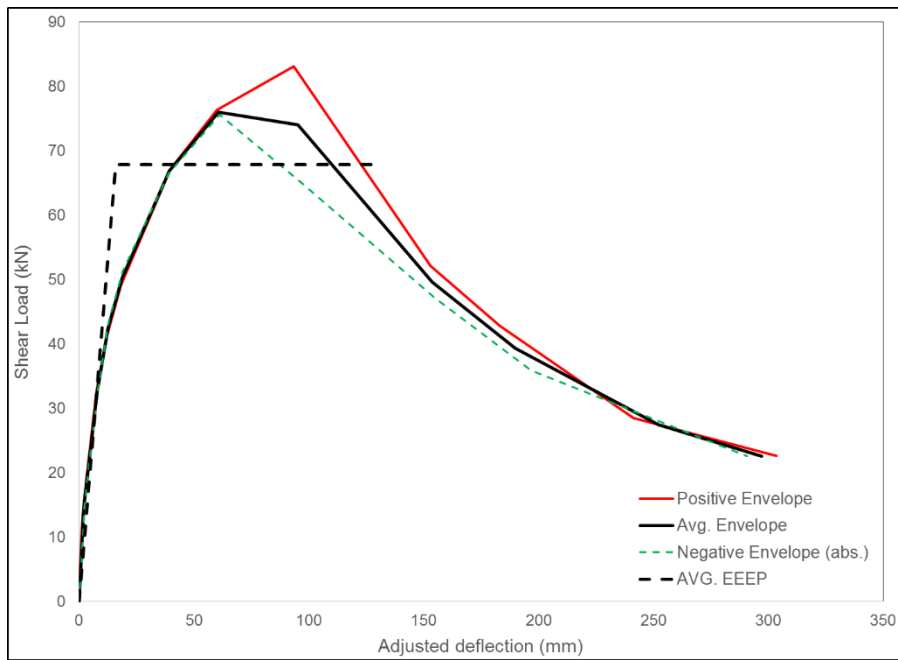


Figure B.30: Average envelop, and EEEP curve of wall 11-2

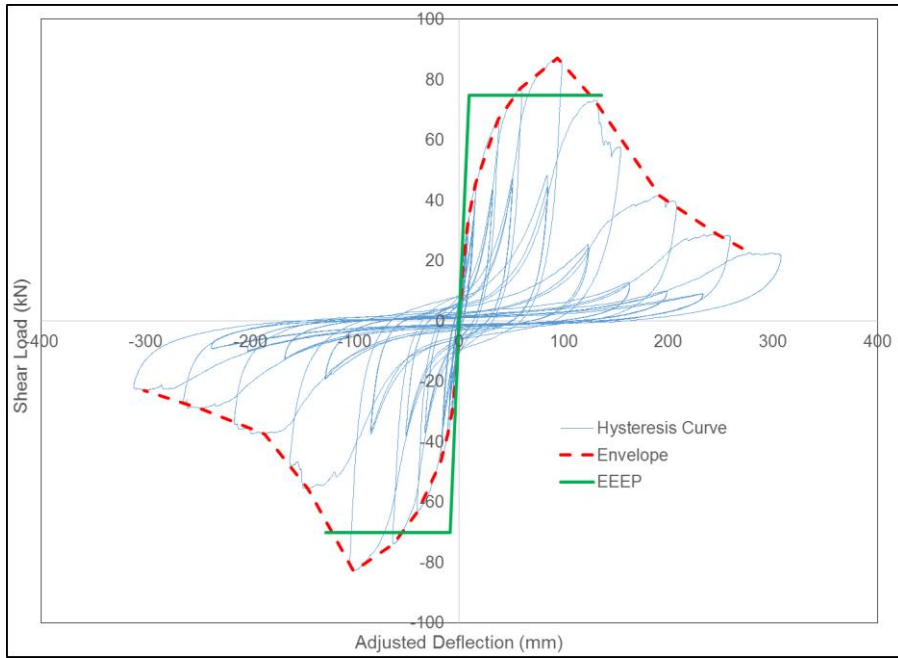


Figure B.31: Hysteresis, Envelop, and EEEP curves of wall 11-3

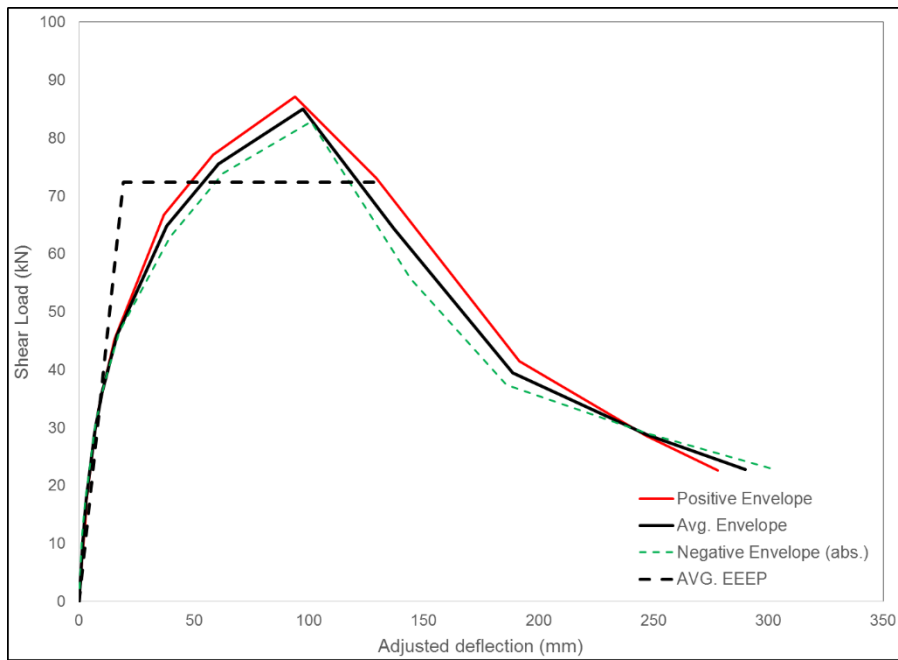


Figure B.32: Average envelop, and EEEP curve of wall 11-3

Table B.8: Average calculated hysteresis parameters. Wall type 11.

Primary Cycle #	$\Delta @$ F_{\max} (mm)	F_{\max} (kN)	$\Delta @$ F_{\min} (mm)	F_{\min} (kN)	Strain Energy (kN mm)	Hysteresis Energy (kN mm)	ζ	Cyclic Stiffness (kN/mm)
1	1.55	9.87	-1.353	-9.556	14.267	6.737	0.075	7.075
3	2.363	14.002	-2.035	-13.946	30.719	2.686	0.014	6.537
5	3.274	18.253	-3.137	-17.952	58.018	8.568	0.023	5.673
7	7.331	30.827	-7.608	-31.538	233.855	128.488	0.087	4.183
9	10.716	37.845	-12.03	-40.662	451.749	282.242	0.099	3.473
11	17.005	47.254	-18.406	-49.005	854.872	620.592	0.116	2.724
13	38.377	66.964	-39.24	-64.743	2555.056	2680.745	0.167	1.699
15	59.246	76.704	-62.071	-74.747	4591.533	4400.261	0.153	1.25
17	93.803	85.113	-99.032	-73.906	7660.29	8591.912	0.18	0.826
19	141.151	62.614	-149.52	-51.428	8191.309	8156.164	0.158	0.399
21	187.433	42.155	-191.402	-36.656	7455.251	6901.457	0.147	0.209
23	244.002	28.555	-255.328	-27.751	7021.52	5273.001	0.12	0.113
25	290.706	22.623	-296.301	-22.739	6657.281	4440.552	0.106	0.078

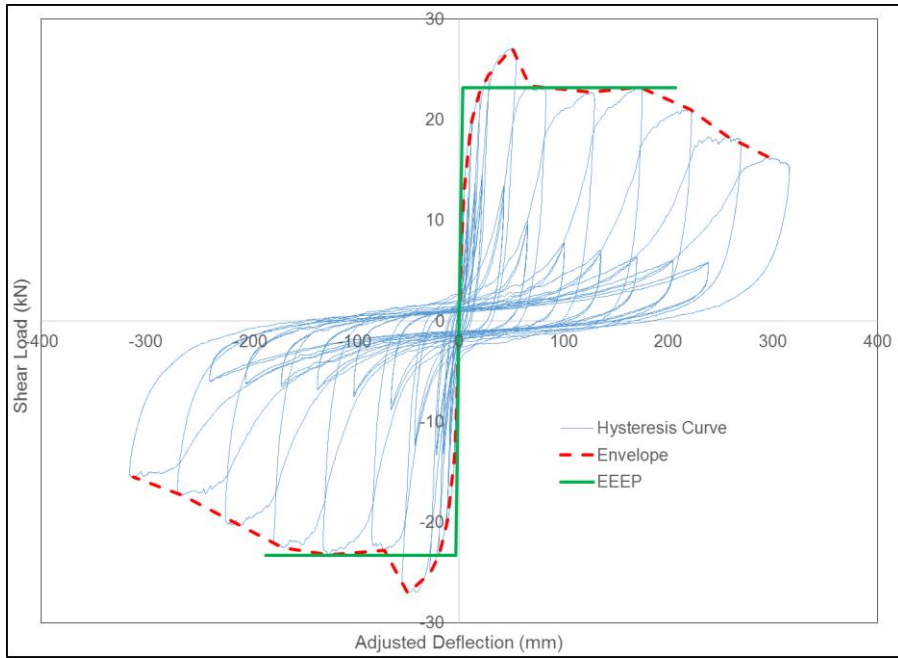


Figure B.33: Hysteresis, Envelop, and EEEP curves of wall 13-1

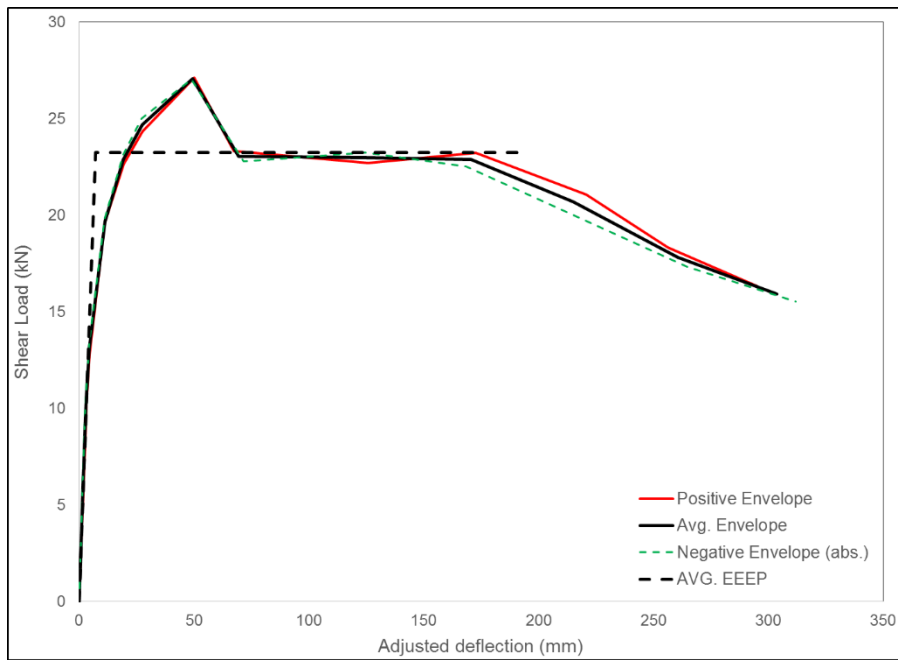


Figure B.34: Average envelop, and EEEP curve of wall 13-1

Table B.9: Average calculated hysteresis parameters. Wall type 13.

Primary Cycle #	$\Delta @$ F_{\max} (mm)	F_{\max} (kN)	$\Delta @ F_{\min}$ (mm)	F_{\min} (kN)	Strain Energy (kN mm)	Hysteresis Energy (kN mm)	ζ	Cyclic Stiffness (kN/mm)
1	2.343	7.262	-1.822	-6.696	14.607	0.973	0.011	3.387
3	3.353	10.321	-2.946	-10.417	32.647	6.086	0.03	3.307
5	4.686	12.81	-4.559	-13.436	60.641	24.229	0.064	2.84
7	11.347	19.617	-11.106	-19.766	221.058	195.151	0.141	1.754
9	19.31	22.636	-19.241	-23.142	441.188	360.583	0.13	1.187
11	27.762	24.344	-27.134	-25.01	677.23	507.376	0.119	0.899
13	50.267	27.112	-48.857	-27.036	1341.868	1642.505	0.195	0.546
15	67.475	23.338	-71.717	-22.785	1604.402	2052.17	0.204	0.332
17	125.73	22.715	-124.752	-23.262	2878.969	2955.387	0.163	0.184
19	172.739	23.245	-168.44	-22.52	3904.293	3311.993	0.135	0.134
21	220.815	21.06	-209.22	-20.322	4451.066	3370.906	0.121	0.096
23	256.477	18.332	-264.757	-17.329	4644.855	3261.987	0.112	0.068
25	295.173	16.346	-311.976	-15.528	4834.631	3191.509	0.105	0.053

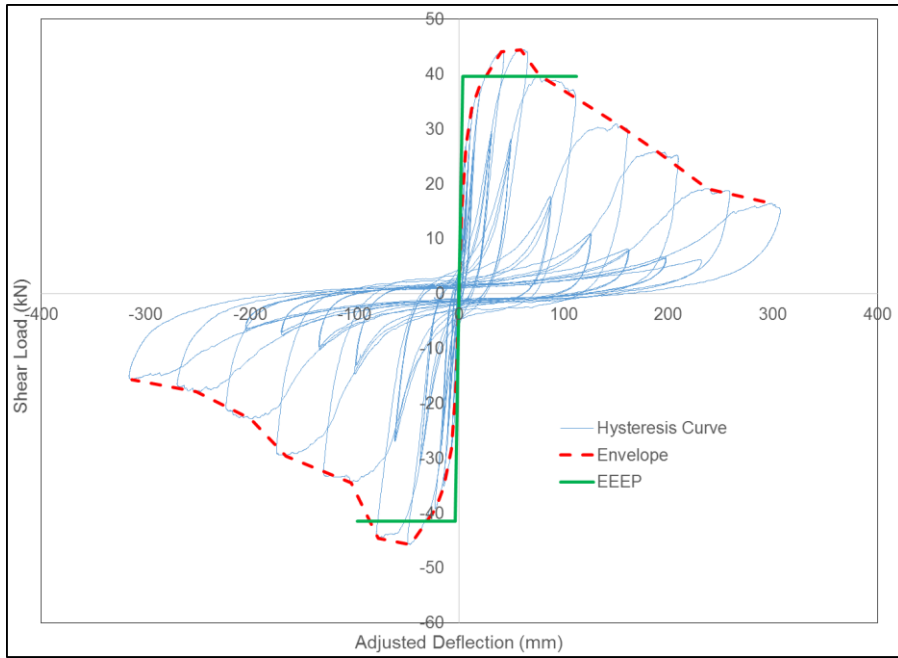


Figure B.35: Hysteresis, Envelop, and EEEP curves of wall 14-1

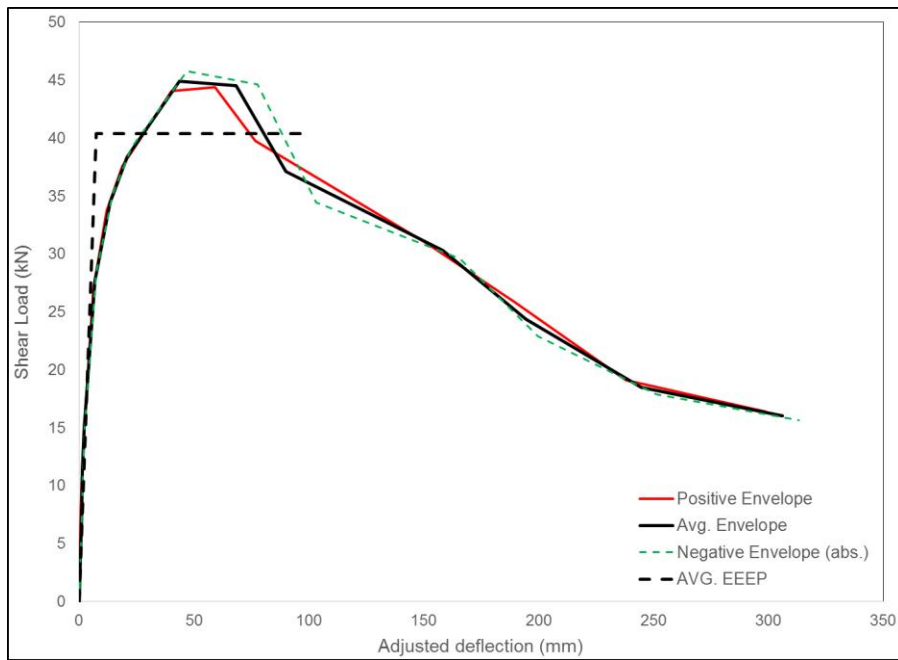


Figure B.36: Average envelop, and EEEP curve of wall 14-1

Table B.10: Average calculated hysteresis parameters. Wall type 14.

Primary Cycle #	$\Delta @$ F_{\max} (mm)	F_{\max} (kN)	$\Delta @$ F_{\min} (mm)	F_{\min} (kN)	Strain Energy (kN mm)	Hysteresis Energy (kN mm)	ζ	Cyclic Stiffness (kN/mm)
1	0.826	7.778	-1.34	-7.146	8	9.799	0.195	7.375
3	1.441	11.036	-1.74	-11.383	17.855	12.573	0.112	7.1
5	2.032	14.479	-2.54	-15.555	34.466	10.129	0.047	6.625
7	6.394	26.953	-7.525	-28.36	192.873	94.067	0.078	3.992
9	12.103	33.693	-14.713	-35.14	462.401	290.67	0.1	2.586
11	19.006	37.6	-22.866	-39.165	805.086	488.95	0.097	1.846
13	40.278	44.062	-46.92	-45.773	1961.199	1746.43	0.142	1.035
15	59.207	44.406	-77.591	-44.648	3046.715	2828.76	0.148	0.663
17	76.638	39.758	-103.219	-34.438	3300.815	5126.852	0.247	0.426
19	150.717	30.979	-165.786	-29.605	4788.578	4694.569	0.156	0.192
21	189.471	25.854	-199.65	-22.891	4734.386	4224.435	0.142	0.126
23	238.004	19.114	-251.212	-17.885	4521.068	3429.559	0.121	0.076
25	298.99	16.399	-313.226	-15.647	4902.092	3141.188	0.102	0.052

**APPENDIX C PREDICTING BEHAVIOR OF STEEL-CLAD, WOOD-FRAMED
SHEAR WALLS UNDER CYCLIC LOADING**

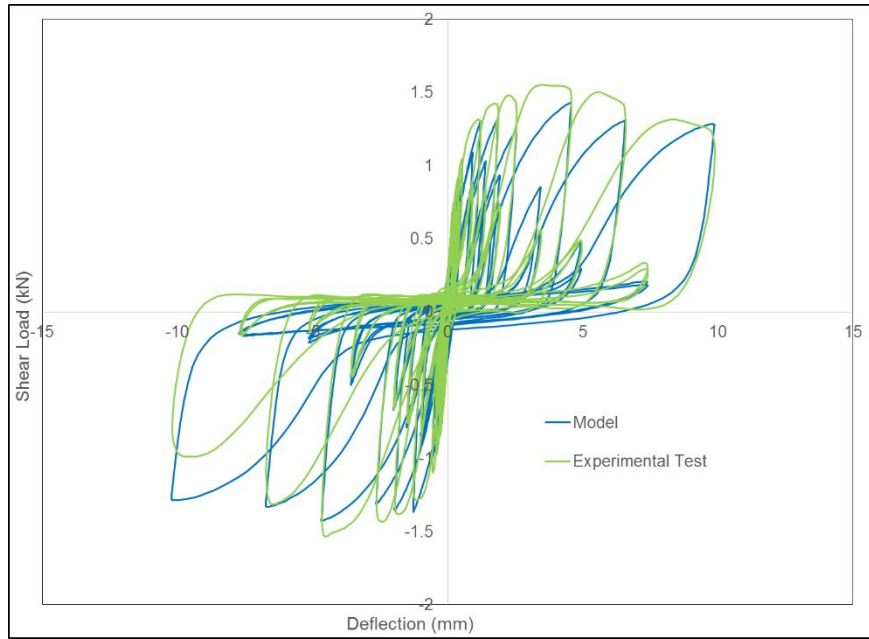


Figure C.1: Load versus displacement of No.10x25.4mm screw connection test 1 (SPF to Grandrib 3)

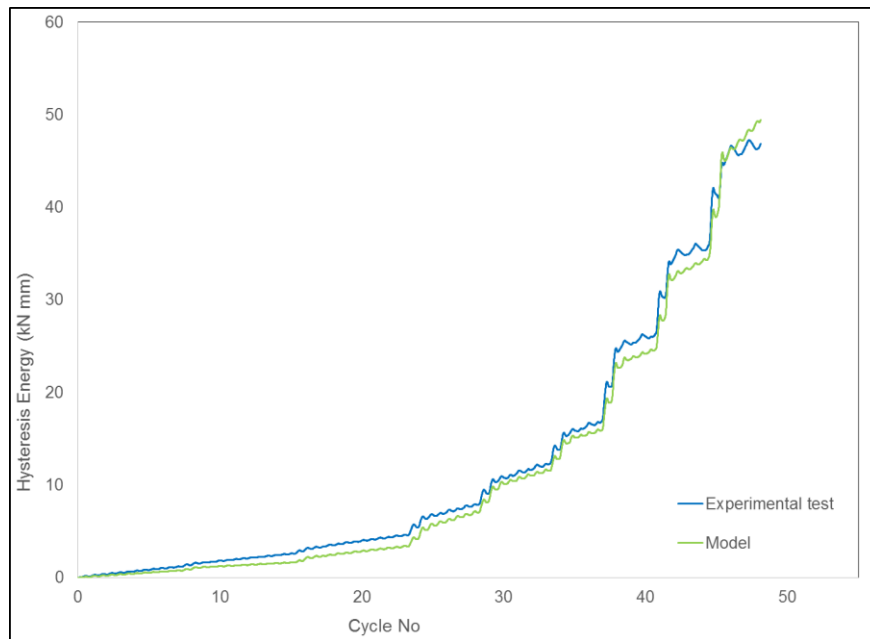


Figure C.2: Cumulative Energy dissipated of No.10x25.4 mm screw connection test 1 (SPF to Grandrib 3)

Table C.1: Parameters estimation of screw connection test 1 (SPF to Grandrib 3)

Parameters	Values
α	0.001715
β	2.49905
ω	1.498048
ζ	0.976314
n	1.031465
ψ_0	0.002562
δ_ψ	0.020648
δ_v	0.014016
ξ_0	0.002624
γ	-1.419993
δ_η	0.106234
p	3.723502
d_{fail}	10.04
SSE / dp	0.013

Where:

SSE: sum square error

dp: number of data point

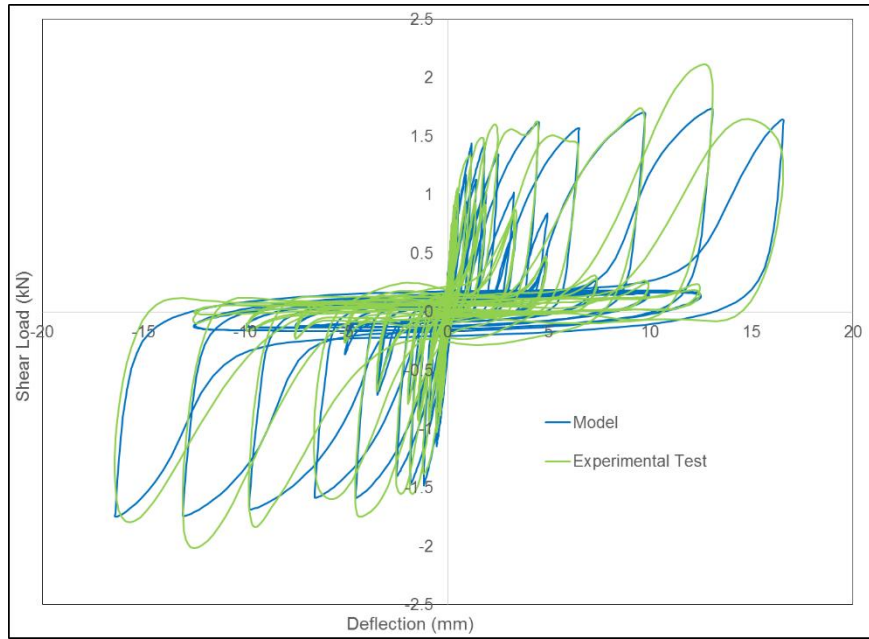


Figure C.3: Load versus displacement of No.10x25.4mm screw connection test 2 (SPF to Grandrib 3)

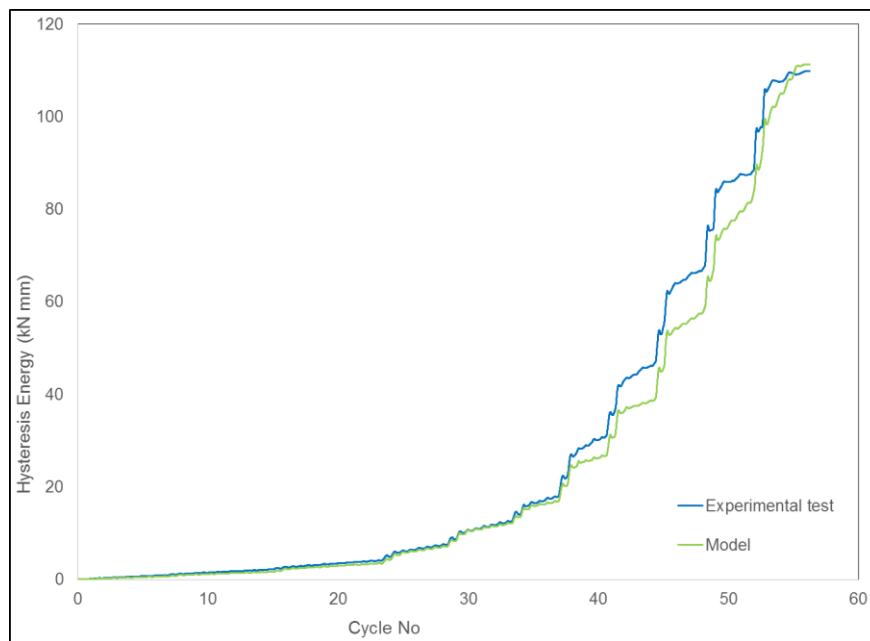
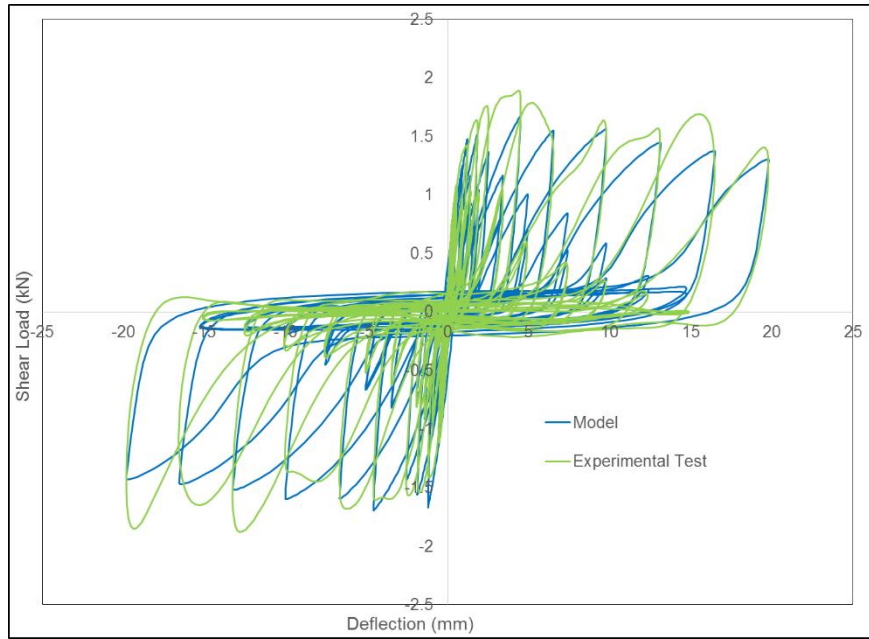


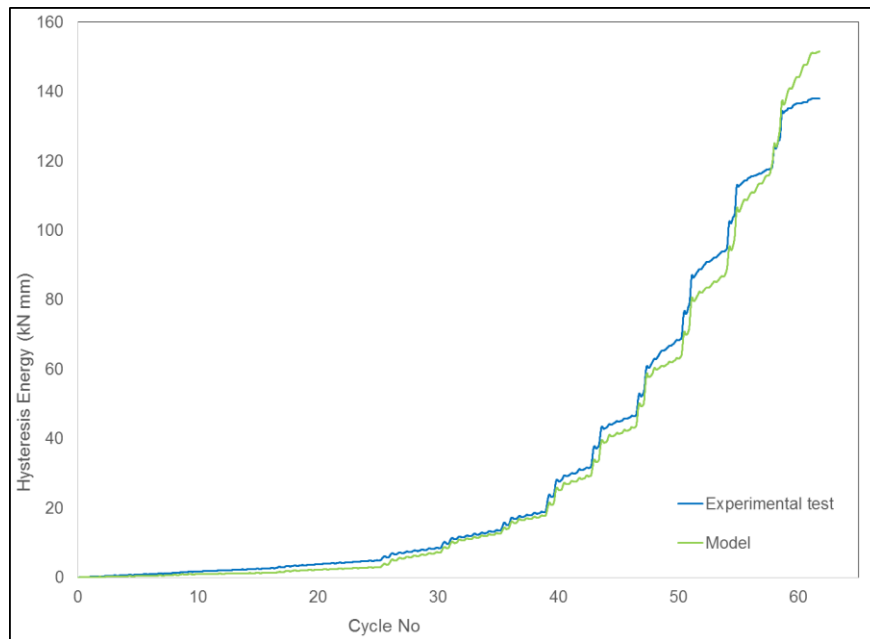
Figure C.4: Cumulative Energy dissipated of No.10x25.4 mm screw connection test 2 (SPF to Grandrib 3)

Table C.2: Parameters estimation of screw connection test 2 (SPF to Grandrib 3)

Parameters	Values
α	0.02313
β	3.576251
ω	1.618767
ζ	0.986264
n	1.107239
ψ_0	0.003591
δ_ψ	0.010735
δ_v	0.035177
ξ_0	0.002869
γ	-2.549417
δ_η	0.152997
p	4.728824
d_{fail}	16.5
SSE / dp	0.012



**Figure C.5: Load versus displacement of No.10x25.4mm screw connection
test 3 (SPF to Grandrib 3)**



**Figure C.6: Cumulative Energy dissipated of No.10x25.4 mm screw connection
test 3 (SPF to Grandrib 3)**

Table C.3: Parameters estimation of screw connection test 3 (SPF to Grandrib 3)

Parameters	Values
α	0.012723
β	2.282357
ω	1.436525
ζ	0.982136
n	1.054614
ψ_0	0.008641
δ_ψ	0.007529
δ_ν	0.032848
ξ_0	0.002588
γ	-1.817625
δ_η	0.143176
p	2.764136
d_{fail}	19.81
SSE / dp	0.017

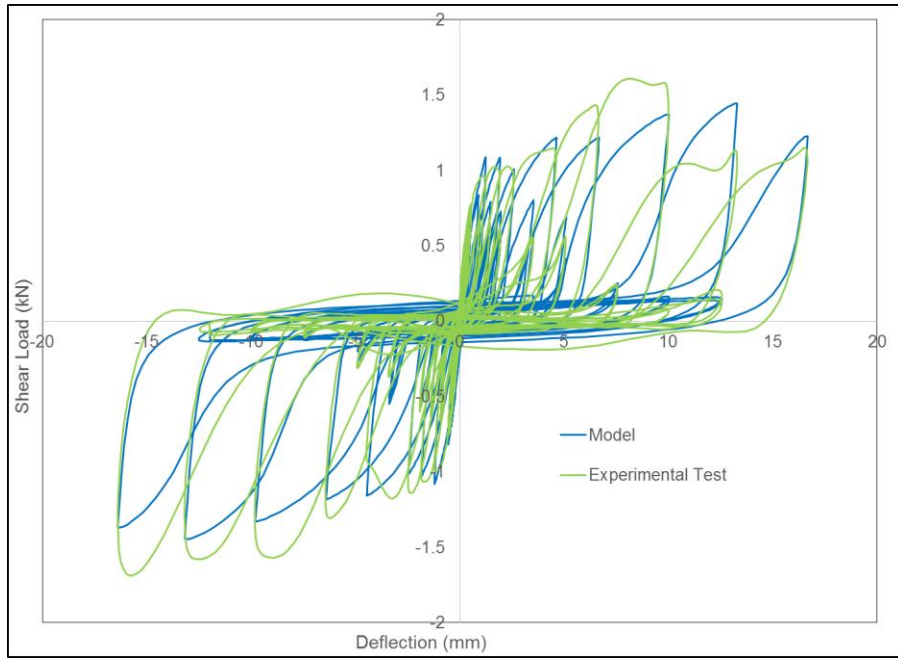


Figure C.7: Load versus displacement of No.10x25.4mm screw connection test 4 (SPF to Grandrib 3)

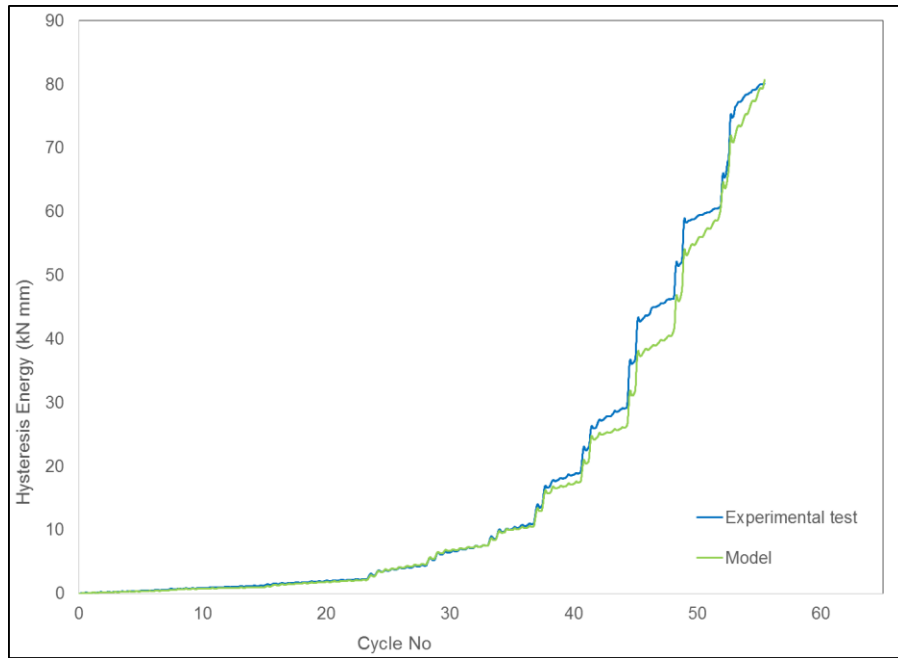


Figure C.8: Cumulative Energy dissipated of No.10x25.4 mm screw connection test 4 (SPF to Grandrib 3)

Table C.4: Parameters estimation of screw connection test 4 (SPF to Grandrib 3)

Parameters	Values
α	0.037093
β	2.482788
ω	1.344332
ζ	0.983281
n	1.183527
ψ_0	0.008966
δ_ψ	0.012802
δ_v	0.097589
ξ_0	0.002266
γ	-1.553872
δ_η	0.21506
p	3.397975
d_{fail}	16.53
SSE / dp	0.007

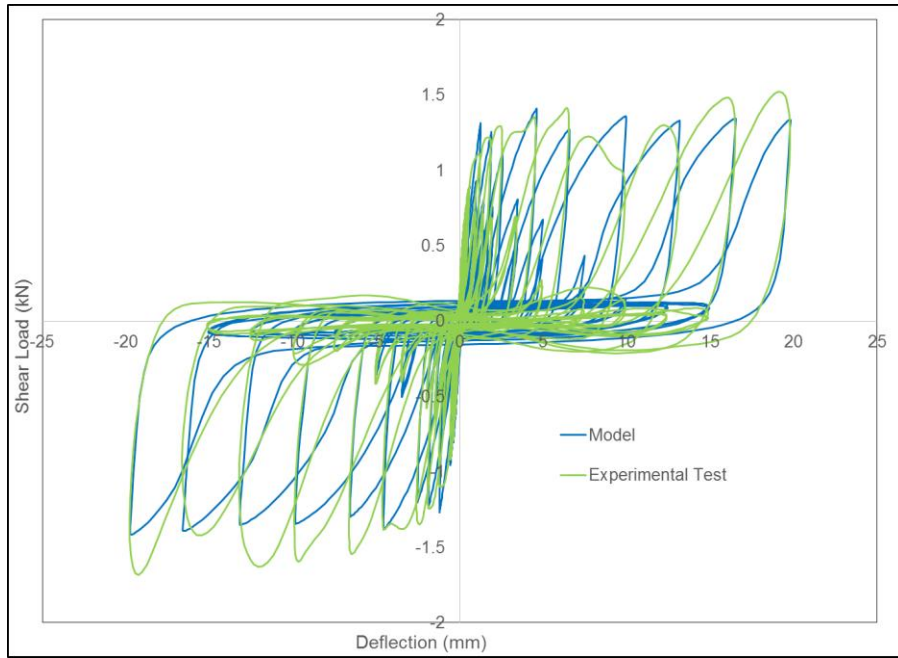


Figure C.9: Load versus displacement of No.10x25.4mm screw connection test 5 (SPF to Grandrib 3)

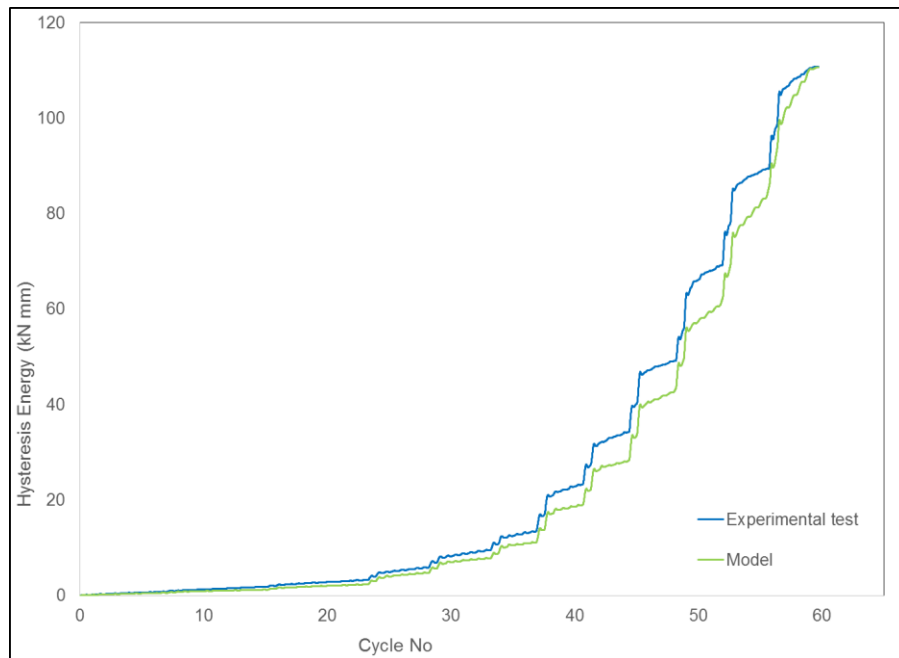


Figure C.10: Cumulative Energy dissipated of No.10x25.4 mm screw connection test 5 (SPF to Grandrib 3)

Table C.5: Parameters estimation of screw connection test 5 (SPF to Grandrib 3)

Parameters	Values
α	0.020119
β	3.268586
ω	1.459071
ζ	0.988848
n	1.285907
ψ_0	0.010931
δ_ψ	0.005418
δ_v	0.166067
ξ_0	0.002053
γ	-2.848378
δ_η	0.293825
p	3.97309
d_{fail}	19.78
SSE / dp	0.009

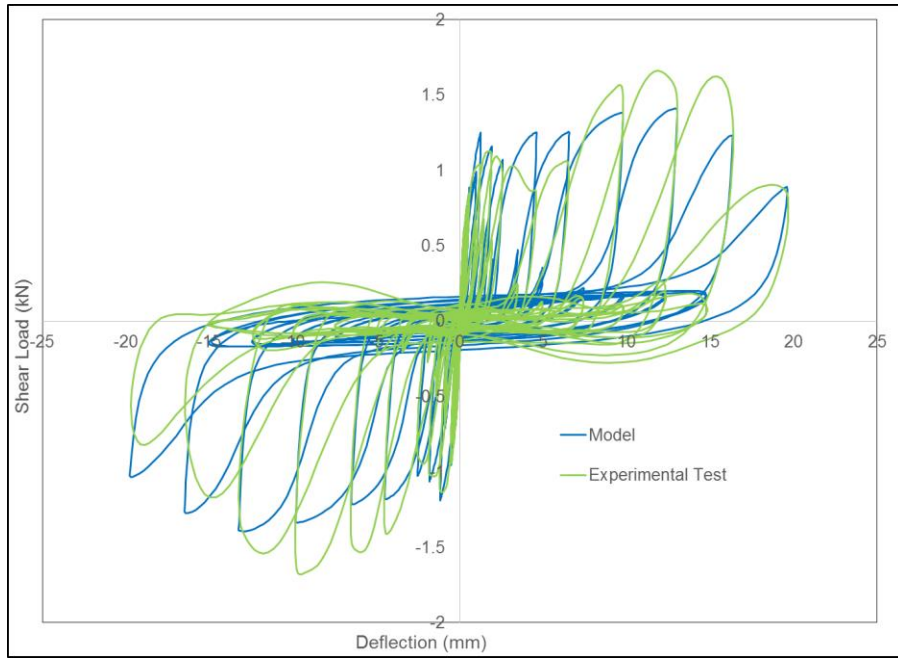


Figure C.11: Load versus displacement of No.10x25.4mm screw connection test 6 (SPF to Grandrib 3)

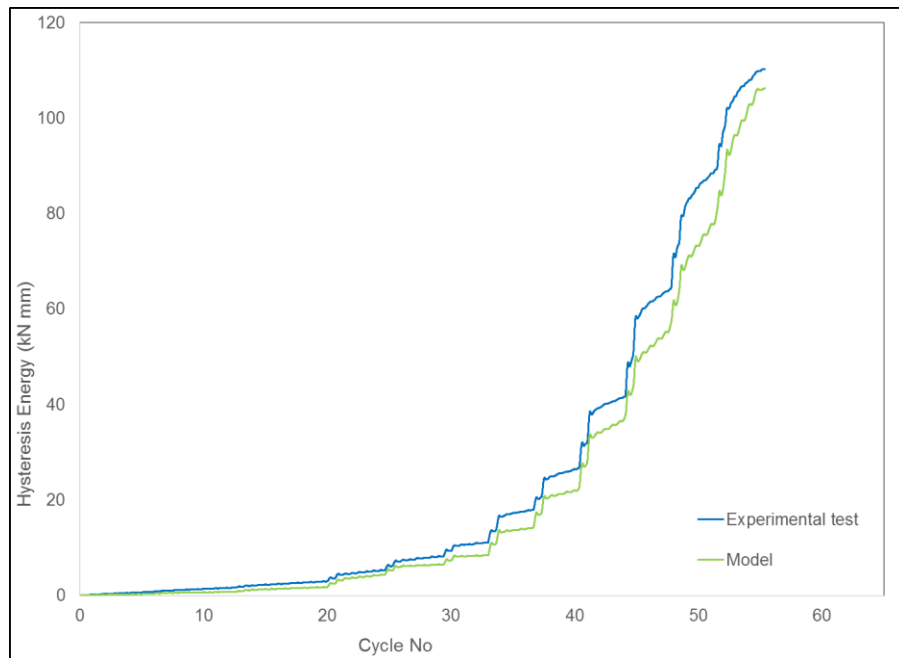


Figure C.12: Cumulative Energy dissipated of No.10x25.4 mm screw connection test 6 (SPF to Grandrib 3)

Table C.6: Parameters estimation of screw connection test 6 (SPF to Grandrib 3)

Parameters	Values
α	0.028502
β	4.205177
ω	1.522016
ζ	0.981786
n	1.614665
ψ_0	0.043733
δ_ψ	0.01094
δ_ν	0.17757
ξ_0	0.002343
γ	-2.687436
δ_η	0.246575
p	2.156789
d_{fail}	19.69
SSE / dp	0.011

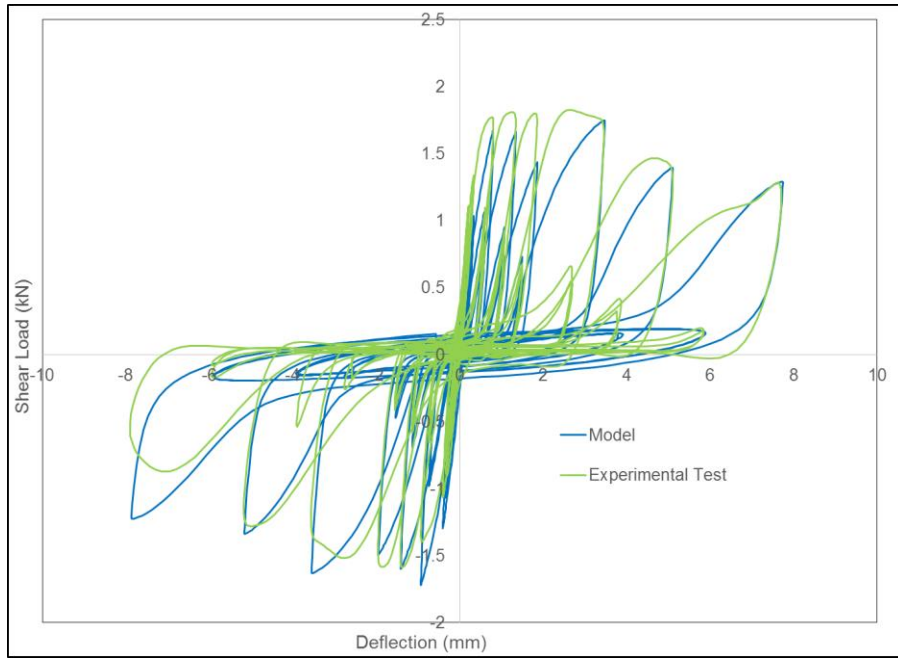


Figure C.13: Load versus displacement of No.12x19.1 mm screw connection test 1 (Grandrib 3 to Grandrib 3)

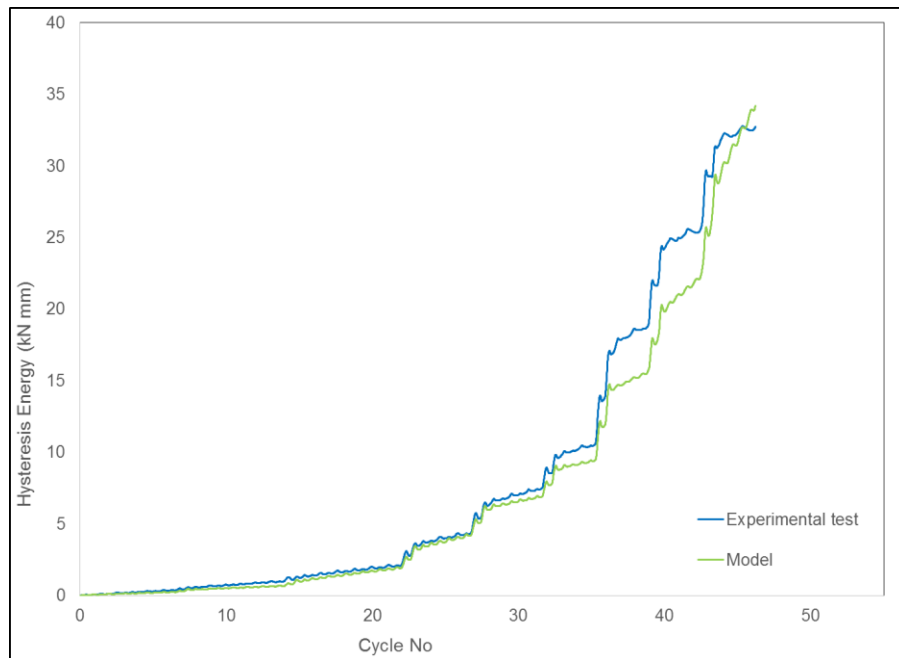


Figure C.14: Cumulative Energy dissipated of No.12x19.1 mm screw connection test 1 (Grandrib 3 to Grandrib 3)

Table C.7: Parameters estimation of No.12x19.1 mm screw connection test 1 (Grandrib 3 to Grandrib 3)

Parameters	Values
α	0.001182
β	3.72756
ω	1.899963
ζ	0.975715
n	1.246145
ψ_0	0.001228
δ_ψ	0.026973
δ_v	0.102096
ξ_0	0.00436
γ	-2.80719
δ_η	0.204871
p	4.899828
d_{fail}	7.81
SSE / dp	0.028

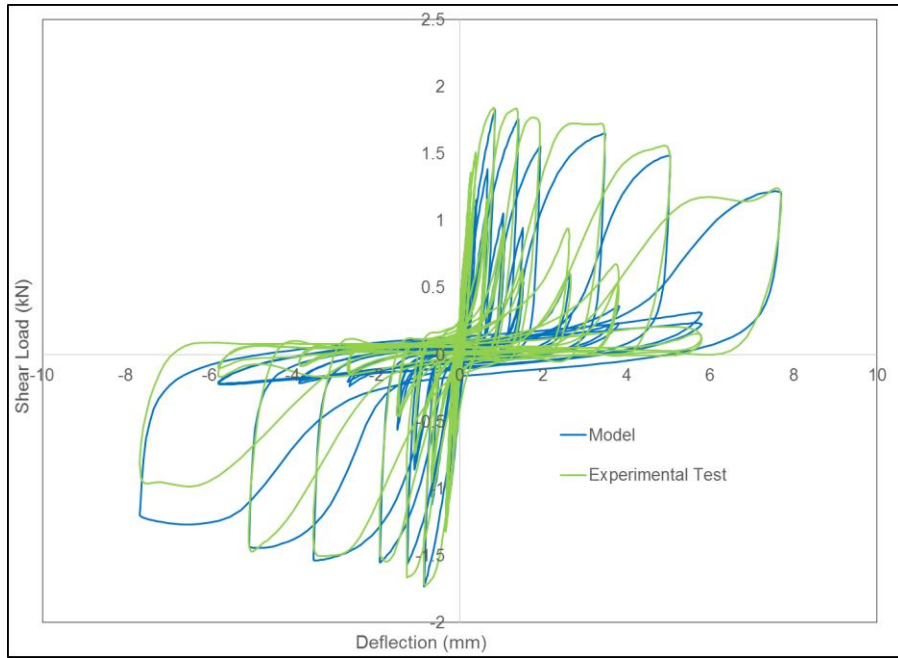


Figure C.15: Load versus displacement of No.12x19.1 mm screw connection test 2 (Grandrib 3 to Grandrib 3)

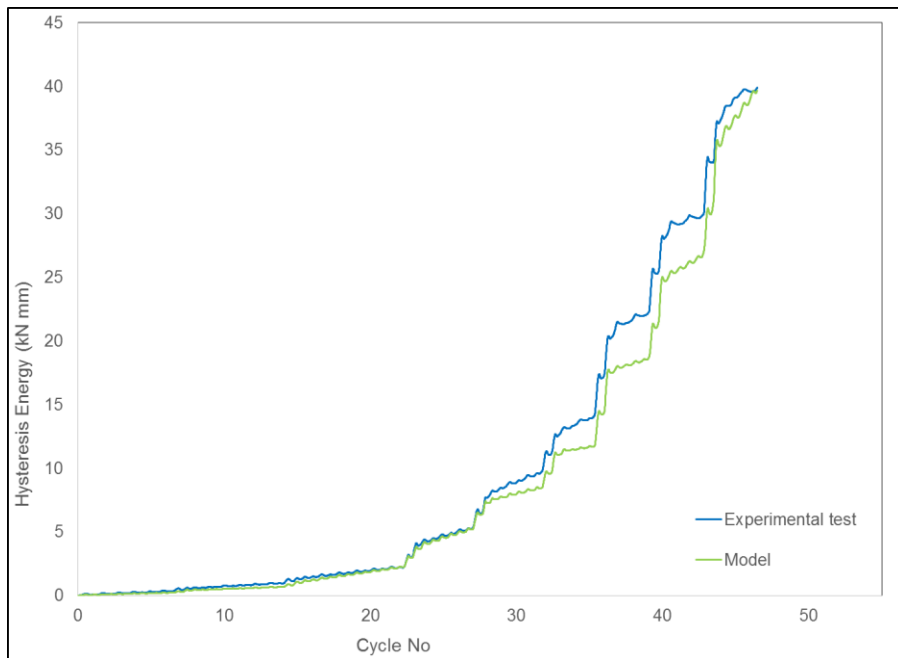


Figure C.16: Cumulative Energy dissipated of No.12x19.1 mm screw connection test 2 (Grandrib 3 to Grandrib 3)

Table C.8: Parameters estimation of No.12x19.1 mm screw connection test 2 (Grandrib 3 to Grandrib 3)

Parameters	Values
α	0.02672
β	3.09421
ω	1.89638
ζ	0.97976
n	1.14233
ψ_0	0.00024
δ_ψ	0.03706
δ_v	0.23127
ξ_0	0.00262
γ	-2.32083
δ_η	0.09441
p	4.8783
d_{fail}	7.68
SSE / dp	0.029

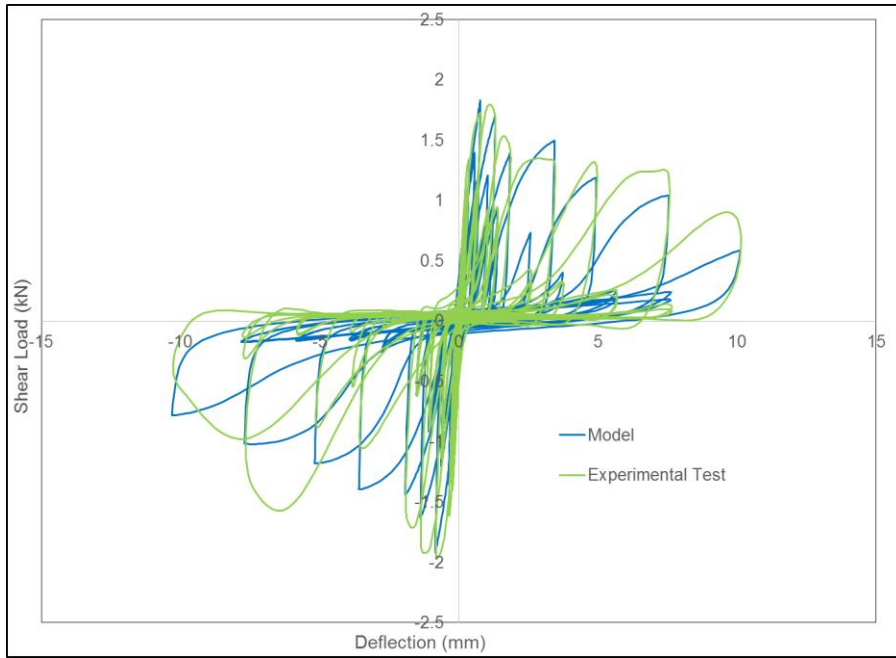


Figure C.17: Load versus displacement of No.12x19.1 mm screw connection test 3 (Grandrib 3 to Grandrib 3)

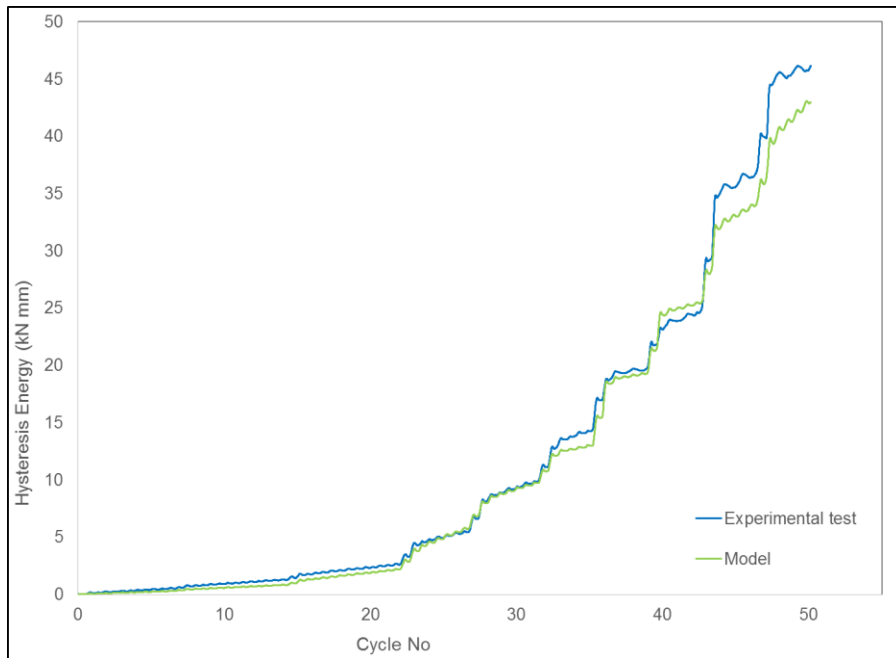


Figure C.18: Cumulative Energy dissipated of No.12x19.1 mm screw connection test 3 (Grandrib 3 to Grandrib 3)

Table C.9: Parameters estimation of No.12x19.1 mm screw connection test 3 (Grandrib 3 to Grandrib 3)

Parameters	Values
α	0.00263
β	3.13569
ω	1.89961
ζ	0.97862
n	1.04898
ψ_0	0.00019
δ_ψ	0.0242
δ_v	0.20842
ξ_0	0.00085
γ	-2.5797
δ_η	0.13327
p	4.71118
d_{fail}	10.21
SSE / dp	0.031

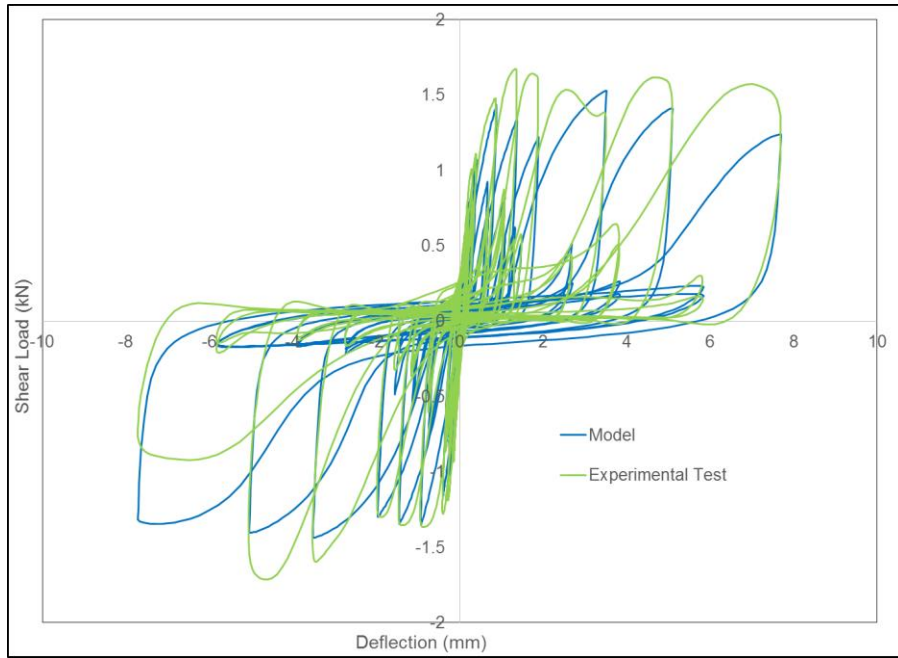


Figure C.19: Load versus displacement of No.12x19.1 mm screw connection test 4 (Grandrib 3 to Grandrib 3)

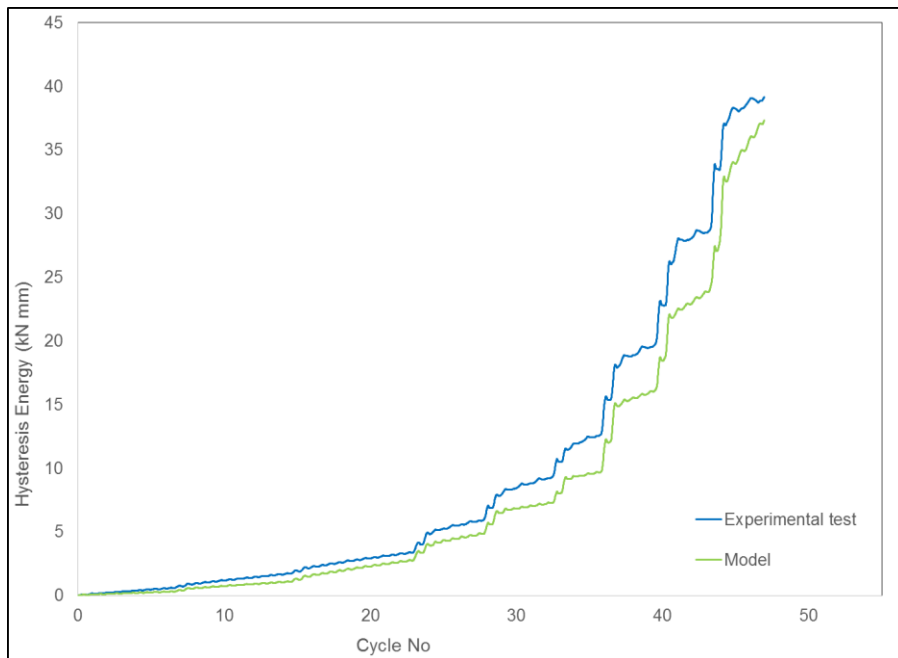


Figure C.20: Cumulative Energy dissipated of No.12x19.1 mm screw connection test 4 (Grandrib 3 to Grandrib 3)

Table C.10: Parameters estimation of No.12x19.1 mm screw connection test 4 (Grandrib 3 to Grandrib 3)

Parameters	Values
α	0.03072
β	3.5295
ω	1.89383
ζ	0.97765
n	1.02127
ψ_0	0.00663
δ_ψ	0.02356
δ_v	0.27596
ξ_0	0.00324
γ	-2.7607
δ_η	0.23341
p	4.95085
d_{fail}	7.7
SSE / dp	0.017

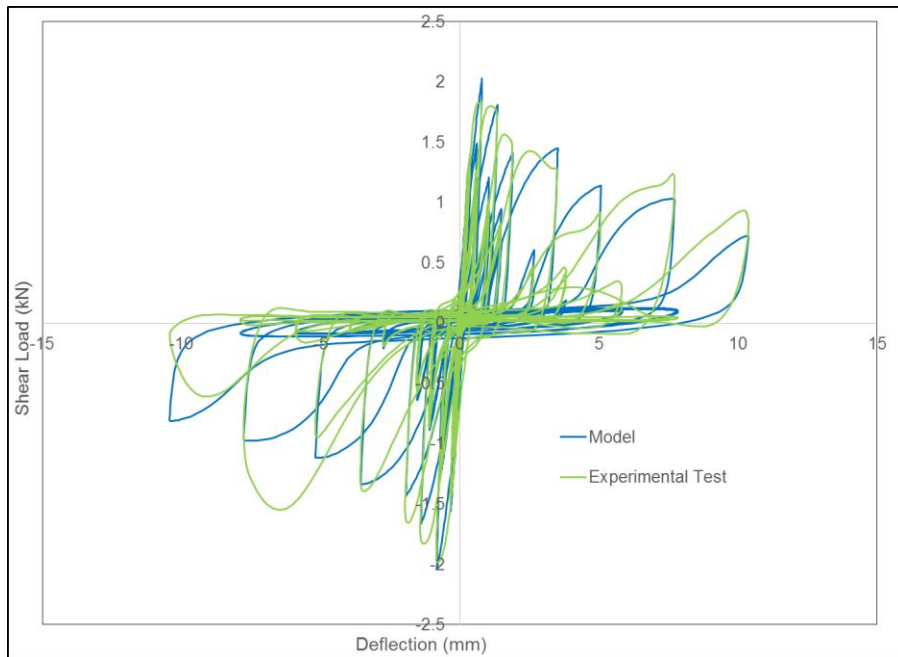


Figure C.21: Load versus displacement of No.12x19.1 mm screw connection test 5 (Grandrib 3 to Grandrib 3)

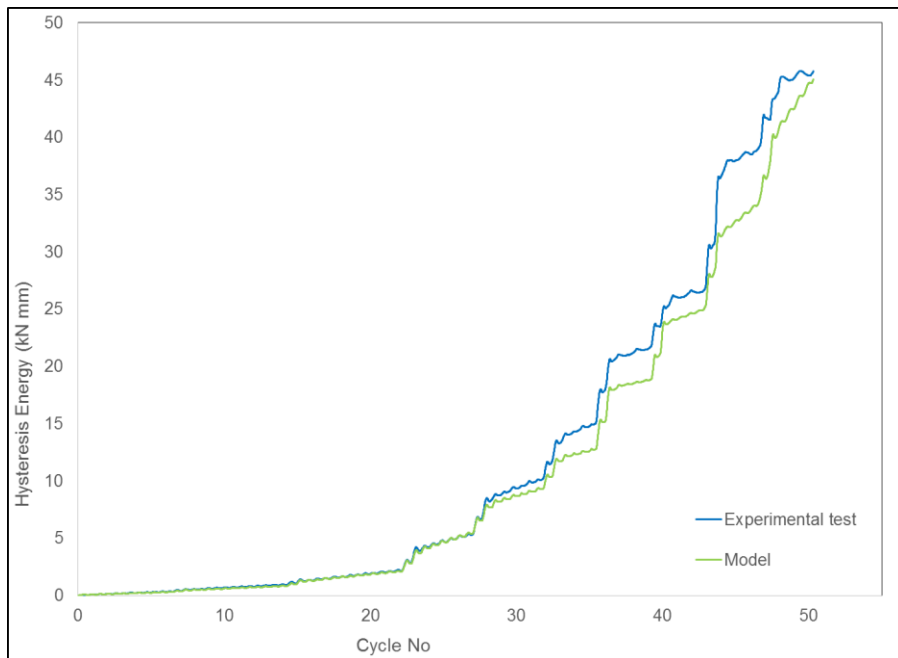


Figure C.22: Cumulative Energy dissipated of No.12x19.1 mm screw connection test 5 (Grandrib 3 to Grandrib 3)

Table C.11: Parameters estimation of No.12x19.1 mm screw connection test 5 (Grandrib 3 to Grandrib 3)

Parameters	Values
α	0.00037
β	2.13538
ω	2.19422
ζ	0.98917
n	1.0062
ψ_0	0.00039
δ_ψ	0.01055
δ_v	0.27021
ξ_0	0.00195
γ	-1.534
δ_η	0.23303
p	5.97144
d_{fail}	10.4
SSE / dp	0.014

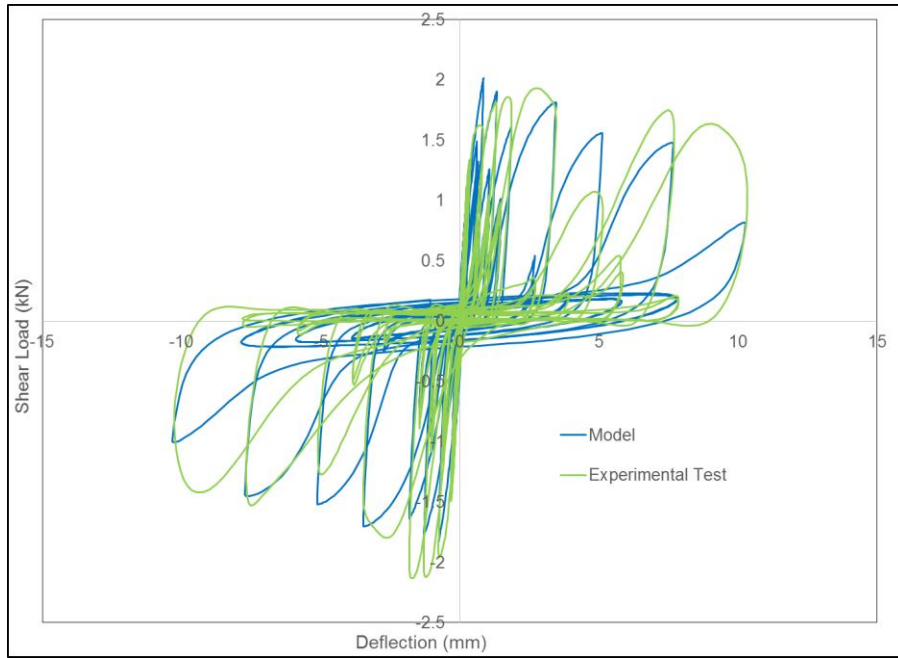


Figure C.23: Load versus displacement of No.12x19.1 mm screw connection test 6 (Grandrib 3 to Grandrib 3)

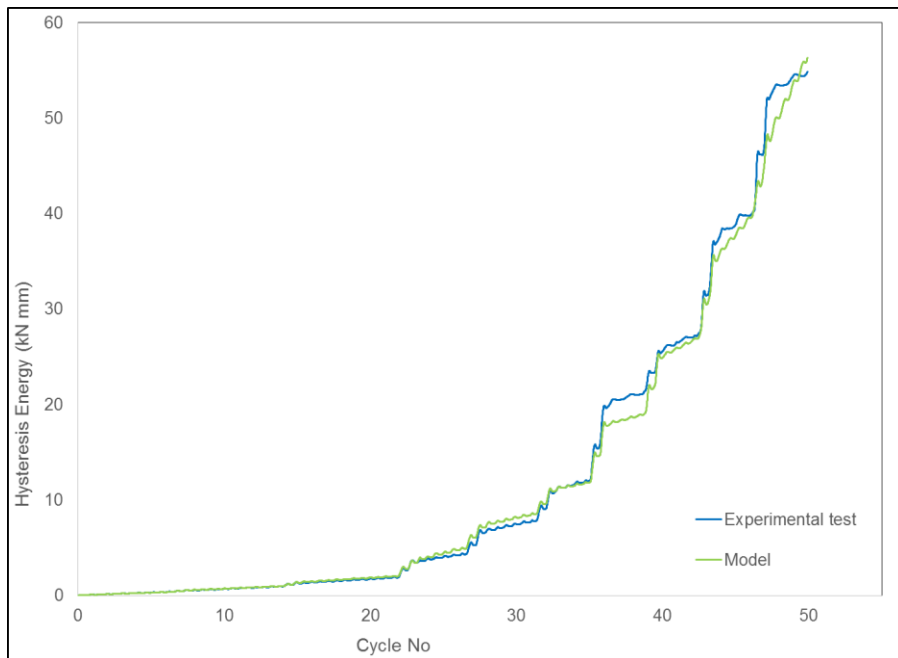


Figure C.24: Cumulative Energy dissipated of No.12x19.1 mm screw connection test 6 (Grandrib 3 to Grandrib 3)

Table C.12: Parameters estimation of No.12x19.1 mm screw connection test 6 (Grandrib 3 to Grandrib 3)

Parameters	Values
α	0.00817
β	2.92786
ω	2.19715
ζ	0.98274
n	1.01689
ψ_0	0.00103
δ_ψ	0.01899
δ_v	0.09093
ξ_0	0.00333
γ	-1.7517
δ_η	0.17926
p	5.98335
d_{fail}	10.3
SSE / dp	0.025

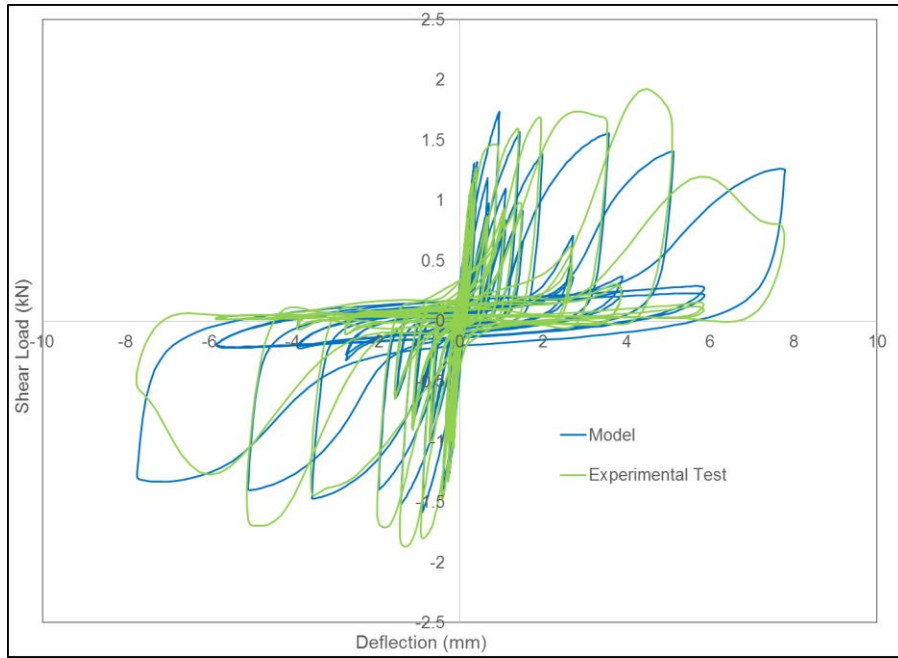


Figure C.25: Load versus displacement of No.12x19.1 mm screw connection test 7 (Grandrib 3 to Grandrib 3)

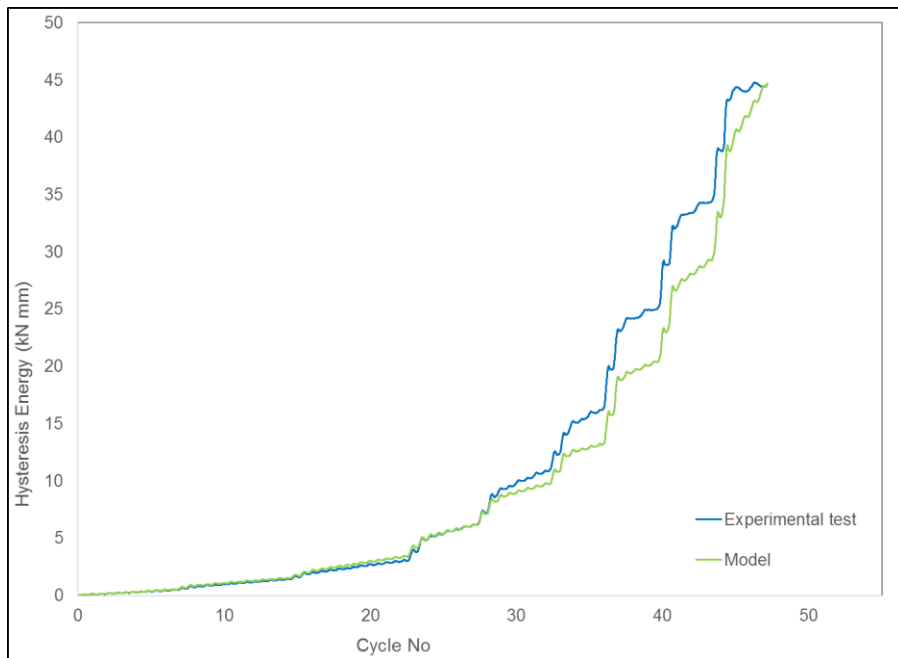


Figure C.26: Cumulative Energy dissipated of No.12x19.1 mm screw connection test 7 (Grandrib 3 to Grandrib 3)

Table C.13: Parameters estimation of No.12x19.1 mm screw connection test 7 (Grandrib 3 to Grandrib 3)

Parameters	Values
α	0.0175
β	3.1195
ω	2.1961
ζ	0.971
n	1.0001
ψ_0	0.0002
δ_ψ	0.0201
δ_v	0.1945
ξ_0	0.0035
γ	-2.174
δ_η	0.2506
p	5.9363
d_{fail}	7.76
SSE / dp	0.019

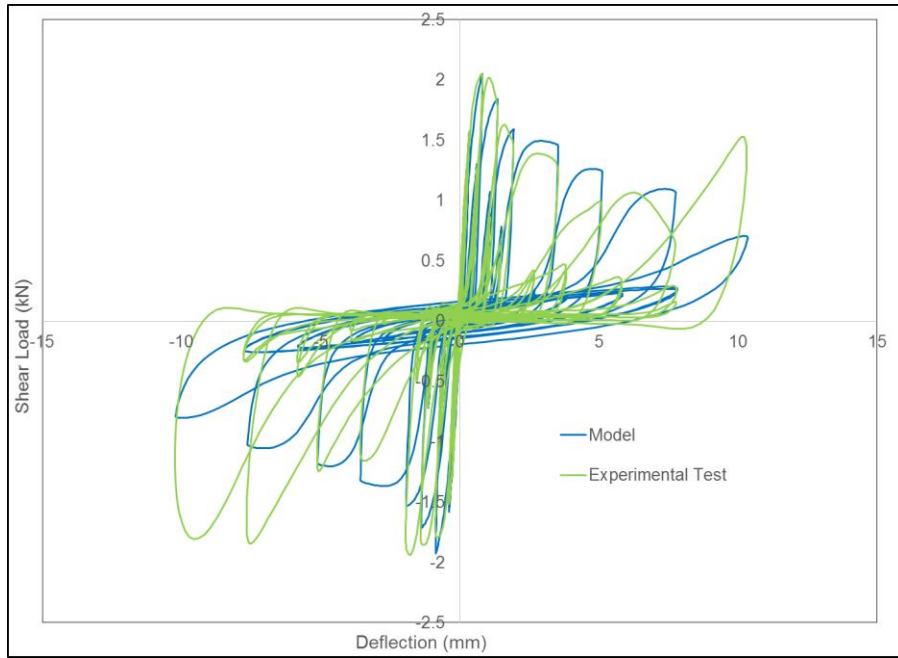


Figure C.27: Load versus displacement of No.12x19.1 mm screw connection test 8 (Grandrib 3 to Grandrib 3)

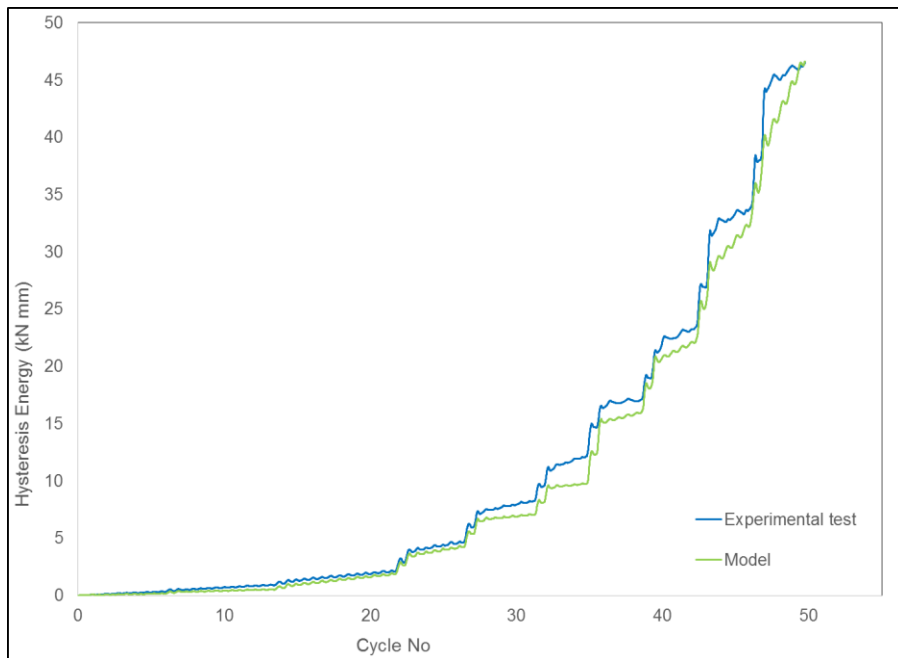


Figure C.28: Cumulative Energy dissipated of No.12x19.1 mm screw connection test 8 (Grandrib 3 to Grandrib 3)

Table C.14: Parameters estimation of No.12x19.1 mm screw connection test 8 (Grandrib 3 to Grandrib 3)

Parameters	Values
α	0.005
β	2.8821
ω	2.1994
ζ	0.9864
n	1.4253
ψ_0	0.0004
δ_ψ	0.0346
δ_v	0.258
ξ_0	0.0028
γ	-1.313
δ_η	0.084
p	5.8622
d_{fail}	10.28
SSE / dp	0.019

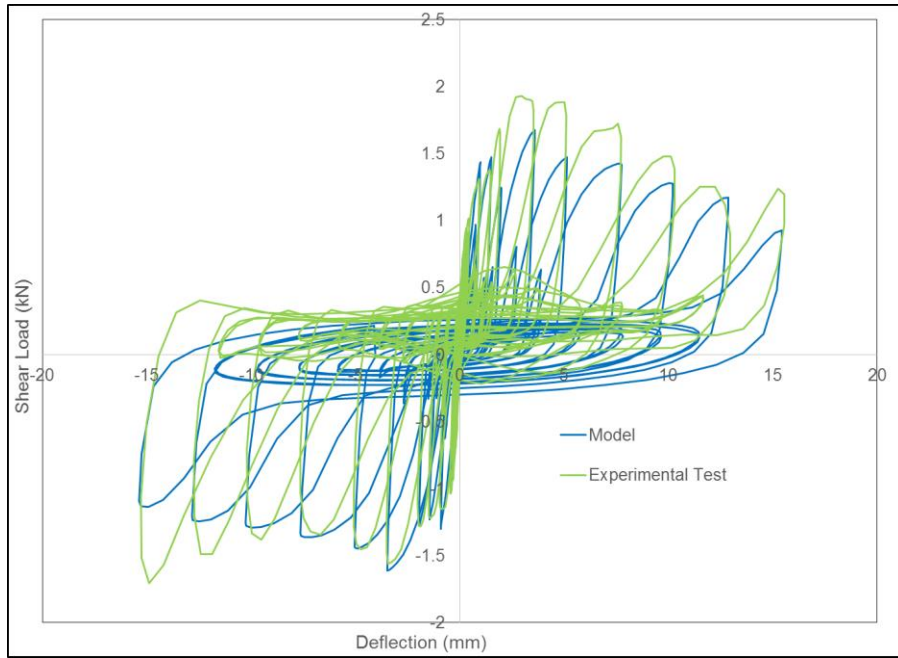


Figure C.29: Load versus displacement of No.12x38.1 mm screw connection test 1 (Grandrib 3 to Grandrib 3)

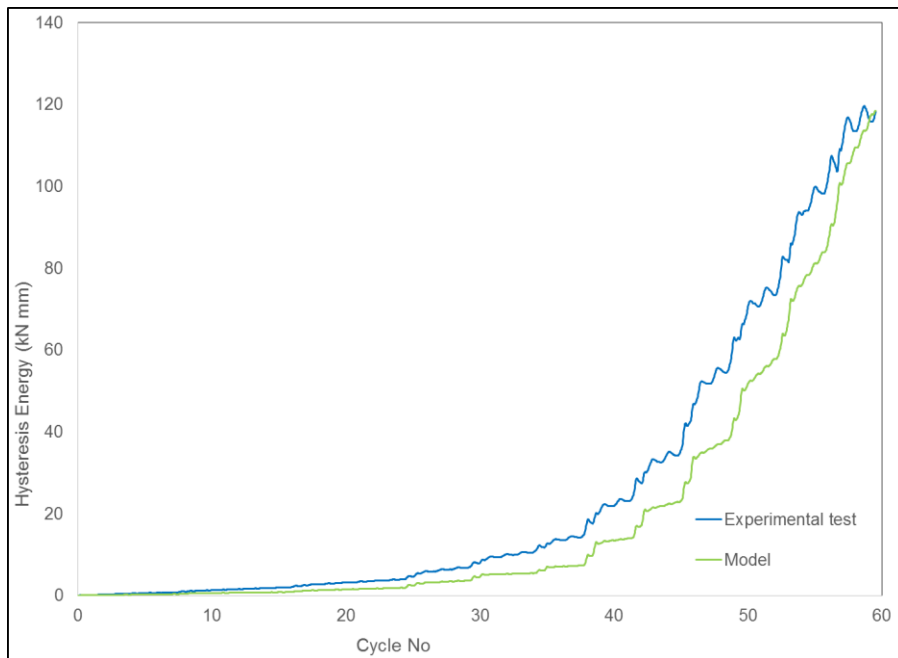


Figure C.30: Cumulative Energy dissipated of No.12x38.1 mm screw connection test 1 (Grandrib 3 to Grandrib 3)

Table C.15: Parameters estimation of No.12x38.1 mm screw connection test 1 (Grandrib 3 to Grandrib 3)

Parameters	Values
α	0.011081
β	2.798202
ω	1.699091
ζ	0.98969
n	1.001066
ψ_0	0.033303
δ_ψ	0.009167
δ_v	0.075755
ξ_0	0.001438
γ	-1.862902
δ_η	0.155305
p	3.830046
d_{fail}	15.4
SSE / dp	0.042

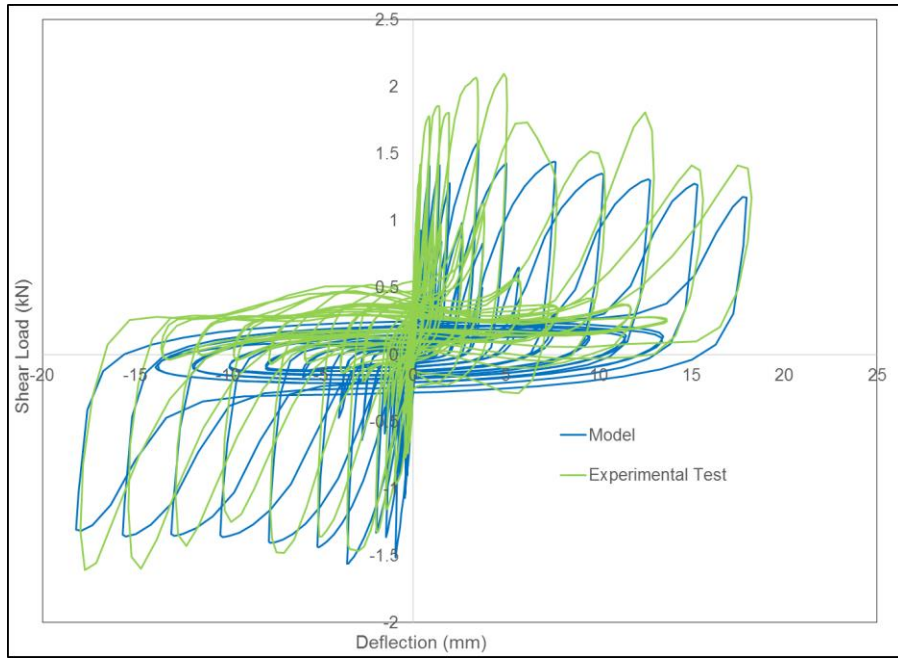


Figure C.31: Load versus displacement of No.12x38.1 mm screw connection test 2 (Grandrib 3 to Grandrib 3)

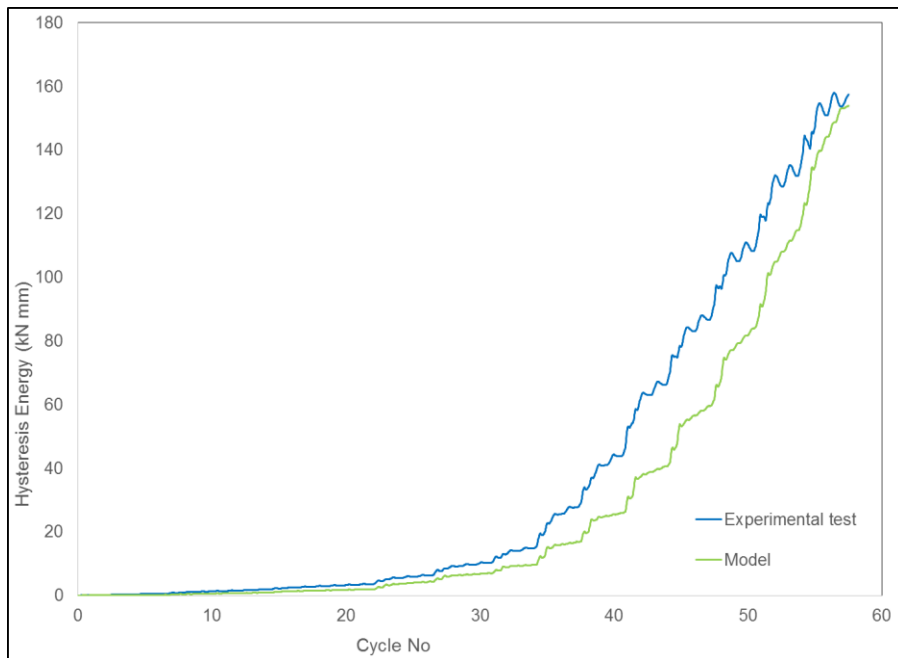


Figure C.32: Cumulative Energy dissipated of No.12x38.1 mm screw connection test 2 (Grandrib 3 to Grandrib 3)

Table C.16: Parameters estimation of No.12x38.1 mm screw connection test 2 (Grandrib 3 to Grandrib 3)

Parameters	Values
α	0.013684
β	2.669789
ω	1.69258
ζ	0.989887
n	1.041919
ψ_0	0.015633
δ_ψ	0.006193
δ_v	0.080234
ξ_0	0.001187
γ	-1.879151
δ_η	0.207109
p	3.815286
d_{fail}	18.08
SSE / dp	0.08

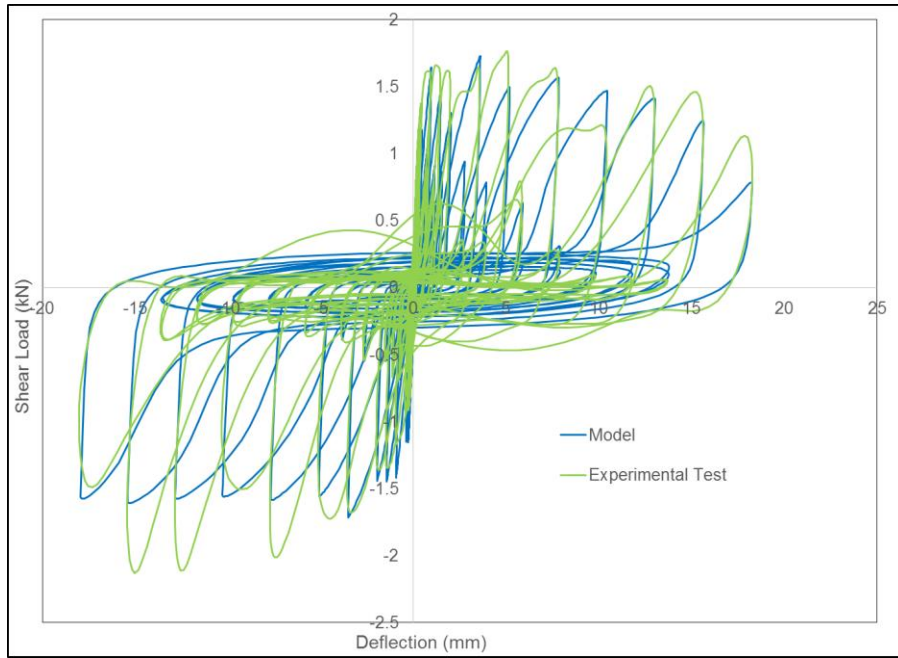


Figure C.33: Load versus displacement of No.12x38.1 mm screw connection test 3 (Grandrib 3 to Grandrib 3)

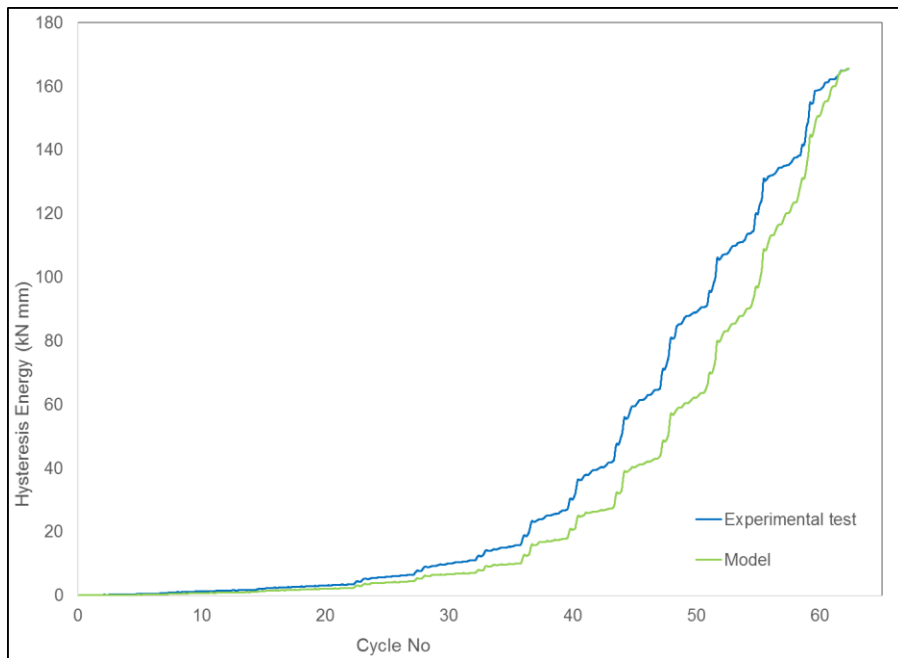


Figure C.34: Cumulative Energy dissipated of No.12x38.1 mm screw connection test 3 (Grandrib 3 to Grandrib 3)

Table C.17: Parameters estimation of No.12x38.1 mm screw connection test 3 (Grandrib 3 to Grandrib 3)

Parameters	Values
α	0.016321
β	3.191365
ω	1.899135
ζ	0.987698
n	1.000829
ψ_0	0.011786
δ_ψ	0.004732
δ_v	0.277255
ξ_0	0.003229
γ	-2.890809
δ_η	0.369118
p	4.940647
d_{fail}	18.11
SSE / dp	0.021

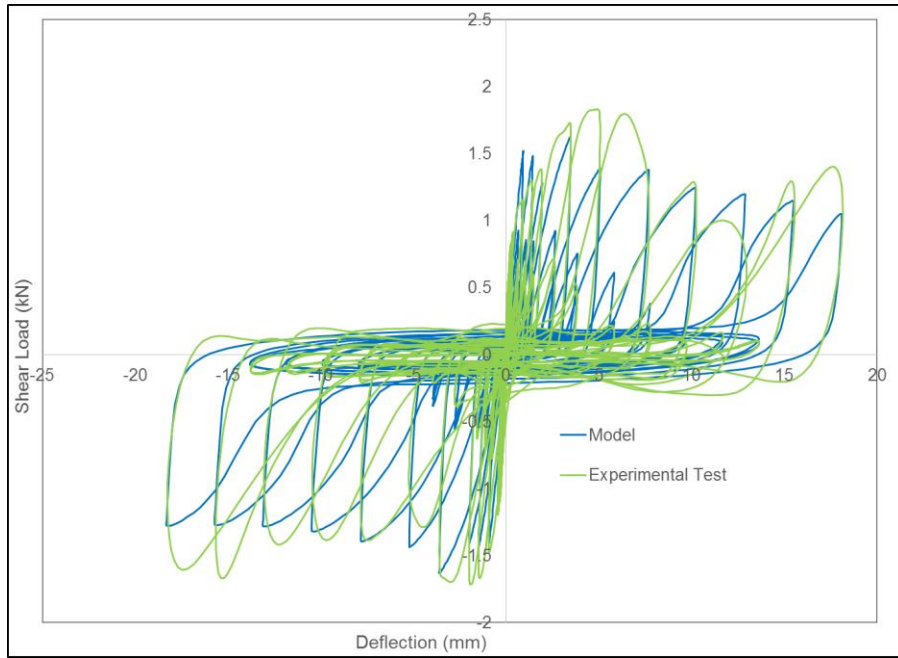


Figure C.35: Load versus displacement of No.12x38.1 mm screw connection test 4 (Grandrib 3 to Grandrib 3)

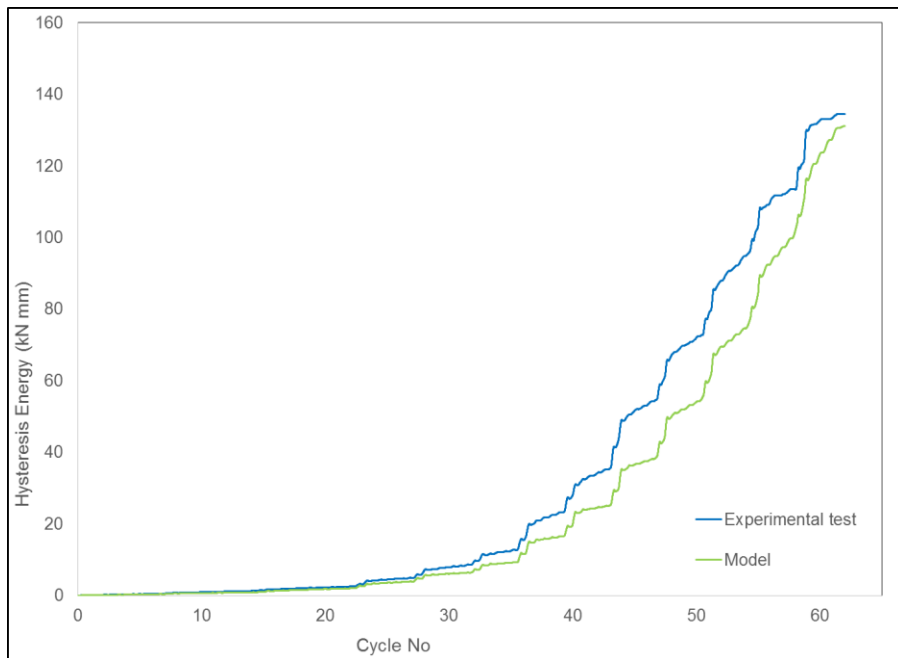


Figure C.36: Cumulative Energy dissipated of No.12x38.1 mm screw connection test 4 (Grandrib 3 to Grandrib 3)

Table C.18: Parameters estimation of No.12x38.1 mm screw connection test 4 (Grandrib 3 to Grandrib 3)

Parameters	Values
α	0.011072
β	3.310131
ω	1.778656
ζ	0.989794
n	1.092169
ψ_0	0.012143
δ_ψ	0.004266
δ_v	0.188539
ξ_0	0.002477
γ	-2.887135
δ_η	0.315528
p	4.95107
d_{fail}	18.21
SSE / dp	0.015

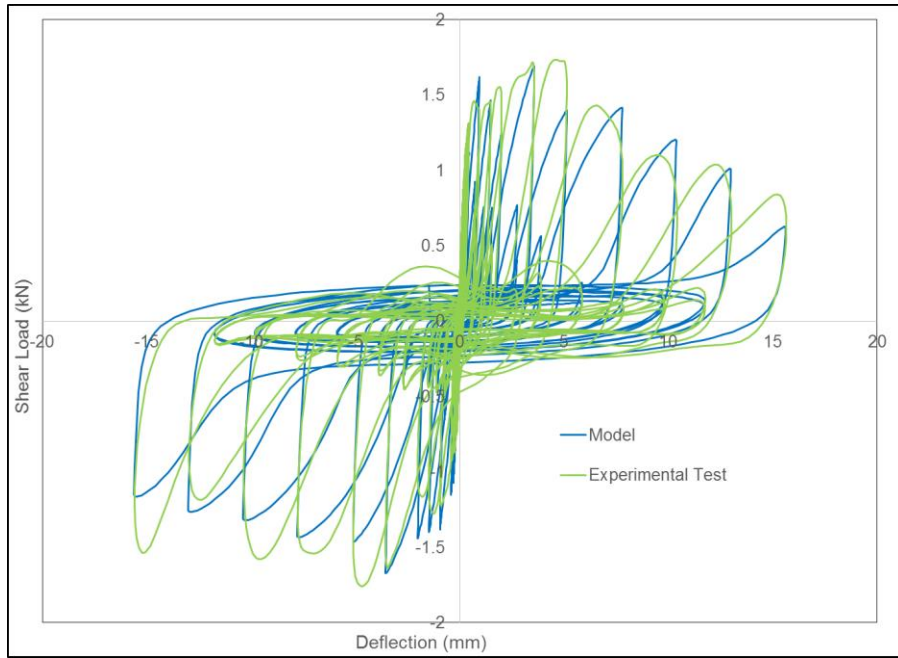


Figure C.37: Load versus displacement of No.12x38.1 mm screw connection test 5 (Grandrib 3 to Grandrib 3)

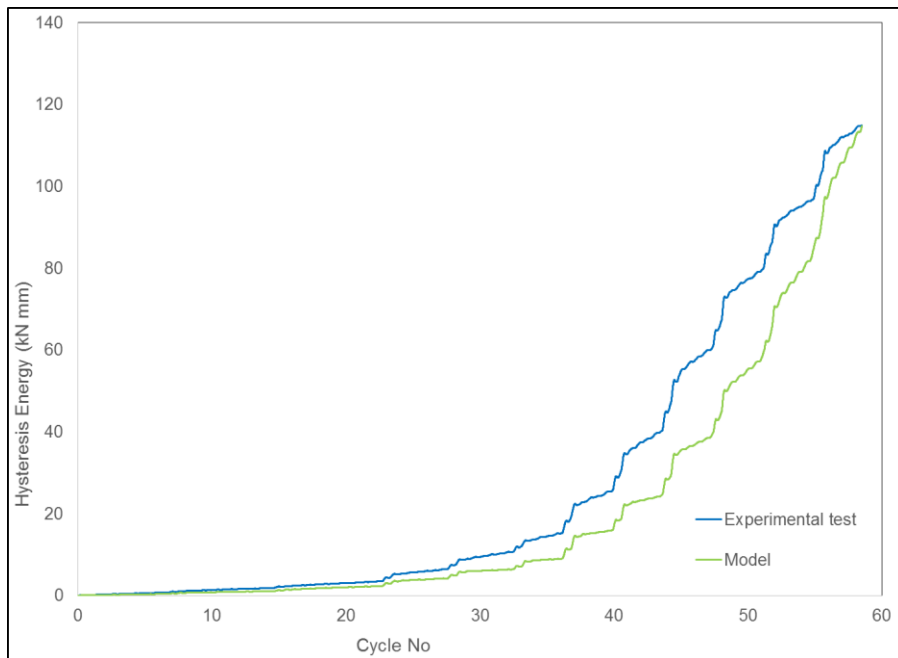


Figure C.38: Cumulative Energy dissipated of No.12x38.1 mm screw connection test 5 (Grandrib 3 to Grandrib 3)

Table C.19: Parameters estimation of No.12x38.1 mm screw connection test 5 (Grandrib 3 to Grandrib 3)

Parameters	Values
α	0.009709
β	3.222305
ω	1.899652
ζ	0.986729
n	1.000896
ψ_0	0.015437
δ_ψ	0.006043
δ_v	0.277035
ξ_0	0.003423
γ	-2.894989
δ_η	0.356066
p	4.717811
d_{fail}	15.61
SSE / dp	0.021

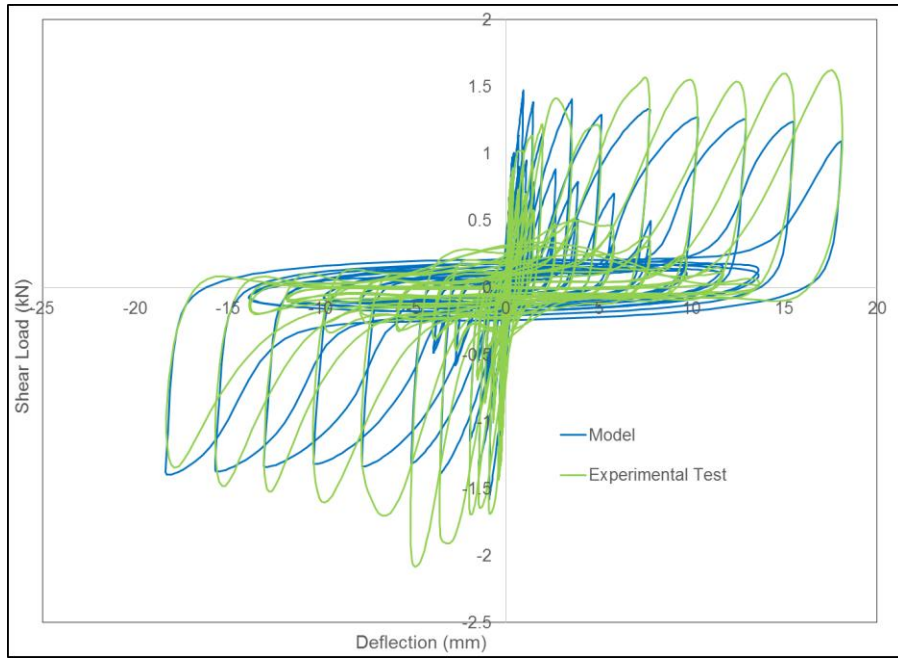


Figure C.39: Load versus displacement of No.12x38.1 mm screw connection test 6 (Grandrib 3 to Grandrib 3)

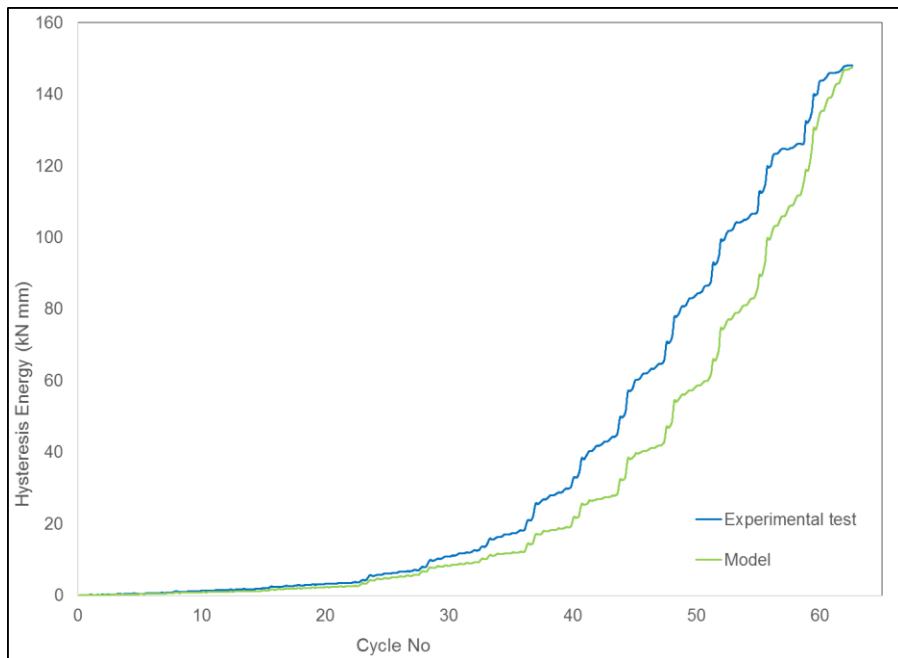


Figure C.40: Cumulative Energy dissipated of No.12x38.1 mm screw connection test 6 (Grandrib 3 to Grandrib 3)

Table C.20: Parameters estimation of No.12x38.1 mm screw connection test 6 (Grandrib 3 to Grandrib 3)

Parameters	Values
α	0.012729
β	3.47183
ω	1.89929
ζ	0.989343
n	1.000134
ψ_0	0.007355
δ_ψ	0.003965
δ_v	0.16033
ξ_0	0.002646
γ	-2.893847
δ_η	0.364467
p	3.260874
d_{fail}	18.22
SSE / dp	0.036

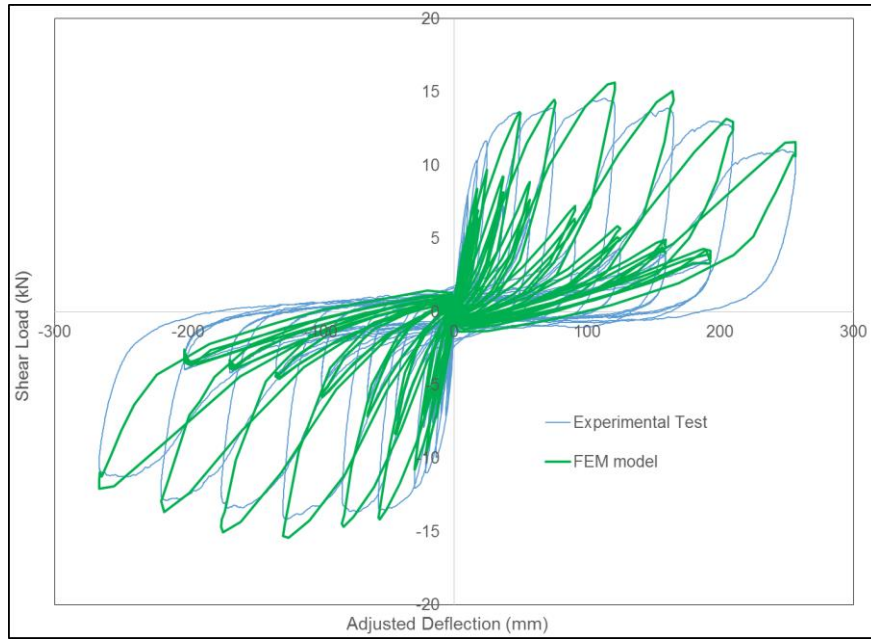


Figure C.41: Load versus deflection of wall type 1 under cyclic loading

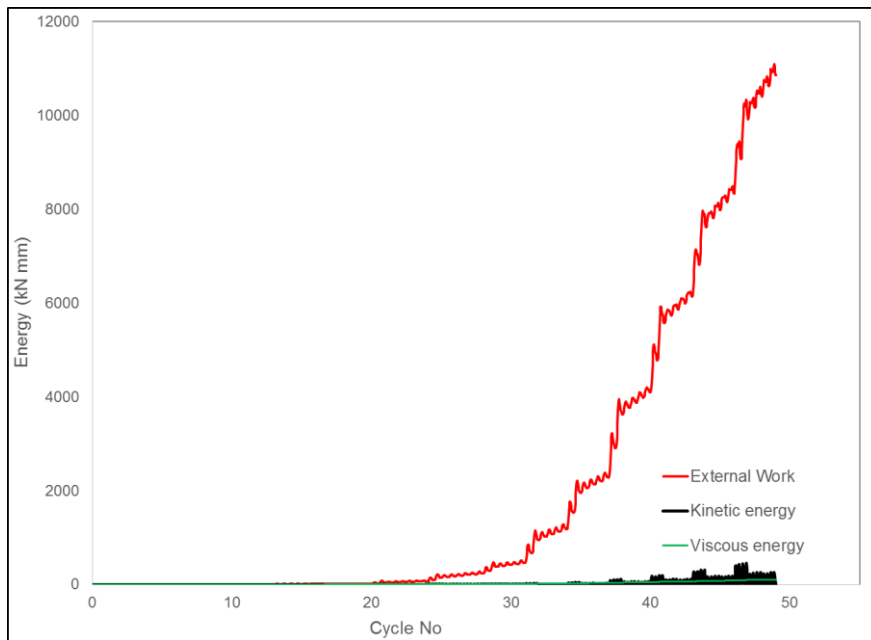


Figure C.42: Energy of wall type 1 under cyclic loading (FEA model)

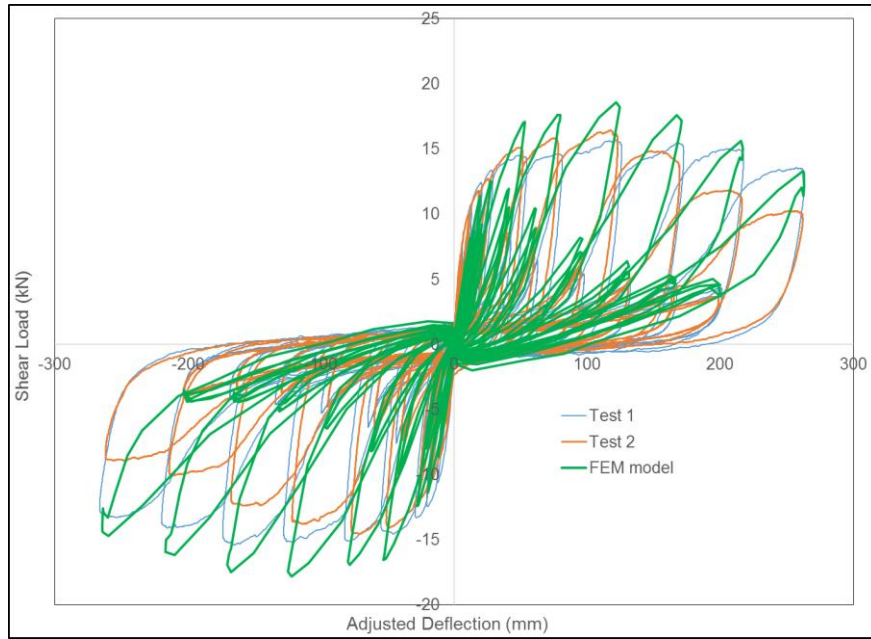


Figure C.43: Load versus deflection of wall type 2 under cyclic loading

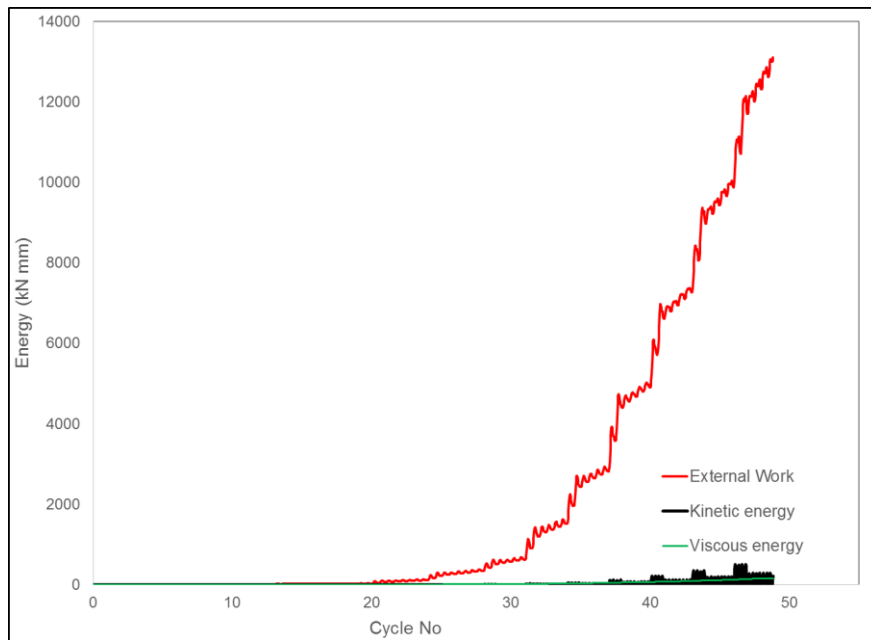


Figure C.44: Energy of wall type 2 under cyclic loading (FEA model)

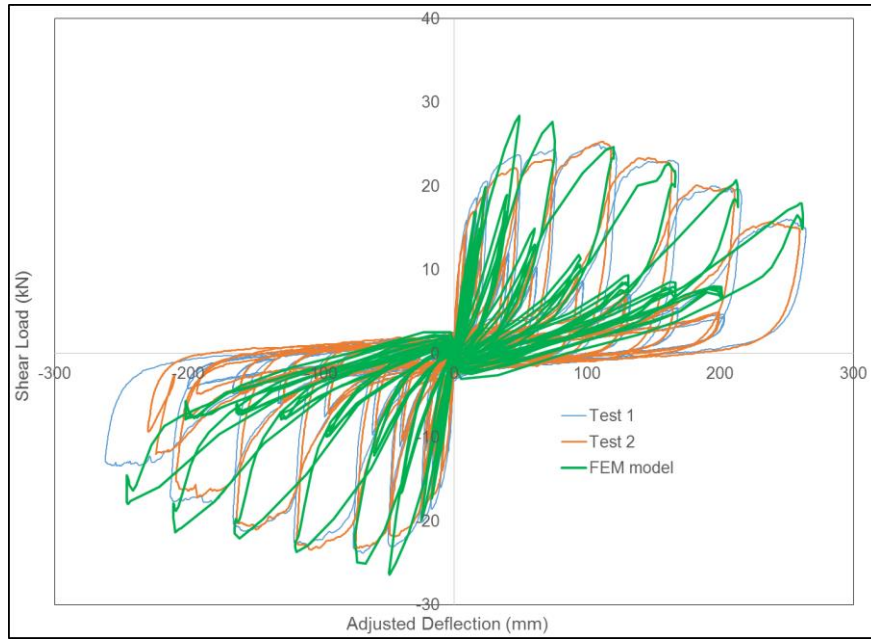


Figure C.45: Load versus deflection of wall type 4 under cyclic loading

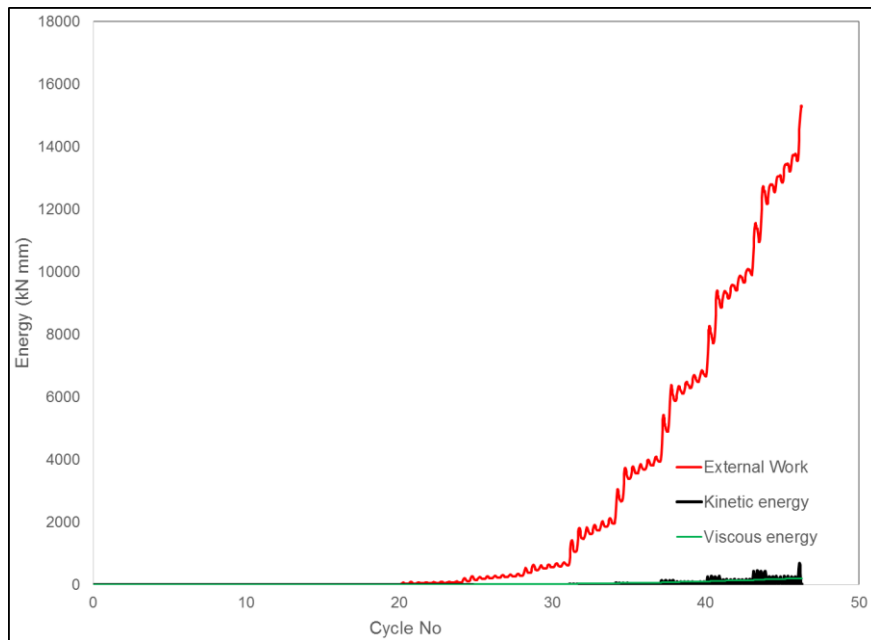


Figure C.46: Energy of wall type 4 under cyclic loading (FEA model)

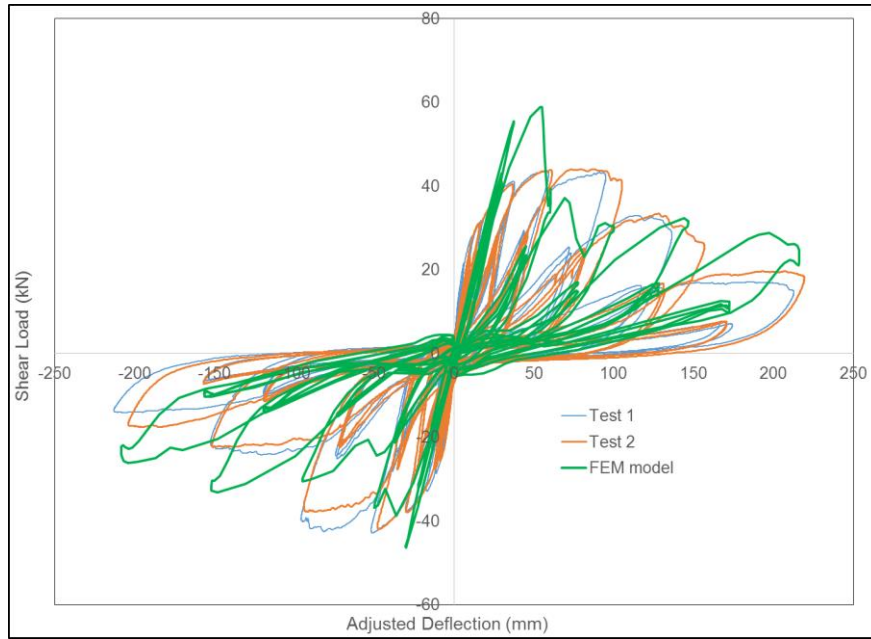


Figure C.47: Load versus deflection of wall type 5 under cyclic loading

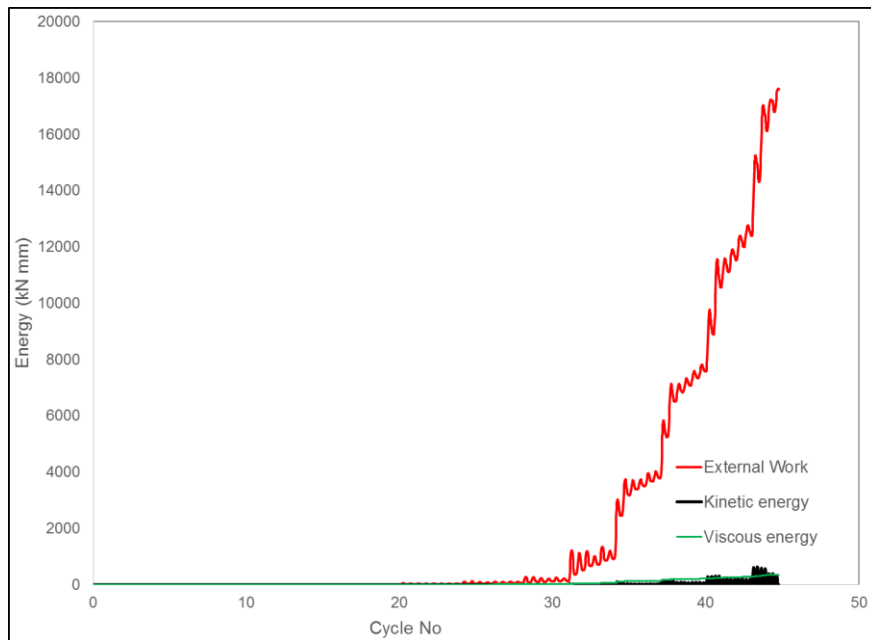


Figure C.48: Energy of wall type 5 under cyclic loading (FEA model)

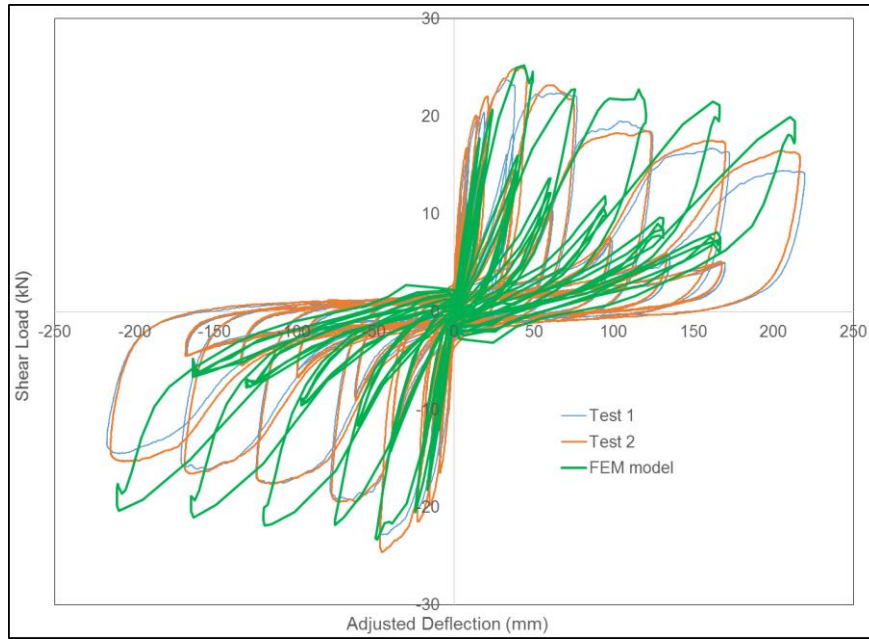


Figure C.49: Load versus deflection of wall type 6 under cyclic loading

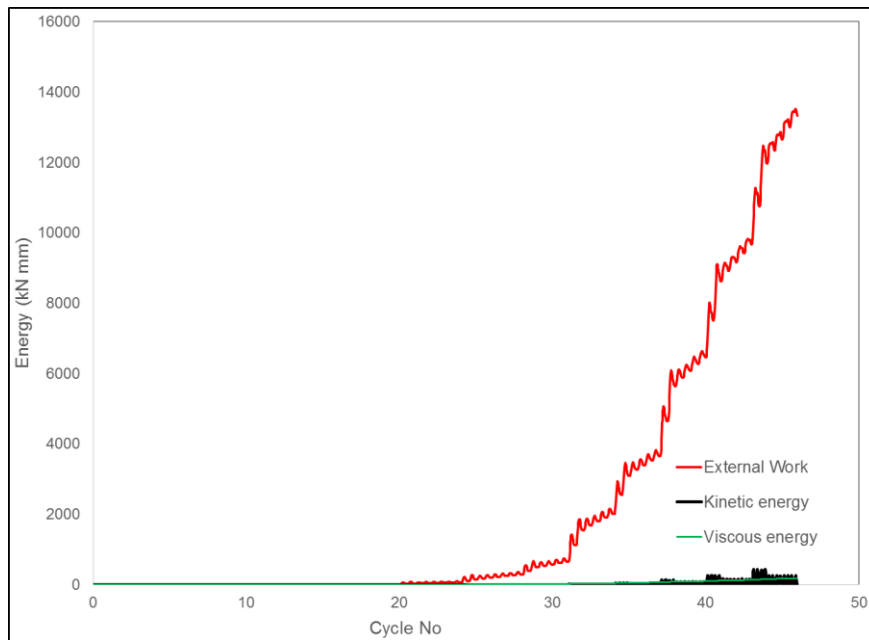


Figure C.50: Energy of wall type 6 under cyclic loading (FEA model)

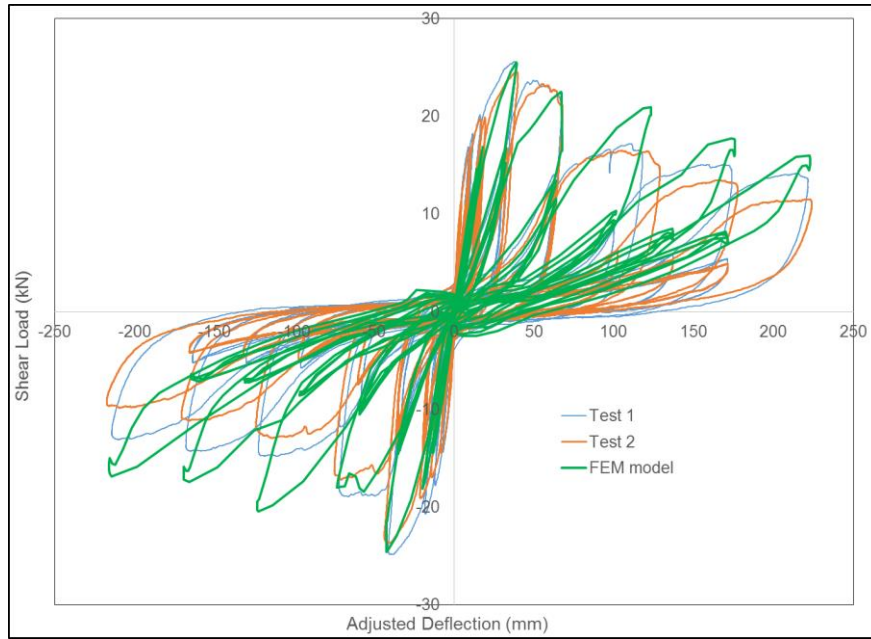


Figure C.51: Load versus deflection of wall type 7 under cyclic loading

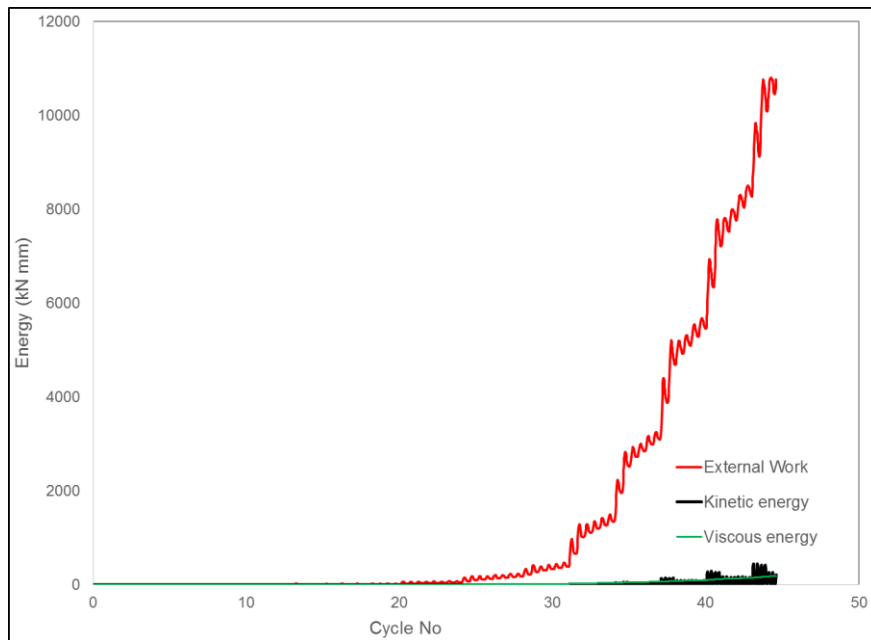


Figure C.52: Energy of wall type 7 under cyclic loading (FEA model)

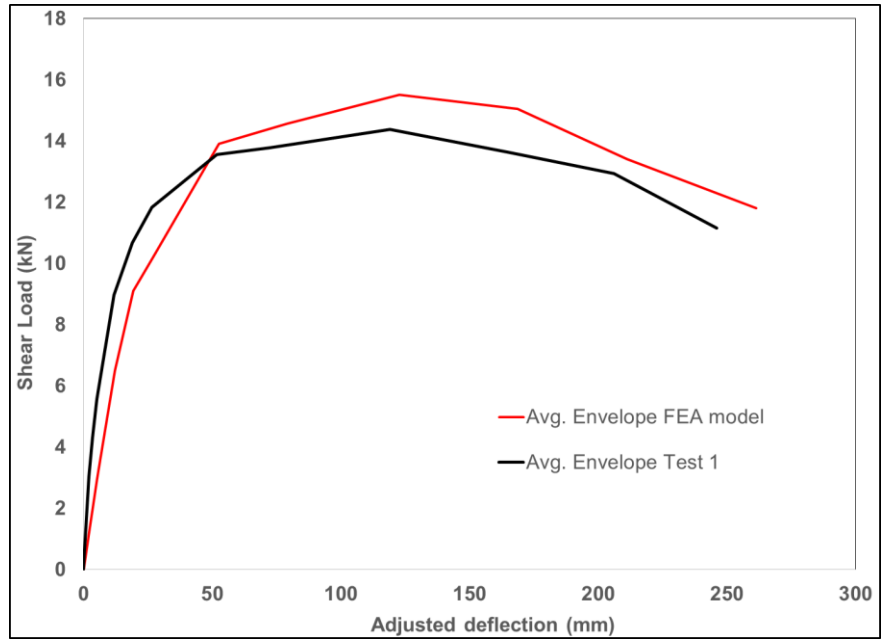


Figure C.53: Backbone curve of FEA model and test. Wall type 1.

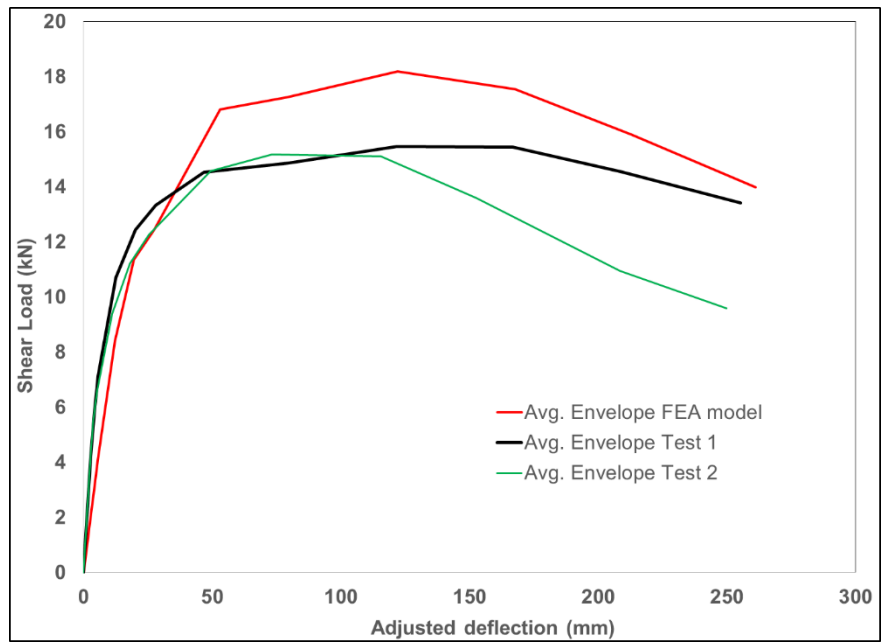


Figure C.54: Backbone curve of FEA model and test. Wall type 2.

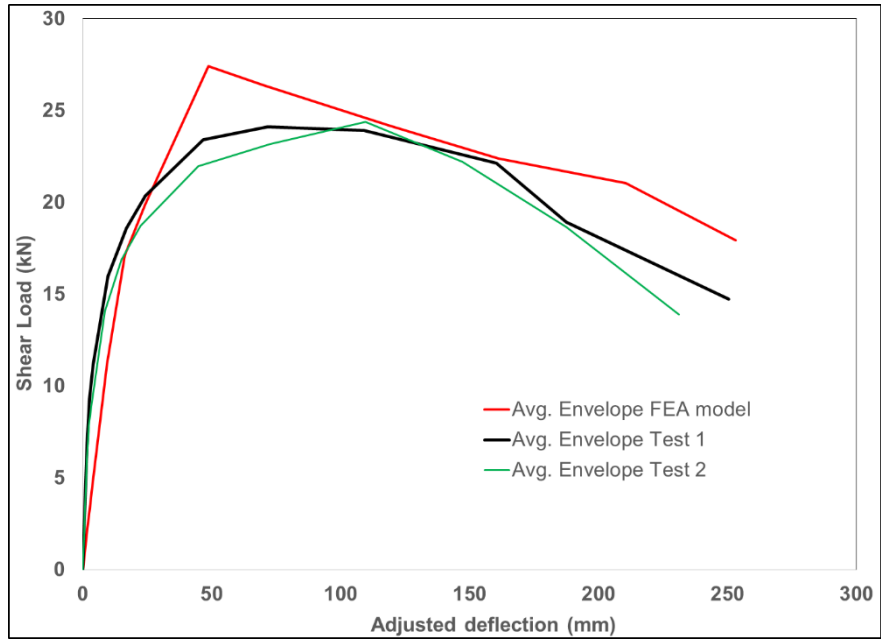


Figure C.55: Backbone curve of FEA model and test. Wall type 4.

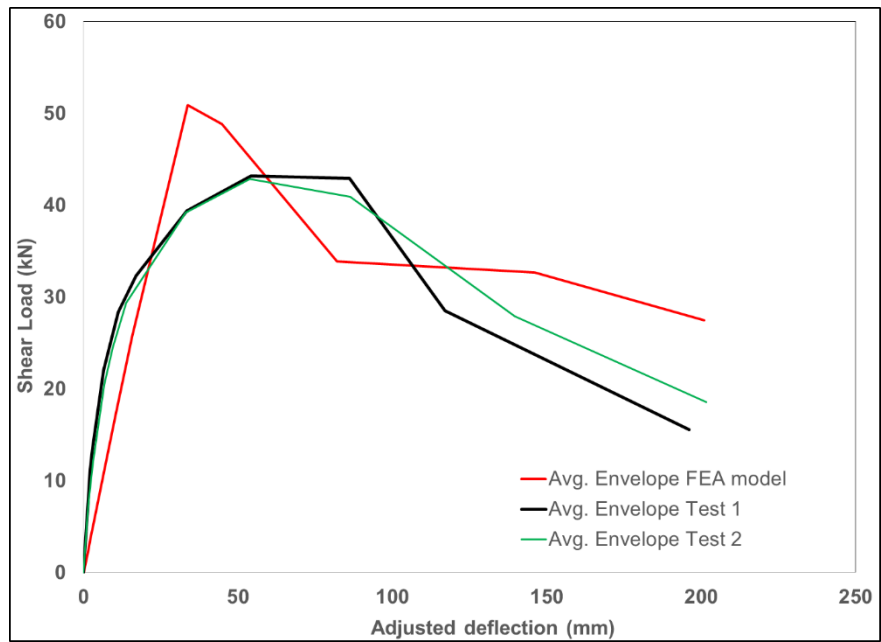


Figure C.56: Backbone curve of FEA model and test. Wall type 5.

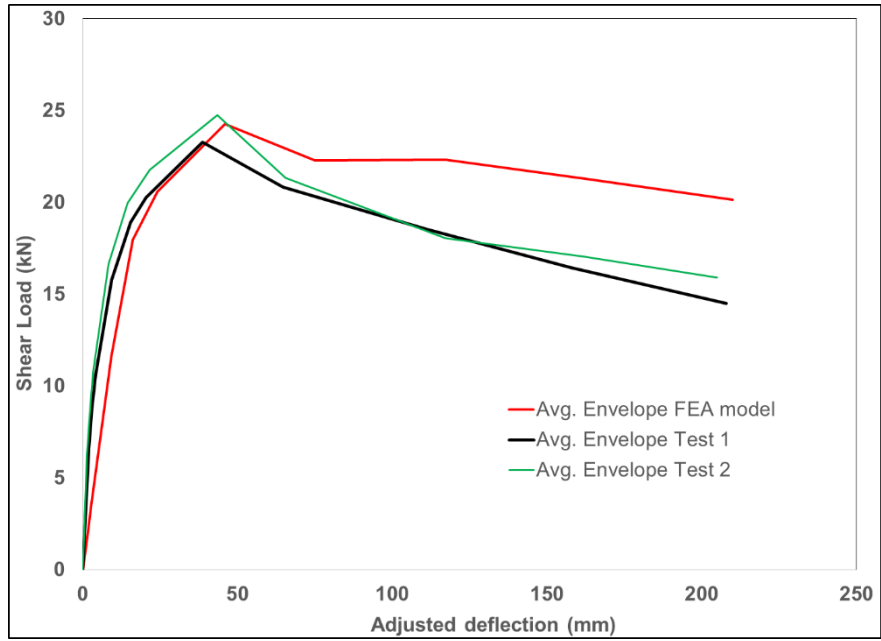


Figure C.57: Backbone curve of FEA model and test. Wall type 6.

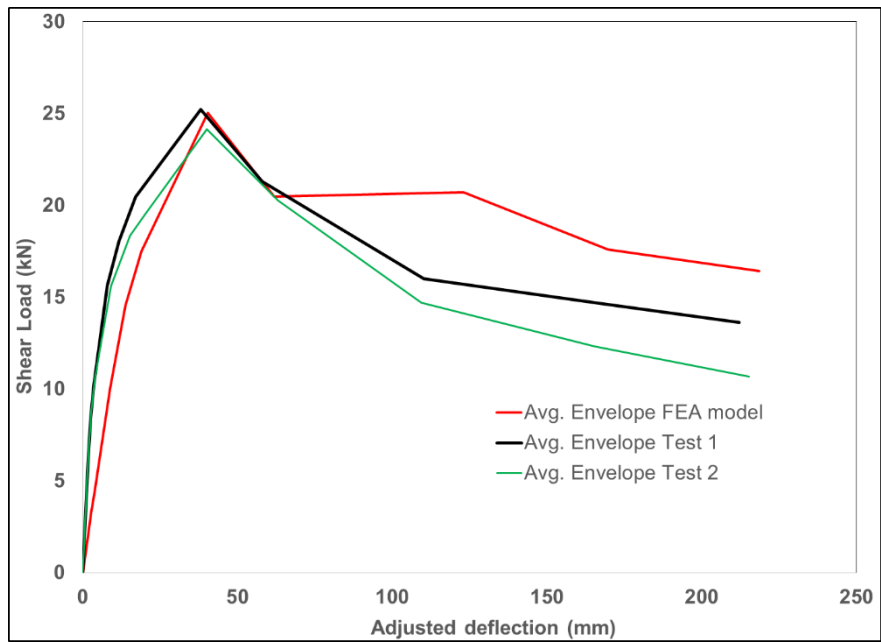


Figure C.58: Backbone curve of FEA model and test. Wall type 7.

Table C.21: AC 322 criteria check for tests and FEA models

Shear		Equivalent to light-frame wood shear walls	
Wall	reps		
ID		Tests	FEA models
1	1	YES	YES
2	2	YES	YES
4	2	YES	YES
5	2	YES	NO
6	2	NO	YES
7	1	NO	YES